Control of MRTF-SRF pathway activity by G-actin

Aleksandra Michrowska

University College London

and

The Francis Crick Institute

PhD Supervisor: Richard Treisman

A thesis submitted for the degree of

Doctor of Philosophy

University College London

September 2024

‘I, Aleksandra Michrowska confirm that the work presented in this thesis is my own. Where information has been derived from other sources, I confirm that this has been indicated in the thesis.'

Abstract

The Myocardin-Related Transcription Factors (MRTF-A and MRTF-B) are G-actin-binding proteins belonging to the RPEL protein family. They regulate the activity of Serum Response Factor (SRF) via activation of the Rho-actin pathway. MRTFs act as G-actin sensors in the cell, with signal-induced depletion of the monomeric actin pool inducing MRTF nuclear accumulation and transcription initiation.

MRTF senses G-actin through its N-terminal RPEL domain, which contains five binding sites for actin, located on three RPEL motifs and two intervening spacers. MRTF binds to SRF through a heptapeptide sequence located downstream of the RPEL domain. Actin regulates MRTF at two levels: it prevents MRTF nuclear localization and inhibits SRF-DNA binding in the nucleus. Since the actin- and SRF-binding sites on MRTF are separate, it presented with a question of how actin could inhibit SRF-DNA binding.

We successfully reconstituted this inhibitory role of actin *in vitro*, showing that actin binding to MRTF prevents the formation of the MRTF-SRF complex. RPEL3 was crucial for this inhibition, and further analysis revealed that sequences downstream of the RPEL domain stabilize its interaction with actin. Using AF2-Multimer *in silico* modelling, we identified a novel actin-binding region on MRTF—the Q-box. This finding was confirmed by HDX-MS analysis, which showed that recruitment of the Q-box to a composite site on RPEL3-actin was dependent on the integrity of RPEL3. Disruption of the interaction between RPEL3 and the Q-box lowered the overall affinity of MRTF for actin.

As the Q-box sequences are proximal to the SRF-binding site, our work suggests mutual exclusivity between MRTF-SRF binding and MRTF-actin binding. This will be further validated *in vivo*.

We propose a model in which actin binds to a composite high-affinity site comprising RPEL3 and the Q-box, nucleating the assembly of a higher-order pentavalent RPEL-actin complex.

Impact Statement

The research presented in this work focused on the Myocardin-Related Transcription Factors (MRTFs), which are signal-regulated cofactors of Serum Response Factor (SRF)—the master regulator of cytoskeletal dynamics in the cell. The MRTF-SRF pathway plays a crucial role in actin-driven cellular behaviours.

A key aspect of MRTF regulation involves its ability to sense monomeric G-actin levels, which controls both its localization and activity in the nucleus. While actin is widely studied as a fundamental component of the cytoskeleton, this work focused on its role as an important regulator of MRTF activity. As MRTF regulates the expression of actin itself, this establishes a negative feedback loop: when actin levels increase, MRTF activity is inhibited, leading to a subsequent reduction in actin expression. This regulatory mechanism is fine-tuned and it is affected by multiple complex processes that ultimately modulate MRTF activity.

Our research explains how actin binding regulates both the nuclear import and export of MRTF. Additionally, we show that actin binding indirectly impacts the stability of the MRTF-SRF interaction by modulating MRTF's ability to bind its cofactor, SRF. This is all governed by the newly identified interaction described in this thesis, highlighting the importance of understanding the detailed molecular mechanisms at play.

Given that MRTF activity has been linked to critical processes such as development, cancer progression, and fibrosis, this discovery has broad implications. By mapping these biochemical interactions between MRTF and actin, this research provides a foundation for future studies to manipulate MRTF activity in various pathological conditions

Publishing these findings will be pivotal for the field of MRTF research, advancing our understanding of MRTF regulation and offering novel avenues for investigation in both basic science and clinical applications.

Acknowledgements

Thank you, Richard, for your guidance throughout my PhD. This project has been an exciting adventure driven by scientific curiosity, and working in your lab has been anything but dull. You fuelled this research—both figuratively and literally—as I wouldn't have made it this far without your morning coffee.

A very special thank you to Stephane Mouilleron, who taught me all I needed to know to survive in the scary world of Structural Biology.

Thank you to everybody in the Crick STPs whose expertise helped develop this project, especially Sarah Maslen for all the HDX data you generated, and Simone Kunzelmann and Laura Masino for their help with the Octet analysis.

To my thesis committee, Michael Way, Caroline Hill and Tariq Enver for your inputs during the thesis meetings.

I want to thank my family, especially my parents, for supporting my scientific journey over the years. Your encouragement allowed me to travel the world and expand my knowledge, helping me reach this point in my career.

Thank you to my partner, Aga, for being there every step of the way.

To all my close friends, thank you for not letting the distance affect our friendship.

A special thank you to dr Tomasz Nawara, who has been my sounding board over the years. Here's to ten years of friendship, almost to the day!

To all the members of the lab, who made coming to work a pleasure. Maria for being my travel buddy, Roman for teaching me not to overcomplicate things, Patrick for being the number one fan of the Q-box from the start, Hector for many fruitful discussions, Noel for always selflessly offering your help. Jessica – thank you so much for always listening and offering your knowledge when most needed.

And to all my fellow PhD's, we did it!

Table of Contents

Table of Figures

List of Tables

Abbreviations

aa	Amino acid
ABP	Actin binding protein
ADF	actin-depolymerising factor
ADP	Adenosine diphosphate
Arp2/3	Actin-related protein
ATP	Adenosine triphosphate
bp	Base pair
BSA	Bovine serum albumin
BSAC	basic, SAP, and coiled-coil domain
CArG box	$CC(A/T)_6GG$ consensus sequence
Cc	Critical concentration
CD	Cytochalasin D
Cdc	Cell division cycle proteins
CDK	Cyclin-dependent kinases
cDNA	Complementary DNA
ChIP	Chromatin immunoprecipitation
CRISPR	Clustered regulatory interspaced short palindromic repeats
Crm1	Chromosomal maintenance 1 (Exportin 1)
CV	Column volume
Da	Dalton
DAPI	4’,6-diamidino-2-phenylindole
DBD	DNA binding domain
DBP	vitamin-D binding protein
dKO	Double knock out
DMEM	Dulbecco’s modified eagle medium
DMSO	Dimethyl sulfoxide
DNA	Deoxyribonucleic acid
DNase	Deoxyribonuclease
dNTP	deoxy-nucleotide triphosphate
Dox	Doxycycline
DTT	Dithiothreitol
E	Embryonic (day)
EDTA	Ethylendiaminotetraacetic acid
EGTA	ethylenbis(oxyethylnitrilo)tetraacetic acid
EMSA	Electrophoretic mobility shift assay
Ena/VASP	Enabled/vasodilator stimulated phosphoprotein
ERK	Extracellular signal-regulated kinases
ES	Embryonic stem cell

Exp	Experiment
F-actin	Filamentous actin
FAK	Focal adhesion kinase
FCS	Foetal calf serum
FGF	Fibroblast growth factor
FITC	Fluorescein
FP	Fluorescence polarization
G-actin	Globular actin
GAP	GTPase-activating proteins
GDI	GDP-dissociation inhibitor
GEF	Guanine nucleotide exchange factor
GFP	Green fluorescent protein
GST	Glutathione S-transferase
GTP	Guanosine triphosphate
GTPase	GTP hydrolase
HA	Hemagglutinin
HEPES	4-(2-hydroxyethyl)-1-piperazineethanesulfonic acid
HIS	Histidine
Imp α/β	Importin α/β
IP	immunoprecipitation
IPTG	Isopropyl β-D-1-thiogalactopyranoside
Kd	Dissociation constant
KO	Knock out
LatA	Latrunculin A
LatB	Latrunculin B
LB	Luria-Bertaini
LIC	Ligation independent cloning
LIMK	LIM kinase
LMB	Leptomycin B
LZ	Leucine zipper
MADS	MCM1, Agamous, Deficiens and SRF
MAL	Megakaryocytic Acute Leukaemia
MAPK	Mitogen-activated protein kinase
MC	Myocardin
mDIA	Mouse diaphanous
MEF	Mouse embryonic fibroblasts
MEF2	Myocyte enhancer factor
MEM	Modified eagle/s minimal media
MKL	Megakaryoblastic leukaemia

MLC	Myosin light chain
MLCK	Myosin light chain kinase
MLCP	Myosin light chain phosphatase
MOI	Multiplicity of infection
MOPS	3-N-morpholinopropanesulphonic acid
mRNA	Messenger RNA
MRTF	myocardin-related transcription factor
N-WASP	Neural Wiskott-Aldrich syndrome protein
NES	Nuclear export signal
NLS	Nuclear import signal
NP40	Nonidet P40
NPF	nucleation-promoting factor
PAGE	Polyacrylamide gel electrophoresis
PAK	p21-activated kinases
PBS	phosphate-buffered saline
PCR	Polymerase chain reaction
PDGF	Platelet-derived growth factor
PFA	Paraformaldehyde
PI(4,5)P2	phosphatidylinositol(4,5)-bisphosphate
PMSF	Phenylmethylsulfonyl fluoride
PP1	Protein phosphatase
RMDS	root mean square deviation
ROCK	Rho kinase
RPEL	Motif name (RPxxxEL), PFAM 2755
rpm	Revolutions per minute
RT-qPCR	Reverse transcription quantitative polymerase chain reaction
SAP	SAF-A/B, Acinus, PIAS
Scar/WAVE	Suppressor of cAMP receptor/WASP-family verpolin
SD	Standard deviation
SDS	Sodium dodecyl sulfate
SEM	Standard error mean
SRE	Serum response element
SRF	Serum response factor
TAD	Transcriptional activation domain
TBE	Tris-boric acid-EDTA
TCF	Ternary complex factor
TEMED	N,N,N’,N’-tetramethylethylenediamine
TEN	Tris-EDTA-NaCl

TPA	12-O-Tetradecanoylphorbol-13-acetate - also known as phorbol 12-myristate 13-acetate (PMA)
TX-100	Triton X-100
U	Unit
UTR	Untranslated region
v/v	Volume to volume
VASP	vasodilator-stimulated phosphoprotein
VCA	Verpolin, cofilin, acidic
w/v	Weight to volume
WASP	Wiskott-Aldrich Protein
WAVE	WASP family Verprolin-homologous protein
WB	Western blotting
WH2	WASP-homology 2
WIP	WASP-interacting protein
WRC	Wave regulatory complex
WT	Wildtype
α-	anti- (in Western Blotting)

Chapter 1. Introduction

1.1 Immediate early genes and the discovery of SRF

Immediate early genes, also known as primary response genes, respond rapidly to external and internal signals without any requirement for new protein synthesis. This reaction leads to changes in cell phenotype and downstream cellular behaviours. These genes respond to ligands such as growth factors, peptide hormones, antigens, and other agents that bind to cell-surface transmembrane receptors (Herschman, 1991). Early research aimed to understand the regulation of immediate early genes and identify the promoter elements and upstream signalling pathways that lead to their activation, as well as understanding how their activation induces changes in cellular behaviour.

1.1.1 Mitogen regulated cell cycle re-entry

The cell cycle is a process that ensures correct execution of two critical events: replication of the genomic DNA and its correct segregation into two daughter cells. This process is tightly regulated by cyclins, which regulate the cyclin-dependent kinases (CDK) at different stages of the cell cycle. Withdrawal from the cell-cycle can be due to several factors: cells reaching confluence, deprivation of serum factors and nutrients and loss of adhesion, and is accompanied by reduced protein and RNA synthesis. Serum and growth factor stimulation leads to new RNA synthesis, followed by protein translation, which triggers cell cycle re-entry. Factors that induce the cell cycle are referred to as mitogens.

Platelet-derived growth factor (PDGF) was one of the first identified mitogens. Early studies showed that PDGF, along with serum, increases protein synthesis rates in mouse fibroblast 3T3 cells (Cochran et al., 1981). The signal for DNA synthesis induced by PDGF was believed to be mediated through an unidentified intermediary. Transfer of cytoplasm from growth factor treated cells into quiescent cells enables them to re-enter the cell cycle (Smith and Stiles, 1981). Similar experiments showed that transfer of RNA from PDGF treated to

untreated cells is crucial for induction of cell cycle re-entry, with RNA synthesis playing a significant role in this process. Inhibition of RNA synthesis prevented cell-cycle entry, while blocking protein synthesis with cycloheximide had no impact.

The first insights into the genes involved are from candidate screening approaches. Research by Kelly et al., 1983 revealed that the accumulation of *c-myc* mRNA in T-cells occurs after PDGF treatment and does not require new protein synthesis, as evidenced by cycloheximide treatment. A three-hour treatment with PDGF, fibroblast growth factor (FGF), and phorbol 12-myristate 13-acetate (TPA) induced mRNA accumulation. This response was observed in fibroblasts and similarly in lymphocytes treated with lipopolysaccharide (LPS). In parallel, differential cDNA screening revealed gene sequences activated by PDGF. It was speculated that the PDGF response involves a combination of oncogenes inducing a mitogenic response (Armelin et al., 1984).

Screening of a pool of oncogenes identified *c-fos*, the cellular homologue of the oncogene isolated from mouse FBJ osteosarcoma virus (Curran et al., 1982; Finkel et al., 1966). It was identified as a gene with increased transcription and protein synthesis following PDGF treatment (Cochran et al., 1984; Greenberg and Ziff, 1984). Serum stimulation increased both *c-fos* and *β-actin* transcription within 15 minutes, while *c-myc* transcription was low as compared to *c-fos*, and only occurred at 30 min post serum treatment. Induction was observed following serum stimulation and also after treatment with purified growth factors such as FGF, PDGF, and TPA, but not after hormone treatments like insulin or in media with low serum concentrations (0.5% serum). The increase in RNA production was transient, peaking at 15 minutes. This was followed by a transition from G0 to G1 and DNA synthesis. This rapid activation and short mRNA lifespan are characteristic of immediate-early genes. Subsequent differential RNA screening studies identified many genes co-regulated with *c-fos*.

A mechanism of transferring the signal from the receptor was thought to be regulated by phosphorylation of kinases which activate downstream pathways and lead to gene activation. TPA can activate protein kinase C and

tyrosine kinase, leading to *c-fos* activation, similarly to treatment with PDGF and serum.

While serum stimulation was established as a mitogenic signal, the downstream regulators that induce DNA synthesis remained unclear.

1.1.2 Identification of Serum Response Factor

The 5' flanking sequence of the *c-fos* gene was shown to be essential for serum-mediated induction of transcription, and the -322 to -277 region of the promotor sequence of *c-fos* was determined to be the sufficient for induction (Treisman, 1985). It was then important to identify proteins that bind to that regulatory sequence upon serum treatment.

Isolation of nuclear extracts from HeLa cells revealed a protein that binds to the promoter region of the 5' *c-fos* gene, specifically to a region of dyad symmetry within the essential sequence element previously identified. The binding site on *c-fos* was called the Serum Response Element (SRE) (Treisman, 1986), and was shown to be sufficient for serum responsive transcription. The protein binding to it, SRF, was identified in parallel by several groups (Gilman et al., 1986; Prywes and Roeder, 1987; Schröter et al., 1987; Treisman, 1987).

A sequence similar to the SRE dyad symmetry has been also identified in the *Xenopus laevis γ-actin* gene (to which SRF binding could be detected), and together with DNA footprinting assays done on the *c-fos* gene, allowed for determining of a consensus binding sequence for SRF termed the CArG box ($CC(A/T)_6GG$).

SRF polypeptide was isolated by DNA affinity chromatography experiments (Prywes and Roeder, 1987; Schröter et al., 1987; Treisman, 1987), and its cDNA was isolated by screening using oligonucleotide probes derived from partial protein sequences within the SRF sequence (Norman et al., 1988). Sequences spanning the 132-223 region were sufficient for DNA binding, with residues 168-222 crucial for dimerization. SRF orthologues were detected in monkey and mouse, as well as fly and frog DNA. The yeast homologue of SRF - MCM1 will be discussed in the next chapter.

It was determined that *srf* transcription itself is regulated by serum stimulation, where about a 5-fold increase could be seen as compared to serum starved conditions (Norman et al., 1988). Interestingly, SRE occupation by protein can be detected before and after serum stimulation, suggesting that regulation of its activity does not occur through DNA binding, but rather through additional mechanism, such as phosphorylation of the protein or binding of another factor to the SRF-SRE complex (Herrera et al., 1989). Subsequent studies showed that this is indeed the case and will be discussed in the following sections (Olson and Nordheim, 2010; Posern and Treisman, 2006; Shaw et al., 1989; Wang et al., 2001).

1.1.3 The MADS-box family of transcription factors

Homologues of SRF have been found in plants and yeast and have been classified into a family based on the presence of a conserved 56 amino acid domain. The domain was called MADS after the first identified members of the family: MCM1(Minichromosome maintenance 1) (Passmore et al., 1989) and Arg80 (Dubois et al., 1987) in yeast, Agamous (Yanofsky et al., 1990) and Deficiens (Sommer et al., 1990) in plants and SRF in animals (Norman et al., 1988). MADS domain is the core DNA interaction and dimerization interface. There is high level of conservation of the MADS domain between species (Figure 1).

Four best described members found in yeast are MCM1, ARG80, Rlm1 and SMP1 and the main metazoan members are MEF2A, B, C and D and SRF. MADS family of proteins is greatly expanded in plants. These transcription factors have been shown to be involved in various processes in the cells such as muscle differentiation, cell proliferation or migration in animals and cell type determination, metabolic pathway regulation and stress response in yeast. In plants they play a part in development (reviewed in (Messenguy and Dubois, 2003)).

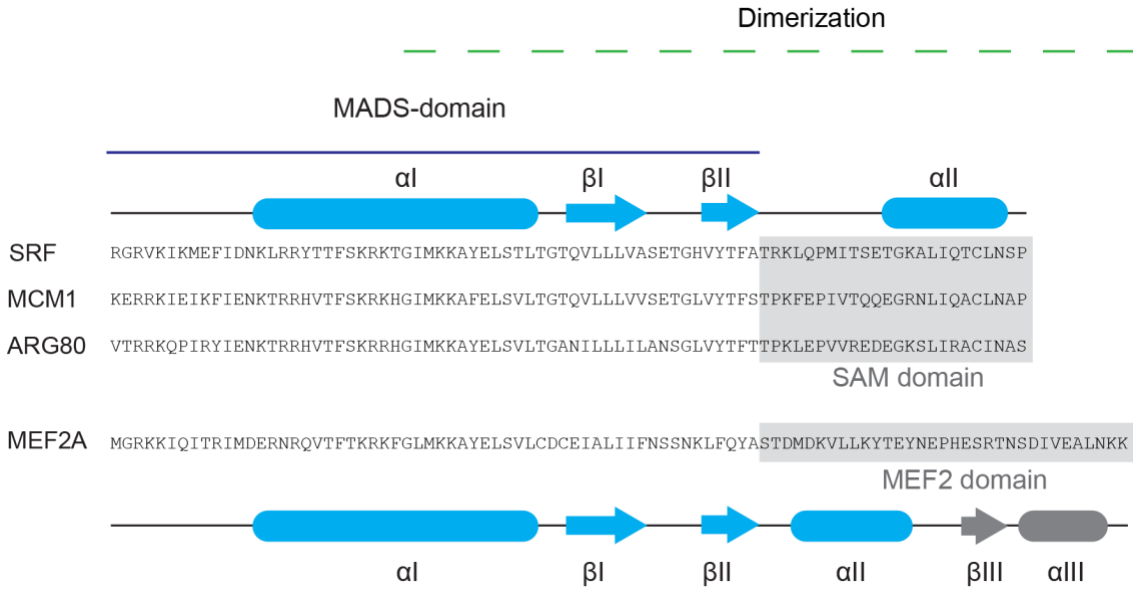

Figure 1. The conservation between MADS-domain between species
Comparison of the domain structure between SRF (animals) and MCM1 & ARG80 (yeast), compared with MEF2A. Regions spanning the MADS domain, and the C-terminal extension are sufficient for dimerization. The DNA-binding domain of the MADS-family of proteins consists of an αI-helix and two β-sheets (I and II).

1.1.4 Structure of the SRF-DNA complex

The structure of the DNA binding domain of SRF-DNA was determined by X-ray crystallography using the 132-223 residues of SRF and an 18bp DNA (α-cell specific *MFα-1* gene found in yeast) sequence containing the SRE consensus sequence with the CArG box in the middle (Pellegrini et al., 1995). SRF binds to DNA as a stable homodimer, consisting of two 10,400 Da monomeric subunits (Figure 2). Two α-helices from two SRF subunits form an antiparallel coiled coil, which is the primary DNA-binding interface, bridging the minor groove to make contacts with the successive turns of the major groove. The N-termini of each SRF subunit is localized to the major groove, with R143 buried in the minor groove, and K171 of the αI-helix positioned over the R143 and making additional electrostatic interactions with both phosphodiester chains. Each subunit is then folded into two antiparallel β-sheets, which are the main dimerization interface of the complex. The following C-terminal sequences are folded into an irregular coil that links to the short αII helix, placed on top of the β sheets.

The DNA is bent by 72º in the complex, and this ability of SRF to bend DNA has been proposed as a possible facilitating mechanism for binding of accessory proteins, which by themselves might not possess the ability bind DNA (Pellegrini et al., 1995).

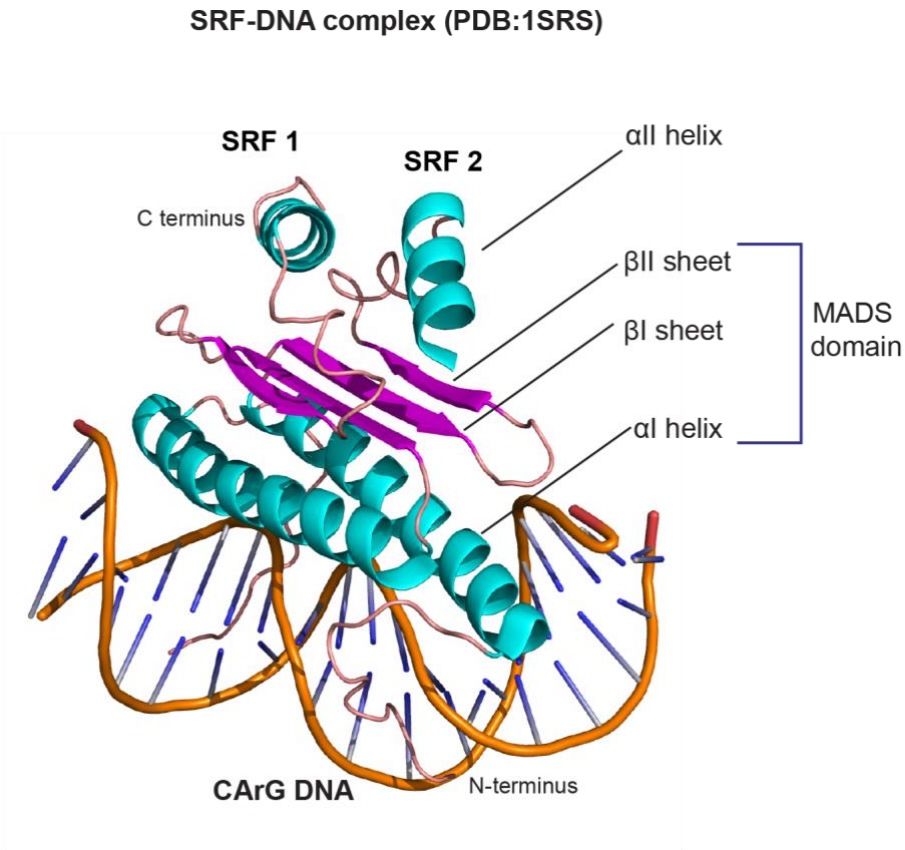

Figure 2. Crystal structure of SRF-binding to CArG DNA sequence
Two SRF molecules (residues 132-223) shown in cyan (αI helix and αII helix) and magenta (β-sheet), 18bp DNA sequence containing the CArG box shown in orange. Each SRF binds to DNA through the αI helix, folds into two antiparallel β sheet, and folds into αII helix. The N terminus of each SRF is buried in the minor groove of DNA, with αI helix making contacts with the major groove of DNA. PDB: 1SRS (Pellegrini et al., 1995) used for making the figure.

1.2 The SRF transcription factor network

SRF activity is regulated by two signal-regulated families of cofactors, the Ternary Complex Factors and Myocardin-family proteins. The three TCFs are activated through the Ras-ERK signalling (Treisman, 1994), while the two MRTFs are novel G-actin binding proteins whose activity responds to signal induced depletion of G-actin via the “Rho-actin” pathway (Miralles et al., 2003)

(Figure 3). Myocardin, the third and founding member of the Myocardin family is constitutively active and expressed specifically in muscle (Wang et al., 2001).

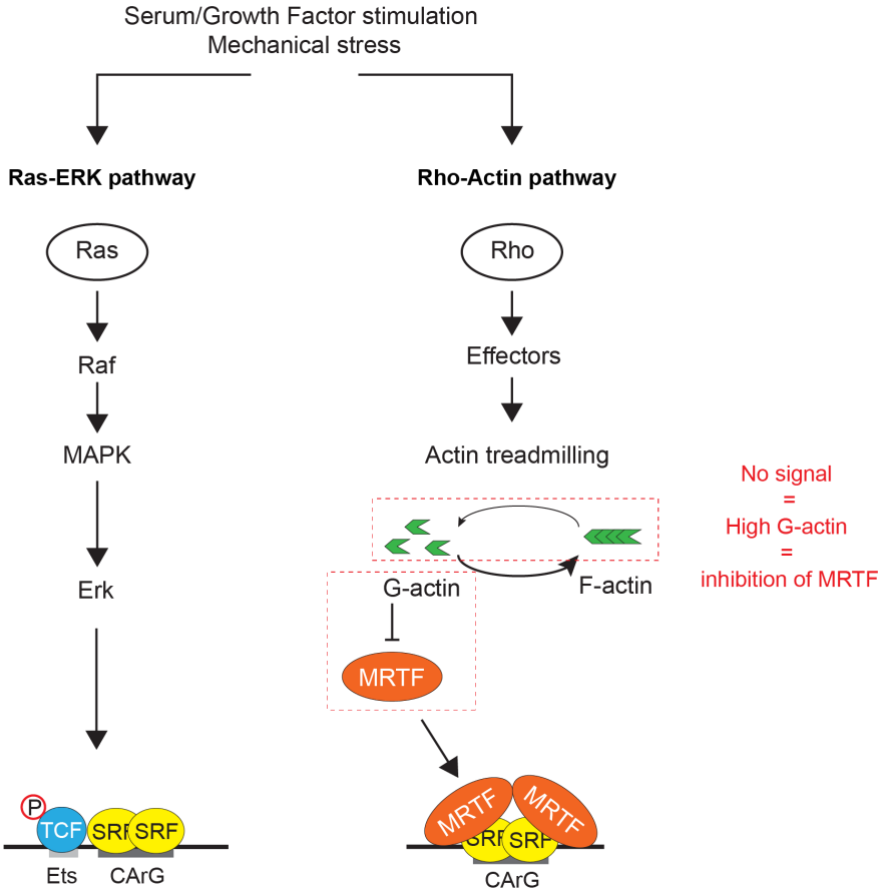

Figure 3. Signal regulated control of SRF activity
Schematic representation of SRF activation through TCFs and MRTFs. Serum stimulation activates two pathways in mouse fibroblasts. Ras activates Raf, which in turn leads to MAP kinase activation and phosphorylation of members of the TCF family. TCFs bind to SRF and DNA leading to expression of genes like *egr-1* and *c-fos*. Rho GTPases activation via serum leads to changes in actin dynamic, with more polymerization and depletion of the G-actin pool. MRTF is in turn activated and binds to SRF, leading to transcription of cytoskeletal genes such as actin or vinculin. In resting cells, MRTF activity is regulated by G-actin, by inhibition of nuclear import and sequestering in cytoplasm (see the red dotted lines).

1.2.1 Identification of TCFs as SRF cofactors

Following the identification of SRF, the mechanism of activation of the downstream gene expression was still unclear. Further research into the signalling pathway found an SRF-binding partner protein called p62, which could only be detected on SRF or p67 in the presence of DNA (Shaw et al.,

1989) and could not bind to DNA without the presence of SRF. Sequences outside the SRE symmetry dyad were shown to be important for p62 binding to SRF. Activation of the c-fos gene was dependent on the formation of the ternary complex between p62 and p67/SRF, as mutation of sequences required for TCF binding blocked serum induction. This was the first indication that SRF signalling is regulated by a ternary complex formation with an accessory protein. The genes encoding TCF were identified by candidate approaches and selection for SRF dependent DNA binding in yeast (Dalton and Treisman, 1992; Giovane et al., 1994; Hipskind et al., 1991; Price et al., 1995). Elk-1 (Hipskind et al., 1991), SAP-1 (Dalton and Treisman, 1992) and Net (Giovane et al., 1994) have been classified as members of the Ets domain containing proteins (Wasylyk et al., 1993) and called the TCFs (Ternary Complex Factors).

TCF's are regulated via the MAP kinase activation through Ras-ERK signalling. Early studies indicated that phosphorylation of TCF C-terminal "C-box" domain potentiated ternary complex formation with SRF *in vitro* (Gille et al., 1992), although this is not consistent with the apparently constitutive binding of TCF *in vivo* (Herrera et al., 1989). Whether phosphorylation affects ternary complex formation with SRF remains to be resolved. Subsequently, the Elk-1 C-terminal sequence was shown to act as a phosphorylation-dependent activation domain (Gille et al., 1995; Janknecht et al., 1994; Marais et al., 1993). The DNA interaction domain is the N-terminal Ets domain and SRF binding occurs downstream through a basic B box (Figure 4) (Treisman, 1994).

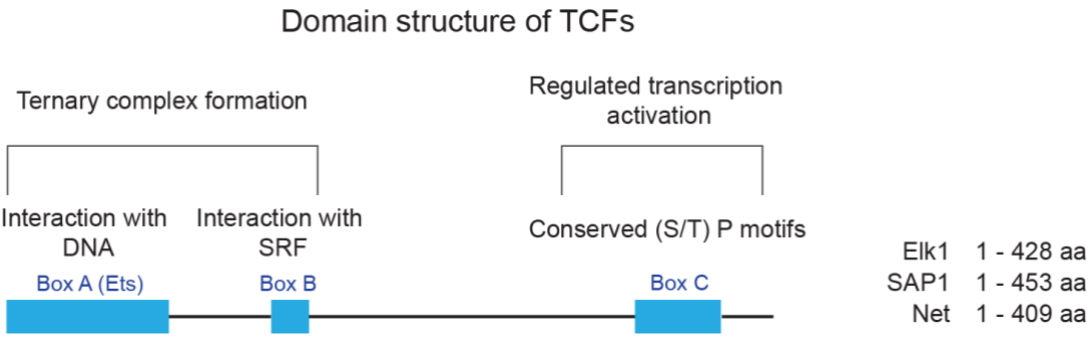

Figure 4. Domain organization of TCF family members
TCF family members (Elk1, SAP1 and Net) share conservation in their structural domains. The Ets binding domain (Box A) is responsible for contacting DNA, Box B binds to SRF and Box C is the C terminal transcriptional activation domain which is a region of multiple phosphorylations.

1.2.2 SRF transcriptional response in the absence of TCF binding

TCF-SRF signalling occurs via activation of the Ras-ERK pathway (Treisman, 1994). Analysis of the TCF-SRF binding revealed that mutation of TCF-binding site in the *c-fos* promoter abolished activation via the Ras-ERK pathway but did not stop a response to serum or PKC-induced signals (Graham and Gilman, 1991; Hill et al., 1994). It was proposed that TCF-independent signalling activated a novel SRF cofactor that interacts with the SRF DBD (Hill et al., 1994).

Analysis of TCF-independent signalling by serum factors showed activation of SRF. LPA (Lysophosphatic acid) signals through G-protein coupled receptors and induces Ras GTP formation, ERK activation, as well as cytoskeletal rearrangement mediated through Rho, a Ras superfamily member of small GTPases (Hall, 1994). Activation through serum and LPA is RhoA dependent. SRF activation can also occur via two other GTPases - Rac1 and Cdc42 and activated forms of any of the three GTPases could activate SRF without extracellular signals (Hill et al., 1995). It was also shown, that TCFs do not respond to the Rho-actin signalling pathway (Ginieitis and Treisman, 2001). Insights into the nature of this pathway come from the finding that RhoGTPases activate SRF independently of TCF (Hill et al., 1995), and that serum activation reflects perturbation of the actin dynamics (Sotiropoulos et al., 1999). Further experiments showed that SRF may be bound to DNA through its DNA binding domain (DBD) to activate transcription via this pathway, and that specific sequences within the DBD were required (Hill et al., 1994).

1.2.3 The Myocardin family of SRF cofactors

The identification of Myocardin as an SRF cofactor in muscle (Wang et al., 2001) led to analysis of its ubiquitously expressed relatives, the MRTFs (MRTF-A and MRTF-B) as candidates for the TCF-independent cofactor (Wang et al.,

2002) (Figure 5). Transfection and reporter experiments showed that MRTF-A had the SRF and DNA binding properties of the putative cofactor, that it was required for the serum response and that it would accumulate in the nucleus in response to signals (Cen et al., 2003; Miralles et al., 2003; Vartiainen et al., 2007). MRTF activity is regulated by actin binding to an N-terminal RPEL domain, which can detect the concentration of monomeric G-actin in the cell. Identification of MRTFs as actin-binding SRF cofactors provided a link between the change in the cytoskeletal dynamics occurring in the cytoplasm and the transcriptional activity in the nucleus (Miralles et al., 2003). Depletion of the actin pool by activation of RhoA and induction of actin treadmilling localizes MRTF to the nucleus and leads to SRF activation (Figure 3). The SRF-binding region was mapped to the B-box and Q-box sequences. A detailed discussion of the MRTFs and their regulation is given in later sections.

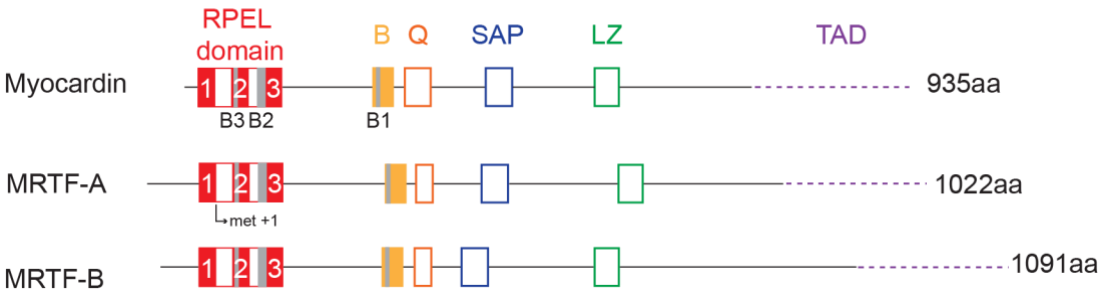

Figure 5. Myocardin family of proteins
Myocardin, MRTF-A and MRTF-B proteins with domain regulatory elements annotated on the schematic. RPELs shown in red, B-box - yellow, Q – orange, SAP – dark blue, LZ – green, TAD domain – purple dotted line (the region has not been mapped to the exact residues conferring transcriptional activity). B1, B2, and B3 NLS indicated in grey.

1.3 SRF – cofactor interactions

1.3.1 Mechanism of Ternary Complex formation

With cDNA clones available, studies of ternary complex formation could be conducted and revealed, that TCFs make DNA contacts independently of SRF, but this was affected by the binding site sequence (Treisman et al., 1992). Structural analysis of the SAP1/SRF ternary complex showed that Ets domain contacts DNA, with B region acting as a flexible tether that interacts with the

SRF MADS-domain (comprising αI-helix, and two β-sheets), adding another strand to the β-sheet. The B-box also makes contacts with DNA. Spacing of Ets and SRF is flexible (Treisman et al., 1992) and reflects independent interaction of the Ets domain with Ets motif on DNA and the B-box with the SRF DBD (Dalton and Treisman, 1992; Treisman et al., 1992). Binding of SAP1 induces an additional bend in the DNA, from 72º angle that can be seen with SRF-DNA alone (Pellegrini et al., 1995), to 77º in the ternary complex (Figure 6A).

The molecular interactions facilitating TCF-SRF binding show striking similarities to these mediating the interaction of the yeast SRF homolog MCM1 with its homeodomain binding partner MATα2. While MCM1 binding partner MATα2 and SRF binding partner SAP1 belong to structurally different families of transcription factors, there are similarities in the way they contact their respective transcription factors. Both have autonomous DNA binding domains, joined to a flexible docking sequence and add a β-strand to the MADS-domain β-strand platform. However in the SAP1/SRF complex, the β-strand is added in an antiparallel manner to SRF, while that in the MCM1/MATα2 complex is added in parallel (Tan and Richmond, 1998) (Figure 6B).

A. **SAP1-SRF-DNA complex (PDB:1HBX)**

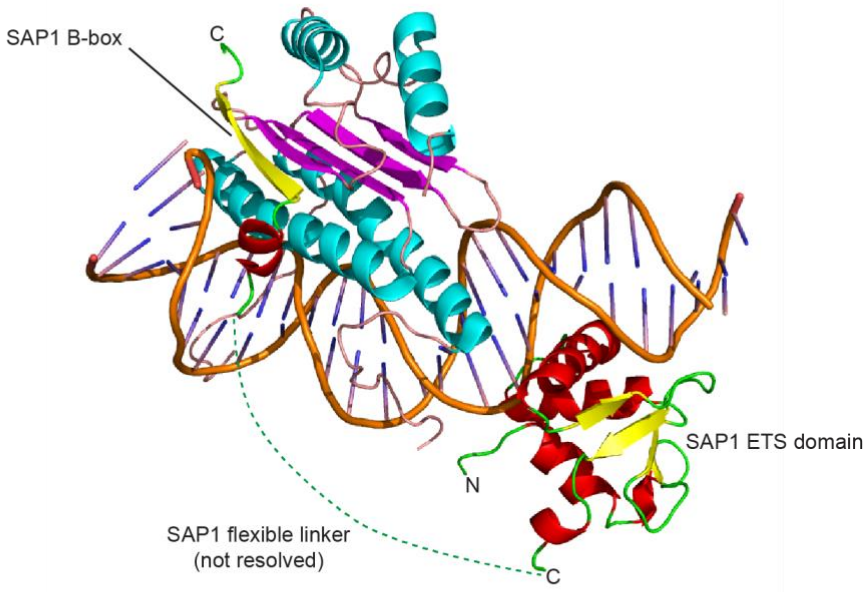

B. **Similarity between SAP1/SRF and MCM1/MATα2 interactions (MCM1-MATα2 PDB: 1MNM)**

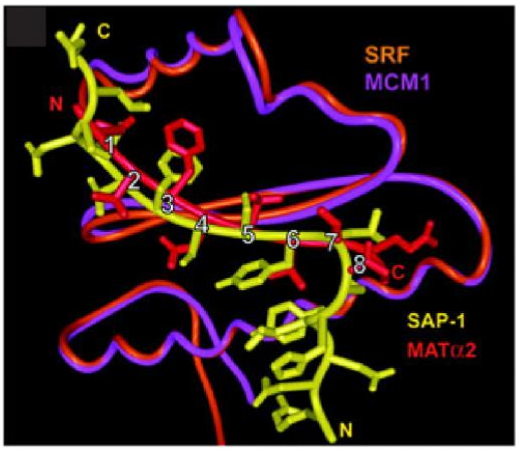

B-box position		1	2	3	4	5	6	7	8	
SAP1 (C←N)	152	L	T	F	S	S	Y	L	G	145
MATα2 (N→C)	114	L	V	F	N	V	V	T	Q	121
MRTF-A (N→C) (sequence mapped by Zaromytidou et al., 2006)	328	L	K	Y	H	Q	Y	I	P	335

Figure 6. TCF-SRF binds SRF with the B-box and DNA via Ets domain
A. Crystal structure of SAP1-SRF-DNA (PDB:1HBX). The SRFdimer (residues 132-223) is shown in cyan (αI helix and αII helix) and magenta (β-sheet), SAP1 (residues 1-156) sequence containing both the B-box and the DNA-binding Ets-domain shown in yellow (β-sheet) and red (α-helix). The flexible linker between the B-box and Ets domain is shown in red dotted line (structure not resolved). SAP1 B-box is placed antiparallel to the SRF β-sheet. **B.** Comparison of SAP-1-SRF binding and MATα2-MCM1 binding (PDB:1MNM). MCM1 binds DNA essentially similarly to SRF shown in A. SAP1 (yellow) and MATα2 (red) contact SRF through 8-residue sequences that add a β strand to their MADS partners β-sheet platform. SAP1 places β-strand in an antiparallel manner, while MATα2 binds with in a parallel orientation. The mapped sequence of the MRTF-A B-box shown below (Zaromytidou et al., 2006). Figure 4B was modified from (Richmond and Hassler, 2001) with a reprinting permission from European Molecular Biology Organization (Licence ID:1526645-1).

1.3.2 MRTF-SRF complex formation

SRF is a common target for TCFs and MRTFs. Competition between the two was shown by transfection experiments (Murai and Treisman, 2002), biochemical studies (Miralles et al., 2003; Wang et al., 2004; Zaromytidou et al., 2006) and genomic analysis (Gualdrini et al., 2016), indicating a shared binding space on SRF.

The MRTF-SRF-DNA complex have not been resolved, but mutagenesis analysis showed that the basic region of MRTF – B-box is necessary for MRTF-SRF interaction, with a heptapeptide within the sequence crucial for binding (Zaromytidou et al., 2006) (Figure 6B). Another element in the MRTF sequence, Q-box was shown to facilitate the interaction. MRTF-SRF binding can only be detected in the presence of DNA. Biochemical data suggests, that MRTF might make specific contacts with the DNA backbone of the MRTF-SRF-DNA complex (Zaromytidou et al., 2006). In Chapter 4 I will show a predicted structure of MRTF-SRF on DNA using AlphaFold3, a new structure prediction software, which confirms the heptapeptide placed as a β-strand on SRF DBD β-sheet platform, indicating competition with TCF for SRF binding.

This thesis will focus on understanding the mechanism underlying the inhibition of MRTF-SRF-DNA binding by actin.

1.3.3 Differential targets of TCF and MRTF

While MRTF and TCF compete for a shared surface on the SRF DBD, functional studies suggest that SRF target genes nevertheless can exhibit a degree of preference for one factor or the other.

RhoA-Actin and Ras-ERK signalling act in a mutually exclusive manner, with immediate early genes such as *egr-1* and *c-fos* dependent on ERK signalling, but independent of RhoA, while *srf* and *vinculin* are Rho-dependent and do not respond to ERK signalling (Gineitis and Treisman, 2001). The initial proposal was that SRF targets could be divided into two distinct groups based on activation of MRTFs or TCFs (Gineitis and Treisman, 2001; Gualdrini et al., 2016). However, analysis of mouse embryonic fibroblasts (MEFs) treated with serum revealed, that most of the serum-inducible genes are regulated by MRTF signalling (Esnault et al., 2014). Conversely, stimulation of MEFs with TPA led to TCF-dependent activation of target genes (Gualdrini et al., 2016), while triple knockout of TCFs (*Elk1*$^{-/-}$, *Elk3*$^{\delta/\delta}$, *Elk4*$^{-/-}$) shown to potentiate MRTF signalling to many genes, suggesting that most genes can bind both cofactors. How the gene-specific preference for one or the other cofactor pathway is achieved remains unclear.

1.3.4 SRF network knockout phenotypes

SRF regulates expression of immediate early genes important for proliferation and cell cycle re-entry, as well as activates expression of cytoskeletal-dynamic regulatory genes. This is governed by binding of MRTFs and TCFs and activation of transcription via two pathways: Ras-ERK and Rho-Actin. An important tool for studying these pathways is inactivation of the genes encoding these proteins and observing the phenotypical and molecular changes.

Knockout of SRF in mice is embryonic lethal, with homozygous deletion mutants of *SRF (srf*-/-) exhibiting reduction in size by E7.5, delayed development, and no viability by E12.5 (Arsenian et al., 1998). Due to this, conditional tissue-specific SRF knockout models were developed to study its

role in different tissues using Cre recombinase. SRF is ubiquitously expressed and was shown to be important for multiple cellular processes in various tissues, such as muscle cells, immune cells, fibroblasts, hepatocytes, neurons and endothelial cells. It also plays a crucial role in tissue development, as well as in the immune and nervous systems, by controlling cell growth, differentiation, proliferation and regeneration (reviewed in Olson and Nordheim, 2010; Onuh and Qiu, 2021). In many contexts, SRF phenotypes can be recapitulated by inactivation of one or more of its cofactors, emphasising that the cofactors activate through SRF.

MRTF-A knockout mice (*Mrtfa-/-*) are viable, but present with an impaired differentiation of the mammary myoepithelium resulting in failure in milk ejection and feeding the litter (Li et al., 2006; Sun et al., 2006). MRTF-B knockout (*Mrtfb-/-*) is embryonic lethal in mice between E13.5 and E14.5 due to severe impairment of branchial arch arteries development and smooth muscle differentiation (Oh et al., 2005a). Similarly to SRF, tissue specific conditional knockouts were generated. MRTFs were shown to be important for neuronal migration and cardiomyocyte function, where deletion led to cardiac fibrosis and dilation of left heart ventricle (Mokalled et al., 2010). Deletion of MRTF in haematopoietic stem cells led to failed colonisation of the bone marrow (Costello et al., 2015). Data from our group showed that deletion of both MRTFs in MEFs led to cell cycle arrest and a senescence-like phenotype, which was also seen with SRF knockout in fibroblast cells (J. Nielsen, manuscript in preparation; S. Bellamy, PhD work).

TCF knockout does not result in embryonic lethality. In thymocyte development, it was shown that there is redundancy between Elk-1 and SAP1 (Costello et al., 2010), with a double knockout Elk1 and SAP1 (*Elk1-/-, Sap1-/-*) mice being viable, but with infertility in the females. SAP1 is required for thymocyte positive selection, where it acts redundantly with Elk1 (Costello et al., 2004). Elk1 knockout (*Elk1-/-*) resulted in spontaneous fibrosis in both liver and lung (Cairns et al., 2020). In contrast, inactivation of Net, the 3rd member of the family revealed that it appears to act in a non-redundant way with the other

family members. Net mutant mice die shortly after birth due to disruption in formation of vasculature (Ayadi et al., 2001).

1.4 Regulation of actin cytoskeleton

In the previous sections, I introduced SRF transcription factor and its regulation through two signalling pathways: Ras-ERK and Rho-Actin. The Rho-Actin pathway signalling regulates the cytoskeletal gene expression through activation of MRTF and SRF, where activation of small GTPases such as Rho affects various downstream effectors that regulate the actin treadmilling cycle.

In this chapter I will focus on describing the regulation of actin cytoskeleton via Rho signalling and introduce the structural basis of actin binding to the MRTF actin binding motif.

1.4.1 Actin classification

Actin belongs to a family of proteins with high conservation of structure between bacteria, archaea and eukaryotes (Bernander et al., 2011; Gunning et al., 2015). It is one of the most abundant proteins in the mammalian cells, with concentrations ranging between 65 to 300μM depending on the cell type (reviewed in Remedios et al., 2003). Actin is a part of cellular microfilament system, and through its ability to treadmill between monomeric and polymerized forms, it takes part in regulating processes such as cell adhesion, motility, cytokinesis, vesicular transport, as well as morphogenesis during regeneration and development.

It is highly abundant in all eukaryotic cells and at least six isoforms of actin have been identified (Vandekerckhove and Weber, 1978). Actins can be divided by different criteria: their isoelectric point (pI) values determined based on their N-terminal residues and their N-terminal processing pre-maturation.

The main difference between actin sequences is localized in their N-terminus, leading to a change in their isoelectric point values, and allowing for first classification into α, β and γ actins by increasing pI values (Garrels and Gibson, 1976).

Another classification can be done based on their N-terminal residue processing (Rubenstein and Martin, 1983). Class I (non-muscle actins), which consist of β and γ cytoplasmic actins, have a D/E residue in the second position after N-terminal Met. Acetylation of Met at the beginning of translation and its removal allows for the second residue to be acetylated, resulting in mature actin folding. Class II (muscle actins) consists of actin with a Met followed by a C-D/E, where in a similar manner N-terminal Met is acetylated and removed, leading to acetylation and removal of C and final acetylation of the N-terminal D or E and mature actin translation (Gunning et al., 1983; Solomon and Rubenstein, 1985). This class consists of α- skeletal and α-cardiac muscle actins, and α-smooth and γ-smooth muscle actins. Class I actins are abundant in almost all cell types, while Class II are tissue specific (Figure 7).

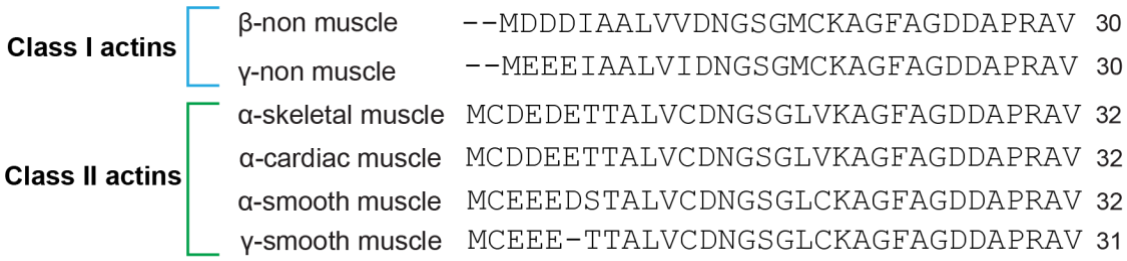

Figure 7. Sequence divergence in the N-terminus between actins
Alignment of N-terminal sequences of Class I and Class II actins (*Mus musculus*). Class I actins undergo removal of N-terminal Met, followed by acetylation leading to mature actin folding (Ac-DDD/Ac-EEE). Class II actins undergo removal of Met and Cys, before acetylation of the following residue (Ac-D or Ac-E).

1.4.2 Monomeric G-actin

Monomeric actin is formed of two major domains: α and β, which in turn can be divided into 4 subdomains (1-4) (Kabsch et al., 1990). The domains are separated by a flexible “hinge” regions, with two clefts formed between the subdomains (Figure 8).

Subdomains 1 and 3 of the β-domain are separated by a target-binding cleft, where a lot of hydrophobic residues are localized. This region is involved both in facilitating contact between actins in the filament and interacting with

majority of G-actin-binding proteins (ABPs) (Dominguez, 2004; Oda et al., 2009).

The nucleotide-binding cleft is localized between subdomains 2 and 4 of the α-domain, where Mg^{+} ions and ATP can bind, stabilizing the two domains (Dominguez and Holmes, 2011). Nucleotide binding to the cleft determines the subdomains position and regulates intra-filament actin binding, as well as ABP binding affinities (Kudryashov et al., 2010).

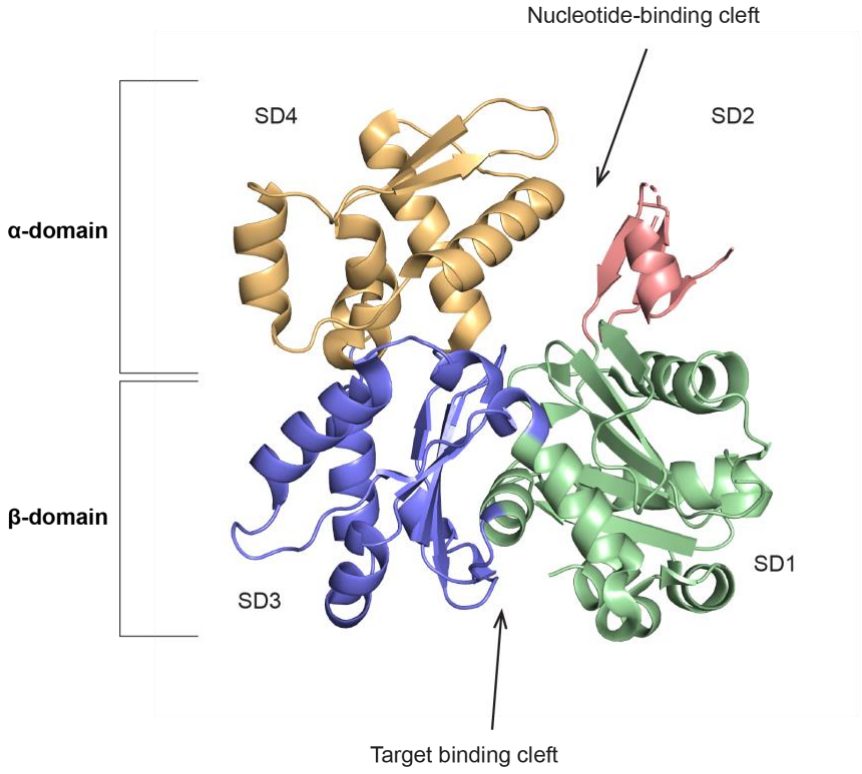

Figure 8. G-actin subdomains
Monomeric actin (rabbit skeletal α-actin, PDB:2V52) with domains and subdomains annotated on the schematic. Residues coloured by subdomains.

1.4.3 Actin treadmilling

Actin treadmilling is a process of polymerization and depolarization of actin filament, which is regulated by binding of actin binding proteins (Figure 9). Polymerization can occur spontaneously in physiological salt concentrations, whereby binding of cations to specific sites on the filament promotes interaction between monomers in the filament (Kang et al., 2013).

Two ends can be distinguished on an actin filament: a barbed end (SD1/3 exposed) and a pointed end (SD2/4 exposed) (Figure 9). Polymerization is favoured at the barbed end, with the ability to add monomers to both ends with different affinities (Pollard and Borisy, 2003). The two ends have a different critical concentration (C_c) of actin, which is the ratio of the dissociation and association constants. For the barbed end, the C_c=~0.1µM, while for the pointed end it's ~0.7µM. This difference is due to the nucleotide bound state of actin molecules within the filament. Hydrolysis of ATP in the actin molecule results in formation of ADP-actin, which has a lower dissociation rate than ATP-actin. When the concentration of the monomeric actin is lowered, ADP-actin at the pointed end dissociates more easily, but the polymerization at the barbed end still occurs (Pollard, 2016; Pollard and Borisy, 2003).

Depolymerization of actin is facilitated by cofilin, which changes the conformation of the actin filament, inducing a helical twist of the filament by inserting itself between the subdomain 2 D-loop (DNAseI-binding loop) and the C-terminus of the adjacent actin molecules (Huehn et al., 2020; McGough et al., 1997; Tanaka et al., 2018). It has been shown, that cofilin efficiently severs actin filaments in a state, where the γ-phosphate is removed from the active site (Oosterheert et al., 2022).

ATP hydrolysis and P_i release favours disassembly (Pollard, 2007). G-actin exhibits a low rate of ATP hydrolysis (Mockrin and Korn, 1980) and the rate limiting step of actin polymerization is formation of dimers and trimers (Pollard and Cooper, 2009).

Incorporation of actin into the filament triggers flattening of the molecule (Oda et al., 2009) to facilitate ATP hydrolysis (Figure 10A). ATP-bound G-actin has a large cavity between SD1 and 3, which accommodates water molecules near the ATP γ-phosphate. An important residue for actin ATPase activity is Q137 localized on subdomain 1 (Iwasa et al., 2008), which in ATP-bound G-actin cannot contact the ATP γ-phosphate. Flattening of the molecule is facilitated by movement of the H-loop (residues 72-77) and the proline-rich loop (residues 108-112), making the SD1/3 cavity narrower. This leads to rearrangement of the water molecules, allowing for the Q137 to make a side-

chain hydrogen bond with a nucleophile water (W_{nuc}) closer to the γ-phosphate of ATP. This movement prompts rearrangement of residues H161 and D154, which in turn form hydrogen bond with another water (W_{bridge}), leading to W_{nuc} accepting a proton from the nucleotide and ATP hydrolysis (Oosterheert et al., 2022) (Figure 10B).

Flattening of the molecule and Q137-facilitated ATP hydrolysis also changes the conformation of the SD2 D-loop (DNase-I-binding loop). Upon ATP hydrolysis, D-loop extends outward and contacts the extended (open) C-terminus of the adjacent actin molecule. This open conformation is tightly regulated by localization of the Q137, acting as a sensor of the nucleotide state of the actin molecule (Oosterheert et al., 2022).

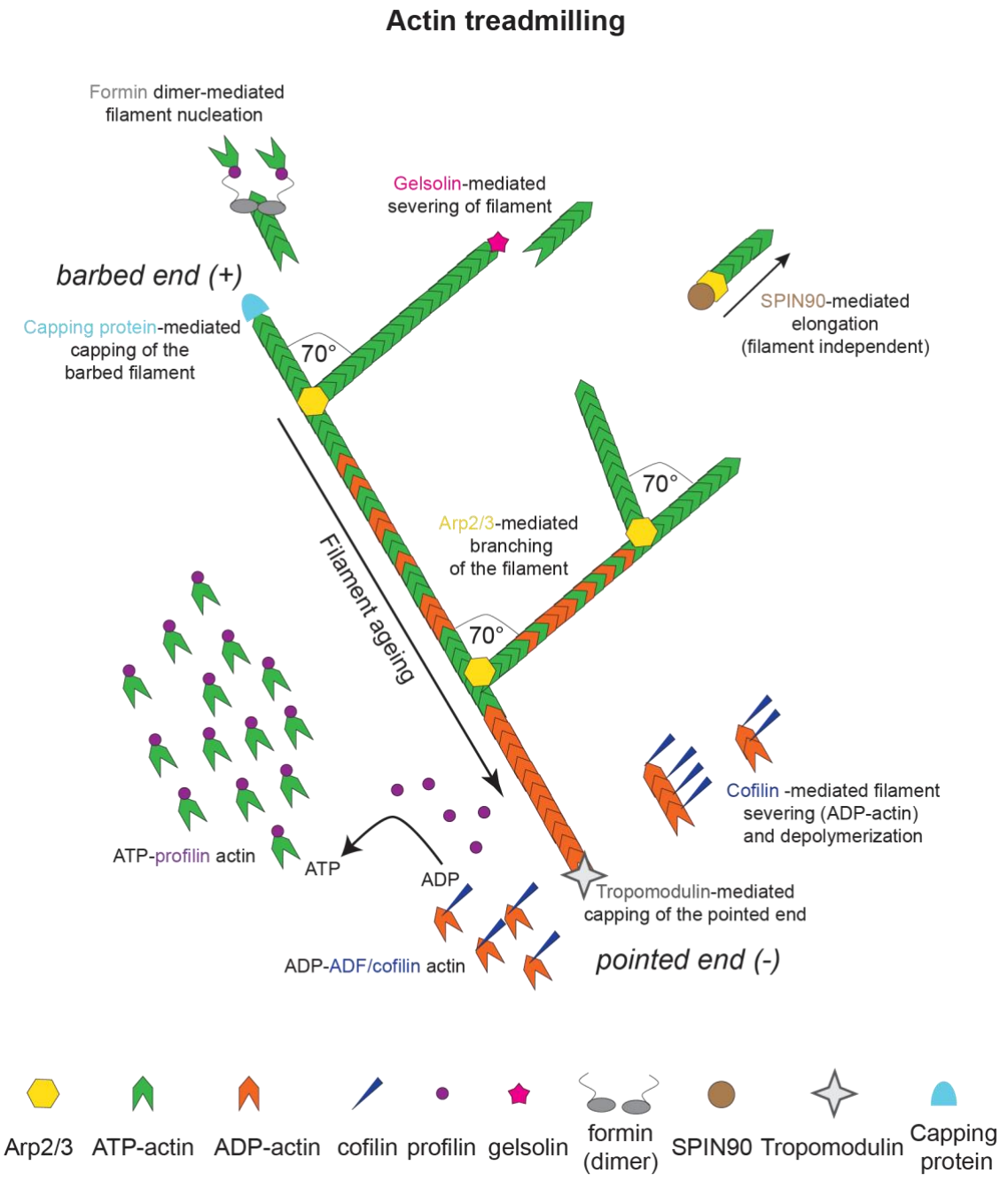

Figure 9. Actin treadmilling
Schematic representation of actin binding proteins regulating polymerization and depolymerization of actin filaments. Filament branching is mediated through Arp2/3; formins nucleate actin dimers; Spin90 elongates filaments by binding Arp2/3 in a filament-independent manner; cofilin severs actin filaments at the pointed end and gelsolin severs and caps the barbed end of the filament; capping protein and tropomodulin cap filament barbed and pointed end, respectively; profilin promotes actin exchange from ADP to ATP and sustains a monomeric pool of actin.

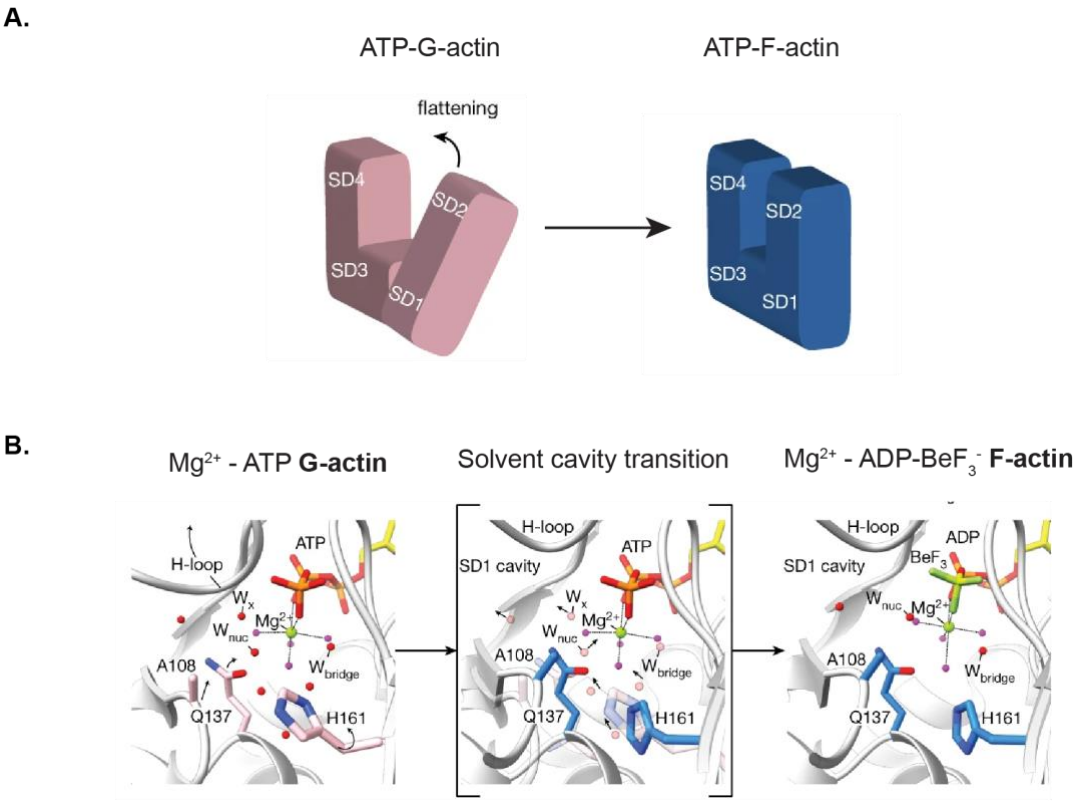

Figure 10. G-actin to F-actin transition
A. Actin flattening of the SD2 and SD1 upon transition into F-actin form. Adapted from (Oosterheert et al., 2022); http://creativecommons.org/licenses/by/4.0/. **B.** Water relocation in the SD1 cavity (between SD1 and SD3) observed in the actin filament leading to ATP hydrolysis. Movement of the H-loop facilitates position change of Q137 and H161 closer to the nucleotide, making hydrogen bond with the nucleophile water (W_{nuc}). Q137 relocates the W_{nuc} closer to another water molecule (W_{bridge}), which together with H161 and D154 (not shown on the schematic) form a hydrogen-bond network, facilitating W_{nuc} accepting of the proton and ATP hydrolysis. ADP-BeF_3 is an ATP analogue. Figure taken from (Oosterheert et al., 2022); http://creativecommons.org/licenses/by/4.0/.

1.4.4 Actin regulation by actin binding proteins

The concentration of actin available in the cell is much higher than that of the C_c required for polymerization and around half of that actin is unpolymerized in cells. This unpolymerized pool is sustained by binding of a variety of Actin Binding Proteins (ABPs), which regulate the amount of polymerized and unpolymerized actin in the cell (Pollard and Borisy, 2003). In turn, ABPs are controlled by extracellular chemical and mechanical signals (Figure 9).

Most of the monomeric actin in the cell is bound by one of two proteins: profilin and thymosin β4 (Pollard and Borisy, 2003).

Profilin is a small, 19kDa protein found throughout eukaryotes (Ampe et al., 1988) and is present in cells at high concentrations (20-100μM), with high affinity for actin binding (K=0.1-0.5μM) (Remedios et al., 2003). Profilin binds to the base of actin monomer between SD 1 and 3, preventing association of actin on the pointed end (Figure 11A). At the same time, profilin catalyses the exchange of ADP to ATP on actin monomers, sustaining a pool of ATP-actin in the cell for association on the barbed end. Profilin-bound actin has been shown to be exported from the nucleus by Exportin 6 (Stüven et al., 2003).

β4 thymosin is a small, 5 kDa protein which has a high affinity for ATP-actin binding (K_d=1.7μM) and prevents polymerization. The N-terminal part of the β thymosin, which has a very strong structural relationship with the WH2 domain, the most abundant actin-binding fold (Paunola et al., 2002), binds as a helix in the target-binding cleft, while the C-terminal portion of the protein binds between SD 2 and 4, consequently preventing actin-bound molecule from interacting with other actin units (Hertzog et al., 2003; Remedios et al., 2003) (Figure 11B). β4 thymosin competes for ATP-actin binding with profilin, and the higher affinity binding of profilin allows for maintaining a pool of ATP-actin competent for association to the actin filament (Pantaloni and Carlier, 1993).

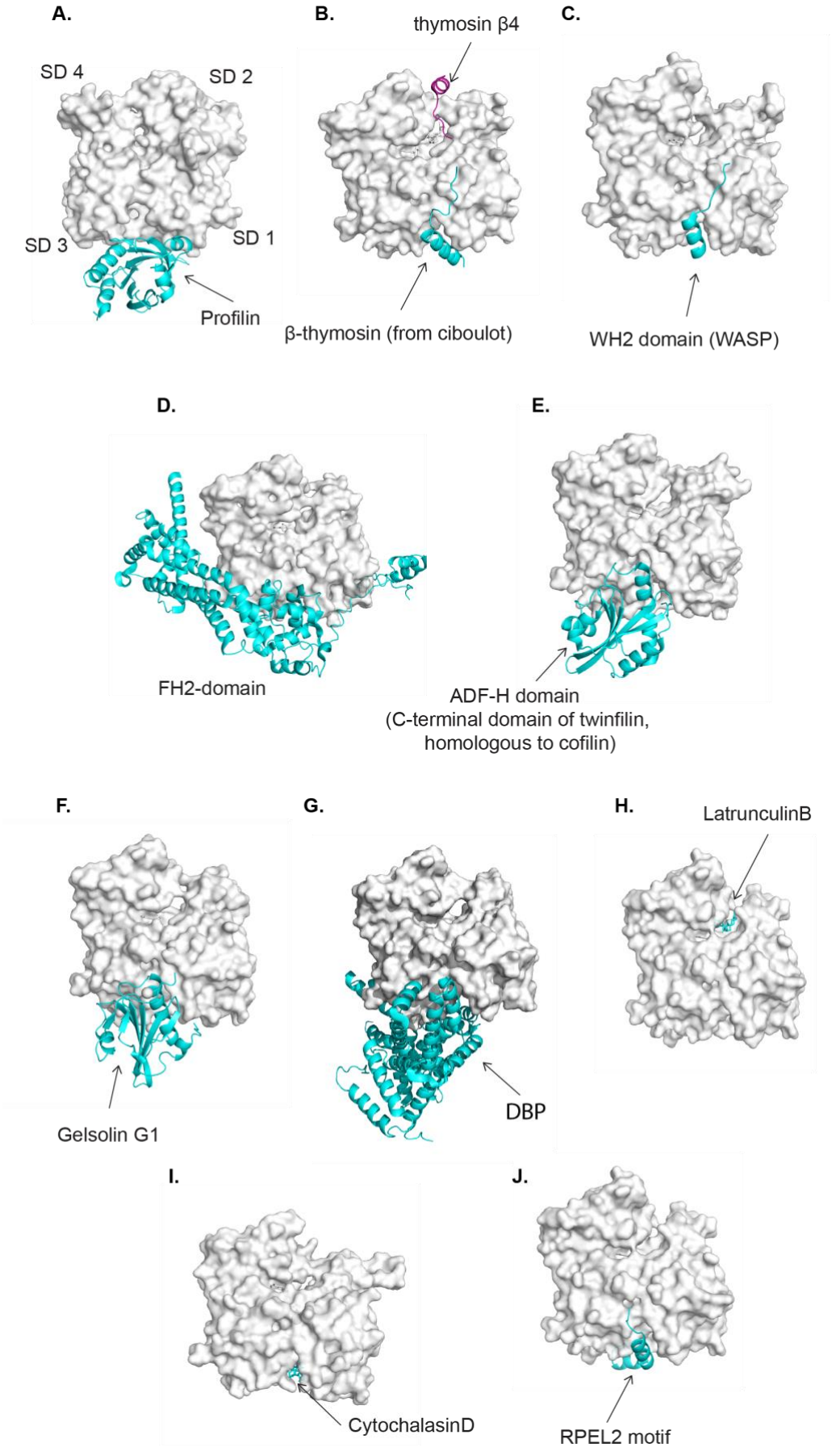
A.
SD 4
SD 2
SD 3
SD 1
Profilin
B.
thymosin β4
β-thymosin (from ciboulot)
C.
WH2 domain (WASP)
D.
FH2-domain
E.
ADF-H domain
(C-terminal domain of twinfilin,
homologous to cofilin)
F.
Gelsolin G1
G.
DBP
H.
LatrunculinB
I.
CytochalasinD
J.
RPEL2 motif

Figure 11. Actin binding proteins shown on the surface of actin monomer
Representation of actin binding proteins on actin surface, shown in classical actin orientation with subdomains 4 and 2 on top and subdomains 3 and 1 on the bottom of the molecule. The nucleotide binding cleft of actin is localized between SD4 and SD2, and the target binding cleft is localized between SD3 and SD1. Actin surface shown in white, with the proteins or drugs binding shown in cyan or magenta. **A.** Profilin (PDB: 2BTF) **B.** β-thymosin-actin binding based on two structures: N-terminal domain (WH2) from *Drosophila* ciboulot (PDB: 1SQK) and the C-terminal domain from thymosin β4 peptide (PDB: 1T44) **C.** WH2 domain of WASP (PDB: 2A3Z) **D.** FH2-domain (PDB: 1Y64) **E.** ADF-H domain of twinfilin (homologous to cofilin) (PDB: 3DAW) **F.** Gelsolin G1 segment (PDB: 1EQY) **G.** DBP (PDB:1KXP) **H.** Latrunculin B (PDB: 2V52) **I.** Cytochalasin D (PDB: 3EKS). **J.** RPEL2 motif (PDB: 2V52). Figure made based on (Dominguez and Holmes, 2011).

1.4.4.1 Actin nucleating proteins

Actin nucleation, which is the formation of actin dimers and trimers is the rate limiting step of filament formation. Stabilization of this process is exerted by proteins that bind to the actin monomers or dimers and prime the growing of the filament.

Arp2/3 complex

Arp (Actin-related protein) 2/3-complex nucleates new filaments ("daughter" filament) by binding to the pre-existing "mother" filament at a characteristic 70º angle (Mullins et al., 1998) (Figure 9). Arp2/3 is formed of seven subunits (Machesky et al., 1994), with a homology of sequence to actin. Its intrinsically inactive (Robinson et al., 2001) and undergoes a conformational change upon nucleation promoting factors (NPFs) binding.

Activation of the Arp2/3 complex is regulated by binding of two types of NPFs. Class I NPFs, which include WASP, N-WASP, WAVE, WASH and WHAMM (Alekhina et al., 2017), contain a VCA (verprolin, central, acidic) domain, which promotes a conformational change of Arp2 and 3 and nucleates branched filament assembly. VCA domain is released from an autoinhibited state by binding of Rho GTPase Cdc42 (Kim et al., 2000). Class I NPFs also have a WH2 domain for actin docking (Figure 11C). Activation of Arp2 and 3 by binding of the VCA domain allows for binding to the existing mother filament of actin, nucleating the assembly of a new daughter filament, mimicking the barbed end of actin filament and allowing elongation.

An important Class II NPF is cortactin, which by binding to Arp2/3 stabilizes new filament formation. It was shown that on its own cortactin can weakly activate the Arp2/3 complex, but cooperation with Class I NPFs enhances the activation (Uruno et al., 2003), where in the presence of the VCA domain cortactin-mediated branching was significantly increased. Cortactin contacts Arp3 with its acidic N-terminal region, while simultaneously binding to actin filament with its C-terminal actin-binding domain. The model for cortactin binding suggested contacts with the mother filament (Helgeson et al., 2014), but it was recently shown that it stabilizes the filament by binding along the daughter filament instead (Liu et al., 2024).

SPIN90 constitutes another nucleating factor that activates Arp2/3 (Wagner et al., 2013). Binding of Spin90, which does not have a VCA domain, leads to a change in conformation of Arp2/3 different than that of VCA activated complex, and leads to formation of linear actin filaments (Luan et al., 2018) (Figure 9). Spin90-Arp2/3 complex has been shown to generate the initial filament used by the WRC (Wave regulatory complex)-Arp2/3 complex to generate dendritic networks, as well as has the ability to regulate the amount of branching by competing with WRC for Arp2/3 binding (Balzer et al., 2019, 2018). It was also recently shown, that VCA domain destabilizes Arp2/3-Spin90 linear filaments (Cao et al., 2023).

Formins

Formins are another family of nucleating ABPs, that contain a formin homology-2 domain (FH2) (Figure 11D), that has an ability to dimerize. Formins bind to the barbed end of the actin filament and can wrap around two actin molecules due to their extended linker placed between the two monomers (Tomchick et al., 2005) (Figure 9). The mechanism of filament nucleation of formins is thought to be due to stabilization of actin dimers within the filament (Pring et al., 2003). Formins also have a FH1 domain which facilitates profilin binding. Many formins activity is regulated through binding of Rho GTPases to the GTPase binding domain in the N-terminal part of the sequence, which in an inhibited state interacts with the diaphanous autoregulatory domain (DAD) localized in the C-terminus of formin (Alberts, 2001).

1.4.4.2 Actin severing proteins

Actin severing proteins affect dynamics of filament assembly, by removing actin monomers from either the pointed end, or from the barbed end. This mechanism is crucial for balancing the amount of monomeric vs polymerized actin in the cell.

Cofilin

Cofilin is a small, 15kDa that can bind both to the actin monomer and to the filament. Cofilin binds ADP-actin with high affinity through its ADF-H domain (Paavilainen et al., 2008) (Figure 11E) and induces a change in the twist of the filament, by inducing a rotation of SD 1 and 2. This antagonizes flattening, changing conformation of actin monomer to a G-actin favoured form and induces a strain on the filament, promoting dissociation of actin from the pointed end (McCullough et al., 2011) (Figure 9). Cofilin can also promote γ-phosphate dissociation from the ADP-Pi-actin molecules (Blanchoin and Pollard, 1999). Cofilin was shown to be important in Importin 9 mediated import into the nucleus, sustaining a pool of nuclear actin (Dopie et al., 2012)

Gelsolin

Gelsolin is a large, multidomain protein comprising six homologous domains (G1-G6), that severs actin filaments from the barbed end (Figure 9). Its activity is regulated by the concentration of $Ca2^{+}$ ions and by phosphorylation. In inactive state, gelsolin domains are interacting within the protein, masking the actin-binding site. Binding of $Ca2^{+}$ partially reveals the actin binding sites on G1 and G4, allowing for binding to the side of the filament between SD 1/3 (Figure 11F). This leads to full exposure of the actin-binding sites, binding of two actin molecules on the two strands of the filament and severing of the actin through a “pincer”-like movement (Burtnick et al., 1997).

A variant of gelsolin, referred to as secretory gelsolin, plays a role in actin depolymerization in the blood. $Ca2^{+}$ concentration is high in the bloodstream, allowing for gelsolin to be in a constitutively active state, where together with vitamin D-binding protein (DBP) it acts as actin-scavenging system. First,

gelsolin depolymerizes the filamentous actin that has been released from damaged cells, after which DBP binds the actin monomers and rapidly clears them from the circulation through the liver (Epstein et al., 1992; Nag et al., 2013).

Vitamin D-binding protein (DBP) binds actin monomers with a high affinity (K_d=1nM) and forms a 1:1 complex (Otterbein et al., 2002) (Figure 11G). DBP crystal structure revealed three α-helical domains with a high degree of flexibility between them. It binds between SD1 and 3 of actin and covers the surface of SD3 with all three subdomains, without inducing conformational changes in actin.

1.4.4.3 Actin capping proteins

Actin capping proteins bind to either the barbed or the pointed end of the filament, preventing dissociation and association of actin monomers and regulating assembly.

Capping protein

Capping protein (CP) works in cooperation with profilin to maintain the monomeric pool of actin in the cell. It binds to the barbed end of the filament as a heterodimer made of two subunits: α and β (Figure 9). Due to its high micromolar concentration in the cell, it attaches to the filament in a matter of seconds, preventing addition of new monomers to the barbed end. Capping protein is important in regulating the number of filaments growing e.g. in leading edge protrusion formation (Edwards et al., 2014; Pollard, 2016).

Capping protein cooperates with gelsolin, which not only severs the barbed end of the filament but also caps it, in nucleation of filaments from the pointed end in skeletal muscle (Littlefield et al., 2001)

Tropomodulin

Tropomodulin caps the pointed end of the actin filament (Figure 9) by wrapping around three actin subunits, preventing monomer addition and loss. Interaction between the N-terminal ends of two tropomodulins increases their capping activity (Rao et al., 2014).

1.4.4.4 Actin binding toxins

Actin conformation can be modulated by binding of toxins, that by direct interaction with actin restrict mobility of its domains and interfere with the normal treadmilling cycle. These toxins are frequently used when studying actin properties.

Latrunculins

Latrunculins are a group of toxins isolated from the sponge *Latrunculia magnifica* (Spector et al., 1983) that bind actin in a reversible manner. Latrunculin A and B bind to the nucleotide binding cleft of actin between SD 2 and 4, preventing nucleotide exchange and flattening of the molecule, keeping actin in a monomeric conformation (Morton et al., 2000) (Figure 11H). LatB binding leads to depolymerization of the cytoskeleton but is compatible with RPEL motif binding (RPEL-actin binding will be described in section 1.4.5.2). It is commonly used as an inhibitor of the MRTF-SRF pathway, by increasing the cellular concentration of G-actin.

Cytochalasin D

Cytochalasins belong to a group of membrane permeable fungal metabolites (Cooper, 1987). They bind to the barbed end of the actin filament between SD 1/3 (Figure 11I), inhibiting association and dissociation of actin monomers to the filament. They also promote the hydrolysis of ATP by stabilizing formation of dimers, leading to an increase in the ADP-actin concentration, although the mechanism of that is unclear. CD-actin binding prevents simultaneous RPEL binding, and it is used as a direct activator of the MRTF-SRF pathway.

1.4.5 Rho GTPases and control of the cytoskeleton

RhoGTPases respond to physical environment and extra and intracellular signals from the cell receptors, coupling the signals to downstream effector proteins.

The Rho family of GTPases belongs to the RAS superfamily of proteins with a weak GTPase activity. In their inhibited state, they are bound to GDI (Guanine nucleotide dissociation inhibitors), and in their inactive state with GDP. Association with GAPs (GTPase-activating protein) and GEFs (Guanine nucleotide exchange factors) regulates their GTPase activity and determines their nucleotide-bound state. GEFs promote exchange from GDP to GTP, and GAPs regulate GTP hydrolysis (Bos et al., 2007) (Figure 12).

Activation of the members of Rho family induces a conformational change and allows for binding of effector proteins and activation of downstream pathways. As members of the Ras family, derivatives of Rho family GTPases can be made, in which specific mutations lock the protein in either the GTP-bound or GDP-bound conformation. For example, RhoA (14V) is equivalent to Ras (V12), and RhoA (N19) equivalent to Ras (N17) (Tang et al., 1999). Mutants of this type have been instrumental in studying the downstream targets of RhoGTPases and their downstream cellular pathways.

Three of the 20 members of the Rho family have been best described: RhoA, Rac and Cdc42 (Heasman and Ridley, 2008) (Figure 13).

RhoA shares a high degree of homology with RhoB and RhoC and is the member of the family that is best described in literature. RhoA activation promotes actin polymerization by activation of its effector proteins (Narumiya et al., 2009). Overexpression of RhoA in cells leads to stress fibre formation (Wheeler and Ridley, 2004). Binding of RhoA to the ROCK kinase (Rho associated coiled coil forming kinase), leads to phosphorylation of the kinase LIMK1 (serin/threonine kinase), which in turn phosphorylates and inactivates cofilin, preventing severing of the actin filaments. ROCK kinase also leads to phosphorylation of the myosin-light chain (MLC), promoting actomyosin contraction and stress fibre formation (Fukata et al., 2001). Another effector protein of RhoA is diaphanous related formin 1 (DIA) protein, activation of which promotes nucleation and assembly of actin filaments through its FH2 domain (Campellone and Welch, 2010).

Out of three Rac isoforms (Rac1, Rac2 and Rac3), Rac1 is the ubiquitously expressed and best described in literature (Moll et al., 1991). Rac1

affects the activity of many effector proteins involved in actin filament nucleation, e.g. WAVE, which in turn activates Arp2/3-mediated branching of actin filaments and formation of lamellipodia cell protrusions (reviewed in (Jaffe and Hall, 2005).

Cdc42 activation of downstream effectors leads to formation of another type of cell protrusion - filopodia, which are formed of parallel actin bundles, extending over cell edge and important for cell-cell signalling and sensing chemoattractants (Gupton and Gertler, 2007). Cdc42 activates N-WASP, which in turn activates Arp2/3 and leads to actin polymerization and filopodia formation (Carlier et al., 1999; Ma et al., 1998). Both Rac and Cdc42 also activate PAK (p21-activated protein kinase), leading to activation of LIMK kinase and phosphorylation of cofilin, regulating actin turnover (Sells et al., 2000; Wittmann and Waterman-Storer, 2001).

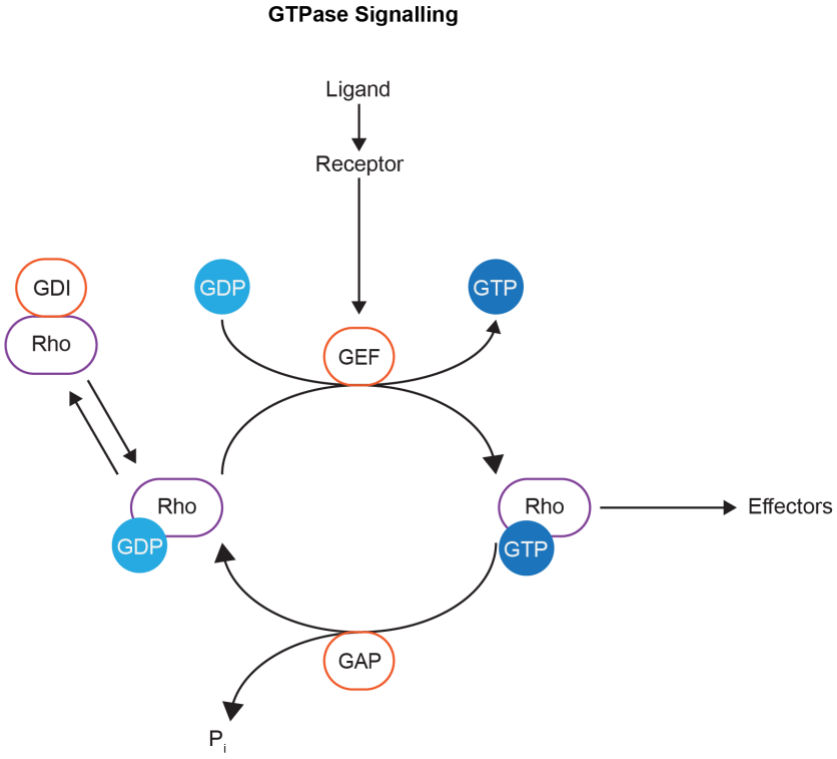

Figure 12. Small GTPase activity regulation
GDI keeps Rho is in an inhibited state, from which it is released by activating signals to the membrane receptors. This leads to activation of small GTPases facilitated by GDP to GTP exchange by GEFs and downstream effector signalling. Hydrolysis of GTP to GDP inactive state is facilitated by GAPs. Figure made based on (Dandamudi et al., 2023).

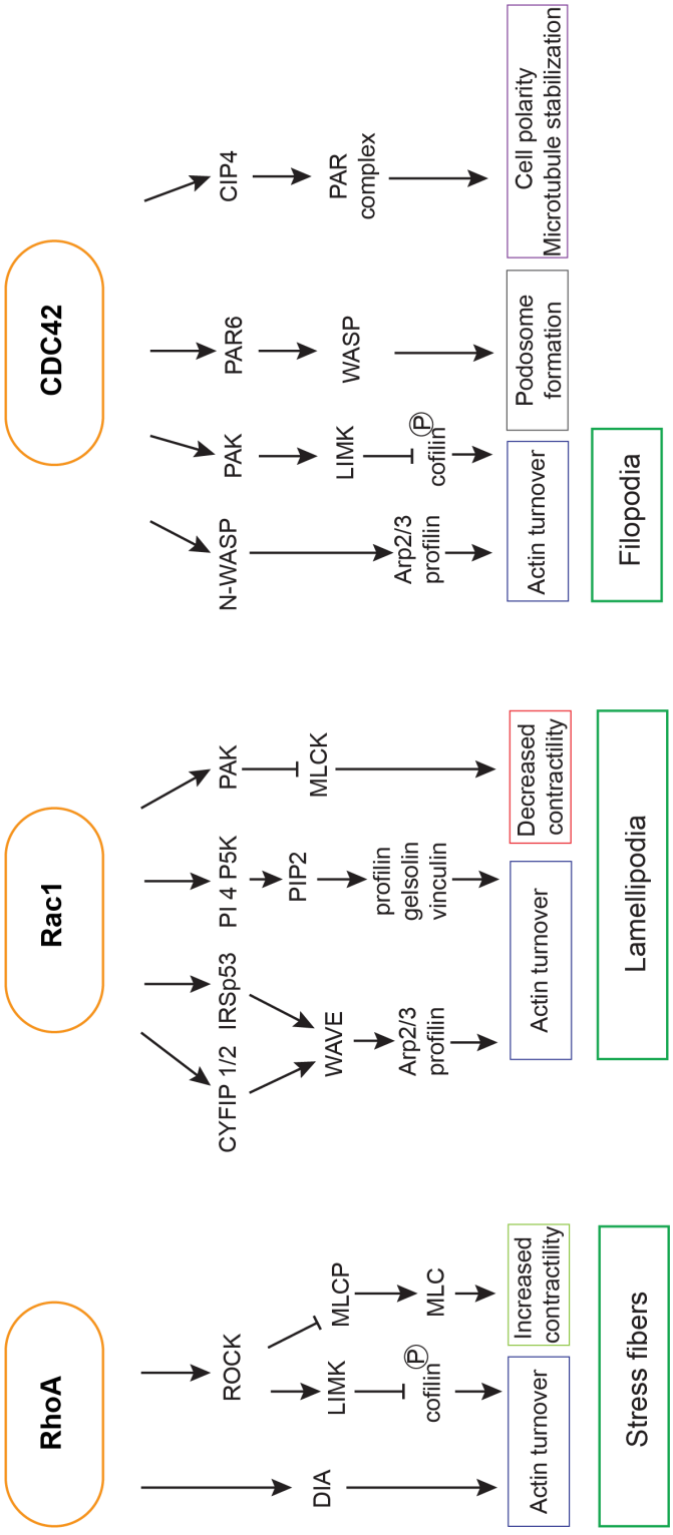

Figure 13. Rho GTPase effector pathways
Three families of RhoGTPases activate downstream effectors, leading to rearrangement of the actin cytoskeleton. RhoA activation leads to stress fibre formation, Rac1 activation leads to formation of lamellipodia, and Cdc42 induces filopodia formation, as well as other actin-based phenotypes. Figure made based on (Mosaddeghzadeh and Ahmadian, 2021).

1.4.5.1 The family of RPEL motif proteins

RPEL proteins constitute a unique family of actin binding proteins. They act as G-actin sensors and compete with other ABPs for G-actin, monitoring the effective concentration of G-actin in the cell and responding to fluctuations in actin dynamics. Actin depolymerizing drugs (LatB and CD) can be used to modulate the pathway, by changing the levels of available monomeric actin for RPEL binding (Figure 14).

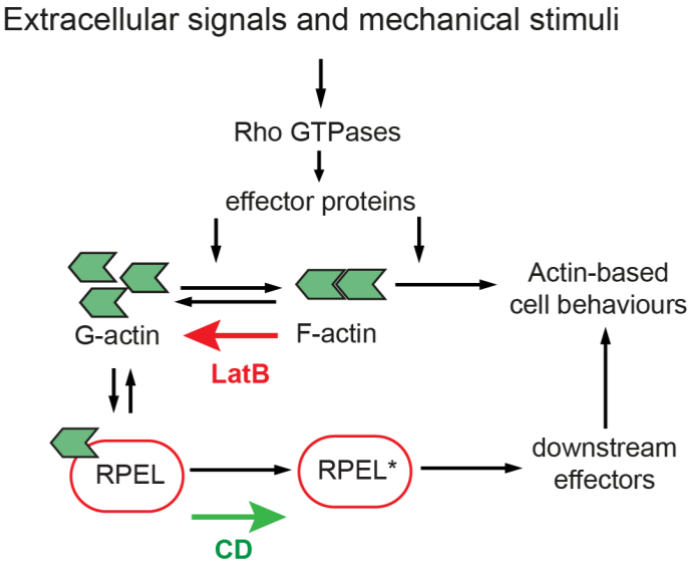

Figure 14. RPEL-motif G-actin sensing
RPEL motifs act as G-actin sensors in the cell and can detect changes in actin concentration, which is influenced by RhoGTPases activation of effector proteins that regulate actin treadmilling. LatB treatment increases G-actin levels, leading to actin binding to the RPEL. CD treatment prevents actin binding to the RPEL, allowing for signalling to downstream effectors.

Three families of G-actin sensing RPEL-motif proteins have been described: Myocardin Related Transcription Factors (MRTFs), the Phosphatase and actin regulators (Phactrs) and the Rho GTPase activating proteins (ArhGAPs) (Figure 15).

MRTF contains three RPEL motifs and can detect the concentration of monomeric actin in the cell by direct binding of actin to the RPEL motifs (Guettler et al., 2008). MRTF regulatory RPEL domain can bind up to five actin molecules (see section 1.5.6). Binding of actin regulates MRTF shuttling between the cytoplasm and nucleus (Vartiainen et al., 2007). Activity of MRTFs

is regulated by RhoA activation, which will be described in detail in section 1.5.3.

ArhGAP family contains a single RPEL motif. ArhGAPs belong to Rac1/Cdc42-specific Rho GAPs. GAP domain binding by actin regulates the GAP activity of ArhGAP12 by occluding its GTPase binding site and direct inhibition of Rac1 and Cdc42 binding (Diring et al., 2019a).

Members of the Phactr family contain four RPEL motifs in their sequence, three in the C-terminal part of the sequence and one in the N terminus. Phactrs acts as a cofactor for PP1 phosphatase. The binding site on for PP1 and actin overlap, competing for Phactr binding, and actin binding inhibits association with PP1 (Fedoryshchak et al., 2020; Mouilleron et al., 2012).

All three families act as G-actin sensors in the cells, where the changes in the monomeric actin concentration regulate their activity.

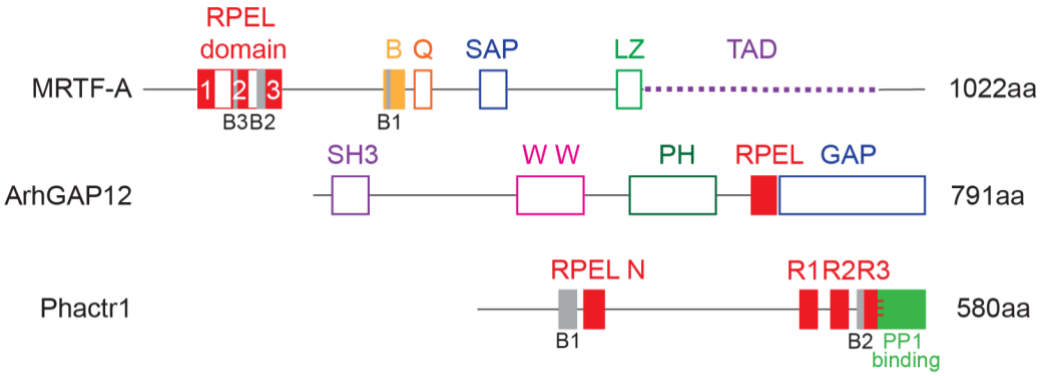

Figure 15. RPEL-family of proteins
Schematic representation of domains of representative members of the RPEL family of proteins. RPELs shown in red, with the basic regions shown in grey. **Top:** MRTF-A *Mus musculus* (AF532597). RPEL1 (72-93), RPEL2 (116-137), RPEL3 (160-181), B3 (119-121), B2 (152-160), B1 basic region (315-341), Q box (356-377), SAP domain (442-476), LZ (620-651), TAD (654-901). **Middle:** ArhGAP12 (UniProt S4R248). SH3 (25-72), 2xWW (266-353), PH (410-523), RPEL (568-599), GAP (600-791). **Bottom:** Phactr1 (UniProt: Q2M3X8). B1 basic (108-129), RPEL N (138-163), RPEL1 (422-443), RPEL2 (460-481), RPEL3 (496-519), B2 basic (493-499), PP1 binding (517-580).

1.4.5.2 RPEL motif-actin binding

The structure of RPEL binding has been resolved for all three members of the family. Upon actin binding, RPEL motif becomes structured and folds into two helices: Helix α-1, which binds to the hydrophobic cleft of actin and Helix α-2 binding to the hydrophobic ledge of actin.

The main contacts with actin will be describe based on crystal structure of RPEL2^{MRTF} (Mouilleron et al., 2008) (Figure 16A). RPEL2^{MRTF} Helix α-1 binds to actin through hydrophobic contacts with the actin cleft through residues L118, I122 and K121. The conserved arginine of the **R**PxxxEL motif, R125 is localized within the flexible linker between the helices, termed the R-loop, and forms a critical hydrogen bond with the C-terminal F375^{actin} carboxylate of actin. Mutation of this motif to alanine (loss-of-contact mutation) has been shown to be sufficient to disrupt actin binding to the RPEL motif (Guettler et al., 2008; Mouilleron et al., 2008). R125 also contacts the Y169^{actin} and E167^{actin} of the actin hydrophobic ledge. Residues within the Helix α-2 make contact through L131, I136 and L137 with actin residues along the hydrophobic ledge. R128 is important for interaction with the Y169^{actin}.

The RPEL^{ArhGAP12} binds to the hydrophobic cleft and ledge in a similar manner to RPEL2^{MRTF} and with similar affinity to that seen for RPEL1^{MRTF} and RPEL2^{MRTF}(Mouilleron et al., 2008). Additional interactions between ArhGAP12 C-terminal GAP domain and actin can be detected within its hydrophobic niche between SD 1 and 3 (Figure 16B). Interestingly, the C-terminal GAP-domain was shown to increase the affinity of actin binding to RPEL^{ArhGAP12}, from ~2µM to ~40nM. This showed the stabilizing effect of C-terminal sequences of an RPEL-motif containing protein on actin binding to the RPEL.

A. **MRTF-A RPEL2 motif - actin (PDB:2V52)**

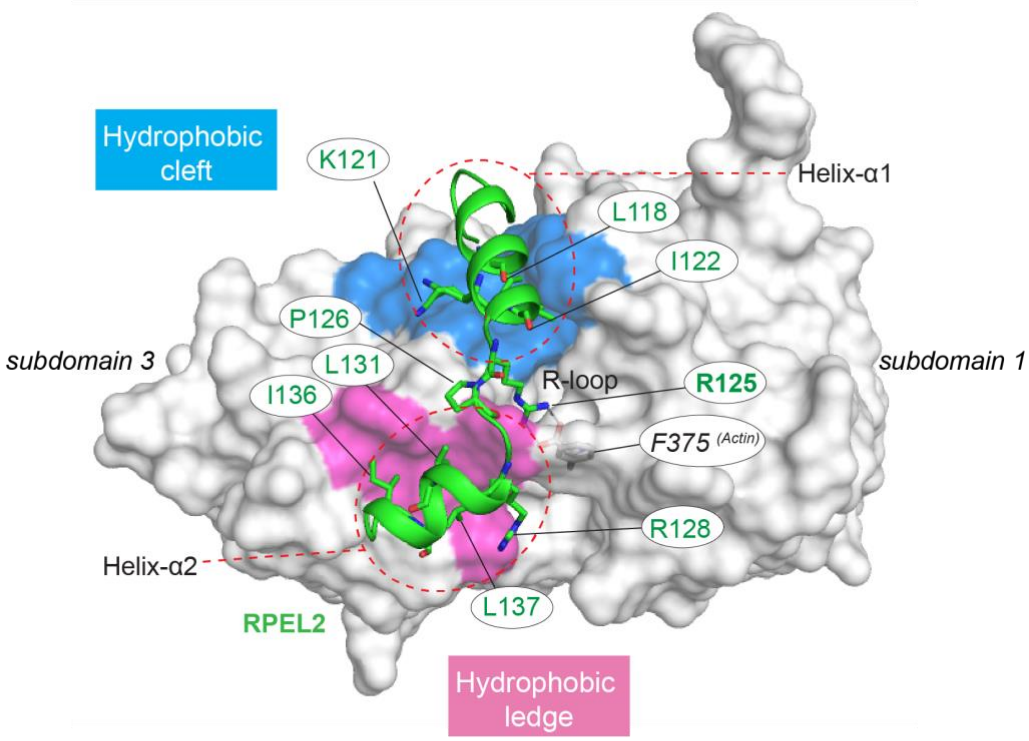

B. **ArhGAP12 - actin (PDB:6GVC)**

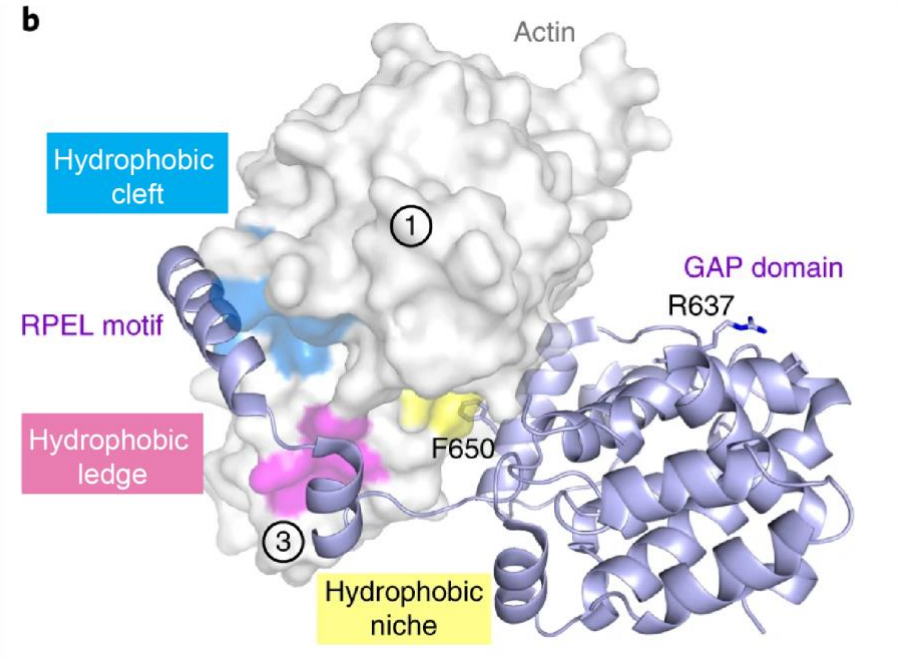

Figure 16. RPEL motif-actin binding
A. Crystal structure of RPEL2 motif on the surface of rabbit skeletal α-actin (PDB: 2V52). RPEL2 shown as a cartoon on actin surface with SD 3 and 1 facing forward. Two hydrophobic surfaces of actin shown: hydrophobic cleft in blue and hydrophobic ledge in magenta. Actin RPEL motif shown in green. Important residues annotated on the surface. Red dotted line indicates Helix α-1 and Helix α-2 of RPEL. Figure made based on (Mouilleron et al., 2008). **B.** ArhGAP12-Actin crystal structure (PDB:6GVC). RPEL motif binds to the hydrophobic cleft and ledge between SD3 and 1. The GAP domain of ArhGAP12 contacts the hydrophobic niche of actin. Figure taken from (Diring et al., 2019a) with permission from Springer Nature (Licence number: 5870780691974).

1.5 Myocardin Related Transcription Factor family

MRTFs are transcriptional coactivators of the Serum Response Factor. They respond to changes in the concentration of monomeric actin in the cell and activate SRF target genes. MRTF-SRF pathway control most of cytoskeletal, muscle specific, structural and regulatory genes.

The founding member of the family, Myocardin, is muscle specific and constitutively active, with low affinity for actin binding. MRTFs are ubiquitously expressed and regulated by actin on two levels. Firstly, actin controls the nuclear import and export of MRTF. Secondly, it controls the activity of MRTF in the nucleus, by inhibiting interaction of MRTF with SRF. The mechanism of this inhibition is unknown, and understanding how actin regulates MRTF-SRF binding will be the subject of this thesis. MRTFs activity is coupled to actin dynamics, with actin being one of the target genes of MRTF-SRF, creating a simple feedback loop (Figure 17).

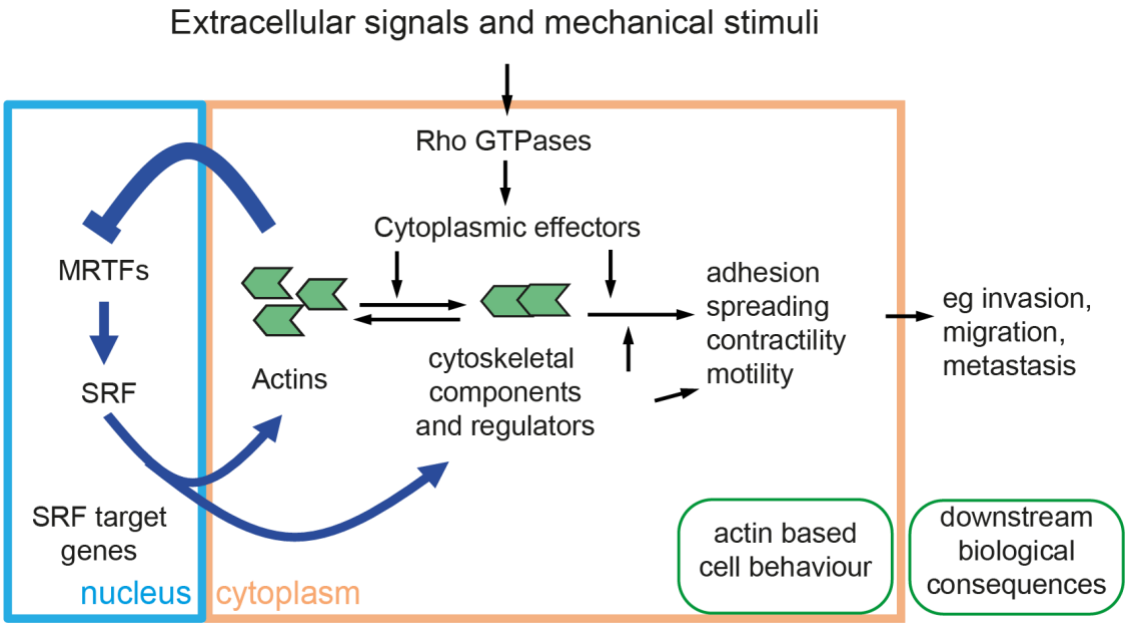

Figure 17. Regulation of the actin treadmilling cycle in the cell
Schematic representation of the effects of the RhoGTPases activation. Signals being received by receptors on the cell membrane activate RhoGTPases and its downstream effectors, leading to increase in actin treadmilling. Rapid actin polymerization decreases the pool of monomeric actin in the cell, leading to MRTF nuclear accumulation and SRF binding. MRTF-SRF activate transcription of cytoskeletal components, which result in actin-based cell behaviour and regulators which in turn control the cycling of actin between monomeric and polymerized forms. Actin is one of the genes expressed downstream of MRTF-SRF, leading to a negative loop formation, where a high concentration of expressed actin will in turn inhibit MRTF activity.

1.5.1 Myocardin family of proteins

The Myocardin family of proteins consists of three members: Myocardin (Wang et al., 2001), MRTF-A/MKL1 (Ma et al., 2001a) and MRTF-B/MKL2/MAL16 (Mercher et al., 2001). There is a high degree of sequence homology between the proteins.

Myocardin was the first member of the family to be discovered in a bioinformatics screen for cardiac specific targets and was shown to be expressed in developing smooth muscle and cardiac tissue. Myocardin was shown to form stable complexes with SRF *in vitro*, establishing it as a bone fide SRF coactivator protein. Myocardin is required for the differentiation of myocardial cells and heart development, as shown in experiments done in *Xenopus* embryos (Wang et al., 2002, 2001), with mice with Myocardin knockout dying by embryonic day (E)10.5 (Wang et al., 2003).

MRTF-A/MKL1 was first identified as a fusion with the RBM15 (Ma et al., 2001b) in the t(1;22), which is a chromosomal translocation occurring in Acute Megakaryoblastic Leukaemia (type M7) patients. Only after Myocardin discovery, the homology between the proteins was analysed and the MKL1 protein was assigned as a member of the Myocardin family of proteins (Wang et al., 2002).

MRTF-B/MKL2/MAL16 was first identified through an enhancer trap scan in mouse embryonic stem cells (Skarnes et al., 1992). MRTF-B is crucial for development, with MRTF-B knockout mice dying between embryonic days (E)13.5-14.5 with severe defects in the branchial arteries formation (Li et al., 2005; Oh et al., 2005b).

1.5.2 Functional elements in the MRTFs

The three members of the Myocardin family share similarities in their sequence with conservation between functional elements. They all have an N-terminal regulatory domain containing three RPEL motifs, a basic domain (B-box), glutamine rich region (Q), SAP domain and the transactivation domain in the C-terminus (TAD) (Wang et al., 2002) (Figure 18). Overall, they share 35% identity in their amino acid sequence, but over 60% in the domains described above, with MRTF-A and MRTF-B being of higher homology to one another than to Myocardin (Figure 19).

MRTF-A open reading frame predicts a protein of 929aa in Mouse Embryonic Fibroblast cell line NIH3T3, starting translation at the 92 amino acid at the first Met, which is localized within RPEL2. This MRTF has been termed MAL(met) and has been used in studies as a full-length version of the protein (Wang et al., 2002) (Figure 18).

However, when looking at the cDNA sequence of MRTF including the 5'UTR, upstream of the first Met the reading frame is open for 92 codons, encoding a further RPEL motif (RPEL1). Insertion of the cDNA sequence into expression vectors resulted in translation of 1022aa protein containing all three RPEL motifs and the sequences N-terminal, with a translation start probably

corresponding to the first Leu in the ORF (AF532597, (Miralles et al., 2003; Wang et al., 2002).

Other MRTF-A cDNAs encode N-terminal splice variants, for example MRTF-A (BSAC) with translation start at position -35 relative to the first Met in the RPEL1 (Sasazuki et al., 2002). The functional significance of these variants remains to be determined. At least some of these variants appear to be conserved in MRTF-B, suggesting they have functional significance. For example, an N-terminal NES is predicted in MRTF-A (FL) (Panayiotou et al., 2016), but not in BSAC. However, the biological role of these different isoforms remains to be elucidated.

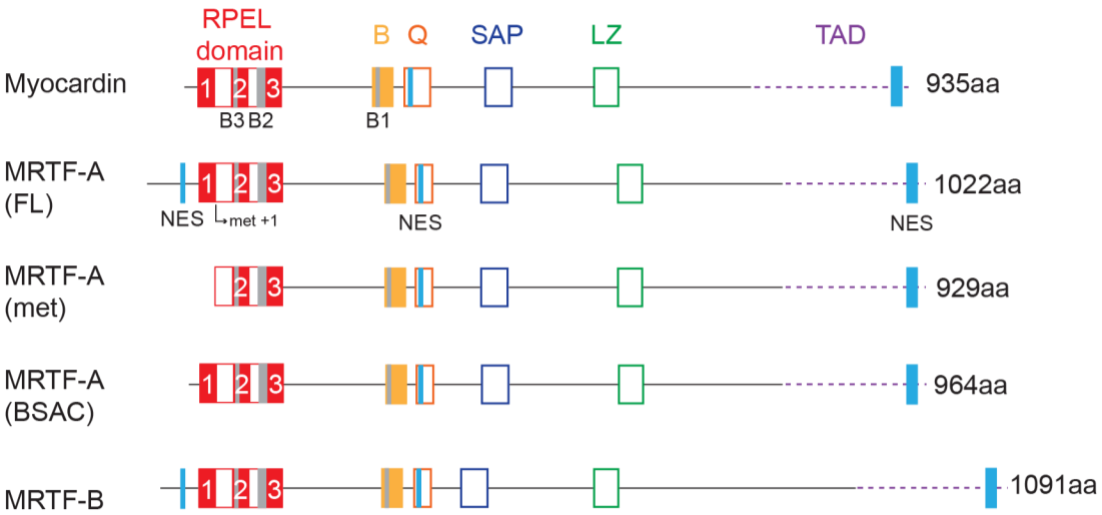

Figure 18. Schematic representation of Myocardin family members
Myocardin and MRTF-B full length proteins shown. Three variants of MRTF-A: MRTF-A (FL) (translation start at the first residue of the ORF, -92 position from the first Met); MRTF-A (met) – translation start at the first Met; MRTF-A (BSAC) – splice variant with translation start at position -35 relative the first Met. RPELs shown in red, B-box - yellow, Q – orange, SAP – dark blue, LZ – green, TAD domain – purple dotted line (the region has not been mapped to the exact residues conferring transcriptional activity). B1, B2, and B3 NLS indicated in grey, NES shown in light blue. The first NES is missing in MRTF-A (met) and MRTF-A (BSAC).

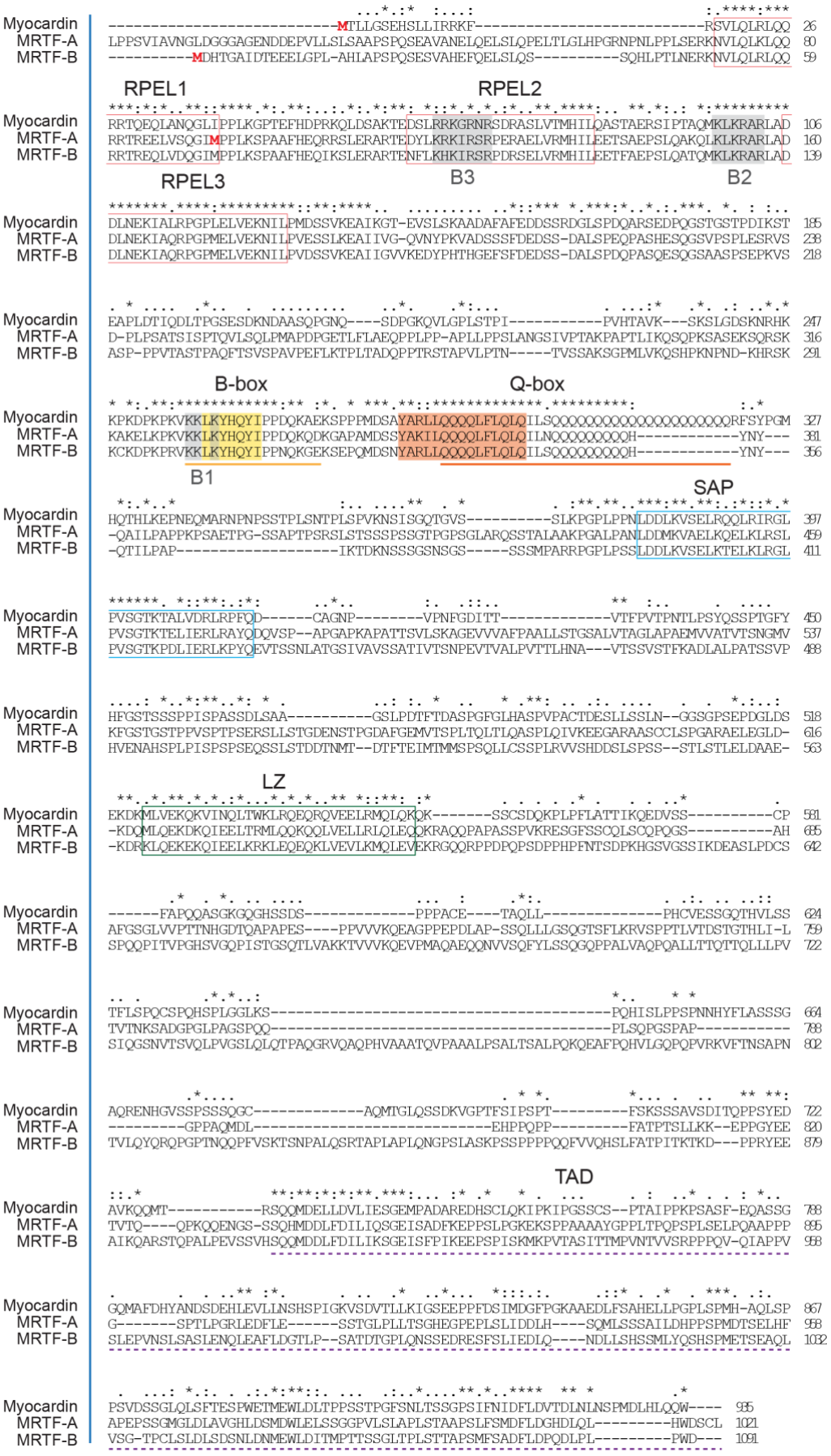
RPEL1
RPEL2
RPEL3
B3
B2
B-box
Q-box
B1
SAP
LZ
TAD
Myocardin
MRTF-A
MRTF-B

Figure 19. Sequence alignment of Myocardin family members shows high degree of homology
Alignment of MRTF family members (Mus musculus), with domains annotated on the sequence. Myocardin (UniProt: Q8VIM5), MRTF-B (UniProt: P59759), MRTF-A (AF532597). RPELs – red, B2 and B3 – dark grey, B1 basic – yellow, Q classical region – light grey (region homologous between vertebrates and invertebrates annotated by an orange line), SAP – blue, LZ – green, TAD has not been exactly mapped, in myocardin the region marked with the dotted purple line has been shown to be necessary for transcriptional activity of Myocardin (Wang et al., 2001). Corresponding regions in MRTF-A and MRTF-B have been marked.

RPEL domain

MRTF-A N-terminal domain comprises of three RPEL motifs that form the regulatory RPEL domain (Guettler et al., 2008; Miralles et al., 2003; Mouilleron et al., 2011, 2008; Vartiainen et al., 2007; Zaromytidou et al., 2006). Each of the motifs is 22-amino acid long with an RPxxxEL core, with the exception of RPEL1, which instead of a Proline has an Arginine in the second position (RRxxxEL). The RPEL domain is conserved through evolution and can be found in various groups of Metazoans (Uniprot: xref:prosite-PS51073). The role of the RPELs was unknown, until the discovery of the Rho-actin pathway in regulation of MRTF, which showed actin binding to the RPEL as a regulator of MRTF activity and cellular localization (Miralles et al., 2003).

Initial biochemical analysis demonstrated that MRTF RPEL1 and RPEL2 bind G-actin with micromolar affinity, while RPEL3 appears to bind weakly (Mouilleron et al., 2008). I will show in this thesis, that this arises from RPEL3-actin complex binding MRTF sequences in the Q region, which facilitates high affinity binding.

In contrast, Myocardin RPEL1 and RPEL2 motifs contain sequence changes that effectively abolish actin binding. This effectively uncouples Myocardin from the Rho-Actin pathway, resulting in it being constitutively active (Guettler et al., 2008). Substitutions of R1 and R2 in Myocardin with those of MRTF was sufficient to convey the regulatory phenotype of MRTF, with Myocardin$^{R1R2\text{-}MRTF}$ shuttling between cytoplasm and nucleus upon Rho-actin pathway activation (Guettler et al., 2008), while R3 was interchangeable between the two. Actin interaction with RPEL domain of MRTF will be discussed further in Section 1.5.6.

Basic and glutamine-rich regions (B1 and Q)

MRTFs bind to the SRF transcription factor via a conserved basic element termed the B-box (Miralles et al., 2003; Wang et al., 2002, 2001). Within this region, a heptapeptide (328-334) was subsequently shown to be crucial for SRF binding (Zaromytidou et al., 2006). The basic region also activates an importin α/β NLS (Miralles et al., 2003; Pawłowski et al., 2010), and is likely to make specific contacts with the DNA phosphate backbone in the MRTF-SRF DNA complex (Zaromytidou et al., 2006).

A second conserved region C-terminal to B1 was identified on the basis of a polyglutamine sequence of Myocardin and termed the Q-box (Wang et al., 2001). Homology of the region can be found in the three members of the Myocardin family. The region consists mainly of glutamine residues and hydrophobics and is the classical sequence that has been used in literature when referring to the Q box. Subsequent analysis has shown that the most evolutionary conserved sequences in the Q-box region are the preceding five amino acids and sequences extending into the hydrophobic section (Zaromytidou et al., 2006) (Figure 20). In this thesis I will show that this conserved element interacts with G-actin and RPEL3 to generate a composite high affinity G-actin binding site.

While the Q-box facilitates MRTF- SRF binding (Zaromytidou et al., 2006), it is essential for Myocardin-SRF interaction, where deletion of Q inhibits formation of ternary complex with SRF (Wang et al., 2001, 2004).

Q-box deletion in MRTF leads to a more nuclear localization of the protein. As it contains a nuclear export signal (NES) within the Q-box sequence, it remains unclear whether the enhanced nuclear localization of MRTF derivatives lacking Q is due to effects of the NES, G-actin binding or both (Muehlich et al., 2008a; Panayiotou et al., 2016).

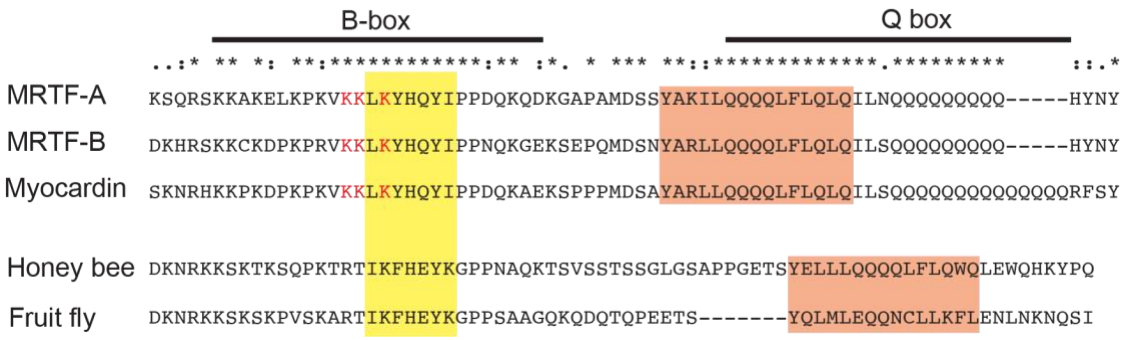

Figure 20. Homology between Q region of MRTF family members
Alignment of the amino acid sequence of the MRTF family members (*Mus Musculus*) with Honeybee (*Apis mellifera*) and Fruit fly (*Drosophila melanogaster*). Basic B and Q box regions are annotated above the alignment, with the heptapeptide in B shaded in yellow, and the evolutionary conserved shown in orange.

SAP domain

SAP (SAF-A/B, acinus, PIAS) domain is a 35-amino acid region, which exerts a DNA-binding function in many proteins, although it has not been shown structurally. It is thought that MRTF could confer transcriptional activity independently from SRF through the SAP domain, mainly of genes involved in chromatin reorganisation, DNA repair and mRNA splicing (Aravind and Koonin, 2000). SAP is not necessary for SRF-complex formation (Miralles et al., 2003), but it is important for myogenic activity of Myocardin (Wang et al., 2003). In Myocardin, the SAP domain appears to enhance activity at a subset of SRF sites, but the mechanism involved is unclear (Wang et al., 2001). Comparison of SAP domain deleted MRTF mutant with MRTF B-box point mutations that prevent SRF binding in mammary epithelial cells allowed for identification of many SRF-independent genes, regulation of which was MRTF dependent (Gurbuz et al., 2014).

Leucine Zipper motif (LZ)

Leucine-rich sequence is a common motif found in transcription factors and DNA-binding proteins, which mediates dimerization by formation of a parallel coiled-coil structure (Hakoshima, 2017).

The leucine zipper-like domain can be found in all three members of MRTF family, which allows for homodimerization of MRTF-A, MRTF-B and

Myocardin (Du et al., 2004; Miralles et al., 2003; Selvaraj and Prywes, 2003; Wang et al., 2003). MRTF-A can also heterodimerize both with MRTF-B and Myocardin (Selvaraj and Prywes, 2003; Zaromytidou et al., 2006). The ability of Myocardin to homodimerize is much weaker than that of MRTF-A and B (Zaromytidou et al., 2006), and although the LZ presence is not necessary for SRF-complex formation, the ability to activate SM genes was diminished in the absence of LZ (Wang et al., 2003), suggesting to the role of dimerization in activation potential of Myocardin. The importance of dimerization of Myocardin in activation of smooth muscle genes has also been shown in ES cells (Du et al., 2004).

Transactivation domain (TAD)

TADs are disordered regions within transcription factors, which interact with transcription initiation proteins, recruiting enhancers and stabilizing the interaction with target promoters (Frietze et al., 2011).

The transcription activation function of Myocardin family of proteins is exerted through their transcription activation domain localized within the C terminal part of the protein, although the exact sequence has not been mapped (Miralles et al., 2003; Wang et al., 2001; Wang and Olson, 2004). Although the similarity of TADs between members of MRTF family is low, they have functional interchangeability (Wang and Olson, 2004). This, combined with the fact the TAD of Myocardin can be replaced with a viral coactivator protein VP15 and still retain it transcriptional activity suggests that there is a low degree of specificity regarding target gene activation (Wang et al., 2001).

1.5.3 Rho-actin pathway in MRTF activity regulation

MRTF shuttles constantly between the cytoplasm and the nucleus. Serum induced activation of Rho induces rapid polymerization of actin, decreasing the overall concentration of monomeric actin in the cell, leading to MRTF nuclear accumulation (Figure 21). This process is governed by exposure of the Importin α/β binding site that is localized within the RPEL domain, as well as decrease in nuclear export, that is mediated by monomeric actin. The same effect can be

seen with treatment of cells with CD, which binds actin and prevents actin-MRTF binding, resulting in MRTF nuclear accumulation. Artificially increasing the concentration of monomeric actin in the cell by treatment with LatB prevents MRTF nuclear import and retained MRTF in the cytoplasm (Vartiainen et al., 2007). Treatment of cells with LMB deactivates the Crm1-mediated export and sequesters MRTF in the nucleus, while not disrupting actin binding.

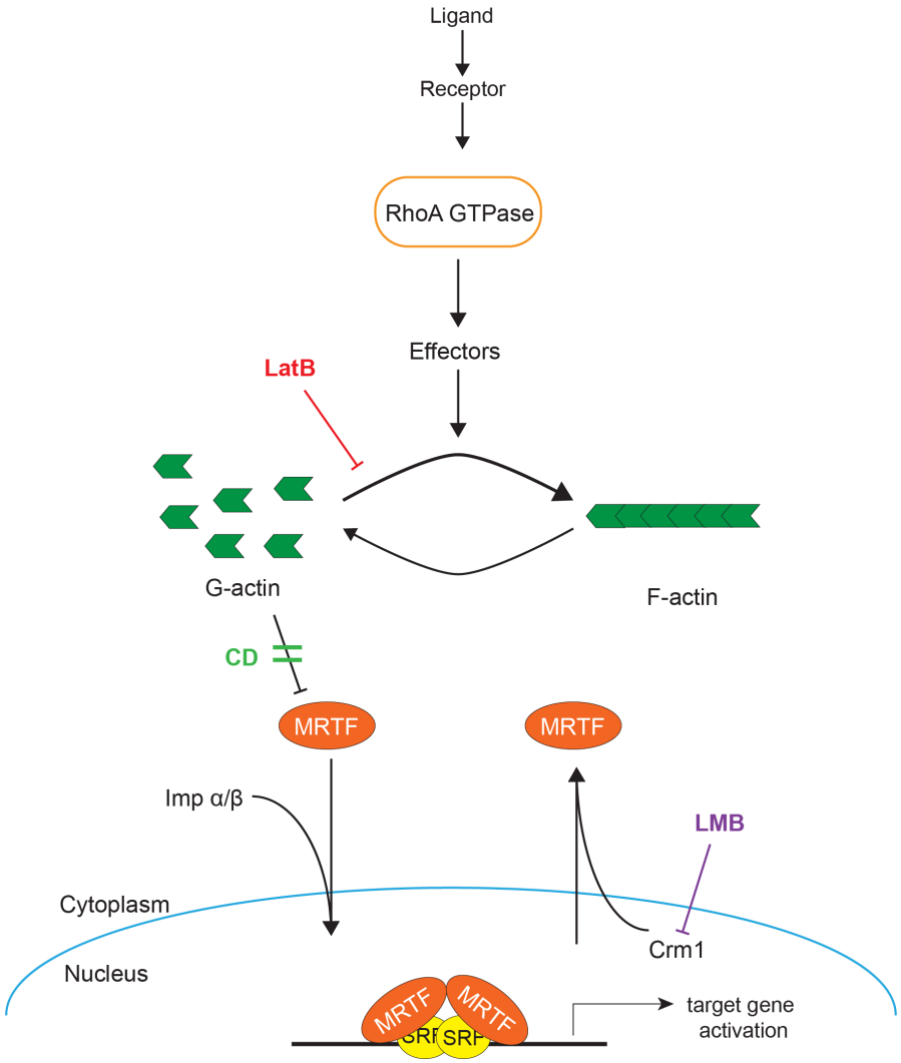

Figure 21. Rho-GTPase signalling couples MRTF activity to actin cytoskeleton Activation of the RhoGTPases leads to rapid polymerization of actin, decreasing the G-actin pool available for MRTF binding. MRTF is free to be transported into the nucleus by binding Importin α/β (bipartite NLS in the RPEL domain), where it binds to SRF and DNA, leading to target gene activation. Export from the nucleus is Crm1 mediated, although the exact mechanism is not yet known. LatB increases the pool of G-actin in the cell, inhibiting MRTF activity and keeping it in cytoplasm. CD disrupts actin binding to MRTF and leading to MRTF-SRF pathway activation. LMB binds Crm1 and inactivates MRTF export from the nucleus, without disrupting actin-binding.

1.5.4 MRTF nuclear import and export

MRTF cellular localization is controlled by Importin α/β regulated import to the nucleus and Crm1-mediated export from the nucleus. Actin binding to MRTF regulates import by occluding the Imp α/β binding sites on MRTF, while also facilitating nuclear export, although the mechanism is not fully understood.

Nuclear import

MRTF nuclear import is regulated by actin binding to the RPEL domain (Pawłowski et al., 2010; Vartiainen et al., 2007). Actin competes with Importin α/β for MRTF binding to the RPEL domain (Pawłowski et al., 2010), while introducing a loss of contact mutation into MRTF (MRTF-12A or "xxx") rendered MRTF nuclear in resting cells (Guettler et al., 2008; Mouilleron et al., 2008; Vartiainen et al., 2007), suggesting that actin binding to MRTF prevents nuclear import.

Two basic NLS sequences can be found in the MRTF RPEL domain, termed B2 and B3. B2 (^{152}KLKRAR^{158}) is localized between RPEL2 and RPEL3 (Miralles et al., 2003; Vartiainen et al., 2007), and B3 (^{119}KRKIRSR^{124}) within RPEL2 sequence (Pawłowski et al., 2010). Another basic sequence (B1) can be found in the SRF binding region of MRTF (residues 315-340) (Miralles et al., 2003).

In the Imp α/β complex, Importin α bids the monopartite or bipartite NLS sequence of proteins and acts as an adapter for Importin β (Görlich et al., 1995), which interacts with nucleoporins and binds to RanGTP, releasing the Impα with bound cargo in the nucleus (Rexach and Blobel, 1995). The crystal structure of Importin α/β binding RPEL peptide with B3-B2 NLS sequences has been determined (Hirano and Matsuura, 2011). MRTF makes direct contact with Importin α, with B2 binding in the major groove and B3 in minor groove of the NLS binding domain.

Functional analysis of the import sites on MRTF revealed cooperativity between the NLS sequences. Combined deletion of B1 and B2 prevented MRTF nuclear localization in serum stimulated cells (Miralles et al., 2003; Vartiainen et al., 2007). Mutagenesis analysis of the B2 and B3 NLS sites

showed cooperativity as well. Mutation of the three basic residues ^{152}KLK^{154} or ^{119}KRK^{121} to alanine in B2 and B3, respectively, prevented nuclear accumulation of MRTF in serum stimulated cells (Pawłowski et al., 2010). B2 was shown to act as a weak autonomous NLS sequence, with B3 being identified as an additional NLS. Together they form a bipartite B2/B3 NLS element (NLS sequences are annotated on Figure 19).

Nuclear export

Nuclear export of MRTF requires the integrity of all the N-terminal actin binding sites (Mouilleron et al., 2011; Vartiainen et al., 2007). Loss-of-contact MRTF mutant was sequestered to the nucleus in FLIP experiments, where overexpression of actin could increase the nuclear export of MRTF (Vartiainen et al., 2007), although the exact mechanism of actin-mediated Crm1 export is unknown. It is also regulated by post-translational modifications, where alanine substitution of S33 which inhibits activity of the N-terminal NES increased MRTF nuclear accumulation (see section 1.5.5). The effect was even more pronounced when combined with additional mutations of other NES sites throughout the sequence (Panayiotou et al., 2016), again showing cooperativity between the sites.

Multiple NES elements have been identified within MRTF sequence. NES element localized in sequences N-terminal to the RPEL domain has been shown to be Crm1-dependent (Muehlich et al., 2008a; Panayiotou et al., 2016). More NES elements were identified within the Q region (Hayashi and Morita, 2013; Muehlich et al., 2008b), SAP region, N-terminal to the LZ and within the TAD domain (Panayiotou et al., 2016). Export of Q-box deleted mutant of MRTF was still regulated (Guettler et al., 2008). Mutagenesis analysis of the NES sites showed that the N-terminal NES mutation had the strongest effect on nuclear localization of MRTF, compared to other NES mutants. However, a combination of two NES mutations resulted in sequestering MRTF to the nucleus, showing cooperativity. Three NES sequences with the strongest effect on MRTF export are annotated on Figure 18.

1.5.5 MRTF phosphorylation

MRTF activity has been coupled to multiple phosphorylation sites identified within the sequence (Panayiotou et al., 2016).

Stimulation of cells with serum was shown to induce MRTF phosphorylation up to 6-8h post treatment, in line with the time MRTF is retained in the nucleus post stimulation (Vartiainen et al., 2007). Treatment of cells with LatB and increasing the concertation of G-actin in the cells resulted in loss of phosphorylation to pre-stimulation levels (Panayiotou et al., 2016). Nuclear localization by using either NLS-fusion or LMB treatment was not sufficient to detect phosphorylation on MRTF, suggesting to a suppressive role of G-actin in MRTF activation.

Twenty-six phosphorylation sites have been identified throughout MRTF sequence with high confidence using proteomics. Two important residues identified to play a role in MRTF activity regulation were S33 and S98. While a phosphomimetic mutant of S98 induced MRTF nuclear localization, an opposing effect could be seen for S33. S98 is localized within R1 on RPEL domain, where phosphorylation could lead to dissociation of actin binding on RPEL. S33 is localized in the sequences N-terminal to the RPEL domain, in close proximity to one of NES signals identified within MRTF sequence. When checking the export rates of the MRTF constructs containing only the residues spanning the NES sequence (2-67), it was shown that S33 phosphorylation significantly increases MRTF nuclear export, as compared to a non-phosphorylatable mutant of S33, which was retained in the nucleus (Panayiotou et al., 2016).

1.5.6 MRTF-Actin binding

The presence of multiple RPEL motifs suggests that MRTF regulatory domain will form multivalent actin complexes. Consistent with this, mutagenesis of individual RPELs shows that all motifs contribute to regulation (Guettler et al., 2008), while in gel filtration experiments a trivalent actin-MRTF complex is detected (Vartiainen et al., 2007). Structural studies of the complex indeed

reveal a trivalent complex, but this contained RPEL1 and 2 with a third actin on the spacer between, and low-affinity RPEL3 unoccupied (Mouilleron et al., 2011). Consistent with actin binding to RPEL3 being unstable, inclusion of actin in the gel filtration buffer allowed detection of a larger pentavalent complex. Substitution of RPEL3 residues by those of RPEL2 revealed that sequences within the RPEL are important for binding affinity, for example the RPEL3$^{GP171/172ER}$ has a 6-fold higher affinity for actin binding than RPEL3^{WT} (Mouilleron et al., 2008). In line with this, to facilitate structural analysis, a GP171/172ER mutation was introduced to RPEL3 to increase its affinity for actin. This allowed the structure of the pentavalent complex to be determined (Figure 22).

Multivalent RPEL domain-actin complex

MRTF has five available sites for actin binding on the RPEL domain: three on each of the RPEL motifs and two on the Spacer regions between the RPELs. In the pentavalent complex, RPEL domain folds into a crank-shaped conformation, with each RPEL folding into two helices (Helix α-1 and Helix α-2) connected by an R-loop. R1, R2 and R3 contact one actin each (RPEL-actins) and the helical N-terminal extensions of the R2 and R3 contact one actin as well (Spacer-actins) (Figure 23). The relative orientation of actins in the MRTF-actin complex is different to that of actins in an actin filament (Holmes et al., 1990; Oosterheert et al., 2022)

Each RPEL-actin can be superimposed with one another, with a rotation of 150º along the crank axis. Within the pentavalent complex two dimers of trimers can be distinguished, where R1-S2-R2 orientation matches that of R2-S2-R3 with RMSD= 2.5Å. Additionally, the trivalent complex of R1-S1-R2^{trivalent} can be superimposed with the pentavalent complex R1-S2-R2^{pentavalent} with a RMSD = 1.9Å.

Analysis of the pentavalent complex revealed that S2-actin has high degree of flexibility within the crystal structure, which on top of weak R3-actin binding could be the reason why a pentavalent complex is unstable. Gel filtration experiments showed that S1-R2 peptide can bind two actins, while the same cannot be seen for S2-R3 (Guettler, 2007, PhD Thesis; Mouilleron et al.,

2011). The suggested model of binding proposed N->C actin loading onto MRTF, with a primary complex on R1-S1-R2, and only in high actin concentrations actin loading on S2-R3 (Guettler et al., 2008).

In this thesis I will provide evidence that actin loads from the C->N through strong composite actin binding site comprising RPEL3 and Q-box, that nucleates actin binding to MRTF.

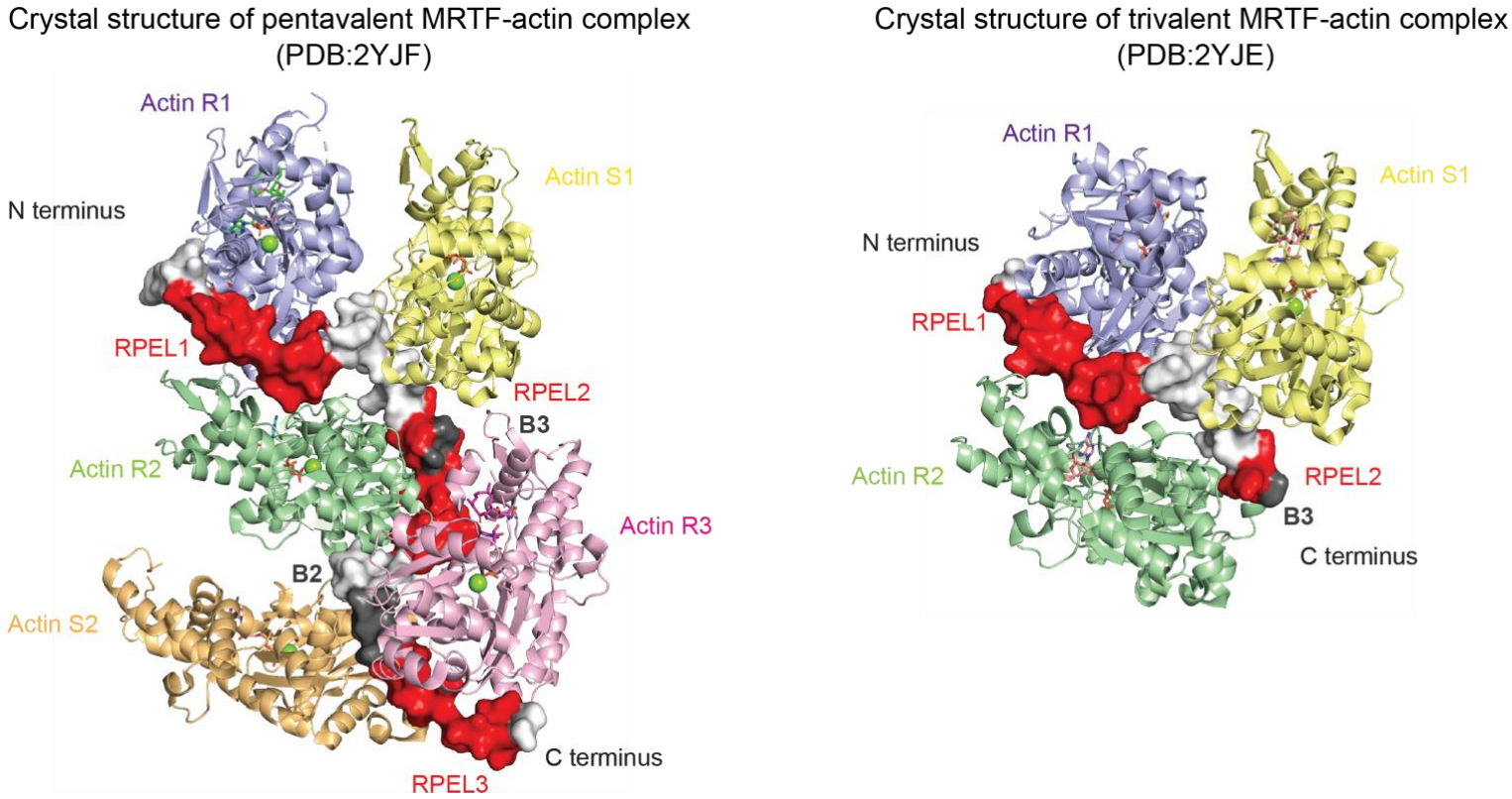

Figure 22. Crystal structure of RPEL-actin binding

MRTF-actin complexes (MRTF residues 67-199; Rabbit skeletal α-actin 1-375): RPEL domain shown as surface, RPEL motif sequences in red, Spacer regions in white, basic B2 and B3 shown in dark grey. Actins shown as cartoon – Actins R1, R2 and R3 bind to RPEL motifs and Actins S1 and S2 bind to Spacer regions. Left: Pentavalent MRTF-Actin complex (PDB:2YJF). Right: Trivalent MRTF-Actin complex (PDB; 2YJE).

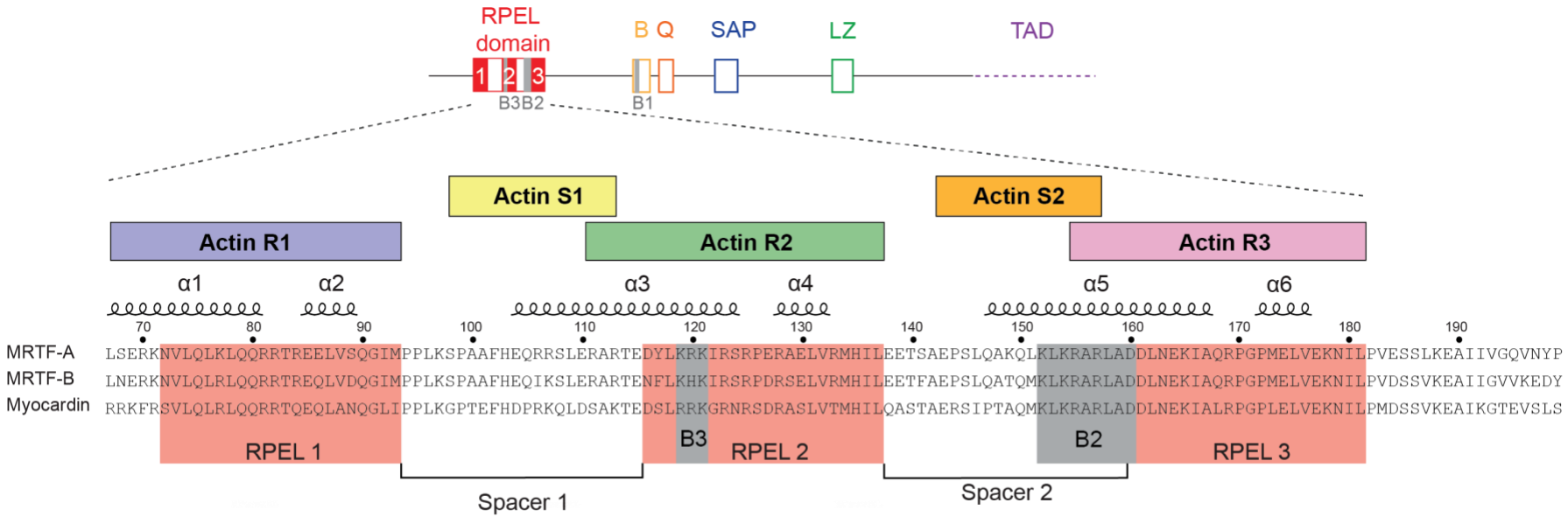

Figure 23. Actin-binding sites on RPEL domain
Alignment of the RPEL domain in Myocardin, MRTF-A and MRTF-B. RPEL motifs shaded in red, basic region shaded in grey. Brackets between RPEL motifs indicate Spacer regions. RPEL motif α-1 and α-2 helices annotated above the sequence. The actin binding sites identified based on crystal structure of pentavalent MRTF-Actin complex (PDB: 3YJF) annotated above the sequences.

1.5.7 Role of actin in regulation of MRTF-SRF complex formation

Myocardin, the founding member of the MRTF family binds to SRF and DNA as monomer (Wang et al., 2001). MRTF binds as a dimer, and its recruitment to DNA is solely dependent on the presence of SRF (Wang et al., 2002; Zaromytidou et al., 2006). Although MRTF cannot bind to DNA on its own, the specificity of the DNA sequence for SRF influences the recovery of MRTF in immunoprecipitation assay (Zaromytidou et al., 2006). MRTF can bind to SRF as a monomer, although it binds less efficiently, and the SRF DBD (DNA binding domain) is necessary and sufficient for MRTF binding. I will exploit this in this thesis to study the dynamics of MRTF-SRF binding *in vitro*.

A heptapeptide (^{328}LKYHQYI^{334}) within the basic B region of MRTF was identified as crucial for MRTF-SRF interaction, with sequences in the Q region downstream of B-box facilitating, but not necessary for DNA binding (Zaromytidou et al., 2006).

MRTF binds not only SRF, but a footprinting assay has shown that it contacts DNA between positions -22 and +22 relative to the SRE dyad (Zaromytidou et al., 2006) (Figure 24). As to date, there is no crystal structure of MRTF bound SRF and DNA, but it has been shown that the presence of MRTF changes SRF-DNA bending as compared to SRF alone (Zaromytidou et al., 2006). This in line with how TCFs contact SRF, with the B region contacting SRF and DNA bending occurring upon cofactor binding (Richmond and Hassler, 2001).

Figure 24. Specific DNA sequence for SRF and MRTF binding
DNA sequence of c-fos with central CArG box, DNA-SRF an DNA-MRTF contacts indicated based on (Zaromytidou et al., 2006).

Investigation of MRTF-SRF interaction *in vivo* was done using Chromatin Immunoprecipitation assay (ChIP) in NIH 3T3 cells (Esnault et al., 2014; Gualdrini, 2016, PhD Thesis; Toteva, 2021, PhD Thesis).

SRF target genes have been identified by SRF-ChIP using serum stimulation to activate the Rho-Actin pathway in mouse fibroblasts (NIH3T3 cells) (Esnault et al., 2014). They were classified as either constitutive or inducible. Most of the inducible sites were MRTF-regulated, and comprised genes involved in regulation of actin cytoskeleton. The MRTF-regulated sites were identified as serum inducible and LatB sensitive. The presence of RNA polymerase II was also detected at the inducible MRTF-SRF sites, as well as nucleosome displacement, both not observed at the constitutive SRF sites.

Productive transcription of MRTF-SRF targets is dependent on disruption of actin binding to MRTF. In line with that, although MRTF nuclear accumulation is sufficient for recruitment to target gene promoters, it is not sufficient to induce target gene expression, and only upon dissociation of actin can transcription occur (Vartiainen et al., 2007).

This was seen both by treatment of cells with LMB (inhibition of nuclear export) and by fusing MRTF to an NLS signal (Gualdrini, 2016, PhD Thesis; Toteva, 2021, PhD Thesis; Vartiainen et al., 2007).

LMB, which inactivates Crm1-mediated export was not sufficient to induce MRTF activation and DNA binding. Treatment with CD, which disrupts actin binding led to detection of MRTF on target DNA. In contrast, DNA binding was abolished with LatB treatment, which increases the monomeric pool of G-actin available for MRTF binding (Gualdrini, 2016, PhD Thesis; Toteva, 2021, PhD Thesis) (Figure 25A). This was dependent on the integrity of actin binding sites on the RPEL domain. MRTF mutant with mutations on each of the RPELs (123-1A or XXX) is constitutively nuclear and binding DNA and does not respond to changes in actin concentration (Figure 25B).

A.

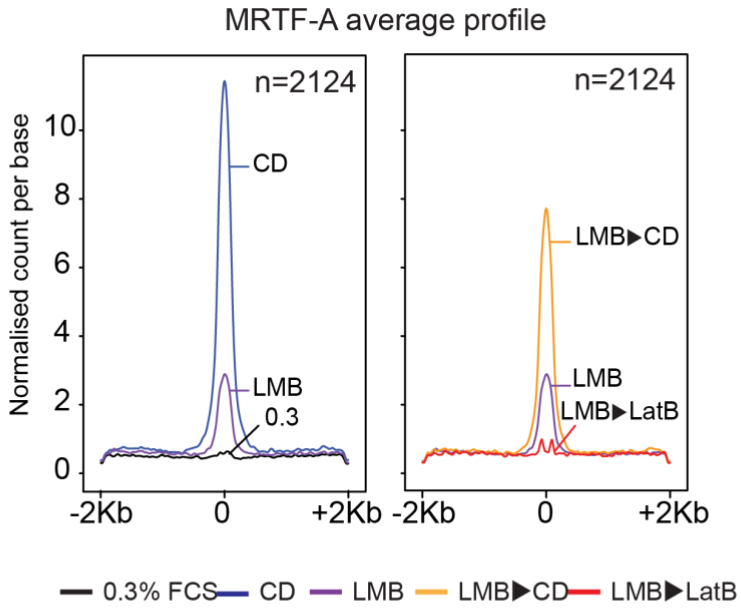

B.

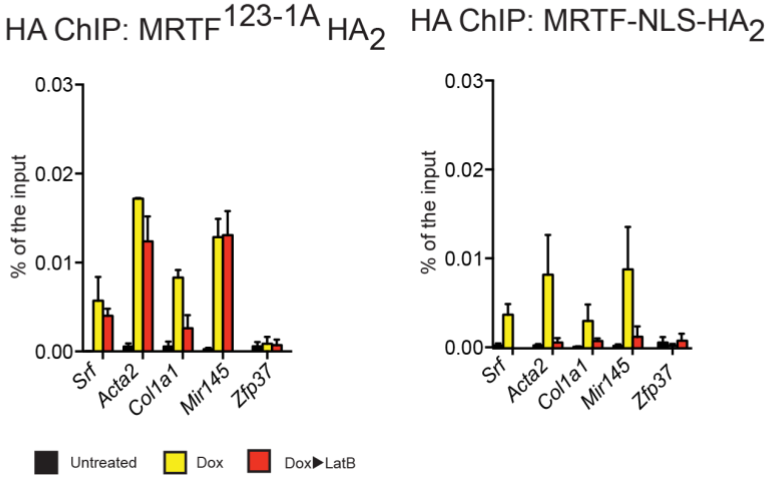

Figure 25. MRTF-DNA binding regulated by nuclear actin

A. MRTF-A Chromatin Immunoprecipitation assay on MRTF targets (2124 targets, defined in (Gualdrini, 2016, PhD Thesis) based on (Esnault et al., 2014)) centered on SRF peak summit. CD (CytochalasinD), LMB (LeptomycinB), LatB (LatrunculinB). **B.** ChIP of MRTF-A (HA) on cells harbouring the $MRTF^{123\text{-}1A}HA_2$ or $MRTF^{WT\text{-}NLS}HA_2$ in a Doxycycline inducible vector. Black: no doxycycline (no vector expression), yellow – doxycycline treatment (expression of the vector), red: doxycycline treatment + LatB treatment. The immunoprecipitate was quantified using RT-qPCR and plotted as percentage of the input material. The binding sites shown include nine bona fide SRF-MRTF targets (*Srf, Acta2, Col1a1, Mir145*) and a negative control *Zfp37*.

1.5.8 The aims of the thesis

MRTF activity and SRF binding is regulated by interaction of the N-terminal RPEL domain of MRTF with actin. SRF and actin binding sites on MRTF are separated, with SRF binding 200 residues downstream of the RPEL domain. In this thesis I aimed to understand what the mechanism of actin inhibition of MRTF-SRF binding is.

1. How does actin binding to the N-terminal RPEL domain inhibit SRF binding to the B and Q-box?
2. Is there additional interaction between actin and SRF-binding site on MRTF that would occlude SRF binding to MRTF?
3. Is SRF and Actin binding to MRTF mutually exclusive?

This thesis will focus on answering these questions.

Chapter 2. Materials and methods

2.1 Expression vectors

Protein expression in *E.coli*	
1C vector (pET His6 MBP Asn10 TEV)	N-terminal His6-MBP-TEV tag (gift from Scott Gradia, Addgene plasmid # 29654; http://n2t.net/addgene:29654 ; RRID:Addgene_29654) All MRTF protein derivatives were expressed using this vector, with mutations and deletions as indicated
1C vector (pET His6 MBP Asn10 TEV-HA)	Modified 1C vector with an N-terminal HA-tag after the TEV cleavage site
pET-41a-3CΔ	Novagen, N-terminal GST-His-S; modified to contain a 3C protease site Used for SRF.DBD (residues 132-223) expression

Table 1. Expression vectors used in *E.coli*

Protein expression in Sf21 cells (insect)	
pFastBac1-Hsβ-Actin-βThymosin	Vector for expression of human cytoplasmic β-actin with C-terminal β-thymosin – chymotrypsin cleavage C-terminal actin residue (F375). A gift from the Way lab, Francis Crick Institute
pFastBac1-Hsβ-Actin-TEV	Modified by removing C-terminal β-thymosin sequence and addition of N-terminal His6 tag and TEV cleavage site (ENLYFQ')
pFastBac1-Hsβ-Actin-TEV-R62D	Addition of R62D mutation (non-polymerizable actin mutant)

Table 2. Expression vectors used in Sf21 cells

Protein expression in mammalian cells	
pEF-FLAG	N-terminal FLAG epitope tag used for expression MRTF-A derivatives. Derived from EF.plink (Hill et al., 1995)

Table 3. Expression vectors used in mammalian cells

2.2 Reagents

2.2.1 ATP preparation

For 250 mM ATP solution (10 ml), 1.378 g of ATP (Merck, A7699-10g) was dissolved in 9.2 ml of H_20, followed by addition of 50 µl 1 M Tris pH=8.8 and 200 µl 10N NaOH. The pH of the solution was adjusted to pH=7 using 10 N NaOH and the solution volume was adjusted with water to 10 ml final volume.

2.2.2 Poly[d(I-C)] preparation

Poly[d(I-C)] (Roche, 10108812001) was prepared by dissolving (in TEN buffer (10 mM Tris-HCl pH=8, 1 mM EDTA, 100 mM NaCl) to a final concentration of 1 mg/ml ($1U_{A260}$ = 50 µg dsDNA). The solution was heated to 72ºC for 10 min to anneal the DNA, left at room temperature for 30 min and sonicated using Biorupor® Plus sonication device (Diagenode) – 2 cycles at high energy 15 sec on, 30 sec off. The resulting DNA fragment sizes should be between 500 bp – 1000 bp.

2.2.3 4X Laemmli buffer

To make a loading buffer for SDS-PAGE 200 mM Tris-HCl pH=6.8, 40% Glycerol, 8% SDS solution was prepared, followed by addition of DTT in powder form to a 400 mM final concentration and a small amount of Bromophenol blue (Sigma, B0126) was added. Buffer was used at 1X in SDS-PAGE samples

2.3 List of antibodies

Antibody	Species	Supplier	Cat. No.	Dilution
HA (16B12)	Mouse	BioLegend	MMS-101R	WB 1:1000
FLAG (M2)	Mouse	Sigma	F3165	IF 1:500
MRTF-A (raised against aa 447-784)	Rabbit	Covalab	Homemade	WB 1:1000 IF 1:500
pan-Actin	Rabbit	Cell Signalling	4968S	WB 1:1000

Table 4. List of primary antibodies

Antibody	Species	Supplier	Cat. No.	Dilution
Alexa Fluor 488 anti - mouse	Donkey	Invitrogen	A21202	IF 1:1000
Alexa Fluor 568 anti - mouse	Donkey	Invitrogen	A31570	IF 1:1000
IRDye 800CW anti-mouse	Donkey	Licor	925-32212	WB 1:10000
IRDye 680LT anti-rabbit	Goat	Licor	926-68023	WB 1:10000
Alexa Fluor® 790 AffiniPure™ anti-mouse	Goat	Stratech Scientific	115-655-174	WB 1:5000

Table 5. List of secondary antibodies

2.4 Mammalian cell culture

2.4.1 Tissue culture conditions

NIH/3T3 cells were cultured in Dulbecco's Modified Eagle Medium (DMEM, Gibco, 41966-029) with 10% Foetal calf serum (FCS, Gibco, 10270-106) and 1% Penicillin/Streptomycin (Sigma, P4333) and kept in an incubator with 10% CO_2 at 37ºC. Cells were passaged twice per week – plates were washed with 1X PBS (137mM NaCl, 2.7mM KCl, 10mM Na_2HPO_4, 1.8mM KH_2PO_4 pH 7.4) and detached using trypsin (Sigma, T4049) by incubation for 5

min. Trypsin was neutralized by adding two volumes of supplemented DMEM and passaged at a 1:10 ratio.

2.4.2 Cell transfection

The numbers here are provided for one well of a 12-well plate. Cells were passaged a day before the transfection and seeded at 100,000/well (for immunofluorescent staining cells were seeded on glass coverslips). Media was changed 30min before the transfection to 1ml of Opti-MEM (Gibco, 31985-047). Transfection reaction was prepared in two separate tubes. pEF-FLAG-MRTF was combined at a 1:10 ratio with an empty pEF-FLAG vector with a total of 1µg DNA (0.1µg MRTF + 0.9µg Empty) and added to 100µl of Opti-MEM. In parallel, 3µl of Lipofectamine2000 (ThermoFisher, 11668-019) was added at 100µl of Opti-MEM. Both reactions were incubated separately for 5 min at room temperature, combined and incubated for another 20 min. The transfection mix was added dropwise to the wells of the 12-well plate and incubated for 4 hours before changing media to DMEM supplemented with 1% Pen/Strep and 10% FCS. Cells were then treated according to the experiment.

2.4.3 Immunofluorescent staining of cells

Following transfection, cells were washed with 1xPBS and starvation media (DMEM with 1% Pen/Strep and 0.3% FCS) was added for 24h prior to treatment and immunofluorescent staining. On the day of the experiment, FCS was added to a final concentration of 15% and incubated for 30 min.

All following steps were done at room temperature, unless stated otherwise. Coverslips were washed twice with 1xPBS and fixed using 4% PFA (Alfa Aesar, J19943.K2) and incubated for 10 min, washed twice with 1xPBS and permeabilised using 0.2%Triton in PBS solution for 20min. The coverslips were blocked with 10% FCS with 0.5% Fish Skin Gelatin (Sigma, G7765) in PBS for 1h, followed by overnight incubation with primary antibody solution (rabbit α-MRTF-A A12 1:500, mouse α-FLAG M2 1:500) at 4ºC. Next day, coverslips were washed three times with 0.1% Triton in PBS solution and incubated with secondary antibodies (α-mouse 488 1:200, α-rabbit 568 1:200,

DAPI 1:1000) for 1h. Coverslips were washed three times with 0.1% Triton in PBS solution and once with water, before mounting on coverslips using Mowiol mounting medium (9.32% (w/v) mowiol 4-88 (Calbiochem, 475904), 2.5% (w/v)DABCO (1,4-diazabicyclo-[2.2.2]octane), 100 mM Tris pH 8.5 and 20% (v/v) glycerol) and stored at 4ºC.

Coverslips were imaged using Zeiss Upright Widefield microscope. Images were processed using ImageJ.

2.5 Nucleic acid work and DNA manipulations

2.5.1 Plasmid DNA purification

Plasmid DNA was isolated from either 5 ml or 200 ml of bacterial cultures, using the QIAGEN Plasmid Mini (Quiagen, 27106) and Maxiprep Kit (Quiagen, 12163), respectively. The DNA was isolated following manufacturers protocol. Briefly, the bacterial cultures were inoculated overnight from bacterial plates. The cells were centrifuged at 2000 rpm and resuspended in P1 buffer, lysed for 5 min using P2 buffer and neutralized using N3 buffer. The lysates were then centrifuged for 30 min at 4°C, cleared lysates were then applied to a binding column, washed twice using Wash buffer and eluted using Elution buffer. The DNA was then precipitated by adding isopropanol and centrifuged for 40 min at 4°C. The pellet was washed using 70% EtOH and centrifugation for 15 min, after which it was left to air dry to remove traces of ethanol. The pellet was then suspended in milliQ H_20 (volume dependent on expression vector, between 100µl-1000µl) and the DNA kept at 20°C for long term storage.

2.5.2 DNA concentration measurement

The DNA was measured using NanoDrop Microvolume Spectrophotometer using the absorbance at 260nm. First, the machine was calibrated using the buffer in which the DNA has been resuspended, followed by measurement of DNA concentration. The output is the concentration of DNA in ng/µl, as well as a ratio of Absorbance at 260/280, which is the measure of DNA purity (A260/280=1.8 is considered as pure).

2.5.3 Bacterial transformation

For plasmid propagation OneShot™ TOP10 Chemically Competent *E. coli* cells (ThermoFisher, C404003) were used, for protein expression purposes Rosetta^{TM} Competent cells *E. coli* cells were used (Merck, 70953).

30 µl of competent cells was thawed on ice and the transformation reaction was assembled by combining 10 ng DNA, 1X KCM buffer, H20 (to a final volume of 30 µl), incubated on ice for 5 min and combined with competent cells. The transformation reaction was incubated for 20 min on ice, followed by 5 min incubation at room temperature. 100 µl of SOC media (ThermoFisher, 15544034) was added and the cells were incubated at 37ºC for 1h shaking at 200rpm. 100µl of the transformed bacteria was spread on LB plates supplemented with antibiotic - Ampicillin (Merck, A0166 - 100 µg/ml) or Kanamycin (Merck, K0254 - 50µg/ml), depending on the antibiotic resistance of the plasmid. The plates were incubated overnight at 37ºC.

KCM 5X buffer

0.5 M KCl

0.15 M $CaCl_2$

0.25 M $MgCl_2$

2.5.4 Molecular cloning

2.5.4.1 Site-directed mutagenesis

Mutations were introduced using overlapping forward and reverse primers, with the mutation localized in the centre of both. Each reaction was prepared in with concentrations of components shown in Table 6. The PCR reaction was run using the programme shown in Table 7.

Components of the PCR reaction (Mutagenesis)			
	Stock concentration	Final concentration	Volume
Forward primer	10µM	0.5µM	2.5µl
Reverse primer	10µM	0.5µM	2.5µl
dNTP	10mM	0.4mM	1µl
Pfu Turbo buffer	10X	1X	5µl
Pfu Turbo DNA polymerase (Agilent, 600252)	2.5 U/µl	0.05 U/µl	1µl
H20	-	-	36µl
Template DNA	10ng/µl	0.4ng/µl	2µl
Final reaction volume			50µl

Table 6. Components of PCR reaction - Mutagenesis

PCR programme		
Temperature	Time	Number of cycles
95ºC	2 min	-
95ºC	30 sec	18
50ºC	1 min	
68ºC	16 min	
72ºC	10 min	-

Table 7. PCR programme - Mutagenesis

The remaining methylated DNA was digested with DpnI (1µl/reaction) for 1h at 37ºC. The DNA was the precipitated with 5.5µl 3M Sodium Acetate pH 5.2 and 160µl 100% EtOH and incubated for 10min at -80 ºC. The samples were centrifuged at 13,000 rpm for 10min, the pellet was washed with 200µl of 70% EtOH and the samples were centrifuged at 13,000 rpm for 5min. The pellet was resuspended in 10µl of Nuclease-Free H_20 and placed on ice for 2min. 3µl of the DNA were used for bacterial transformation into 25µl of One Shot™ TOP10 Chemically Competent *E.coli* cells (ThermoFisher, C404003). Cells were incubated with the DNA on ice for 30min, followed by 30s heat shock at 42ºC, and 5min on ice. 250µl of warm SOC media was added and the cells were incubated at 37ºC for 1h shaking at 200rpm. 150µl of the transformed bacteria

was spread on LB plates supplemented with antibiotic - Ampicillin or Kanamycin depending on the antibiotic resistance of the plasmid. Plates were incubated overnight at 37ºC, with chosen colonies used for inoculation of antibiotic-supplemented LB media (Kanamycin at 30µg/ml and Ampicilin at 100µg/ml) followed by purification of plasmid DNA (2.5.1 Plasmid DNA purification) and evaluated by sequencing (Sanger sequencing, Genewiz).

2.5.4.2 Insertions and deletions

Insertions and deletions were done using Q5® Site-Directed Mutagenesis Kit (New England Biolabs, E0554S). The primers were designed based on the recommendation of the manufacturer. The components of the reaction and the PCR programme is indicated in the Table 8 and Table 9. Annealing temperature of the primers was calculated using the NEB T_m calculator (https://tmcalculator.neb.com/#!/main) and the elongation time was adjusted based on the size of the plasmid.

Components of the PCR reaction (Insertion or Deletion)			
	Stock concentration	Final concentration	Volume
Forward primer	10µM	0.5µM	1.25µl
Reverse primer	10µM	0.5µM	1.25µl
Q5 Hot Start High-Fidelity 2X Master Mix (NEB, M0494AVIAL)	2X	1X	1µl
H20	-	-	9µl
Template DNA	10ng/µl	0.4ng/µl	1µl
Final reaction volume			25µl

Table 8. Components of PCR reaction – Insertion/Deletion

PCR programme		
Temperature	Time	Number of cycles
98ºC	30 min	-
98ºC	10 sec	25
50-72ºC	20s	
72ºC	20s/kb	
72ºC	2 min	-

Table 9. PCR programme – Insertion/Deletion

Digestion, phosphorylation and ligation of the PCR product was done with the KLD Enzyme Mix (NEB, M0554AVIAL), using 0.4µl of PCR product, 0.4µl of the 10X KLD Enzyme Mix, 2µl of 2X KLD Reaction Buffer and 1.2µl H_20. The reaction was incubated for 5min at room temperature (RT). NEB® 5-alpha Competent E.coli bacteria were transformed with 2µl of the PCR/KLD product and incubated for 30min on ice, followed by heat shock at 42ºC for 30s. 500µl of warm SOC media was added and the cells were incubated at 37ºC for 1h shaking at 200rpm. 150µl of the transformed bacteria was spread on LB plates supplemented with antibiotic. Plates were incubated overnight at 37ºC, with chosen colonies used for inoculation of antibiotic-supplemented LB media followed by purification of plasmid DNA (2.5.1 Plasmid DNA purification) and evaluated by sequencing.

2.5.4.3 Ligation Independent Cloning (LIC) into 1C vector

Insertion of MRTF and SRF sequences into the 1C vector was done using LIC cloning. Primers were designed by addition of a LIC tag to the 5'end (Table 10).

FW primer LIC tag	5' TACTTCCAATCCAATGCA 3'
RW primer LIC tag	5' TTATCCACTTCCAATGTTATTA 3'

Table 10. LIC tags for addition to PCR primers – LIC

PCR reaction of the DNA template (insert) was assembled. The components of the reaction and the PCR programme is shown in Table 11 and Table 12. Annealing temperature of the primers was calculated using the NEB

T_m calculator (https://tmcalculator.neb.com/#!/main) and the elongation time was adjusted based on the size of the amplified DNA.

Components of the PCR reaction (LIC cloning)			
	Stock concentration	Final concentration	Volume
Forward primer	10µM	0.5µM	1.25µl
Reverse primer	10µM	0.5µM	1.25µl
Q5 High-Fidelity 2X Master Mix (NEB, M0492S)	2X	1X	1µl
H20	-	-	9µl
Template DNA	10ng/µl	0.4ng/µl	1µl
Final reaction volume			25µl

Table 11. Components of PCR reaction – LIC

PCR programme		
Temperature	Time	Number of cycles
98ºC	30 min	-
98ºC	10 sec	30
50-72ºC	30s	
72ºC	20s/kb	
72ºC	2 min	-

Table 12. PCR programme – LIC

The 1C vector linearized using SspI restriction digestion enzyme (Table 13). The LIC tags added to the primers for PCR product of the insert are designed to match the open ends of the vector.

1C Vector linearization	Volume
1C vector DNA (500ng)	3µl
10X NEBuffer 2.1 (NEB, B6002S)	2.5µl
SspI (NEB, R0132S/L)	0.5µl
H_20	19µl

Table 13. 1C vector linearization reaction components

The PCR product (insert) and the digested 1C vector were run on a 0.7-1% Agarose Gel in TBE buffer (100 mM Trizma Base, 100 mM Boric Acid, 5 mM EDTA in water) at 100V. The bands corresponding to the size of the PCR product and the linear vector were cut out of the gel and purified using QIAquick Gel Extraction kit (Qiagen, 28704). The purified insert and vector were eluted using 30µl of elution buffer supplied with the kit.

The LIC reactions were assembled as indicated in Table 14 and incubated in the thermocycler: 30min at 22ºC, 20min at 75ºC.

LIC reaction - insert		**LIC reaction - vector**	
dCTP (Bioline, BIO-39026)	10ul	dGTP (Bioline, BIO-39026)	10ul
NEBuffer 2.1	2ul	NEBuffer 2.1	2ul
DTT 100mM	2ul	DTT 100mM	2ul
T4 DNA polymerase (NEB, M0203S)	1ul	T4 DNA polymerase	1ul
H20	0.4ul	H20	0.4ul

Table 14. LIC reaction

2µl of LICed insert and 2µl of LICed vector were combined with 8µl of H_20 and incubated for 10min at room temperature. NEB® 5-alpha Competent E.coli bacteria were transformed with 2µl of the combined DNA and incubated for 30min on ice, followed by heat shock at 42ºC for 30s. 900µl of warm 2X YT media was added and the cells were incubated at 37ºC for 1h shaking at 200rpm. 150µl of the transformed bacteria was spread on LB plates supplemented with Kanamycin. Plates were incubated overnight at 37ºC, with chosen colonies used for inoculation of antibiotic-supplemented LB media followed by purification of plasmid DNA (2.5.1 Plasmid DNA purification) and evaluated by sequencing.

2.6 Insect cell work

2.6.1 Insect cell tissue culture

Sf21 and HighFive cells were cultured in Sf-900™ III SFM (ThermoFisher, 12658027) at 27ºC shaking at 140 rpm. Cells were passaged three times per week at to a final concentration of $0.5x10^6$ cells/ml. The viability of cells was monitored with every passage by adding 1:1 Trypan Blue solution (Gibco, 15250061) and cell size was monitored. Healthy Sf21 are between 14-16µm in diameter and healthy HighFive cells are between 17-18µm in diameter.

2.6.2 Transposition of pFastBac1 DNA into Bacmid

1µg of DNA (pFastBac1-Hsβ-Actin-TEV-R62D) was used for electroporation into DH10EMBacY (Genova Biotech, MultiBac^{TM}) competent cells. DNA was added to 50µl of cells and transferred to a 2mm Electroporation Cuvette and electroporated at 15kV/cm, followed with addition of 950µl of warm SOC media and incubated for 6h shaking at 220rpm at 37ºC. 50µl of the cells was passed over LB agar plates supplemented with 7 µg/mL Gentamycin (ThermoFisher, 15710064), 50 µg/mL Kanamycin, 10 µg/mL Tetracycline, (Merck, T7660-25G) 100 µg/mL X-gal (Sigma, 46026217) and 40 ug/mL IPTG (Generon, I1003-25GM). The plates were incubated for 2 days at 37ºC (day 1 – colonies formation, day 2 – blue/white colour develops; white colonies indicate successful transposition of the vector into Bacmid).

2.6.3 Bacmid DNA purification

A single white colony from the plates generated in 2.6.2 was used to inoculate 3 ml of LB supplemented with 7 µg/mL Gentamycin, 50 µg/mL Kanamycin and 10 µg/mL Tetracycline and incubated overnight shaking at 220rpm at 37ºC. The cells were centrifuged for 3 min at 13,000 rpm. The pellet was resuspended in 0.3 ml of P1 buffer (all the buffer used from the QIAGEN Plasmid MiniKit) and lysed by adding 0.3 ml of P2 buffer. Cells were incubated for 5 min at room temperature and the reaction was neutralized by addition of 0.4 ml of cold N3 buffer and incubated on ice for 5 min. Lysates were

centrifuged for 10 min at 13,000rpm and 0.8 ml of the supernatant was transferred to a fresh tube, followed by another centrifugation at 13,000 rpm for 3 min. 0.6 ml of the supernatant was transferred to a fresh tube and DNA was precipitated by adding 0.8 ml of Isopropanol and incubated for 10 min at room temperature. The reaction was centrifuged for 5 min at 13,000 rpm, the DNA pellet was washed twice using 0.75 ml of 70% Ethanol (3 min centrifugation steps between washes at 13,000 rpm). The pellet was air-dried under a sterile cell culture hood and resuspended in 50 µl filter-sterilized Elution Buffer. DNA concentration was measured using NanoDrop.

2.6.4 Baculovirus production in insect cells

2.6.4.1 Insect cell transfection – V0 production

To produce the initial viral stock (V0) the Sf21 cells were seeded at $2x10^6$ cells/well in a 6-well plate in a volume of 2 ml and incubated for 30 min to allow adherence to the bottom of the plate. The transfection reaction was prepared by combining: 95µl of Sf21 medium, 2µg of Bacmid and 3µl of FugeneHD (Promega, E2311), incubated at room temperature for 15 min and the reaction was added dropwise to the cells. The plate was incubated for 72h at 27ºC in a humid chamber to allow baculovirus production. The cells used for Bacmid purification have an RPF protein expressed under a separate promoter than actin, resulting in production of RFP and visual evaluation of the transfection efficiency.

2.6.4.2 V1 production

V0 made in 2.6.4.1 was used to make a viral stock of a higher titre. V0 viral titre was estimated at $1x10^6$-$1x10^7$ pfu/ml. Cells should be infected at MOI between 0.05-0.1 and the calculation of the required volume was done using the below formula (Equation 1).

$$Inoculum\ required\ (ml) = \frac{MOI\ \left(\frac{pfu}{cell}\right)\ x\ number\ of\ cells}{titer\ of\ viral\ stock\ (\frac{pfu}{ml})}$$

Equation 1. Calculation of inculcation volume for viral stock propagation

Sf21 were inoculated with the calculated volume of V0 at $1.5x10^6$ cells/ml and incubated for 3 days at 27ºC shaking at 140 rpm. The cells were inspected to see whether RFP expression can be observed. The viral supernatant was collected by centrifugation at 500 x g for 5 min and transferred to a fresh tube. The V1 was stored at 4ºC in black tubes to protect from light until further manipulation.

2.6.4.3 V2 production

The final baculovirus stock (V2) was made by inoculating Sf21 cells with V1. V1 viral titre was estimated at $1x10^7$-$1x10^8$ pfu/ml. Cells should be infected at MOI between 0.05-0.1 and the calculation of the required volume was done using Equation 1. Sf21 were inoculated with the calculated volume of V0 at $1.5x10^6$ cells/ml and incubated for 3 days at 27ºC shaking at 140 rpm. The viral supernatant was collected by centrifugation at 500 x g for 5 min and transferred to a fresh tube. The V2 is stored at 4ºC in black tubes to protect from light until further manipulation. V2 can be used for protein expression in Sf21 cells of HighFive cells.

2.6.4.4 Determination of the V2 viral titre

Viral titre of the V2 was assessed in order to determine the amount of Baculovirus needed for efficient infection of cells for protein expression. Infected insect cells stop division and proliferation within 24 hours post-infection. The diameter of the cells increases with protein production (Sf21: non-infected 14-16µm diameter, post-infection: 17-19µm; HighFive: non-infected: 17-18µm, post-infection: 20-21µm).

Insect cells were prepared at $1.5x10^6$ cells/ml and infected at 1:10, 1:50, 1:100, 1:250 and 1:500 dilution of the V2. The cell size and diameter was assessed 24 hours post infection. The most efficient concentration of the Baculovirus was used for following protein expression.

2.6.4.5 Protein expression in Sf21 cells

Sf21 or HighFive cell suspensions of required volume were prepared at $1.5x10^6$ cells/ml, infected with the V2 (see 2.6.4.4 for determining the viral titre) and incubated for 72 hours at 27ºC shaking at 140 rpm. The cells were centrifuged at 2000 rpm for 5 min and the supernatant was discarded (as there are viral particles in the supernatant it is disposed of by addition of virucidal disinfectant). Cell pellets were placed on ice, resuspended with ice-cold 1xPBS and centrifuged for 5 min at 2000 rpm. Cell pellets were snap-frozen in liquid nitrogen and stored at -80ºC until further manipulation.

2.7 Protein purification

2.7.1 Actin purification

2.7.1.1 Recombinant human cytoplasmic β – actin R62D protein purification

All the steps in this protocol were performed on ice. The cell pellets from step 2.7.1.1 were resuspended in 100 ml of Lysis buffer / 1L of insect cell culture (Hepes pH 7.5 20mM, NaCl 300mM, Imidazole 10mM, DTT 0.5mM, $CaCl_2$ 0.25mM, ATP 0.5mM, Protease inhibitor tablet – 1/50ml of lysis buffer) with addition of 2µl of Benzonase® Nuclease (Merck, E1014). Lysates were sonicated (2 cycles, 2min, 40%, cycles of 5 sec on – 5 sec off), followed by ultracentrifugation at 4ºC, 41000 rpm for 45 min using Beckman Coulter Rotor Ti-45. The supernatant was filtered with a 0.40µm cell strainer and incubated for 1 hour with 1 ml of Ni-NTA agarose (Quiagen, 30210) rotating at 4ºC. The supernatant was then transferred to a Chromabound column (FisherScientific, 730380) and the resin was washed twice using 10 CV of Buffer A. The protein was eluted from the resin using Buffer B and injected onto a Size Exclusion Chromatography column - HiLoad 16/60 Superdex 200 attached to ÄKTA pure™ chromatography system. The column was equilibrated with SEC buffer. The localization of the protein in the fractions was determined by SDS-PAGE (2.8.1) and Quick Coomassie (Generon, NB-45-00078-1L) staining of the gel to

visualize protein. The fractions were pooled and concentrated, followed by incubation with Ni-NTA agarose for 1h at room temperature. 50 µl of S-TEV protease (10mg/ml) was added to the protein bound to resin (the concentration of TEV based on 1L of insect cell culture) and incubated overnight at 4ºC, rotating. The cleaved protein was eluted from the beads by washing three times with Buffer A, concentrated and snap-frozen using liquid nitrogen. Protein concentration was determined using the ε_{290}=26,600 $M^{-1}cm^{-1}$ and calculated using Equation 2.

$$A = \boldsymbol{\varepsilon} * \mathbf{c} * \mathbf{l}$$

Equation 2. Lambert-Beer law calculation of protein concentration
A - absorption; ε - molar extinction coefficient in $M^{-1}cm^{-1}$; c - concentration in M; l - cell path length in cm

Buffer A:
25 mM Tris pH=8
500 mM NaCl
10 mM Imidazole

Buffer B:
25 mM Tris pH=8
500 mM NaCl
250 mM Imidazole

SEC Buffer:
20 mM Tris pH=8
150 mM NaCl
0.2 mM $CaCl_2$
0.2 mM ATP
0.5 mM DTT

2.7.1.2 Rabbit skeletal α-actin purification

Rabbit skeletal muscle actin was purified based on a protocol described in (Feuer and Molnar, 1948; Spudich and Watt, 1971).

Preparation of acetone powder from rabbit muscle

All steps were done at 4ºC unless stated otherwise. White muscle from rabbit leg was minced until homogenized. The homogenate was washed using the following buffers while vigorously stirring and the muscle tissue was drained by filtering through a gauze between each washing step:

- 2L 10 mM KCl (10 min)
- 2L 50 mM $NaHCO_3$ (10 min)
- 3L 1 mM EDTA
- 3.5L H_20 (5 min – swelling)
- 3.5L H_20 (5 min) – after this, next steps at room temperature
- 3.5L cold acetone (quickly)
- 2 volumes of acetone (10 min)
- 2 volumes of acetone (10 min)
- 2 volumes of acetone (10 min)

The homogenate was dried overnight by spreading out on 3MM Whatman paper under a fume hood, divided into 5 g aliquots and kept at -80ºC until further use.

Purification of actin from acetone powder

All steps were done at 4ºC unless stated otherwise. Rabbit skeletal α-actin was extracted from the acetone powder by rehydration in ice-cold G-buffer. This step was done overnight while stirring in the cold room.

G-buffer base
5 mM Tris pH=8
0.2 mM $CaCl_2$

G-buffer for rehydration
G-buffer base
0.2 mM ATP
0.5 mM DTT
0.15 mM PMSF

The rehydrated powder was filtered through four layers of gauze and collected into a fresh beaker. The powder was rehydrated again for 1h and filtered through gauze. The pooled filtrates were centrifuged at 27,000 rpm for 90 min, following which the supernatant is collected. Next step induces actin polymerization and is done under slow stirring in the cold room by addition of 1 mM ATP, 2 mM $MgCl_2$ and 50 mM KCl – incubate for 30 min. Solid KCl was added to a final concentration = 600 mM and incubated under stirring for 75 min in the cold room. Polymerized actin was pelleted by ultracentrifugation using Beckman Coulter Rotor Ti-45 at 100,000 x g for 90 min. The lens-resembling polymerized pellet was resuspended in G-base buffer with 0.5 mM ATP and 1 mM DTT followed by Dounce homogenization. Actin was dialyzed against G-buffer with ATP and DTT (buffer changed daily and concentrations adjusted accordingly):

Day 1: 0.5 mM ATP and 0.5 mM DTT
Day 2: 0.3 mM ATP and 0.5 mM DTT
Day 3: 0.2 mM ATP and 0.5 mM DTT
Day 4: 0.2 mM ATP and 0.5 mM DTT
Day 5: Mg+ G-buffer

Mg+ G-buffer
2mM Tris-HCl pH=8
0.2 mM ATP
0.5 mM DTT
0.2 mM EGTA
0.3 mM $MgCl_2$

Actin concentration was determined using the ε_{290}=26,600 $M^{-1}cm^{-1}$ (as described in 2.7.1.1). Latrunculin B (Sigma, 428020-5MG) was added at a 5-molar excess (5 mg of LatB / 5 g of acetone powder) and incubated overnight stirring in the cold room. Polymerization of unbound Actin-LatB was done by addition of 20X Initiation Buffer and incubation in the cold room stirring.

20X Initiation Buffer

2 M NaCl

10 mM ATP

60 mM $MgCl_2$

Actin filaments and any insoluble material was removed by ultracentrifugation at 200,000 x g for 15 min using Beckman Coulter rotor TLA 120.2. The protein was injected onto a Size Exclusion Chromatography column - HiLoad 16/60 Superdex 200 attached to ÄKTA pure™ chromatography system. The column was equilibrated with SEC buffer (20 mM Tris pH=8, 150 mM NaCl, 0.2 mM $MgCl_2$, 0.2 mM ATP and 0.5 mM DTT). The fractions containing actin were pooled, concentrated to 50 µM, aliquoted in 1.5 ml Eppendorf tubes, snap-frozen in liquid nitrogen and stored at -20ºC.

2.7.2 MRTF purification

2.7.2.1 Protein expression of MRTF in E.coli

Protein expression plasmids were transformed into Rosetta Competent cells (see 2.5.3) and a single colony was used for inoculation of Terrific Broth (made inhouse) supplemented with antibiotic. Cells were incubated at 37ºC shaking at 220 rpm until reaching OD=1.2-1.5, followed by addition of 0.5 mM IPTG to induce protein expression and incubated overnight at 18ºC shaking at 220 rpm. Cells were centrifuged at 3500 rpm for 15 min at 4ºC and the cell pellet was resuspended in Lysis buffer and snap-frozen in liquid nitrogen and stored at -80ºC until further manipulations.

Lysis buffer:

50 mM Tris pH=8

500 mM NaCl

1% v/v Triton X-100

0.1 mM PMSF

10 mM Imidazole

2.7.2.2 Protein purification of 1C-His6-MBP-TEV-MRTF

Cell lysates were prepared as described in 2.7.2.1. All steps were done at 4ºC unless stated otherwise. Lysates were thawed on ice and sonicated on ice for 2 cycles of 2 min at 45% amplitude. Cell lysates were centrifuged at 25,000 x g for 45 min for 1h. Following this step the protocol was divided into two methods depending on whether the protein was purified as a His6-MBP-fusion without cleavage, or as a TEV-cleaved final product.

Purification of His6-MBP-MRTF

Protein was purified using two-step automated protein purification protocol on ÄKTA pure™ chromatography system. In step one the lysate was loaded on 1 ml HisTrap HP column (Cytiva, 17524701) using a Sample pump, washed with Buffer A and protein was eluted in 9 CV using Buffer B into a 10 ml Capillary Loop. In step two the protein was injected onto HiLoad 26/600 Superdex 200 pg column equilibrated with Gel Filtration buffer. Protein fractions were pooled, concentrated, with concentration assessed by measuring A_{280} and snap-frozen in liquid nitrogen and stored at -80ºC.

Buffer A:
25 mM Tris pH=8
500 mM NaCl
10 mM Imidazole

Buffer B:
25 mM Tris pH=8
500 mM NaCl
250 mM Imidazole

Gel Filtration buffer:
20 mM Tris pH=8
250 mM NaCl
0.5 mM TCEP

Purification of MRTF cleaved with TEV-protease

The lysate was incubated with Ni-NTA agarose (1 ml / 1L bacterial culture) for 1h at 4ºC, then transferred to a Chromabound column and the resin was washed twice using 10 CV of Buffer A. Protein-bound Ni-NTA resin was resuspended in in Buffer A and transferred into a fresh tube. S-TEV was added (50 µl of 10 mg/ml / 1l of bacterial culture) and the resin was incubated overnight rotating at 4ºC. Protein was recovered from the beads using Buffer A, concentrated and injected on HiLoad 16/60 Superdex 200 column equilibrated with Gel Filtration buffer. Protein concentration was assessed as described in 2.8.3, the proteins were snap-frozen in liquid nitrogen and stored at -80ºC.

2.7.3 SRF.BDB purification

2.7.3.1 Protein expression of SRF in E.coli

Protein expression plasmids were transformed into Rosetta Competent cells (see 2.5.3) and a single colony was used for inoculation of LB supplemented with antibiotic. Cells were incubated at 37ºC shaking at 220 rpm until reaching OD=0.6, followed by addition of 0.5 mM IPTG to induce protein expression and incubated overnight at 18ºC shaking at 220 rpm. Cells were centrifuged at 3500 rpm for 15 min at 4ºC and the cell pellet was resuspended in Lysis buffer and snap-frozen in liquid nitrogen and stored at -80ºC until further manipulations.

Lysis buffer:
50 mM Tris pH=8
300 mM NaCl
0.5 mM EDTA
0.1 mM PMSF
0.5 mM TCEP

2.7.3.2 Purification of SRF.DBD

Cell lysate prepared in 2.7.3.1 was thawed and sonicated on ice in 6 cycles of 1 min at 45% amplitude and centrifuged at 25,000 x g for 45 min at 4ºC. The lysate was submitted to Anion Exchange Chromatography by using Q

Sepharose Fast Flow resin (Merck, GE17-0510-10) (0.5 ml /1L bacterial culture) and the flow-through was collected. It was incubated with GST-resin (Cytiva, 17075601) for 1h rotating at 4ºC, then transferred to a Chromabound column and the resin was washed twice using 10 CV of Buffer 1 and twice using Buffer 2. Resin was collected in Buffer 2 and 3C-protease was added (10 µl of stock / 1L culture) and the protein-bound resin was incubated overnight rotating at 4ºC.

Buffer 1
50 mM Tris pH=8
300 mM NaCl
0.5 mM EDTA
0.1 mM PMSF
0.5 mM TCEP

Buffer 2
50 mM Tris pH=8
500 mM NaCl
0.5 mM EDTA
0.1 mM PMSF
0.5 mM TCEP

Protein was recovered from the beads, concentrated and diluted 2X with Buffer 1 to reduce the salt concentration from 500 mM NaCl to 250 mM NaCl. A Cation Exchange was done using ResourceS column (Cytiva, 17118001) to remove any DNA bound to SRF. Protein was injected on the column equilibrated with Buffer A' and eluted with a gradient of 0-100% Buffer B'.

Buffer A'
25 mM Hepes pH=7.5
250 mM NaCl
0.5 mM EDTA
0.5 mM TCEP
0.1 mM PMSF

Buffer B'

25 mM Hepes pH=7.5

1.5 M NaCl

0.5 mM EDTA

0.5 mM TCEP

0.1 mM PMSF

Fractions containing the protein were pooled and injected onto Superdex^{TM} 75 10/300 GL column (Cytiva, 17-5174-01) equilibrated with Gel Filtration' buffer. Protein fractions were pooled, concentrated, snap-frozen in liquid nitrogen and stored at -80ºC.

Gel Filtration Buffer'

25mM Tris pH=8

100mM NaCl

0.1mM EDTA

0.5mM TCEP

0.1mM PMSF

2.8 Protein analysis

2.8.1 SDS-PAGE Electrophoresis

Proteins were separated based on their size by SDS-Polyacrylamide Gel Electrophoresis (SDS-PAGE) using NuPAGE™ 4-12% Bis Tris Protein Gels (ThermoFisher, NP0321BOX). Samples were prepared with 4X Laemmli buffer, incubated at 95ºC for 5 min, loaded onto the gel and run at 120-150V in MOPS buffer (Merck, NP0001). Gels were either stained using Quick Coomassie (for protein purification visualization purposes) or were submitted to Western Blotting.

2.8.2 Western Blotting

Proteins were transferred onto a 0.45 μm nitrocellulose membrane (Amersham, 10600003) by Western blotting. A wet transfer method was used where the gel and nitrocellulose membrane were sandwiched between two layers of Whatmann 3MM blotting paper (ThermoFisher, 12668356). The transfer was run for 90 min at 200 mA in 1x Transfer Buffer (10% methanol, 192 mM glycine, 25 mM Trizma Base). The membranes were incubated with 3% BSA (Sigma, A7030-100G) in TBS-T (0.05 M Tris pH=7.5 , 0.15 M NaCl with 1% v/v Tween-20) for 1h rotating at room temperature. Incubation with primary antibodies in 3% BSA in TBS-T was done overnight at 4ºC. Membranes were washed three times with TBS-T, followed by 1h incubation with secondary antibodies diluted in 3% BSA in TBS-T (protected from light) at room temperature, washed three times with TBS-T and developed using Oddyssey CLx (Licor).

2.8.3 Quantification of protein concentration using Standard Curve

For proteins with low content of aromatic amino-acids determination of protein concentration using A280 is not reliable. Protein concentration calculated from a linear equation of a Standard Curve. SC samples were prepared using BSA (SC concentrations in ng/μl: 200, 400, 600, 800, 1000) and run on SDS-PAGE electrophoresis alongside the protein sample of interest. The gel was stained with Quick Coomassie and the intensity of the corresponding bands was used to generate a SC linear equation ((x) SC protein concentration, (y) band intensity).

2.9 Affinity measurement assays

2.9.1 Octet Biolayer Interferometry Assay (BLI)

Affinity measurement of MRTF derivatives binding actin was done using the His6-MBP-MRTF protein and LatB-rabbit skeletal α-actin on the Octet Red96 (ForteBio) machine. All the protein manipulations were done in Octet Buffer. MRTF was immobilized on Ni-NTA sensor (VWR, 733-2142) using a

concentration of 50 ng/µl and the MRTF-loaded biosensors were incubated with actin at different concentrations (0.3125 µM, 0.625 µM, 1.25 µM, 5 µM, 10 µM and 20 µM). For the determination of the K_d of binding steady state analysis was used by plotting the Response at equilibrium (y) over Actin concentration (x). Equation 3 was used to calculate the K_d of binding for high-affinity binding of MRTF derivatives.

$$y = \frac{Rmax * x}{(Kd + x)}$$

Equation 3. Kd calculation based on Rmax value in the Octet assay

For MRTF derivatives with low affinity of binding, a range K_d was generated by constraining the R_{max} in Equation 3 to the value of a high-affinity binder (Rmax = ~1). This is made under the assumption that given high enough concentration of ligand (actin), MRTF would be able to reach the Rmax of the high-affinity binder. Binding curves were stimulated using constant Rmax which allowed for determining a range of Kd values based on whether a curve could be fitted over the data points collected.

Octet Buffer:
20 mM Tris pH=8
150 mM NaCl
0.1% Tween-20
1 mg/ml BSA
0.5 mM TCEP

2.9.2 Fluorescence Polarization Anisotropy assay (FP)

FITC-conjugated RPEL2 peptide generated by the Cancer Research UK peptide synthesis facility was used for affinity measurement of LatB-rabbit skeletal α-actin and human β-cytoplasmic actin R62D. The reaction was prepared in 10 µl final volume with FITZ-RPEL2 peptide at 100 nM and actin serial dilution with a top concentration of 20 µM by diluting the proteins and peptide in SEC buffer (2.7.1.1).

The plates were read immediately after assembly of the reaction using the BMG Labtech CLARIOstar Plus microplate reader. Anisotropy values were calculated using the raw values of fluorescent intensities parallel and perpendicular to the excitation plane, respectively (Equation 4). The binding constants were calculated in GraphPad Prizm 8 software using Equation 5.

$$Anisotropy = \frac{(\boldsymbol{I}parallel - \boldsymbol{I}perpendicular)}{(\boldsymbol{I}parallel + 2 * \boldsymbol{I}perpendicular)} * 1000$$

Equation 4. Calculation of Anisotropy in FP assay

$$A = Af + (Ab - Af) * (Kd + L + C - \frac{(Kd + L + C)^{0.5}}{2 * L})$$

Equation 5. Binding constants (K_d) calculation in FP assay
A - anisotropy measured; Af - anisotropy of free peptide; Ab - anisotropy of bound peptide; L -labelled peptide concentration; C - protein concentration (X axis); Kd - binding constant.

2.10 DNA pulldown assay

The DNA pulldown assay was assembled using purified components: cleaved HA-MRTF 2-404 derivatives (2.7.2.2), SRF.DBD (2.7.3.2), human cytoplasmic β-actin R62D (2.7.1.1) and DNA oligonucleotide (Table 15).

c-fos (T)	5′ CGTCAATCCCTCCCCCCTTACACAGGATGTCCATATTAGGACATCTGCGTCAGCAGGTTTCCACGGCCGG 3′
c-fos (B)	5′ CCGGCCGTGGAAACCTGCTGACGCAGATGTCCTAATATGGACATCCTGTGTAAGGGGGGAGGGATTGACG 3′
mcm1 (T)	5′ CGTCAATCCCTCCCCCCTTACACAGGATGTCCCAATCGGGACATCTGCGTCAGCAGGTTTCCACGGCCGG 3′
mcm1 (B)	5′ CCGGCCGTGGAAACCTGCTGACGCAGATGTCCCGATTGGGACATCCTGTGTAAGGGGGGAGGGATTGACG 3′

Table 15. Sequence of DNA oligonucleotides used in DNA pulldown assay
C-fos promoter sequence of the top (T) and bottom (B) strand, mcm1 promoter sequence of the top (T) and bottom (B) strand. Biotin tag on the bottom strand of both at 3'. Synthetized and purified by HPLC (Merck).

Dynabeads™ M-280 Streptavidin (Invitrogen, 11206D) (30 µl / reaction) were washed twice with 1X DW buffer, resuspended in 0.5X DW buffer and incubated with 1 µg of DNA / reaction for 30 min rotating at room temperature.

The beads were washed three times with 1X DW buffer, once with TE/NP-40 buffer and once with 1X Buffer G and incubated with SRF.DBD (Binding reaction in 200µl: 40 nM SRF.DBD, 1.5 mM Spermidine, 1 µg Poly[d(I-C)], 2X Buffer G, Water) for 20 min at 30ºC shaking at 500 rpm. Beads were washed three times with 1X Buffer G and incubated with HA-MRTF (Binding reaction in 200µl (water volume adjusted to include actin volume in reaction: 50 nM HA-MRTF, 1.5 mM Spermidine, 1 µg Poly[d(I-C)], 2X Buffer G, Water + actin at 0.4 µM, 0.8 µM and 1.6 µM). Beads were incubated for 20 min at 30ºC shaking at 500 rpm, and the supernatant of the reaction was transferred to clean Eppendorf tubes for a later step of HA-Immunoprecipitation. The beads were washed three times with 1X Buffer G, 1X Laemmli buffer was added, and the samples were incubated for 5 min at 95ºC. The proteins were recovered from the beads and run on SDS-PAGE followed by Western Blotting using α-HA and α-pan-actin antibody (Table 4).

For the HA-Immunoprecipitation, the supernatant of the HA-MRTF – actin binding reaction indicated in the steps above was incubated with anti-HA magnetic beads (ThermoFisher, 88837) for 30 min at room temperature shaking at 500 rpm. The beads were washed three times with 1X Buffer G, 1X Laemmli buffer was added and the samples were incubated for 5 min at 95ºC. The proteins were recovered from the beads and run on SDS-PAGE followed by Western Blotting using α-HA and α-pan-actin antibody (Table 4).

1X DW buffer
20 mM Tris-HCl pH=8
2M NaCl
0.5 mM EGTA
0.03% NP40

TE/NP-buffer
10 mM Tris-HCl pH=8
1 mM EDTA
0.02% NP40

2X Buffer G
20 mM Tris-HCl pH=8
3 mM MgCl2
200 mM NaCl
0.4 mM EGTA
0.04% NP-40
20 mM DTT

2.11 Hydrogen-Deuterium Mass Spectrometry (HDX-MS)

For the HDX-MS analysis, cleaved MRTF proteins were prepared alone and with LatB-rabbit skeletal α-actin. The samples were assayed either at five molar excess of actin (25 µM) with 5 µM MRTF. For actin titration on MRTF 2-404 WT actin was used at 25µM, 5µM, 1.5µM and 0.5µM. For actin titration on MRTF 2-404 GP171/172ER actin was used at 25µM, 10µM, 5µM and 1.5µM. Samples were diluted in Gel Filtration buffer (2.7.1.1) and the concentration of ATP and DTT was adjusted to match the Gel Filtration buffer.

HDX reaction, data acquiring and processing as described in the below protocol was done by Sarah Maslen (Crick Proteomics STP).

The samples were incubated with 40 µl of D_2O buffer on ice for 2 sec and at room temperature for 3 and 30 seconds (in triplicate). The labelling reaction was quenched by addition of chilled 2.4% v/v formic acid in 2M guanidinium hydrochloride and snap-frozen in liquid nitrogen. Samples were stored at -80°C prior to analysis. The samples were rapidly thawed and subjected to proteolytic cleavage by pepsin, followed by Reversed-phase HPLC separation. Briefly, the protein was passed through an Enzymate pepsin column (Waters, 186007233) at 200 µl/min for 2 min and the peptic peptides were trapped and desalted on a 2.1 x 5 mm C18 trap column (Acquity BEH C18 Van-guard pre-column, 1.7 µm; Waters, 186003975). Trapped peptides were subsequently eluted over 11 min using a 5-43% gradient of acetonitrile in 0.1% v/v formic acid at 40 µl/min. Peptides were separated on a reverse phase column (Acquity UPLC BEH C18 column 1.7 µm, 100 mm x 1 mm; Waters, 186002346). Peptides were detected on a Cyclic mass spectrometer (Waters, UK) acquiring over a *m/z* of 300 to 2000, with the standard electrospray ionization (ESI) source and lock mass

calibration using [Glu1]-fibrino peptide B (50 fmol/µl). The mass spectrometer was operated at a source temperature of 80°C with a spray voltage of 3.0 kV. Spectra were collected in positive ion mode.

Peptide identification was performed by MS^e (Silva et al., 2005) using an identical gradient of increasing acetonitrile in 0.1% v/v formic acid over 12 min. The resulting MS^e data were analysed using Protein Lynx Global Server software (Waters, UK) with an MS tolerance of 5 ppm. Mass analysis of the peptide centroids was performed using DynamX software (Waters, UK). Only peptides with a score >6.4 were considered. The first round of analysis and identification was performed automatically by the DynamX software; however, all peptides (deuterated and non-deuterated) were manually verified at every time point for the correct charge state, presence of overlapping peptides, and correct retention time. Deuterium incorporation was not corrected for back-exchange and represents relative, rather than absolute changes in deuterium levels. Changes in H/D amide exchange in any peptide may be due to a single amide or several amides within that peptide. All time points in this study were prepared at the same time and individual time points were acquired on the mass spectrometer on the same day.

2.12 AlphaFold Structure prediction

AlphaFold2-Multimer structure prediction was generated using (“AlphaFold open-source code. https://github.com/deepmind/alphafold,” n.d.)on the internal Crick High-Performance Computing platform (HPC). Sequences in FASTA format of mouse MRTF RPEL3 + C (residues 155-404), MRTF (residues 2-404), MRTF GP171/172ER (residues 2-404) and human cytoplasmic β-actin (residues 1-375) were provided. The output was 15 relaxed protein predictions, ranked by the software in the order of confidence, with files encoding pLDDT and PAE provided in PKL format. Protein structure analysis was done using UCSF Chimera which allows for visualization of pLDDT values on the amino-acid sequence in the prediction. Figure generation was done using PyMOL.

AlphaFold3 structures were generated on the AlphaFold server (https://alphafoldserver.com/). Sequences used: SRF.DBD (132-222), MRTF

(residues 2-404), *c-fos* DNA (70bp, see Table 15), MRTF B-box & Q-box (residues 305-404) and human cytoplasmic β-actin (residues 1-375). The output was of 5 protein predictions, with JSON files provided containing the pLDDT and PAE data. Analysis and processing were done as described for AF2-Multimer.

Chapter 3. In vitro reconstitution of MRTF-DNA-SRF binding and MRTF-actin interactions

Previous studies have shown that G-actin controls not only MRTF's subcellular localization, but also its activity in the nucleus (Vartiainen et al., 2007). G-actin regulates MRTF nuclear accumulation in two ways: it prevents Importin α/β binding to the Nuclear Localization Signal (NLS) within the RPEL domain, and G-actin binding to the RPEL domain is required for Crm1-dependent export of MRTF (Panayiotou et al., 2016; Pawłowski et al., 2010; Vartiainen et al., 2007).

Several lines of evidence indicate a role for actin in regulation of MRTF activity in the nucleus. When MRTF is sequestered in the nucleus after treatment of cells with LMB, which inactivates the exportin Crm1, MRTF is still responsive to changes in actin dynamics – a decrease in DNA binding and gene expression is observed (Gualdrini, 2016, PhD Thesis; Toteva, 2021, PhD Thesis; Vartiainen et al., 2007). MRTF constructs localized to the nucleus by fusion to an NLS signal still respond to fluctuations in G-actin levels (Gualdrini, 2016, PhD Thesis; Toteva, 2021, PhD Thesis). Additionally, treatment of cells with LatB, which increases the pool of G-actin in the cell inhibit MRTF-DNA binding (Gualdrini, 2016, PhD Thesis; Toteva, 2021, PhD Thesis).

The possible mechanism of this inhibitory regulation remains unclear. MRTF-actin binding occurs within the RPEL domain, around 200 residues N-terminal to the B region crucial in SRF interaction. How does then actin binding to MRTF its interaction with SRF (Figure 26A)?

Two possible models can be proposed for how actin inhibits MRTF-SRF interaction (Figure 26B). First, actin binds an additional actin binding site within the C-terminus of MRTF, possibly in the B-Q region crucial for SRF binding. This might either prevent interaction with SRF or sequester SRF into an inhibited complex that cannot bind DNA. The latter is unlikely, as the inhibition is MRTF dependent and SRF targets are not inhibited. In the second proposed model, sequences C terminal to the RPEL domain, including B and Q, are

recruited into the RPEL domain/actin complex, thereby preventing MRTF-SRF interaction with DNA (Figure 26).

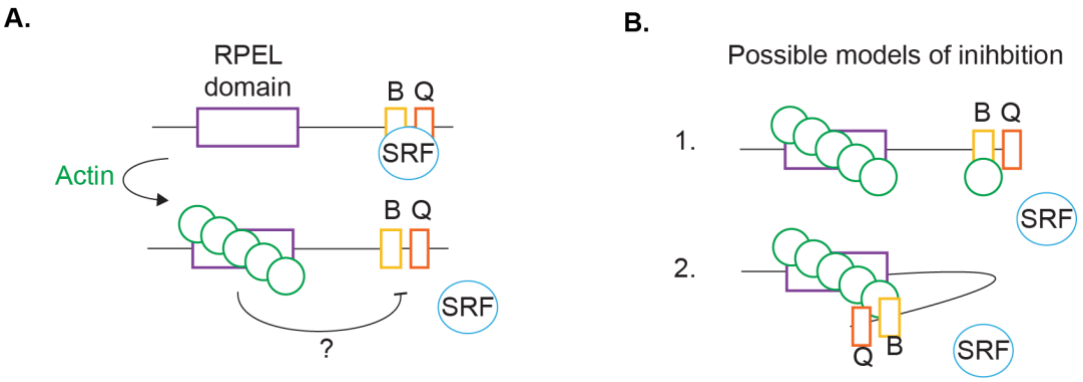

Figure 26. Schematic representation of actin inhibition of MRTF-SRF-DNA binding **A.** Schematic representation of actin inhibition of MRTF-SRF binding. **B.** Two possible models of how actin binding to MRTF inhibits SRF binding.

3.1 Experimental approach

DNA pulldown experiments show that actin inhibits MRTF-SRF interaction (Gualdrini, 2016, PhD Thesis), but it is not clear whether the interaction is direct, or if there are other proteins involved. I therefore set out to establish the simplest possible system in which actin could inhibit MRTF-SRF interaction using purified components. Such an assay would allow for mapping of the MRTF sequences involved in the inhibition.

3.1.1 Monomeric HA-MRTF-A 2-404 protein

Previously, a full length MRTF purification was attempted by expression using baculovirus (Gualdrini, 2016, PhD Thesis). This approach poses challenges due to its size (1022aa) and dimerization properties. The fact that MRTF is an intrinsically disordered protein makes it hard to purify and it aggregates in solution. Expression in insect cells is also complicated by MRTF co-purifying with actin.

MRTF binds as a dimer to SRF on DNA in cells. For this assay, I used a monomeric MRTF derivative, expressed in bacteria. The founding member of the MRTF family, Myocardin, binds as a monomer, and monomeric MRTF derivatives, which lack the Leucine Zipper sequences can still bind SRF on

DNA, although less efficiently than the intact protein (Miralles et al., 2003; Zaromytidou et al., 2006).

I decided to use the N-terminal fragment of MRTF-A (residues 2-404). This contains the actin-binding RPEL domain and the B and Q regions required for interaction with SRF and DNA. MRTF-A (2-404) was expressed as an N-terminal HIS_6-MBP fusion that maintains protein solubility during purification, and an N-terminal HA-tag to allow detection by immunoblotting (Figure 27A). After association of the protein with Nickel beads (NI-NTA), the protein can be recovered in soluble form, by cleaving the HIS_6-MBP tag with TEV-protease.

3.1.2 Monomeric SRF-DNA binding domain

For SRF purification I followed the same approach of simplifying the interaction and only using the minimal fragment needed for both MRTF and DNA interaction. I used the SRF-DBD (DNA-binding domain) core domain (residues 132-222) ((Norman et al., 1988; Pellegrini et al., 1995), which has been shown to be sufficient for both DNA and MRTF binding (Miralles et al., 2003; Zaromytidou et al., 2006). SRF-DBD was expressed as an N-terminal GST-fusion (Figure 27B), cleaving the tag using 3C-protease on GST resin.

3.1.3 CArG box containing oligonucleotide

SRF binds to a specific Response Element (SRE) sequence on its targets (Treisman, 1995, 1986), with a consensus sequence $CC(A/T)_6GG$, referred to as a CArG box. In the ternary complex with MRTF, however, additional contacts are apparently made by MRTF with the DNA within 30 base pairs relative to the SRF dyad (Zaromytidou et al., 2006). For DNA pulldown experiments I used a 70bp double stranded oligonucleotide derived from the c-fos SRE region (Figure 27C), with Biotin tag on the 3'end of the bottom strand, allowing its attachment to streptavidin beads for use in the DNA pulldown assay.

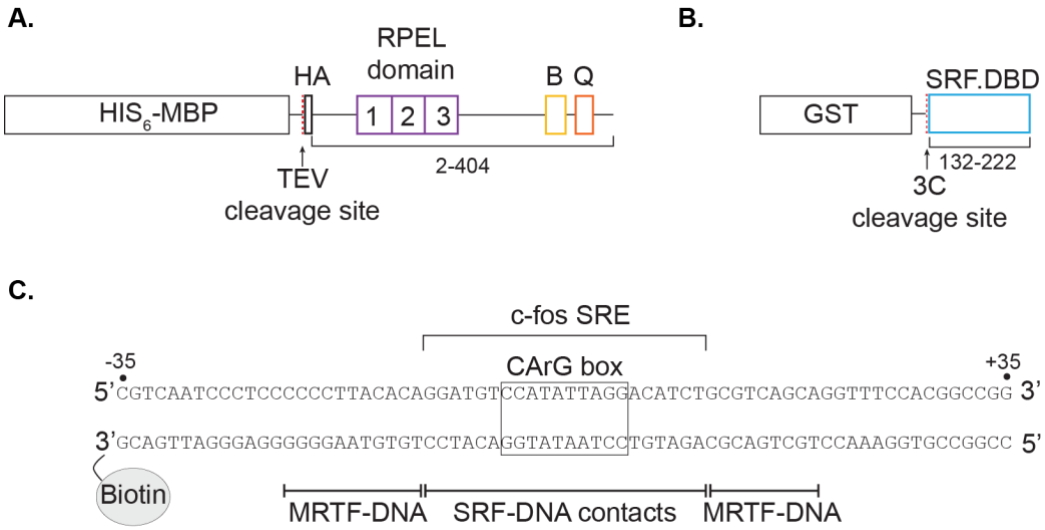

Figure 27. Schematic representation of the DNA pulldown assay components
A. 6xHIS/MBP-MRTF 2-404 fusion with an HA N-terminal tag, cleaved by TEV protease. **B.** GST-SRF.DBD 132-222 fusion, cleaved by 3C protease (DBD-DNA binding domain). **C.** Double-stranded oligonucleotide with the CArG box in the middle. The top strand is untagged, whereas the bottom strand has a Biotin tag on the 3' end to allow recovery with Streptavidin magnetic beads.

3.1.4 Monomeric Actin

Actin purification presents technical difficulties, as it polymerizes at low salt concentrations. Moreover, because correct folding of actin requires the CCT chaperonin, production in bacteria is not feasible. The structure of G-actin alone is unclear, as all the crystal structures were resolved with actin binding proteins, drugs preventing polymerization or with C-terminal modifications (Dominguez and Holmes, 2011).

To generate monomeric actin, many studies utilize α-actin purified from rabbit skeletal muscle acetone powder (Feuer and Molnar, 1948; Spudich and Watt, 1971) and bound to LatB to prevent polymerization (Figure 28A). LatB binds between subdomains 2 and 4 of actin, preventing flattening of the molecule into F-actin conformation and keeping it in monomeric state (Morton et al., 2000). While α-actin differs from the β and γ-cytoplasmic actins that are implicated in MRTF regulation, functional and structure-based experiments indicate that it interacts in a similar manner with MRTF (Mouilleron et al., 2011, 2008).

In recent years methods for expression and purification of recombinant actin have been developed, allowing for expression of all actin isoforms in yeast, insect cells or cultured mammalian cells. The problem of purification has been solved by expressing actin fused to C-terminal β-thymosin moiety, which stabilizes actin in its monomeric form during purification, but does not interfere with folding (Noguchi et al., 2007). Following purification, β-thymosin is removed using Chymotrypsin, which cleaves at the C-terminal phenylalanine. This actin can be used in biochemical assays in no-salt conditions and for polymerization studies. Unfortunately, chymotrypsin also cleaves internally generating small amounts of lower molecular products, known as “split” actin (Konno, 1987). To circumvent this, actin has been purified as an N-terminal HIS_6-tag fusion, with a partial TEV cleavage site before the N-terminal methionine, allowing purification of tag-free recombinant actin using baculovirus expression (designed based on Ceron et al., 2022) (Figure 28B).

Although both methods above allow for purification of recombinant actin, it still polymerizes and needs to be complexed with LatB to keep it in monomeric form. To rectify this, I introduced an R62D mutation into cytoplasmic human β-actin. R62 is localized in the salt bridge between subdomains 2 and 4, and its mutation to aspartate disrupts the interaction, stabilizing actin in a monomeric form (Posern et al., 2002).

Most of the biochemical assays I use in this thesis, such as affinity measurements and binding assays require G-actin in salt containing buffers, which is why I compared the LatB rabbit skeletal α-actin with the cytoplasmic human β-actin R62D purified using the TEV-cleavage protocol. While α-actin can be purified at high yield and is stable when bound to LatB, it also has PTMs and can dissociate from LatB at high protein concentrations. In contrast, R62D β-actin is more biologically relevant, does not require LatB-binding to maintain it in G-actin state and there are no PTMs (it still has the N-terminal Met), but the expression yields are lower.

I compared the ability of the two actins to bind the RPEL motif using a fluorescence polarization anisotropy assay (FP). LatB-rabbit skeletal α-actin and recombinant R62D β-actin both bind to FITZ-conjugated RPEL2 with similar

K_d of around 2µM. Addition of LatB to the recombinant R62D actin did not change the affinity of binding (Figure 28C).

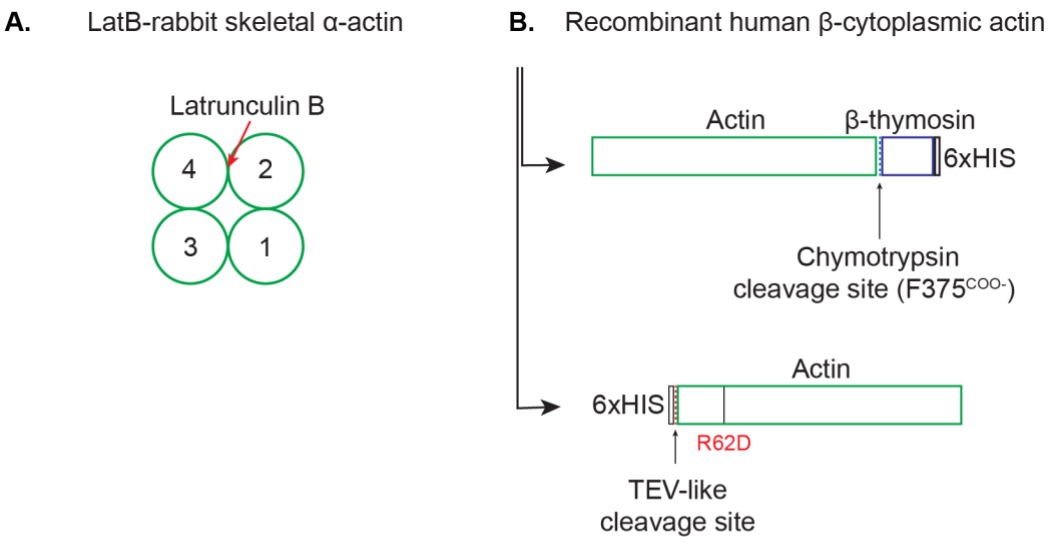

C.

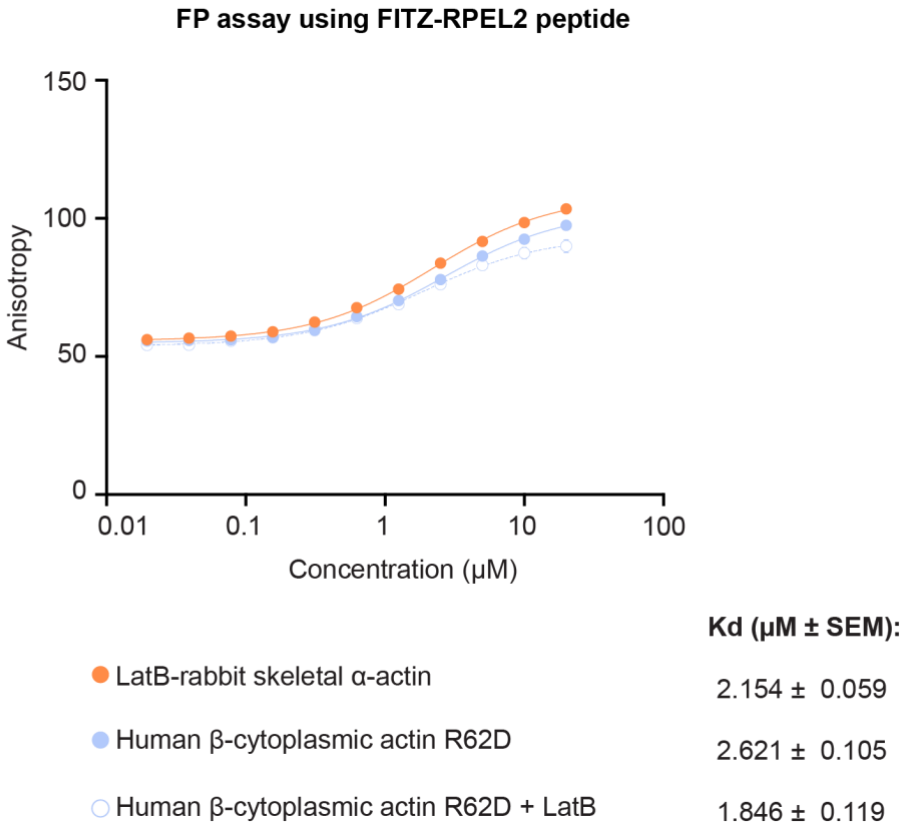

Figure 28. LatB-α-actin and R62D β-actin bind RPEL with similar affinities
A. A schematic representation of actin subdomains (1-4). Latrunculin B binding between subdomains 1 and 2. **B.** Two approaches for expression of recombinant human cytoplasmic β-actin in eukaryotic cells. Top: actin C-terminal fusion to β-thymosin which prevents polymerization during purification. Chymotryptic cleavage site after actin F375 Bottom: N-terminal HIS_6 fusion with added partial TEV cleavage site. The non-polymerizable R62D mutation in subdomain 4, prevents the formation of the salt bridge between subdomains 2 and 4. **C.** Fluorescence polarization anisotropy assay (FP) using FITZ-RPEL2 peptide and two sources of monomeric actin: LatB-Skeletal muscle actin and Human β-cytoplasmic actin R62D with or without LatB. The assay was done using 100nM peptide and actin with a concentration range between 0.02µm-20µM. (n=1, technical replicates=4).

3.1.5 DNA pulldown assay

To assess the inhibitory effect of actin on DNA-SRF-MRTF binding, I used the DNA pulldown assay *in vitro*. Biotinylated DNA was immobilized on streptavidin-coated magnetic beads and incubated for 30min, followed by addition of SRF and 20min incubation. After washing the beads to remove any excess SRF, MRTF was added, followed by addition of actin at increasing concentration. The binding reaction was then incubated for additional 20min, following which the beads were recovered and the associated proteins analysed by Western Blotting. Detection of MRTF was done by using α-HA antibodies (N-terminal HA-tag on MRTF) and actin using α-pan actin antibody (Figure 29, top).

3.1.6 HA IP assay

To test whether MRTF can bind to actin in solution, I used the N-terminal tag on MRTF to immunoprecipitated MRTF from the DNA pulldown reaction, after assembly of the complex on the streptavidin beads (Figure 29). Excess HA-MRTF in the supernatant was immunoprecipitated using HA-beads and analysed by Western blotting, to assess the ability of MRTF to bind actin in solution.

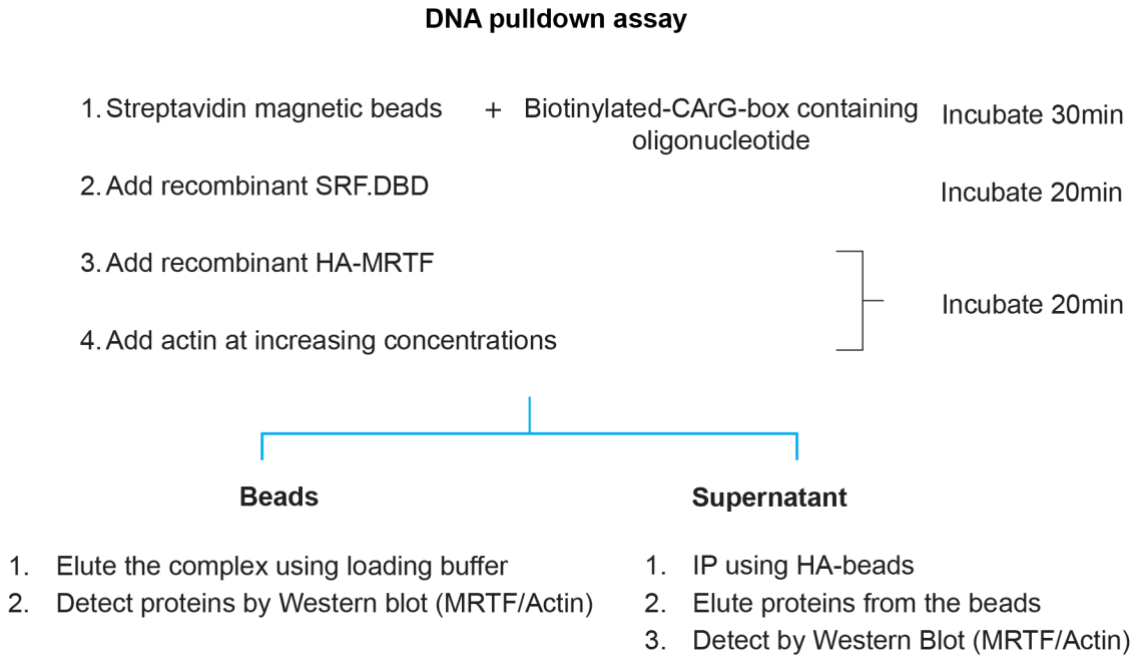

Figure 29. Assembly of the DNA pulldown assay
Flow chart of the DNA pulldown assay. DNA was bound to streptavidin beads, followed by incubation with SRF. Next, the beads were washed, MRTF was added, followed by actin titration. The beads were recovered, and the supernatant was used for an HA-IP using HA-magnetic beads. Next, both sets of beads were washed, resuspended in SDS-PAGE loading buffer and the samples were analysed by SDS-PAGE and Western Blotting.

3.1.7 Setting up the DNA pulldown assay

Although MRTF makes contacts with DNA when bound to SRF, it does not stably bind to DNA in the absence of SRF (Zaromytidou et al., 2006). SRF-DNA binding results in DNA bending, which facilitates consequent MRTF - DNA binding (Pellegrini et al., 1995; Zaromytidou et al., 2006). Consistent with this, MRTF recovery in the DNA pulldown assay required the presence of SRF in the reaction (Figure 30, Lane 1).

The reaction conditions were set with 21pmoles of DNA and 4pmoles of SRF, effectively saturating SRF with DNA. MRTF was used at three concentrations, using 3, 10 and 30 pmole of the protein.

Mutation of SRF binding site on DNA substantially lowered MRTF recovery (Figure 30, Lane 8-10 - compare with Lanes 3-5), which remained SRF dependent (Figure 30, Lane 6). The residual recovery presumably reflects the very high concentrations of SRF and DNA used in the assay.

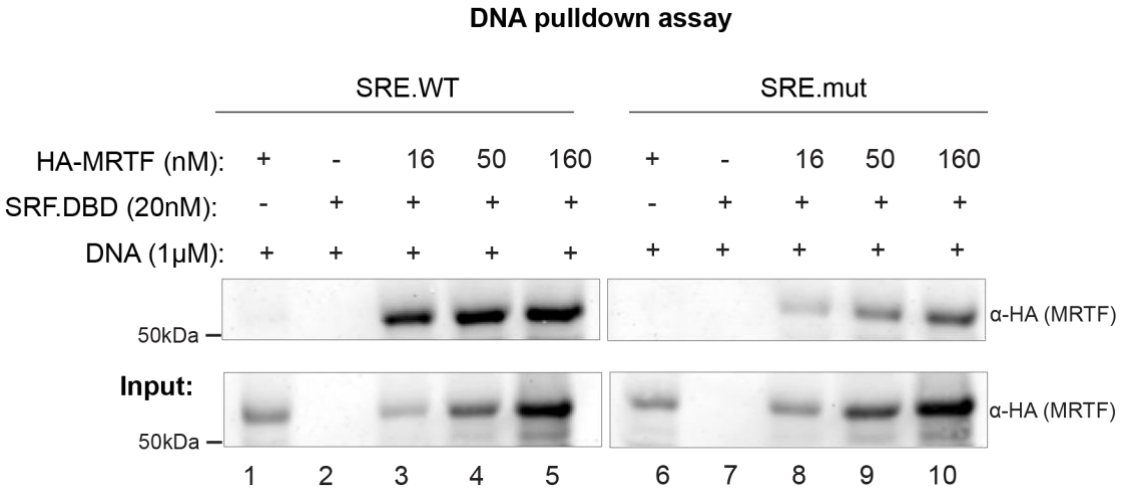

Figure 30. Recovery of MRTF on DNA is SRF specific
A control DNA pulldown assay, where two oligonucleotide sequences were used to check specificity of binding. Lanes 1-5: SRE.WT (CCATATTAGG) and Lanes 1-5 SRE.mut (CCCAATCGGG) (Hill and Treisman, 1995; Wagner et al., 1990). DNA was used at 21pmole/reaction, SRF.DBD at 4pmole/reaction, HA-MRTF 2-404 at 3pmole/reaction (+), 10 pmole/reaction (++) and 30 pmole/reaction (+++).

3.2 Actin-RPEL domain interaction is crucial for inhibition of DNA binding

MRTF interaction with SRF and DNA can be disrupted by increasing the concentration of actin in the system. This has been shown previously in *in vivo* experiments, whereby increasing the available pool of monomeric actin in cells by treatment with LatB, MRTF was less efficiently detected on DNA in ChIP assay (Gualdrini, 2016, PhD Thesis). This DNA-binding inhibition is dependent on the ability of the RPEL domain to bind to actin. Introduction of a loss of contact mutation to each of the RPEL motifs (MRTF 123-X: R81A, R125A, R169A, also referred to as MRTF XXX) (Guettler et al., 2008; Mouilleron et al., 2011) which substantially lowers actin binding affinity, renders MRTF insensitive to actin and no DNA-binding inhibition is observed *in vivo* (Gualdrini, 2016, PhD Thesis) (Figure 25).

After establishing the conditions necessary for MRTF binding to SRF and DNA *in vitro*, I tested both LatB-rabbit skeletal α-actin and recombinant human β-actin R62D in the assay. While increasing LatB α-actin concentrations inhibited MRTF-SRF interaction, actin could be recovered in the DNA pulldown (Figure 31A). This was not dose dependent and was not seen when human

R62D β-actin was used in the assay (Figure 31B). I have not investigated the basis for this, but it may reflect the dilution of the LatB α-actin in the assay, leading to polymerization and sedimentation with the beads. Since the R62D β-actin performed consistently, I decided to use it for this assay.

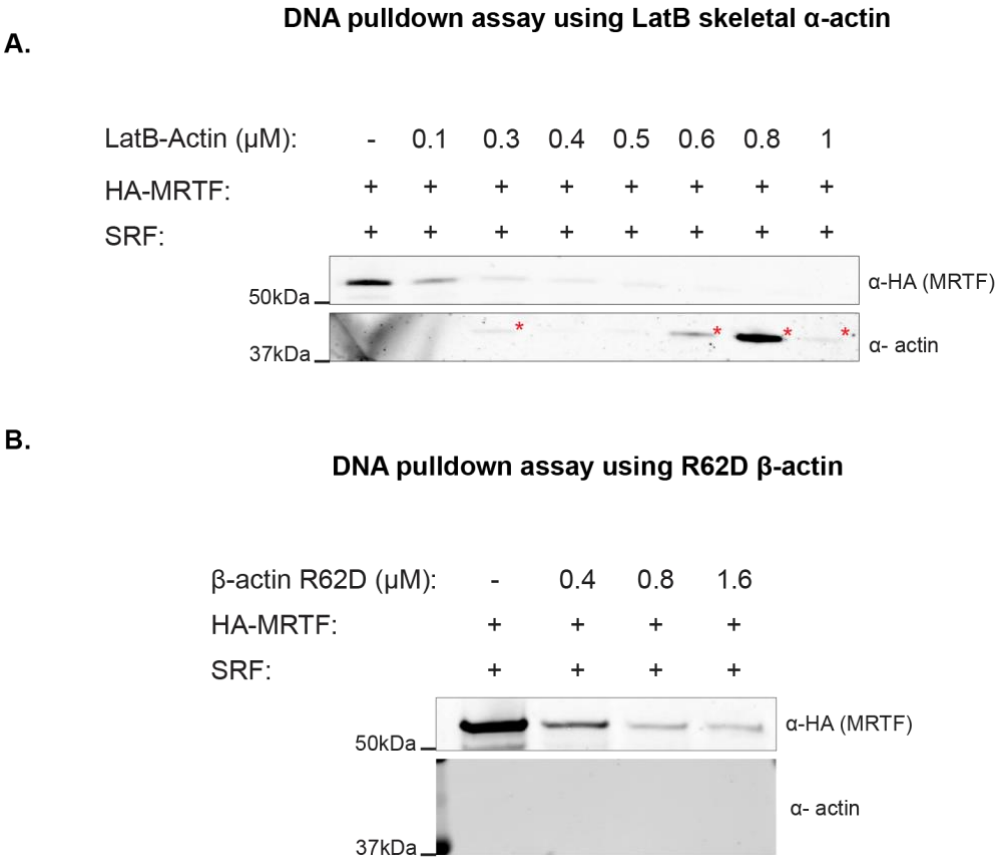

Figure 31. MRTF-SRF binding inhibited by both LatB-α-actin and R62D β-actin
A. DNA pulldown assay done using LatB-rabbit skeletal muscle actin. DNA at 21pmole/reaction, SRF - 1pmole/reaction, MRTF - 6pmole/reaction. Red asterisks indicated actin detected on beads in the reaction **B.** DNA pulldown assay done using Human cytoplasmic β-actin R62D. DNA at 21pmole/reaction SRF - 4pmole/reaction, MRTF at 10pmole/reaction. MRTF was detected using anti-HA antibody, actin was detected using anti pan-actin antibody.

MRTF-DNA binding is inhibited by increasing the concentration of actin in the solution. Actin can also be recovered by immunoprecipitation of the supernatant, together with MRTF (Figure 32A). I used the MRTF (XXX) mutant to investigate whether the inhibition required MRTF-actin interaction. Recovery of MRTF (XXX) in the DNA pulldown was insensitive to inclusion of actin in the

reaction and as expected actin was not recovered in HA-IP (Figure 32B). This shows that DNA binding inhibition of MRTF is dependent on its ability to bind actin.

As one of the proposed models of inhibition was actin biding to sequences C-terminal to RPEL domain, we decided to introduce a loss of contact mutation (R169A) to RPEL3, which is on the 3’ end of the RPEL domain. In contrast to MRTF WT, MRTF 12X recovery in the DNA pulldown was much less sensitive to actin, and recovery of MRTF from the pulldown supernatant was also diminished (Figure 32C).

The decreased effectiveness of actin inhibition by MRTF 12X, coupled with reduced recovery from solution is consistent with RPEL3 facilitation of cooperative actin binding to form the pentavalent RPEL-actin complex (Mouilleron et al., 2011). It should be considered that RPEL3-actin directly contacts C terminal sequence in the SRF-interacting region. Such a situation is seen in another member of the RPEL-family of actin regulated proteins, ArhGAP12, where RPEL-actin binding is significantly increased in the presence of the C-terminal GAP domain, which makes additional contacts with RPEL-bound actin (Diring et al., 2019).

A.

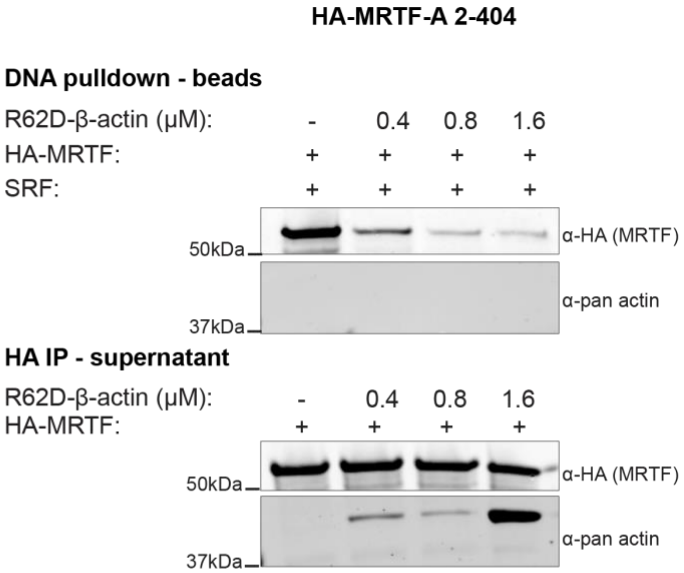
HA-MRTF-A 2-404
DNA pulldown - beads
R62D-β-actin (μM): - 0.4 0.8 1.6
HA-MRTF: + + + +
SRF: + + + +
50kDa
37kDa
α-HA (MRTF)
α-pan actin
HA IP - supernatant
R62D-β-actin (μM): - 0.4 0.8 1.6
HA-MRTF: + + + +
50kDa
37kDa
α-HA (MRTF)
α-pan actin

B.

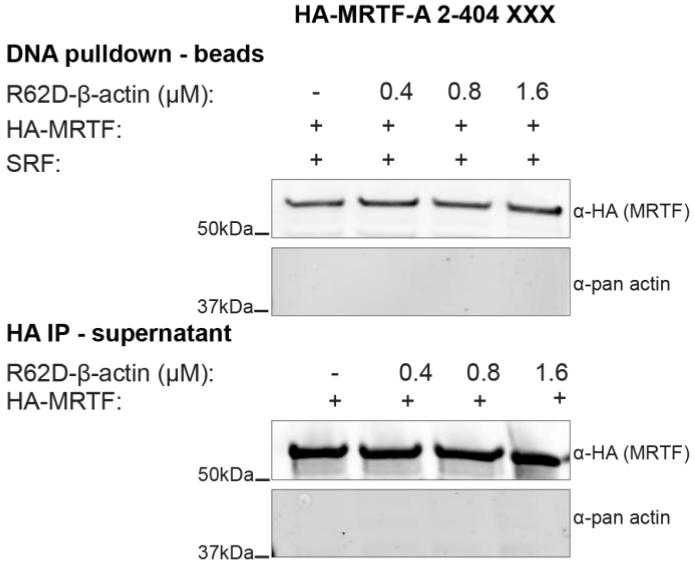
HA-MRTF-A 2-404 XXX
DNA pulldown - beads
R62D-β-actin (μM): - 0.4 0.8 1.6
HA-MRTF: + + + +
SRF: + + + +
50kDa
37kDa
α-HA (MRTF)
α-pan actin
HA IP - supernatant
R62D-β-actin (μM): - 0.4 0.8 1.6
HA-MRTF: + + + +
50kDa
37kDa
α-HA (MRTF)
α-pan actin

C.

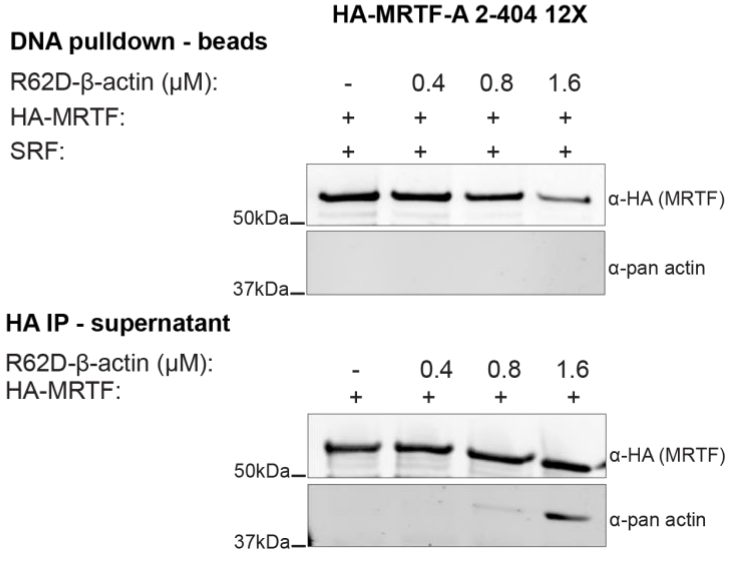
HA-MRTF-A 2-404 12X
DNA pulldown - beads
R62D-β-actin (μM): - 0.4 0.8 1.6
HA-MRTF: + + + +
SRF: + + + +
50kDa
37kDa
α-HA (MRTF)
α-pan actin
HA IP - supernatant
R62D-β-actin (μM): - 0.4 0.8 1.6
HA-MRTF: + + + +
50kDa
37kDa
α-HA (MRTF)
α-pan actin

Figure 32. MRTF recovery in the DNA pulldown assay actin dependent
DNA pulldown assay done using Human cytoplasmic β-actin R62D. DNA at 21pmole/reaction SRF - 4pmole/reaction, MRTF at 10pmole/reaction. Human cytoplasmic β-actin R62D at 0.4µM, 0.8µM and 1.6µM. Top panel in each is DNA pulldown, bottom panel is HA IP of the pulldown supernatant. MRTF was detected using anti-HA antibody, actin was detected using anti pan-actin antibody. **A.** HA-MRTF WT (2-404). **B.** HA-MRTF XXX (2-404). **C.** HA-MRTF 12X (2-404).

3.3 MRTF C-terminal sequences stabilize RPEL3-actin binding

The data presented in the previous section suggested a role of RPEL3 in both actin binding and inhibition of MRTF-SRF interaction. I therefore decided to test whether RPEL3 -actin interacts with sequences C-terminal to the RPEL domain. The Biolayer Interferometry (BLI) assay was used to measure the affinity of actin-binding to MRTF.

BLI is an analytical method that measures the interference pattern of white light going through the tip of a biosensor. The light goes through two layers vertically – an internal reference layer and a biocompatible layer at the tip of the sensor; the interreference pattern between the two is detected, and the output is presented as thickness of the optical layer. The ligand is immobilized on the tip of the biosensor using an affinity tag, upon which the distance between the two layers increases, leading to a shift of the interreference pattern. This change in the optical layer can be further followed upon titration of analyte and is a function of the thickness of the molecular layer.

In the assay, the analyte is titrated at increasing concentration. At equilibrium, the binding curve will reach plateau where association and dissociation rates of analyte to ligand are equal (R_{eq}). Highest level of analyte binding (R_{max}) can be reached if the top concentration of the analyte is ~10x K_d of binding. Low affinity binding cannot be measured accurately using this method, due to limitations of the assay. If the K_d of binding is 20µM, to obtain R_{max} value, a top concentration of 200µM of analyte is required, an amount of protein which would interfere with a correct readout of the assay. Without reaching the R_{max} of binding, it is not possible to accurately determine the affinity of binding. This being the case, a range of K_d is determined by fixing the R_{max} value to that of a strong binder (R_{max}=~1), under the assumption that given a high enough concentration of the analyte, the R_{max} would be reached by the

weak binder. Fitting stimulated binding curves using a constraint of R_{max} and a testing different K_d values provides with a range of binding affinities.

MRTF was used as a HIS_6-MBP fusion to immobilize it on the NI-NTA sensor. RPEL3 alone (residues 155-187) and RPEL3+C (residues 155-404) actin binding affinity was compared.

RPEL3 alone is a weak actin binder (Mouilleron et al., 2008). Addition of the C terminal sequences increased binding affinity of RPEL3 significantly (Figure 33B) to around 2µM, as compared to RPEL3 alone, where the R_{max} of R3+C was used to determine a range of binding to be between 76-120µM (Figure 33A). This observation strongly suggests that MRTF sequences C terminal to the RPEL domain somehow interact with actin-bound RPEL3.

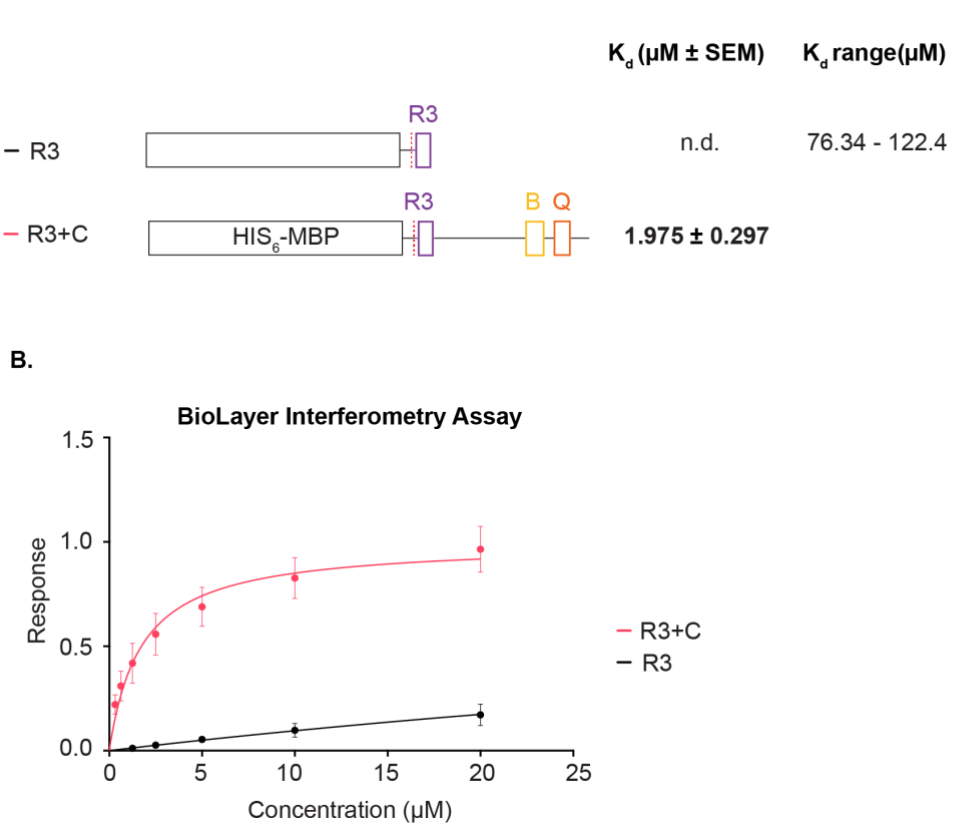

Figure 33. C-terminal sequences of MRTF increase actin binding affinity of RPEL3
BLI assay using HIS_6-MBP R3 (155-187) and R3 + C (155-404) with LatB-rabbit skeletal muscle α-actin (top concentration of actin = 20µM). The values of K_d are based on a non-linear curve fit, with R_{max} constraint =0.9965. K_d values were calculated by steady state, using Response values of each protein over Concentration. For low affinity binders, K_d values shown as range. **A.** Schematic representation of tested proteins. **B.** R3 (n=3) and R3+C (n=6) binding curves. Technical replicates were performed for each experiment. The error bars indicate SD values for constructs n>3.

3.4 Summary

In the DNA pulldown *in vitro*, addition of G-actin inhibits MRTF-SRF interaction, in parallel with actin loading onto MRTF. Inhibition requires the integrity of the actin binding RPEL motifs, with RPEL3-actin binding playing a crucial role in SRF inhibition. MRTF binding to actin and SRF appear mutually exclusive.

Strikingly, MRTF sequences C terminal to the RPEL domain increase the affinity of RPEL3 for actin, suggesting a model in which the actin bound RPEL domain directly sequesters sequences that interact with SRF. This could explain why actin and SRF cannot bind to MRTF at the same time.

In the following chapters I will provide evidence for such a model and test it using *in silico* modelling and biochemical analysis of interactions.

Chapter 4. AF2-Multimer prediction of MRTF complexes

Previous work has established that the MRTF regulatory RPEL domain forms a pentavalent complex with G-actin with one actin bound to each RPEL motif, and additional actins at the intervening spacers (Guettler et al., 2008; Miralles et al., 2003; Mouilleron et al., 2011, 2008; Vartiainen et al., 2007). The data presented in the previous chapter suggest that sequences C-terminal to the RPEL domain stabilize G-actin binding to RPEL3.

Due to the fact that all the structural data of MRTF-actin binding has been obtained using RPEL domain alone, there is a lot of information still missing about where the additional interactions might occur. This is because MRTF is an intrinsically disordered protein, and it is known that the N-terminal RPEL domain becomes folded only upon binding to actin (Mouilleron et al., 2011). The fact that the C-terminal sequences remain unstructured poses a challenge in obtaining crystallography data of the whole protein.

4.1 AlphaFold structure prediction programmes

I used the *in silico* protein interaction prediction programme – AlphaFold2-Multimer (Evans et al., 2022), developed based on the structure prediction programme - AlphaFold2 (Jumper et al., 2021), an artificial neural network trained using the PDB database. By using Multiple Sequence Alignment (MSA) of proteins with homologous sequences from various species, it tracks conservation of proteins in evolution and utilizes the information of co-evolution between amino-acids based on the MSA. Then, through deep learning it produces MSA representation and pair representation between residues in the sequence to predict the relative distances between the amino acids. Each residue is then placed accordingly in the structure prediction based on both the MSA and the pair representation, considering physical interactions between residues within a protein.

AlphaFold2-Multimer uses MSA of multiple amino acid sequences to predict binding of multiple proteins. Like AF2, it takes into account the MSA and

pairwise comparison between amino acids in the protein sequence to predict the structures of protein chains based on homologues sequences in different species in evolution. Additionally, it uses known inter-chain interactions of proteins from the same species, either homomeric or heteromeric and compares the input sequences to generate a probable position of the chains in relation to one another. All of the above allows for prediction of interaction between proteins taking into consideration evolutionary, physical and geometric constrains of protein structure (Evans et al., 2022).

Recently, AlphaFold3 structure prediction programme was released, which allows for structure prediction using sequences of not only protein sequences, but it includes DNA and RNA interactions, as well as allows for placing ions and small ligands. This new version reduces the amount of MSA processing, and uses raw atom coordinates of molecules, instead of using amino-acid specific frames and side-chain torsion angles (Abramson et al., 2024).

The results in this chapter will utilize AlphaFold2-Multimer. Early use of this programme was initially constrained by available computing power, so initial studies were performed with RPEL3 and a single actin molecule, which we know based on biochemical data shown in Chapter 3 is sufficient for high affinity binding. Development of AF during the period of this research allowed predictions of the full pentavalent MRTF-actin complex, which will also be presented in this chapter. With the recent development of AF3, I was also able to predict MRTF binding to SRF on DNA, which will be presented in this chapter.

AF3 was also used to predict the structures of MRTF-actin complexes to confirm the accuracy of the AF2-Multimer prediction, but all the analysis of MRTF-actin binding presented in this section was done using the AF2-Multimer.

4.1.1 Outputs of AF2-Multimer

The pLDDT (predicted local distance difference test) is a measure of per-residue confidence levels. Each residue is valued on a scale of 0-100, where a higher score indicates more accurate prediction. Values over 90 are of very high accuracy, where both the backbone and sidechains prediction can be

trusted. Values above 70, while still of high confidence, correspond to a correct prediction of a backbone, with the possibility of the side chains being misplaced.

PAE (Predicted Aligned Error) describes the error between residues (x,y) in inter and intra-chain contacts. The PAE allows for visualization of the confidence with which the relative positions of residues can be assigned. Each point on the PAE plot (x,y) represents the error in the predicted position of residue (y) if it's aligned to residue (x), as well as the error in the predicted position of residue (x) if it's aligned to residue (y). This results in asymmetrical error prediction, as the confidence of the relative positions between two residues can vary depending on which direction the alignment was made. This arises from the confidence of the predicted residues surrounding the residue in question, e.g. if residue (x) is predicted as part of a high confidence region, the PAE values will be lower for its interaction with residue (y), while if residue (y) is part of a lower confidence region, the PAE values of its interaction with residue (x) may be higher. The PAE is assigned on a scale of 0-30, with lower values corresponding to lower predicted error. The scale is colour coded, with lower error values presented in dark green, and higher error values in yellow. This allows for not only validating whether the prediction is of high confidence within one chain, but also determining the level of confidence between chains.

When analysing AlphaFold predictions, it is important to consider both of the outputs, which in a high confidence prediction can be correlated, e.g. the residues with a high pLDDT levels will have a low Predicted Aligned Error.

4.2 AlphaFold2-Multimer prediction of R3+C / G-actin binding

The biochemical data I have described in the previous chapter show, that RPEL3 alone is a weak G-actin binder, but the presence of MRTF sequences C-terminal to the RPEL domain, including the B and Q region stabilizes binding and increases the affinity for actin. For initial studies, MRTF sequence spanning residues 140-404 was used, which includes the RPEL3 motif and the B and Q regions, implicated in interaction with SRF, together with one human β-cytoplasmic actin. AlphaFold2-Multimer was initially set up as remote server by Roman Fedoryshchak, and later established inhouse at the Francis Crick

Institute. The original structural analysis of the prediction done with input from Stephane Mouillerone (Crick Structural Biology STP).

4.2.1 AF2-Multimer prediction implicates Q-box in interaction

AlphaFold-Multimer ("AlphaFold open source code. https://github.com/deepmind/alphafold,"; Evans et al., 2022) was programmed to generate fifteen structure predictions between MRTF and actin with Amber relaxation to allow for accurate side chain positions. The predictions were then ranked by the confidence levels calculated by the software, represented by the two parameters: pLDDT and PAE.

I first examined the MRTF fragment demonstrated to increase the affinity of RPEL in the BLI experiments with one human β-cytoplasmic actin. The pLDDT values shown in Figure 34A indicate to high degree of confidence for residues spanning RPEL3 (residues:145-156 high, 157-181 very high, 182-184 high) as well as for a region encompassing the Q-box (residues: 349 high, 350-363 very high, 364-378 high). It also predicts low confidence interaction for residues 185-202 downstream from the RPEL3, and residues 347-348 and 379-384 around the Q-box region.

The PAE output on the x axis shows predicted error of aligning (y) to (x), and on the y axis, the error of aligning (x) to (y). There was a low error of intrachain interaction between residues within RPEL3, as well as in the region corresponding to the Q-box. The PAE values were also low for intrachain interactions between residues of actin. When looking at interchain PAE values, MRTFs RPEL3 region had a low PAE error in relation to actin, as well as in relation to the Q region. Q region was also predicted with low PAE as contacting both RPEL3 and actin (Figure 34B).

Taken together, the prediction shows high confidence for RPEL3, Q and actin, indicative of a fixed spatial relationship between these regions.

A. Predicted local distance difference test (pLDDT) of AF2-Multimer prediction

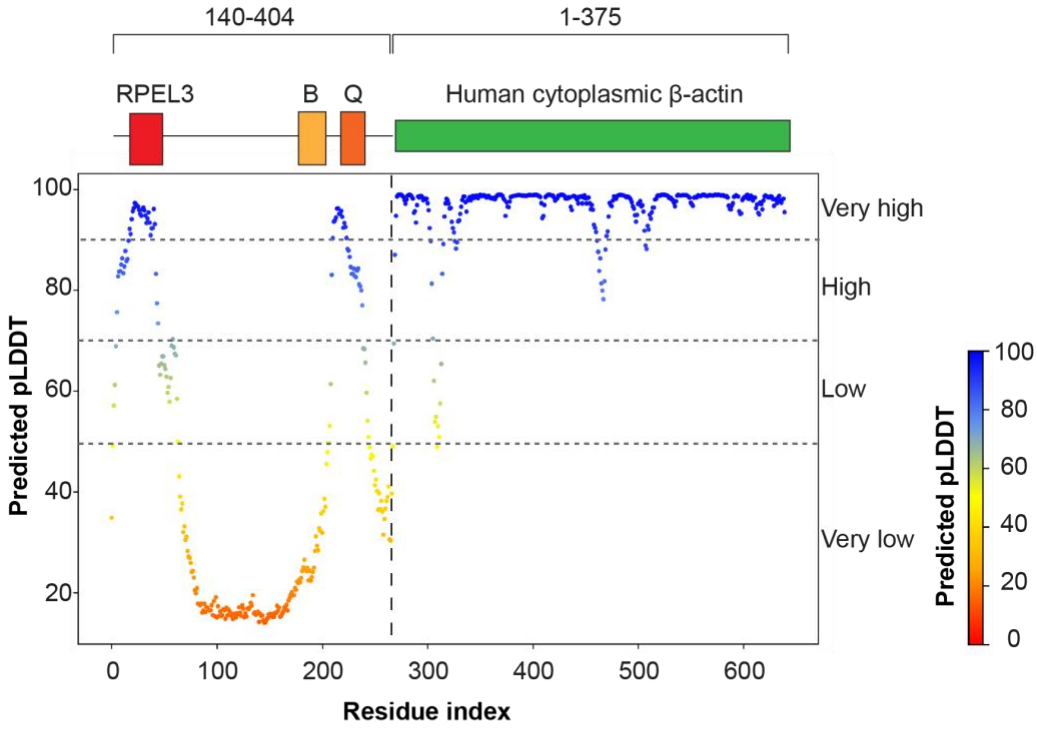

B. Predicted aligned error (PAE) of AF2-Multimer prediction

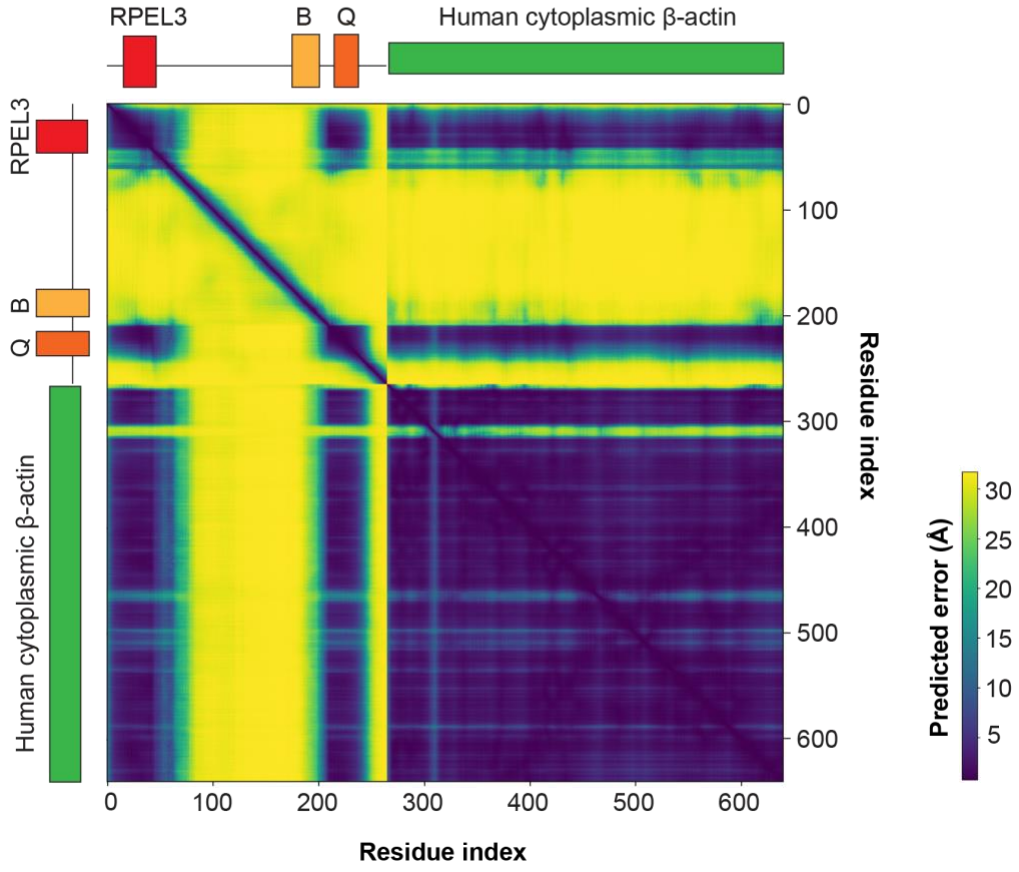

Figure 34. PAE and pLDDT values of AlphaFold2-Multimer prediction
AlphaFold2-Multimer prediction using MRTF (140-404) and human β-cytoplasmic actin (1-375). **A.** pLDDT values are colour-coded on a scale of 1-100, where 90-100=Very high accuracy (main chain + side chain) , 70-90=High accuracy (main chain only), 50-70=Low accuracy and <50=Very low accuracy. **B.** Predicted aligned error (PAE) values are coloured on a scale of 1-30, with lower values in dark indicating lower error, and higher values in lighter shade indicating high error of prediction. Sequence schematics have been aligned to the graph to indicate the PEA for specific regions.

The prediction is displayed in Figure 35, with actin shown as surface representation, with indicated hydrophobic regions, and MRTF as cartoon ribbon. In Figure 35A, the pLDDT values were plotted onto MRTF structure, with colours indicating the confidence of the prediction. Very low confidence prediction is not shown. In Figure 35B, the sequences are annotated to indicate the regions of MRTF that were predicted. RPEL3 (red) is placed between the subdomains 3 and 1 of actin, with Helix α-1 on the surface of the hydrophobic cleft (blue) and Helix α-2 on hydrophobic ledge (magenta) of actin (Table 16). RPEL3 is followed by additional helix predicted with low confidence (50<pLDDT<70, white), which has been termed the O-box, followed by a long, disordered loop including the B region, which was of very low confidence (pLDDT <50, residues not shown). The prediction places the Q-box (orange) of MRTF on another hydrophobic surface of actin, which we termed the wall (green) (Table 16), in close proximity to RPEL3.

I will analyse the prediction, starting by describing the classical RPEL-actin interactions, followed by comparison of those contacts with the prediction. Then, individual sets of interactions will be described between Q-box with actin and Q-box with RPEL3 and O-box.

A. AF2-Multimer R3+C/G-actin - pLDDT values plotted on MRTF structure

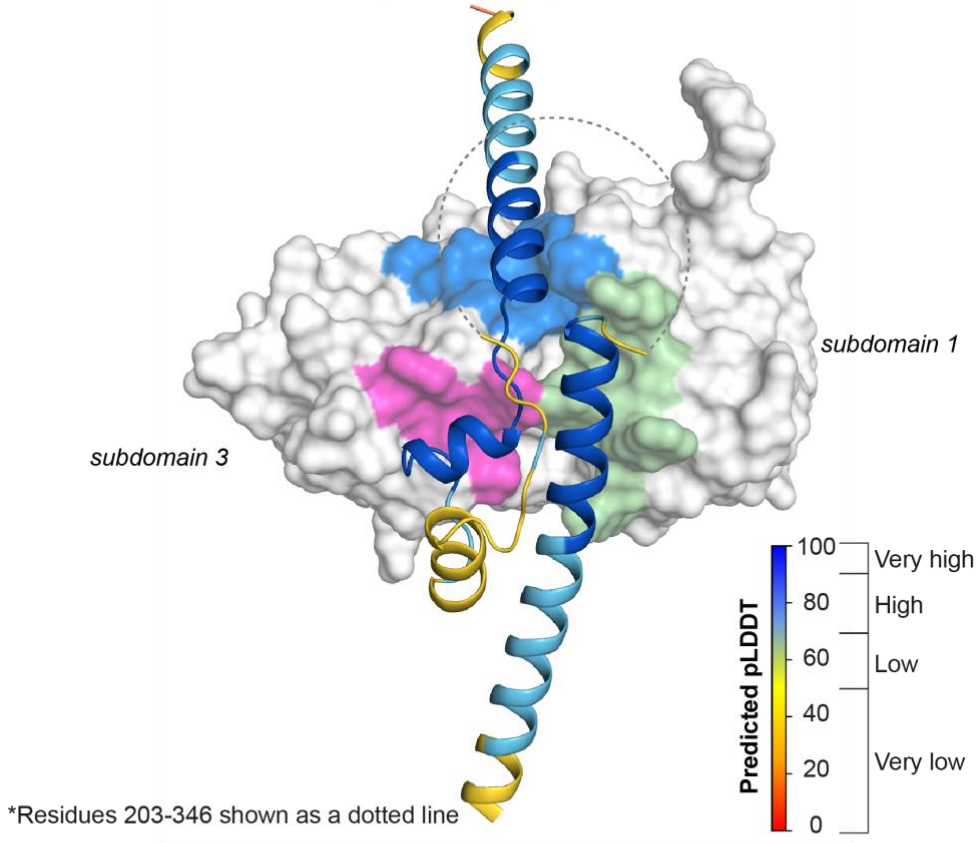

B. AF2-Multimer R3+C/G-actin with annotation

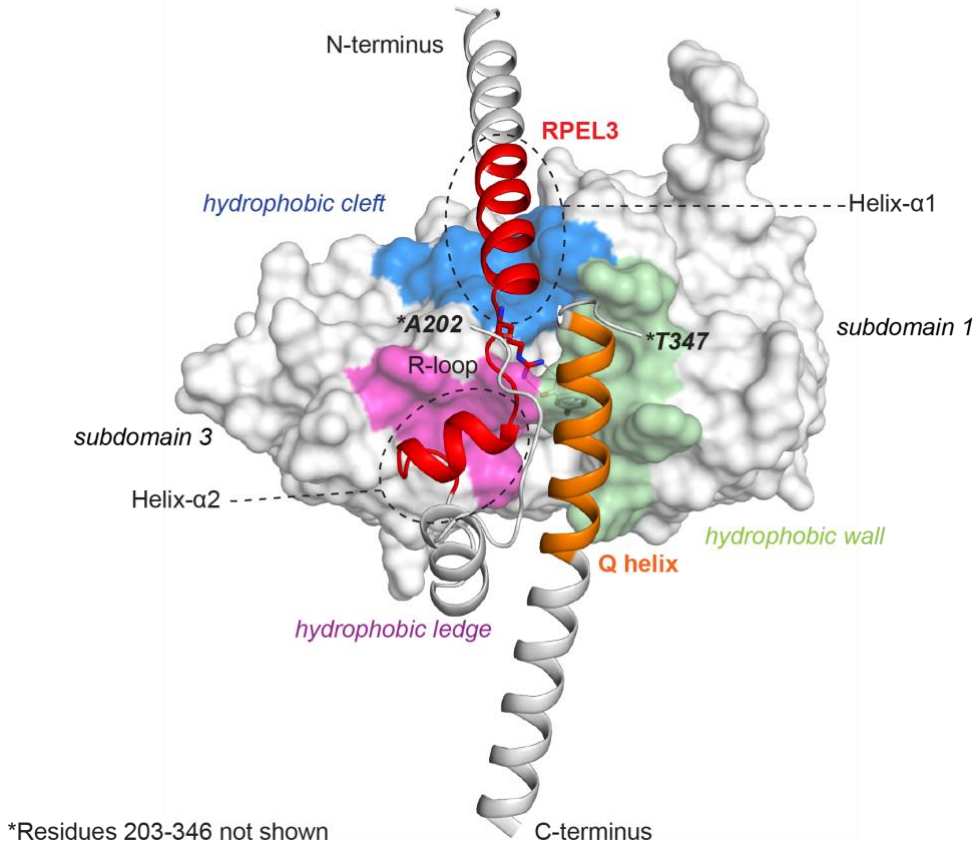

Figure 35. AF2-Multimer prediction of R3+C/G-actin interactions
Actin is shown as surface (white) with MRTF sequence shown as cartoon ribbon. Prediction shown with subdomains 3 and 1 facing front. **A.** pLDDT values of MRTF prediction shown on the structure. pLDDT>90– very high (dark blue), 90>pLDDT>70 – high (light blue), 70>pLDDT>50 – low (yellow), pLDDT<50 – very low (orange, residues not shown). **B.** RPEL3 (155-179) shown in red, Q region corresponding to high confidence prediction shown in orange (350-364). This Q region also corresponds to the residue of high homology between vertebrates and invertebrates (discussed in Introduction). Residues 203-346 of MRTF not shown with values of pLDDT <50. Actin: hydrophobic cleft – blue, hydrophobic ledge – magenta, hydrophobic wall – green. Residues marked with * indicate where the disordered loop starts (A202) and ends (T347).

Actin surface	Residues
Hydrophobic cleft	Y143, G146, R147, T148, I345, L346, L349, T351, F352
Hydrophobic ledge	Y166, Y169, A170, L171, P172, I289
Hydrophobic wall	K113, Q354, M355, H371, R372, K373, F375

Table 16. Hydrophobic surfaces of actin

4.2.2 RPEL3 – actin interactions

The low affinity of RPEL3 for actin has precluded the determination of the RPEL3 / Actin complex at the structural level. I therefore compared the AF2-Multimer prediction for RPEL3 with the previous RPEL2 / actin structure. RPEL2 motif crystal structure was overlayed with RPEL3 motif AF2-Multimer prediction with RMSD=0.364Å. Helix α-1 and α-2 of both RPELs are placed in the same orientation on the surface of actin hydrophobic cleft and ledge, with $R125^{RPEL2}$ (green) and $R169^{RPEL3}$ (red) making the same contact with the C-terminal carboxylate of $F375^{actin}$ (Figure 36A).

A. **RPEL2 (crystal structure) and RPEL3 (AF prediction) on actin surface**

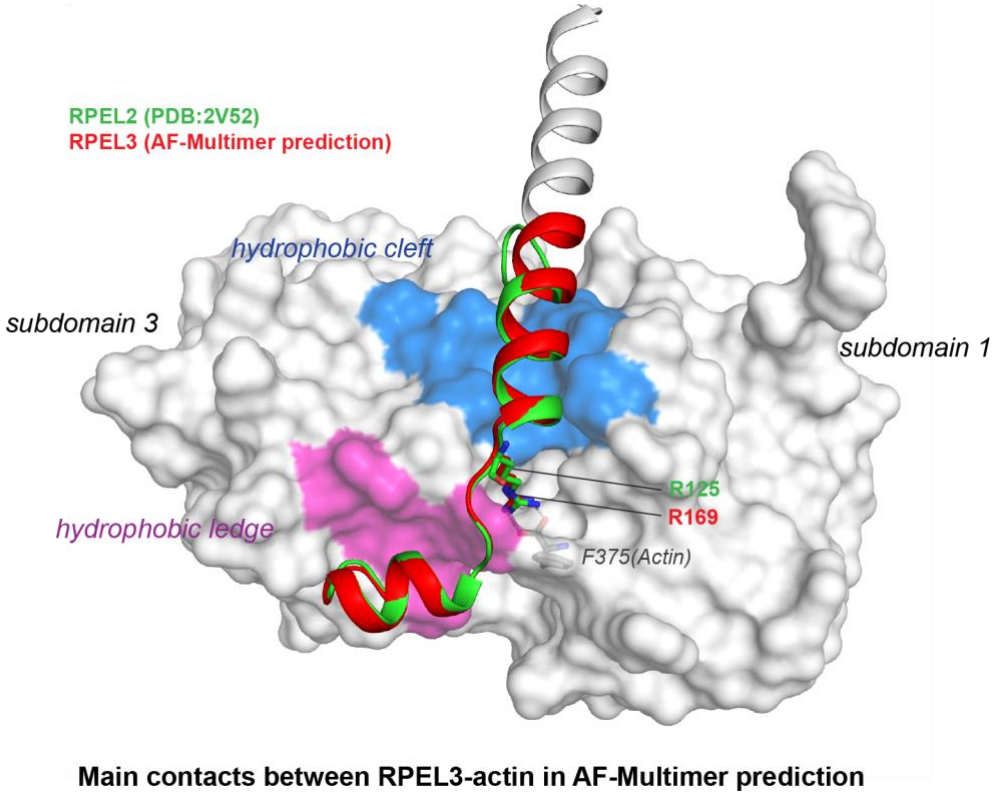

B. **Main contacts between RPEL3-actin in AF-Multimer prediction**

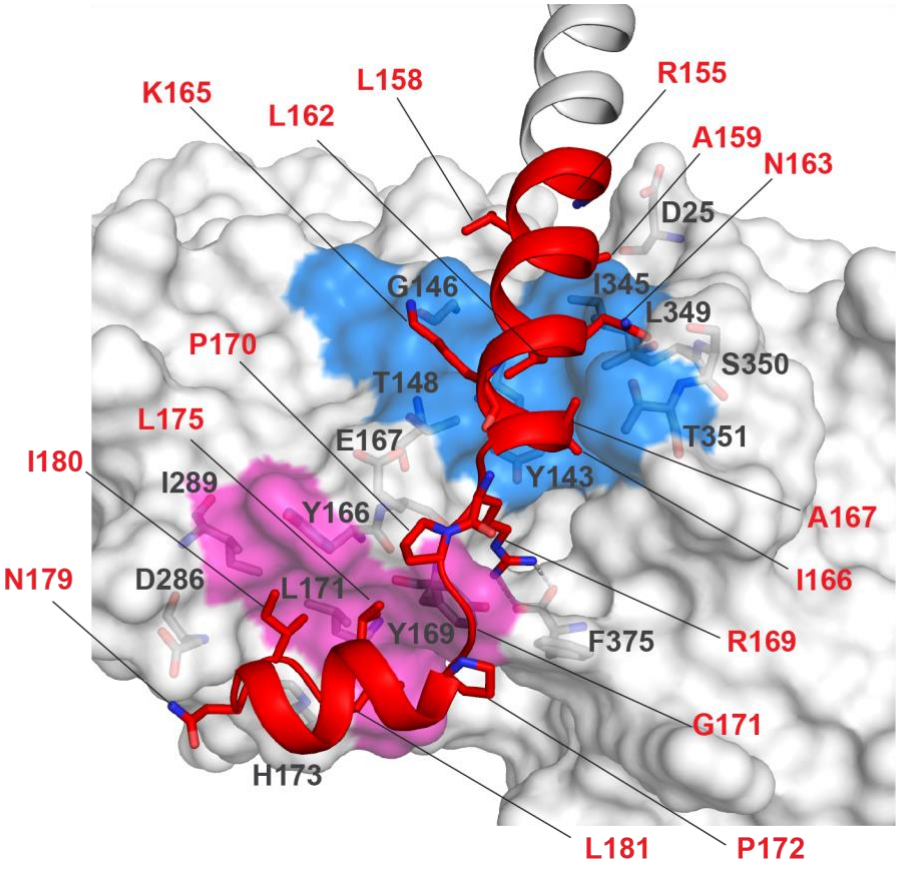

Figure 36. RPEL3-actin interaction predicted by AF2-Multimer
AF2-Multimer prediction of RPEL3 binding to the actin surface. Blue-hydrophobic cleft, Magenta-hydrophobic ledge RPEL3 motif in red, RPEL2 motif in green. **A.** RPEL2 crystal structure (PDV:2V52) overlayed with the RPEL3 motif AF prediction on the surface of human β-cytoplasmic actin. The main contact between the RPEL and actin F375 is labelled for both: $R125^{RPEL2}$ and $R169^{RPEL3}$. Actin is orientated with the subdomain 3 and 1 facing front. **B.** RPEL3 motif from the AF prediction on the surface of actin. Residues in red are RPEL3, in black cursive – actin.

RPEL3 prediction was analysed and the residues making contact with actin with high pLDDT values were annotated on the prediction (Figure 36B). Residues $L158^{RPEL3}$, $L162^{RPEL3}$ and $K165^{RPEL3}$ within the Helix α-1 of RPEL3 are predicted to make hydrophobic contacts with the hydrophobic cleft in a similar manner to RPEL2. The conserved $R169^{RPEL3}$ of the RPxxxEL motif contacts side chain of $Y169^{actin}$, main chain of $E167^{actin}$ and a critical contact with the $F375^{actin}$ carboxylate. An important difference between RPEL2 and 3 is localized to residues in the 3rd position of the RPxxxEL: in RPEL 2, $E127^{RPEL2}$ stabilizes the interaction within Helix α-2 of RPEL2, whereas in RPEL3, in the same position $G171^{RPEL3}$ does not make the same contacts within the helix, instead binding the side chain of $Y169^{actin}$. This difference has been stipulated to be one of the reasons why RPEL3-actin binding might be of lower affinity as compared to RPEL2. $P172^{RPEL3}$ main chain nitrogen contacts the $Y169^{actin}$ side chain, in a similar manner to that of $R128^{RPEL2}$. This is a new finding, as $P172^{RPEL3}$ was thought not to make main chain contact with the $Y169^{actin}$ based on the position in the sequence alone (Mouilleron et al., 2008). Helix α-2 residues $L175^{RPEL3}$, $I180^{RPEL3}$ and $L181^{RPEL3}$ contact the hydrophobic ledge of actin. A table of all contacts between RPEL2 and actin identified in the crystal structure (Mouilleron et al., 2008) is shown in Table 17, while those of predicted RPEL3 and actin in Table 18.

RPEL2 (from PDB: 2V52)	Actin
L118 (side chain) I122 (side chain)	Hydrophobic cleft
K121 (side chain)	G146 (main chain) E167 (side chain)
R125	E167 (main chain) Y169 (side chain) **F375**$^{coo-}$
P126 (side chain)	Y166 (main chain) E167 (side chain)
P126 (main chain)	Y169 (side chain)
R128 (main chain)	Y169 (side chain)
L131 I136 L137 (all side chain mediated)	Hydrophobic ledge

Table 17. List of main RPEL2 – actin interactions in crystal structure

RPEL3 (AF2-Multimer)	Actin	Type of interactions
R155 L158 A159 L162 N163 K165 I166 A167 (all side chain mediated)	Hydrophobic cleft	Hydrophobic
R169 (side chain)	E167 (main chain) Y169 (side chain) **F375^{coo-}**	Ionic Hydrogen bond Ionic
P170 (side chain)	E167 (side chain)	Hydrophobic
P170 (main chain)	Y169 (side chain)	Hydrophobic
G171 (main chain)	Y169 (side chain)	Hydrophobic
P172 (side chain)	Y169 (side chain) F375 (side chain)	Hydrophobic Hydrophobic
L175 I180 L181 (all side chain mediated)	Hydrophobic ledge	Hydrophobic
N179 (side chain)	D286 (side chain)	Ionic

Table 18. RPEL3 – actin contacts predicted by AF2-Multimer

4.2.3 Q-box – actin interactions

The whole Q region (residues 339-378) is predicted with high confidence to form a long helix (9-turns) contacting the hydrophobic surface of actin, which we termed the hydrophobic wall (Table 16).

The Q-box was originally defined as a glutamine-rich region in Myocardin (Wang et al., 2002, 2001). The corresponding sequence in MRTF-A is 356-QQQQLFLQLQILNQQQQQQQQ-377. This nomenclature has been therefore used in further studies regarding the role of Q (Zaromytidou et al., 2006). However, the most conserved region throughout evolution between Myocardin family members from insects to man corresponds to MRTF-A 351-YAKILQQQQLFLQLQ-365. Interestingly, it is this region that AF2-Multimer predicts as interacting with RPEL3-actin (Figure 37, orange). For purposes of the following discussion, I will consider Q to encompass Y351-L355.

$Y351^{Q\text{-}box}$ side chain makes hydrophobic contacts with $Q354^{actin}$, $M355^{actin}$ and $K373^{actin}$ of actin. $I354^{Q\text{-}box}$ contacts the side chain of $F375^{actin}$ through hydrophobic interactions, while $L355^{Q\text{-}box}$ makes contact with $R372^{actin}$ main chain. $Q358^{Q\text{-}box}$, $Q359^{Q\text{-}box}$ and $Q365^{Q\text{-}box}$ bind actin through hydrogen bond with $H371^{actin}$, $R372^{actin}$ and $K113^{actin}$, respectively. $L362^{Q\text{-}box}$ binds actin through hydrophobic contacts with $R372^{actin}$ and $H371^{actin}$. Full list of contact identified is shown in Table 19.

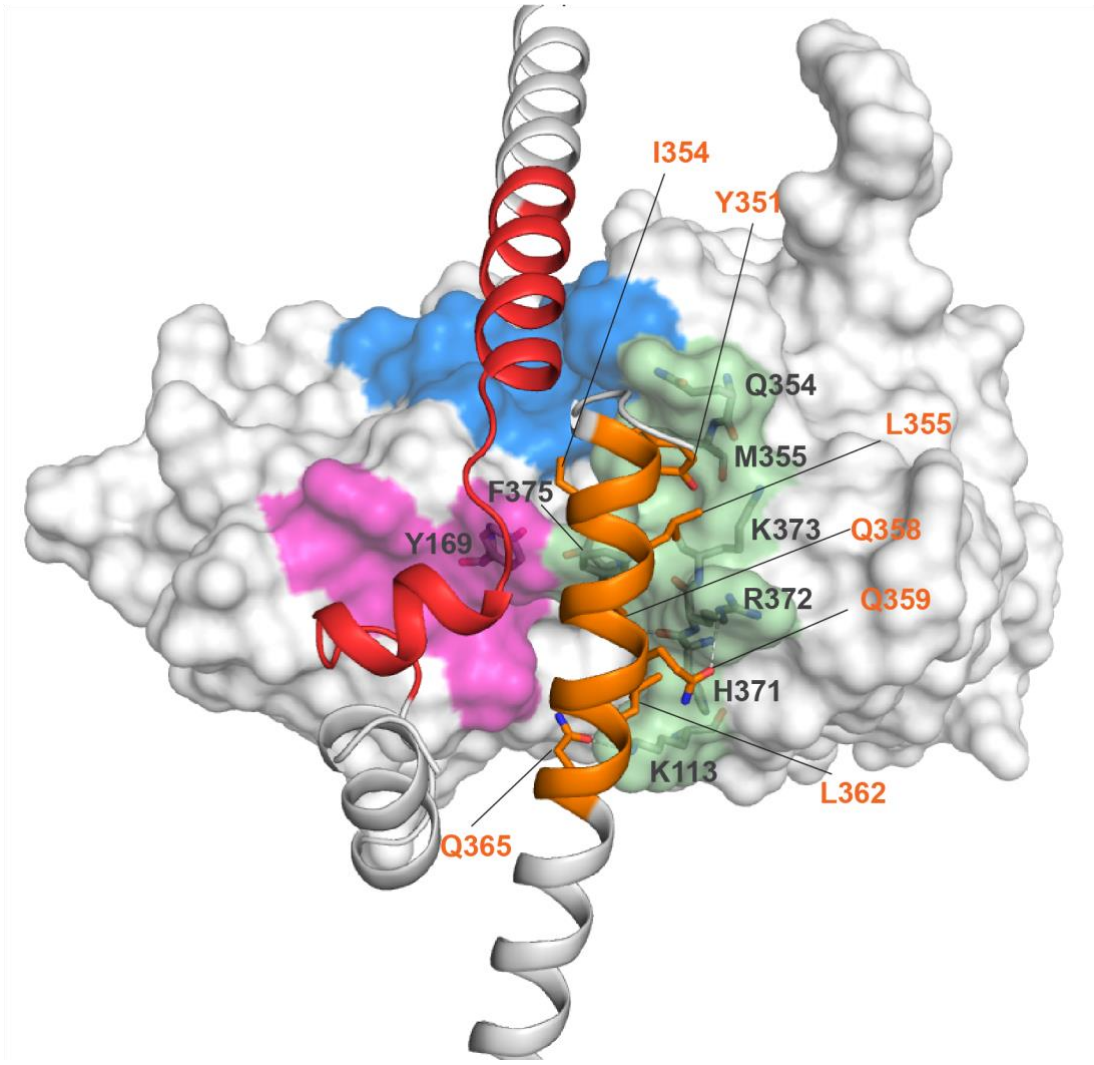

Figure 37. Q region – actin interaction as predicted by AF-Multimer
The prediction of RPEL3 and Q helix placed on the surface of actin, RPEL3 (red) on the hydrophobic cleft and ledge, conserved Q helix (orange) on the hydrophobic wall. Main interactions between Q and RPEL3 are highlighted – Q residues in orange, actin residues in black cursive.

Q-helix	Actin	Type of interaction
Y351 (side chain)	Q354 (side chain) M355 (main chain) K373 (side chain)	Hydrogen bond Hydrophobic Polar interaction
I354 (side chain)	F375 (side chain) Y169 (side chain)	Hydrophobic Hydrophobic
L355 (side chain)	F375 (side chain) K373 (side chain) R372 (main chain)	Hydrophobic Hydrophobic Hydrophobic
Q358 (side chain)	F375 (side chain) H371 (main chain)	Hydrophobic Hydrogen bond
Q359 (side chain)	R372 (side chain)	Hydrogen bond
L362 (side chain)	R372 (main chain) H371 (side chain) K113 (side chain)	Hydrophobic/Ionic Hydrophobic Hydrophobic
Q365 (side chain)	K113 (side chain)	Hydrogen bond

Table 19. List of Q-helix and actin interactions predicted by AF2-Multimer

4.2.4 RPEL3 – O-box – Q-box interactions

Besides multiple identified interactions with actin, the Q-box is also predicted to make multiple contacts with RPEL3.

Q-box contacts RPEL3 R-loop and Helix α-2 (Figure 38). $I354^{Q\text{-}box}$ binds RPEL3 residues in the R-loop $R169^{RPEL3}$, $G171^{RPEL3}$ and $P172^{RPEL3}$. $G171^{RPEL3}$ also interacts with $Q357^{Q\text{-}box}$ side chain, stabilizing binding of Q to the R-loop. $P172^{RPEL3}$ interacts with the aromatic chain of $F361^{Q\text{-}box}$ through both hydrophobic effect and interaction between the negatively charged π face of $F361^{Q\text{-}box}$ side chain with C-H bonds of proline. Both $G171^{RPEL3}$ and $P172^{RPEL3}$ interactions with the Q-box are specific to RPEL3, as these residues are absent in RPEL2 and facilitate binding to Q. Helix α-2 residues make additional

contacts with Q. M173^{RPEL3} interacts both with Q357$^{Q\text{-}box}$ and L360$^{Q\text{-}box}$; E174^{RPEL3} with Q357$^{Q\text{-}box}$ through hydrophobic effects. V176^{RPEL3} and L181^{RPEL3} interact with F361$^{Q\text{-}box}$. Full list of contacts can be found in Table 20.

Q	RPEL3	Type of interactions
I354 (side chain)	R169 (side chain) G171(main chain)	Hydrophobic Hydrophobic
I354 (main chain)	P172 (side chain)	Hydrophobic
Q357 (side chain)	G171 (main chain) E174 (side chain) P172 (side chain) M173 (side chain)	Hydrogen bond Hydrogen bond Hydrophobic Hydrophobic
L360 (side chain)	M173 (side chain)	Hydrophobic
F361	P172 (side chain) V176 (side chain) L181 (side chain)	π/CH Hydrophobic Hydrophobic

Table 20. Q-RPEL3 interactions identified by AF2-Multimer

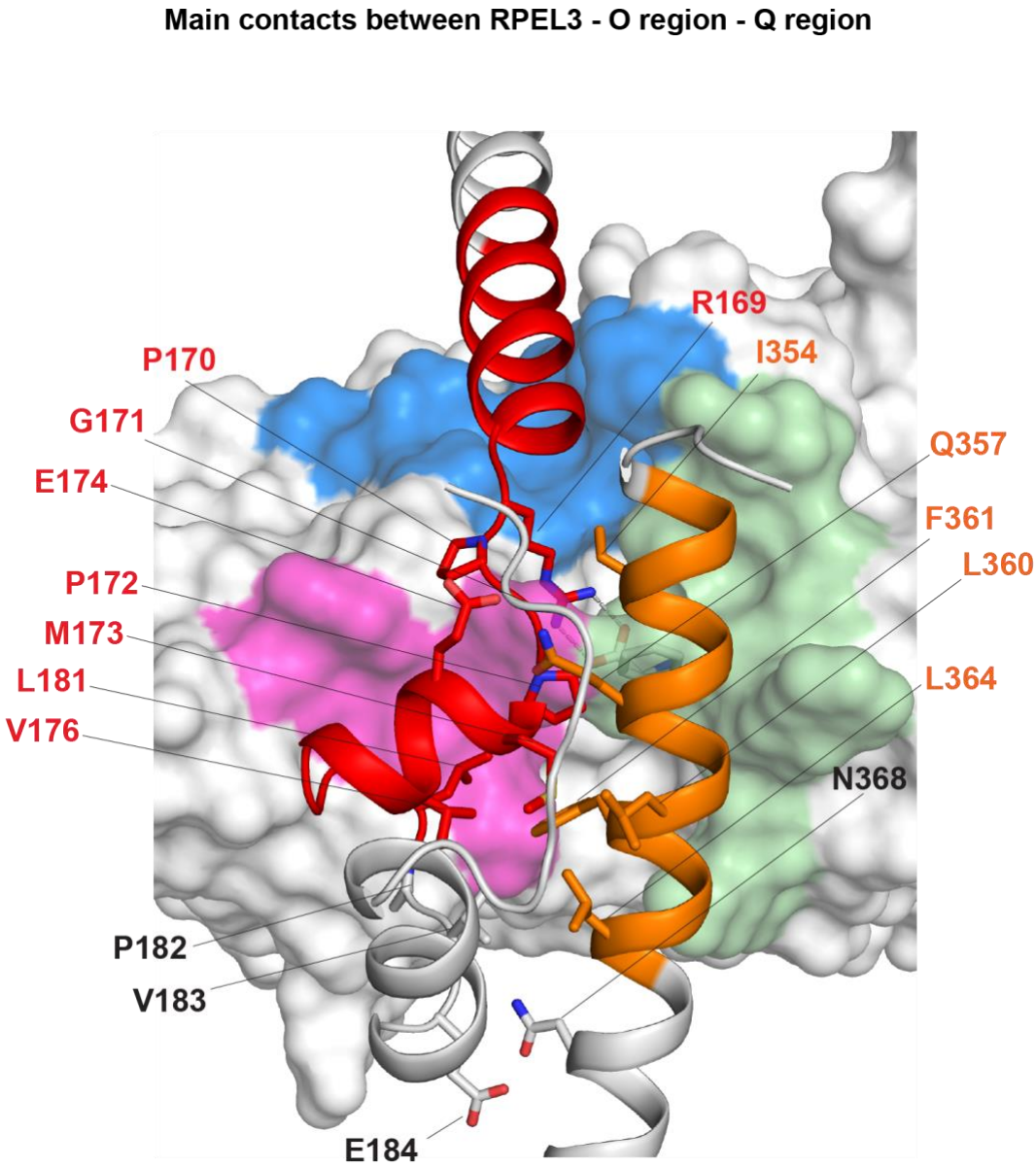

Figure 38. RPEL3 – O-box – Q-box interactions
The prediction of RPEL3 -O box and Q helix shown on the surface of actin, RPEL3 (red) on the hydrophobic cleft and ledge, Q helix (orange – high pLDDT and main interactions, white low pLDDT) on the hydrophobic wall. Main interactions between Q (orange)– O (black) - RPEL3 (red) are highlighted. Actin shown in white with coloured hydrophobic surfaces.

AF-Multimer predicted an extension region of RPEL3, with high confidence prediction of residues P182$^{O\text{-}box}$, V183$^{O\text{-}box}$ and E184$^{O\text{-}box}$. These residues are part of a loop connecting RPEL3 with another helix, region we termed “O-box”, which was predicted with low confidence, and spanned residues 185-202 (shown in grey, Figure 38).

P182$^{O\text{-}box}$ contacts RPEL3 N179^{RPEL3} and I180^{RPEL3}, whereas V183$^{O\text{-}box}$ interacts with both Q – F361$^{Q\text{-}box}$ side chain, L364$^{Q\text{-}box}$ side chain and N368$^{Q\text{-}box}$ side chain. Contacts with RPEL3 are made through main chain carbon α with L181^{RPEL3} and V176^{RPEL3} through side chain interactions. All contacts between O and RPEL3 can be found in Table 21, and between Q-box and Q-box in Table 22.

O-helix	RPEL3	Type of interactions
P182 (side chain)	N179 (side chain)	Hydrophobic
	I180 (main chain)	Hydrophobic
V183 (side chain)	L181 (main chain)	Hydrophobic
	V176 (side chain)	Hydrophobic

Table 21. O-box – RPEL3 interactions predicted by AF2-Multimer

O-helix	Q-box	Type of interactions
V183 (side chain)	F361 (side chain)	Hydrophobic
	L364 (side chain)	Hydrophobic
	N368 (side chain)	Hydrophobic

Table 22. O-box – Q interactions predicted by AF2-Multimer

The high confidence of the prediction and in-depth analysis of the interactions have provided a probable model of additional interaction with the Q-box sequences that facilitate formation of a composite site on RPEL3, increasing its affinity for actin binding.

4.3 MRTF 2-404 – actin binding

To confirm the Q-box interaction in the context of an intact RPEL domain, AF2-Multimer was used, with MRTF sequence spanning the N-terminus, RPEL domain and the C terminal sequences including B and Q as input (residues 2-404), together with five molecules of human cytoplasmic β-actin.

The N-terminus prior to the RPEL domain is unstructured (residues 2-64), as well as the loop between the RPEL domain and Q-box (residues 203-347). RPEL domain and the C terminal Q region are determined to be of high confidence, both by high pLDDT values (Figure 39A) and low PAE error (Figure 39B). This is in agreement with the crystal structure of the RPEL domain and the AF2-Multimer prediction of R3+C – actin binding described in the section 4.2. Each actin molecule was predicted to be folded with a high degree of confidence.

Next, the prediction was compared with the known structure of the RPEL domain in a pentavalent complex with actin. The structure of the MRTF with actin (PDB:2YJF) was resolved using the RPEL domain sequence (residues 63-199) with five molecules of rabbit α-skeletal muscle actin. Crystal structure of the pentavalent complex could only be obtained upon stabilization of actin binding on RPEL3 by introducing “RPEL2-like” mutations. Residues in position 3 and 4 of the RPxxxEL were mutated to G173E and P172R. $E127^{RPEL2}$ interacts with residues within the Helix α-2, while $R128^{RPEL2}$ binds to the side chain of $Y169^{actin}$. As discussed above, $G171^{RPEL3}$ and $P172^{RPEL3}$ are involved in interaction with the Q-box, which is where the difference between the RPELs sequence might be derived. A side-by-side comparison of the crystal structure with the prediction is shown in Figure 40.

On the left, the crystal structure of the RPEL domain with five actins bound is shown. On the right, the AF2-Multimer prediction with human cytoplasmic β-actin.

A. pLDDT of AF2-Multimer prediction (MRTF 2-404 / 5xG-actin)

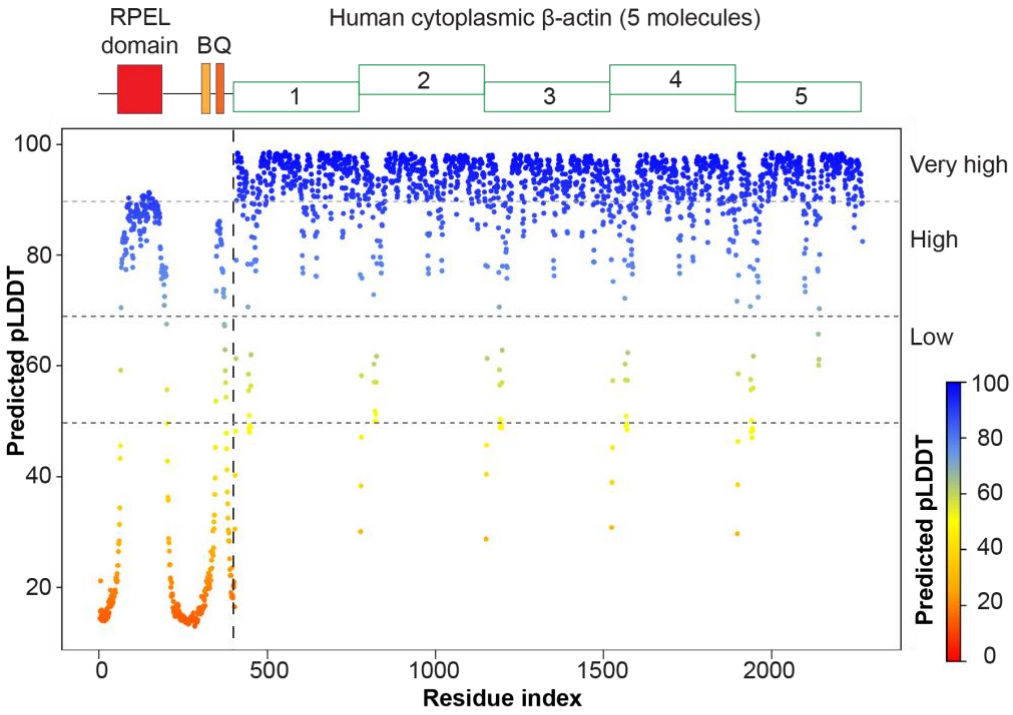

B. PAE of AF2-Multimer prediction (MRTF 2-404 / 5xG-actin)

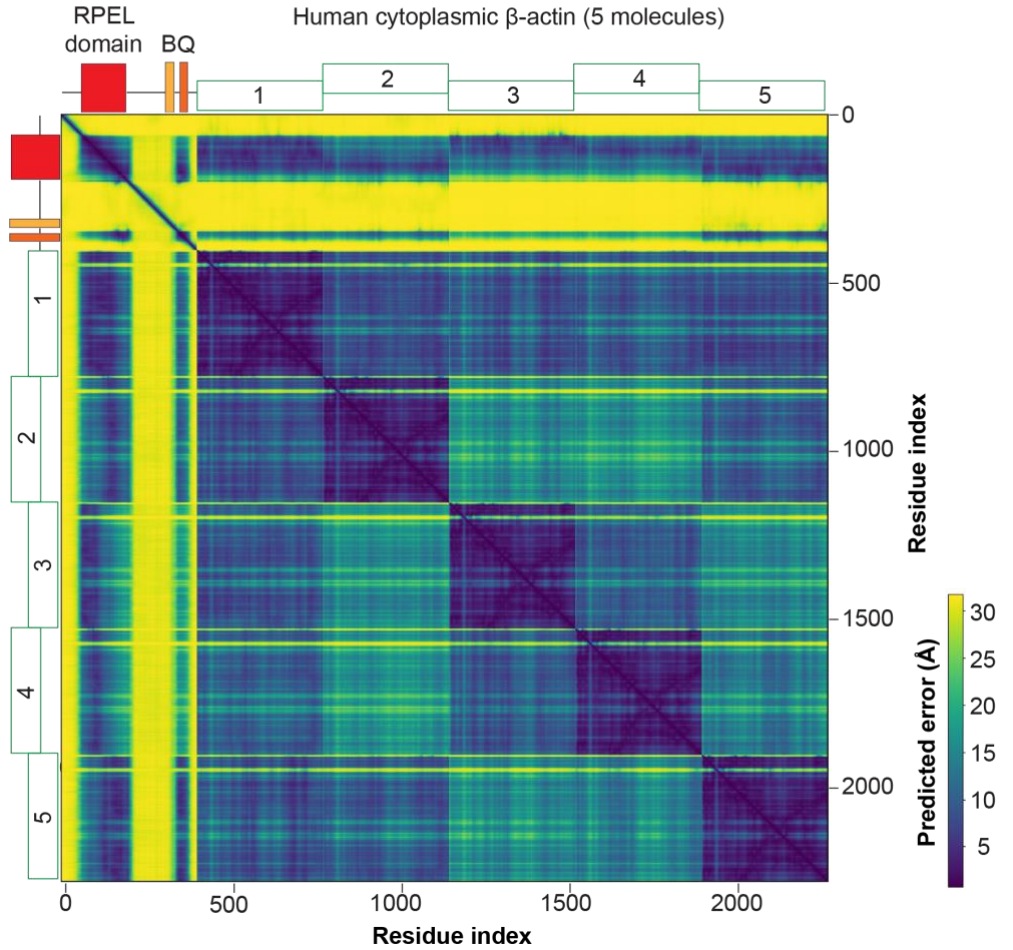

Figure 39. PAE and pLDDT plots of the AF2-Multimer prediction of MRTF with actin
AlphaFold2-Multimer prediction using MRTF (2-404) and five human β-cytoplasmic actin (1-375). **A.** pLDDT values are colour-coded on a scale of 1-100, where 90-100=Very high accuracy, 70-90=High accuracy, 50-70=Low accuracy and <50=Very low accuracy. **B.** Predicted aligned error (PAE) values are coloured on a scale of 1-30, with lower values in dark indicating lower error, and higher values in lighter shade indicating high error of prediction. Schematic sequence representation has been aligned to the graph to indicate the PEA for specific regions.

RPEL domain is localized between the actins in a crank-shaped conformation, with a left-handed super helical twist along the axis. Each of the RPELs is folded into two helices and engages one actin, with the N-terminal extensions of RPEL2 and RPEL3 recruiting another actin molecule to bind to the Spacer region between the RPELs. One distinct difference between the two is the presence of the Q region placed in the same orientation as in the R3+C prediction on the hydrophobic wall of actin, in close proximity to the RPEL3.

To better visualize the Q-box, the prediction was rotated, with the SD 1 and 3 of Actin^{R3} facing forward, which shows the same placement of the Q-box relative to both Actin and RPEL3 as described for R3+C (Figure 41).

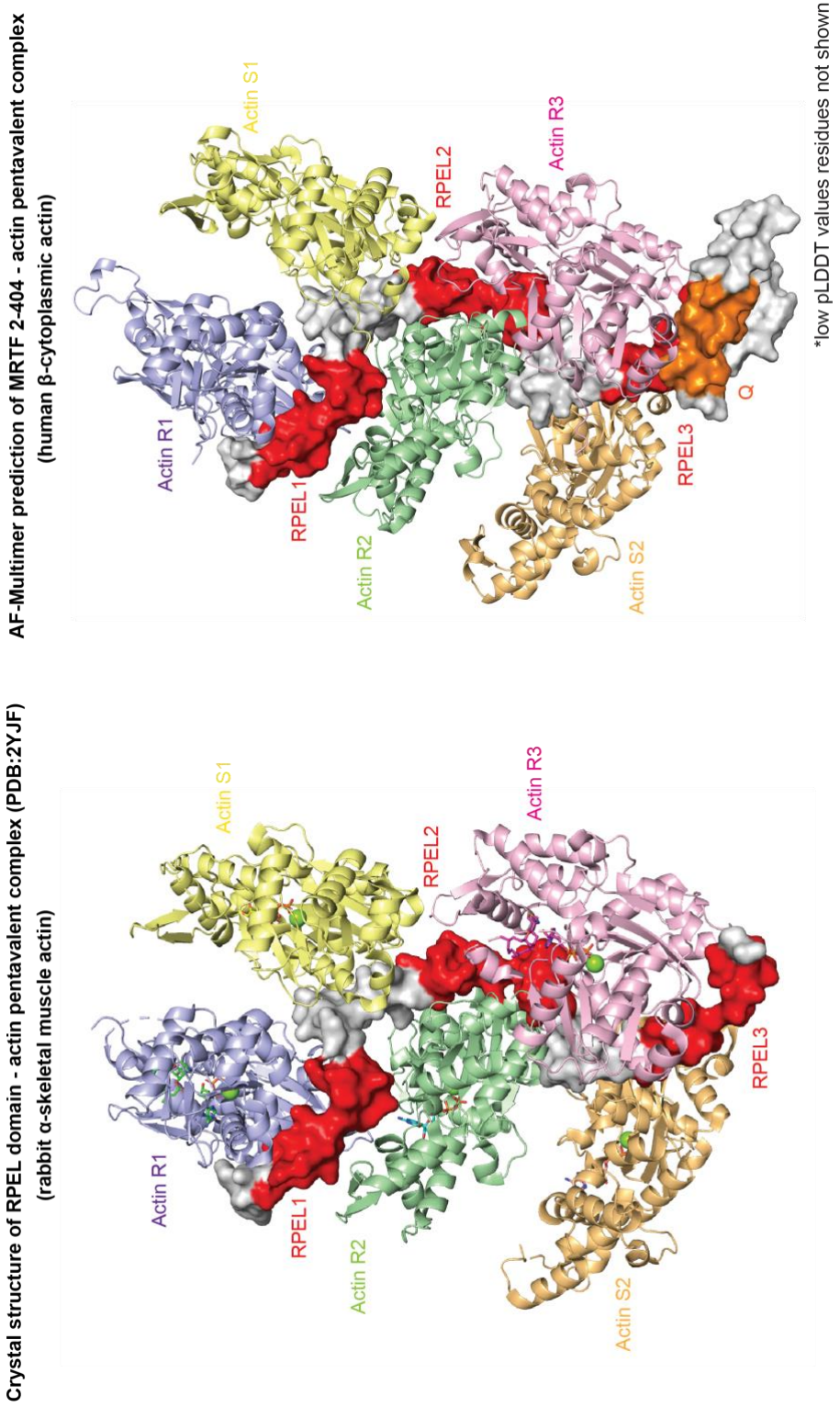

Figure 40. Side-by-side comparison of crystal structure and AF prediction
Left: Crystal structure of RPEL domain with five rabbit α-skeletal muscle actin molecules. Each actin in shown in a different colour, with RPEL motifs coloured in red (PDB:2YJF). **Right:** AF2-Multimer prediction of MRTF 2-404 with five human β-cytoplasmic actin molecules. Unstructured N-terminus (2-64) and the loop between RPEL domain and Q (203-347), as well as C terminal residues (379-404) are not shown. Q helix shown in orange. Actins shown as cartoon, with MRTF presented as surface.

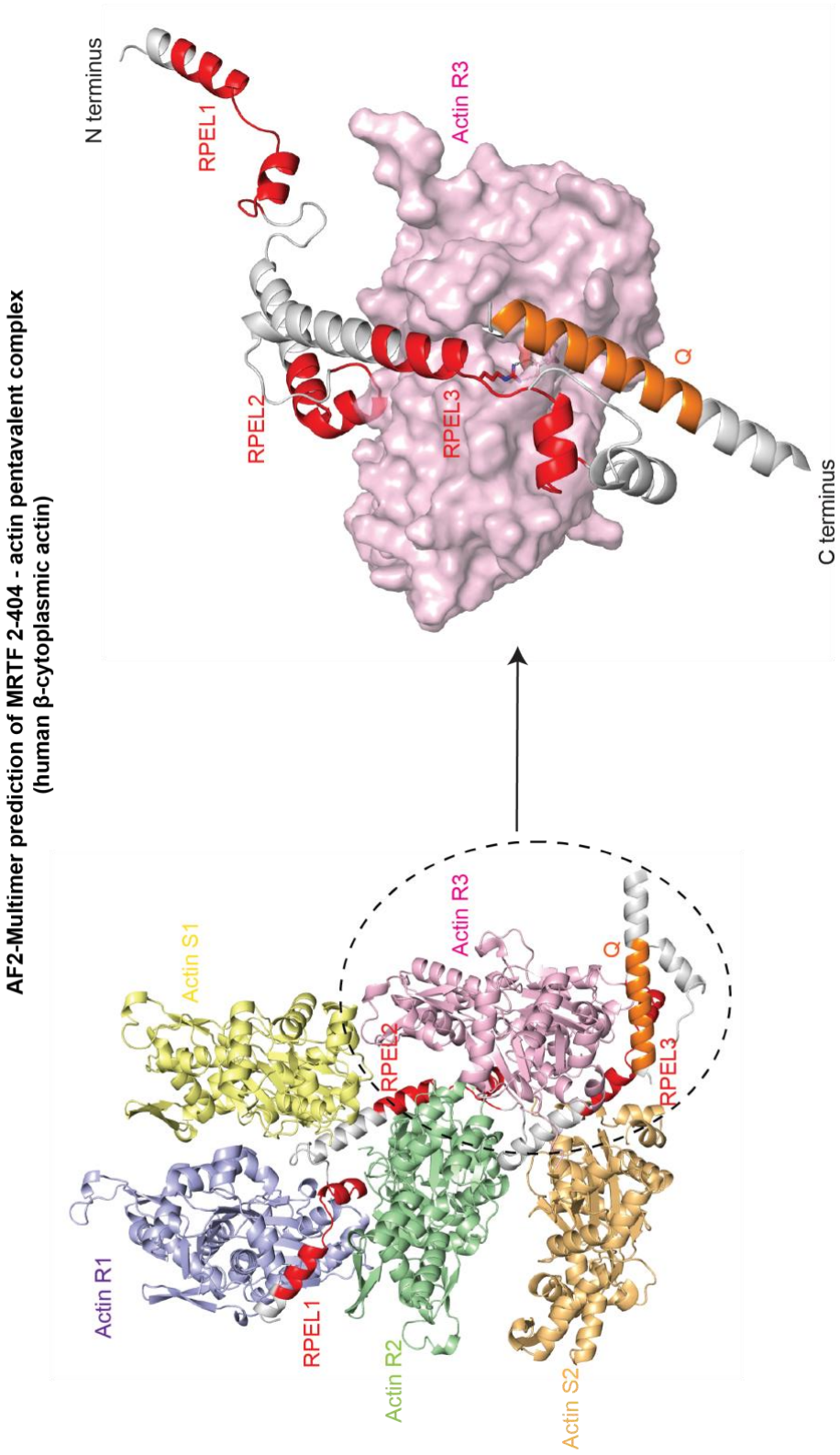

Figure 41. AF2-Multimer prediction of pentavalent complex with exposed Q region
Left: The MRTF 2-404-five actins AF2 prediction, with MRTF and actins presented as cartoons. **Right:** Magnified view of the predicted interaction of Actin R3 (shown as surface) with RPEL domain and the Q-box region. Actins R1, S1, R2 and S2 omitted for clarity.

4.4 AlphaFold3 prediction of MRTF / SRF / DNA

MRTF exerts its transcriptional activity by binding to SRF on DNA. The structure of DNA-SRF complex was resolved by X-ray crystallography, but there is no crystal structure of MRTF-SRF-DNA complex.

Through biochemical analysis it was determined that the B-box of MRTF, specifically a heptapeptide within that region, is crucial for SRF binding (Zaromytidou et al., 2006). MRTF binds to SRF as a dimer, although it can make contacts as a monomer, with a lower affinity of binding. As MRTF-SRF binding can be detected only in the presence of DNA, the limitation of AF2-Multimer as a protein-prediction software precluded determining the structure.

Recently, AlphaFold3 was developed which allows for prediction of interactions between proteins and nuclei acids. Using the software, I investigated the structure of SRF-DNA with MRTF B-box and Q-box sequences. The structure confirmed the biochemical data, where the heptameric peptide in B-box makes the interaction with SRF, consistent with the way TCF family of proteins contacts SRF in ternary complex. Although Q-box was not predicted with high confidence, the placement in the structure suggests to a possible dimerization between the two Q-helixes, which could have a stabilizing effect on binding to SRF.

In this section, I will present the AF3 prediction of MRTF-SRF-DNA complex, as well as compare the structure to that of TCF family member-SAP1.

4.4.1 AF3-prediction

For the AF3 prediction, 70bp DNA sequence of the *c-fos* promoter was used, containing the CArG box, as well as two SRF.DBD (residues 132-222) and B- and Q-box containing sequence of MRTF (residues 305-404), with the heptapeptide (residues 328-334) previously mapped as crucial for SRF binding. AF3 generates five structure predictions, providing the PAE and pLDDT values, as described at the beginning of this Chapter.

Next, MRTF-SRF binding was analysed using the AF3 outputs that inform about the confidence of the prediction. PAE plot indicates correct placement of

MRTF B-box and Q box within the protein structure. In SRF there is a low error of predicted placement of all residues, indicating correct domain folding and their placement within the structure.

B-box placement towards SRF is of low PAE error. Q-box residues are also placed with relatively low PAE towards SRF. There is an asymmetry in the alignment of MRTF and SRF, which could be due to the fact that SRF is well packed and of high global confidence, which will reflect the confidence of residue interactions. Alignment of MRTF to SRF has lower PAE values, as the alignment is done towards a molecule that is of higher global confidence with residues within its sequence (Figure 42).

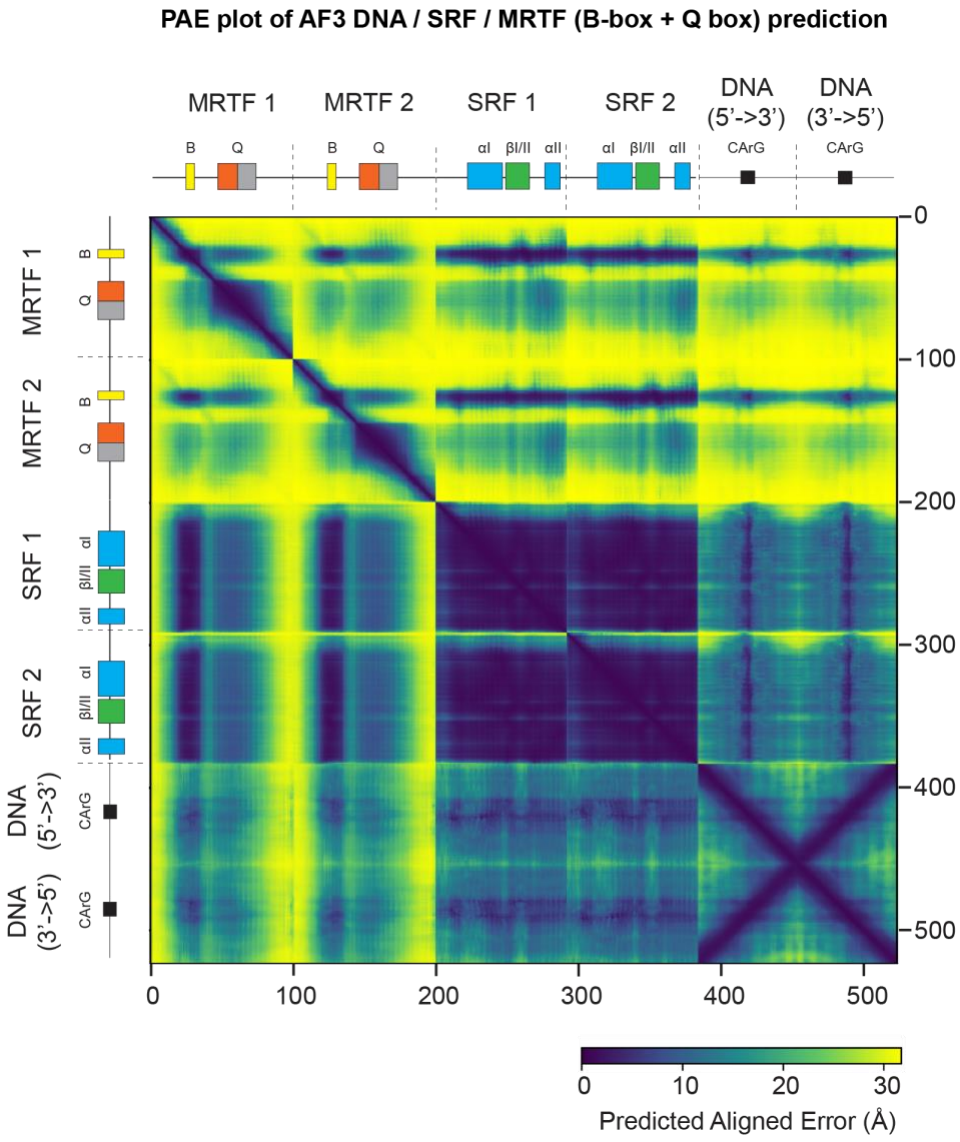

Figure 42. PAE of the AF3-prediction of SRF / DNA / MRTF (B + Q box)
AlphaFold3 prediction using 2xMRTF B-box + Q-box (305-404, 2xSRF.DBD (128-223) and *c-fos* promoter DNA (70bp) with a central CArG box. Predicted aligned error (PAE) values are coloured on a scale of 1-30, with lower values in dark indicating lower error, and higher values in lighter shade indicating high error of prediction. Sequence schematics have been aligned to the graph to indicate the PEA for specific regions.

When looking at the confidence levels of the prediction (pLDDT), both DNA and SRF are predicted with high or very high confidence (pLDDT>70), with a high confidence prediction of the heptapeptide in B-box (residues 328-334). Q-box prediction was of low confidence, with higher values (50>pLDDT>70) of sequence containing residues that show homology in evolution (residues 352-368). The pLDDT of the prediction is shown on the structure in Figure 43A, with the colours indicating the confidence of the prediction. In Figure 43B the structures are annotated as follows: two SRF molecules of SRF are shaded in light pink and light green, MRTF B-box in yellow, and MRTF Q-box in magenta.

Alignment of the AF3 prediction of SRF-DNA to that of SRF-DNA crystal structure is shown in Figure 44, with RMSD=0.351Å of the alignment, confirming the validity of the prediction.

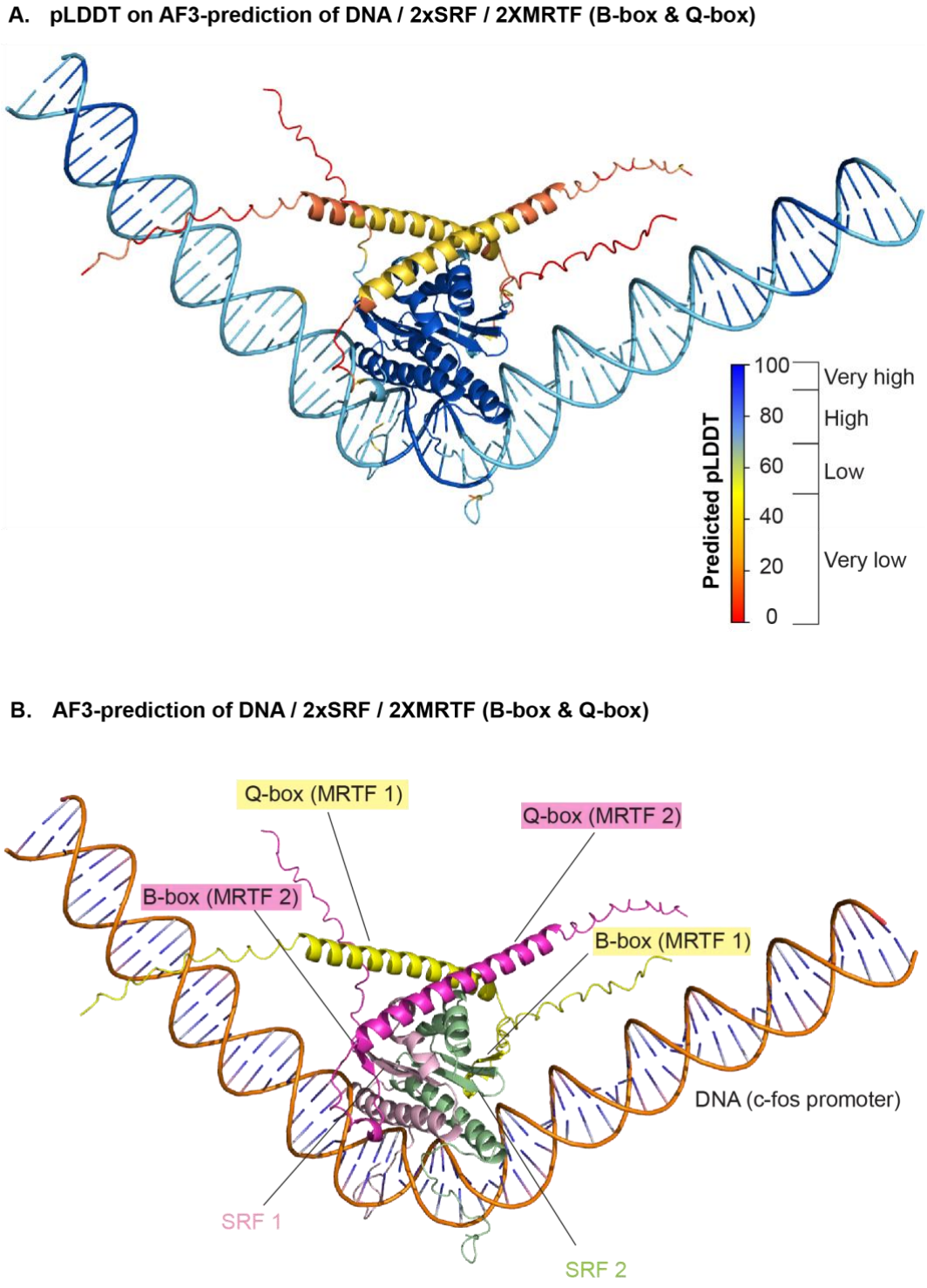

Figure 43. AF3 predicts the binding surface of MRTF on SRF-DNA complex
A. AF3 prediction with the pLDDT values plotted on the structure. pLDDT values are colour-coded on a scale of 1-100, where 90-100=Very high accuracy, 70-90=High accuracy, 50-70=Low accuracy and <50=Very low accuracy. **B.** AF3 prediction with annotations. MRTF Q-box shown in orange (evolutionary conserved sequence), B-box heptapeptide shown in yellow. SRF1 shown in pink, SRF2 in green.

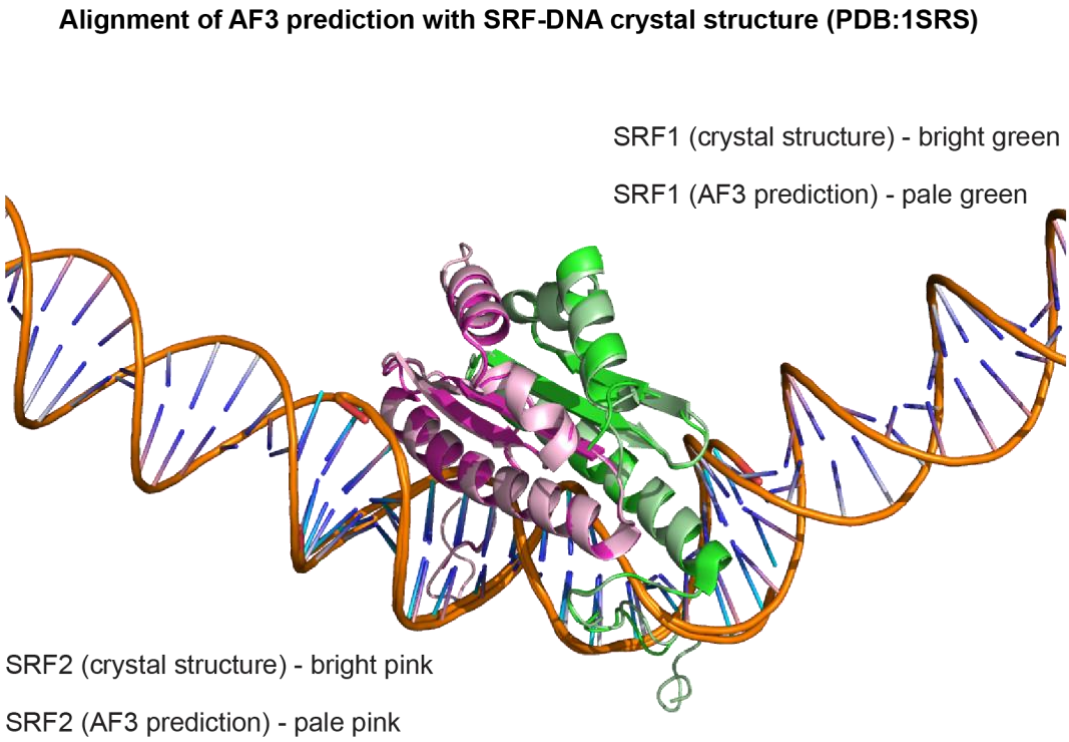

Figure 44. SRF-DNA crystal structure alignment with AF3-prediction
SRF-DNA crystal structure (PDB:1SRS) aligned to the MRTF-SRF-DNA AF3 prediction (). The RMSD of the alignment =0.351. SRF crystal structure: SRF1 – bright green, SRF2 – bright pink; SRF AF3-prediction: SRF1 - pale green, SRF2 – pale pink. MRTF B-box in yellow for both MRTF1 and MRTF2.

A detailed view of B-box contacting SRF is shown in Figure 45A. The heptapeptide sequence of both MRTFs is folded into a β-sheet and placed in a parallel manner to the β-sheet-folded subunit of SRF, making contact with all three subunits of SRF: αI-helix, β-sheets and the αII-helix (the list of contact can be found in Table 23). Interestingly, Q-box of each MRTF is folded into a left turn helix and situated on the top of the SRF complex forming a structure similar to an anti-parallel coiled-coil (Figure 45B). Typically, a coiled coil is formed of two-five helices wrapped around into a left-handed helix. The main interaction interface which was predicted with low confidence consists of seven turns. Coiled-coil domains have been implicated in dimerization, with both hydrophobic and hydrophilic contacts between the two helixes stabilizing the structure (Mason and Arndt, 2004). Based on literature, it is known that Q is not necessary for SRF-MRTF binding, but it facilitates the interaction, with Q-box

deleted MRTF mutants not binding SRF as efficiently (Zaromytidou et al., 2006). This low confidence prediction of Q placement in the complex nevertheless provides an idea of how Q-box might facilitate binding of MRTF to SRF.

A. B-box - SRF interactions

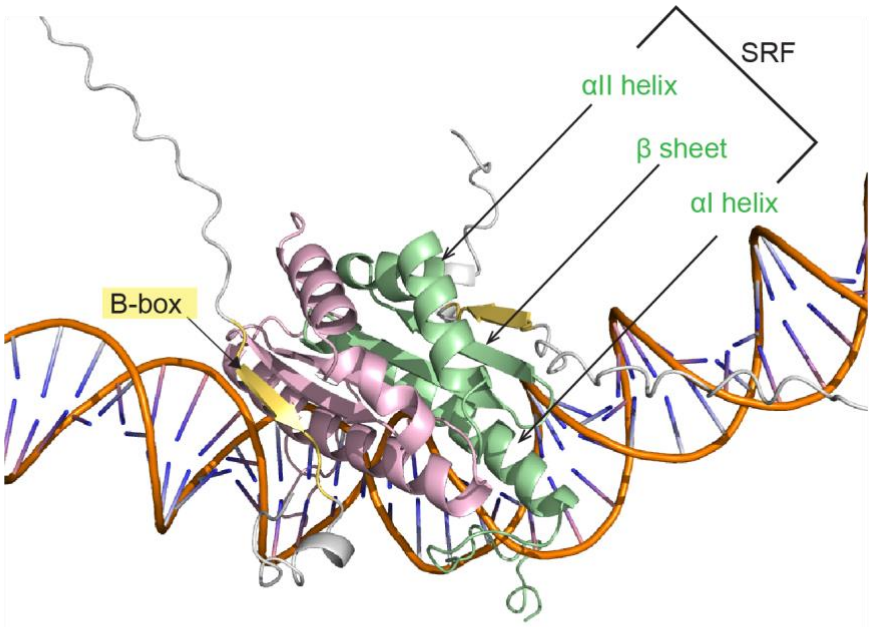

B. Q-box placement in the complex (top view)

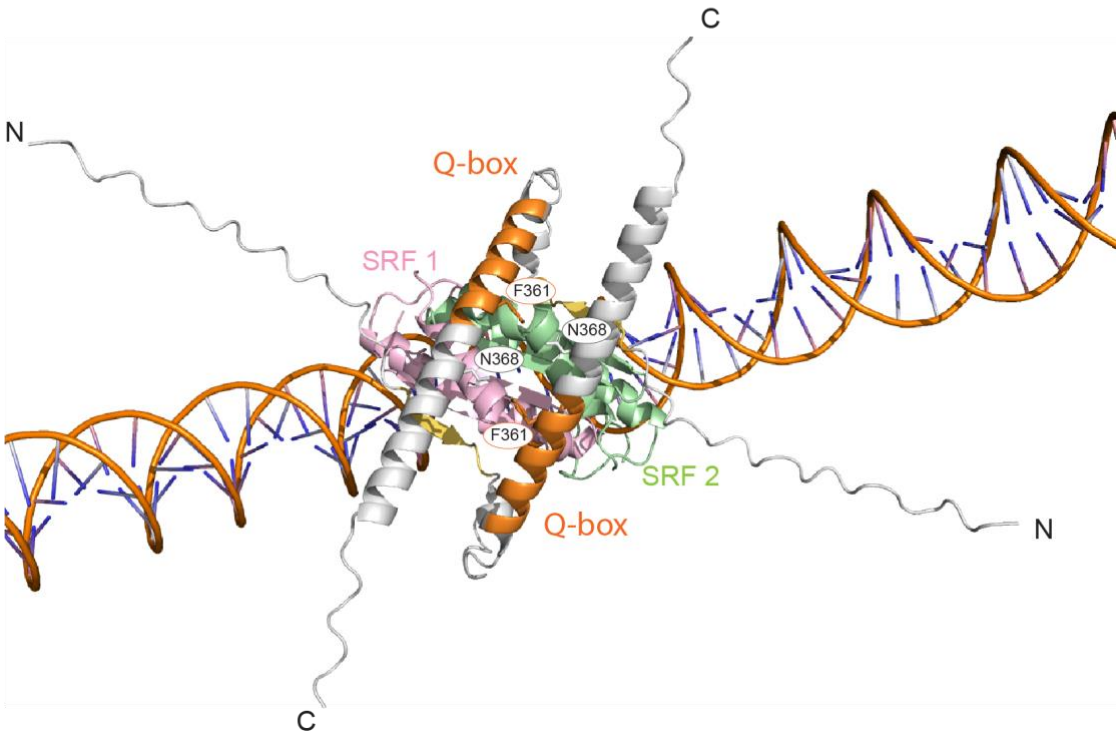

Figure 45. B-box / Q-box / SRF interactions
A. AF3 prediction with focus on the B-box / SRF interaction. Two SRF molecules (1 – pale pink, 2 – pale green), MRTF B-box – yellow. B-box is placed in a parallel manner to the β-sheet subunit of SRF. **B.** Placement of Q-box on the surface of the SRF-DNA complex in a coiled-coil formation. MRTF Q-box conserved part is coloured in orange. Residues that were indicated to make contact with low confidence are shown on the structure.

MRTF B-box	SRF
L328	L219 (αII-helix) Q216 (αII-helix)
K329	G182 (β-sheet) H193 (β-sheet) V194 (β-sheet)
Y330	V194 (β-sheet) I125 (αII-helix) K212 (αII-helix)
H331	H193 (β-sheet) V194 (β-sheet) Y195 (β-sheet)
Q332	T196 (β-sheet)
Y333	T196 (β-sheet) F197 (β-sheet) Y173 (αI-helix) M169 (αI-helix)

Table 23. List of MRTF B-box heptapeptide contacts with surfaces on SRF

4.4.2 Comparison of MRTF and TCF binding to SRF

Another family of proteins that have been described as SRF coactivators are TCFs. Biochemical and functional data suggest that they contact the same surface on SRF as MRTFs, through B-box interaction (Miralles et al., 2003; Murai and Treisman, 2002; Wang et al., 2004; Zaromytidou et al., 2006). The crystal structure of one of the members of the TCF family, SAP1 with SRF on DNA was resolved by X-ray crystallography (Richmond and Hassler, 2001).

TCF contacts SRF and DNA as a monomer, with binding of the B-box to SRF and an additional domain making contact with DNA (Ets-binding domain). In Figure 46A I used the crystal structure of SAP1-SRF-DNA to align with the AF3 prediction of MRTF-SRF binding to compare the mode of binding to SRF between the two.

MRTF B-box is aligned with the TCF B-box, making contacts with all three subunits of SRF. The main difference is in the placement of the B-box β-sheet towards SRF. TCF B-box binds in an antiparallel manner, while MRTF B-box is placed in a parallel orientation (Figure 46B). Yeast homologue of SRF – MCM1 binds its cofactor protein MATα2 in the same orientation as MRTF.

This is, to our knowledge, the first visualization of the structure of MRTF-SRF binding to DNA, with high confidence prediction of the surfaces in MRTF responsible for contacting SRF, validating the biochemical data that identified the residues important for contact with SRF to be the heptameric peptide within the B-box. Further work needs to be done to fully understand the role of Q-box and formation of stabilizing coiled coil structures in formation of the ternary DNA-SRF-MRTF complex.

A. Alignment of AF3 prediction with SRF-SAP1-DNA crystal structure (PDB:1HBX)

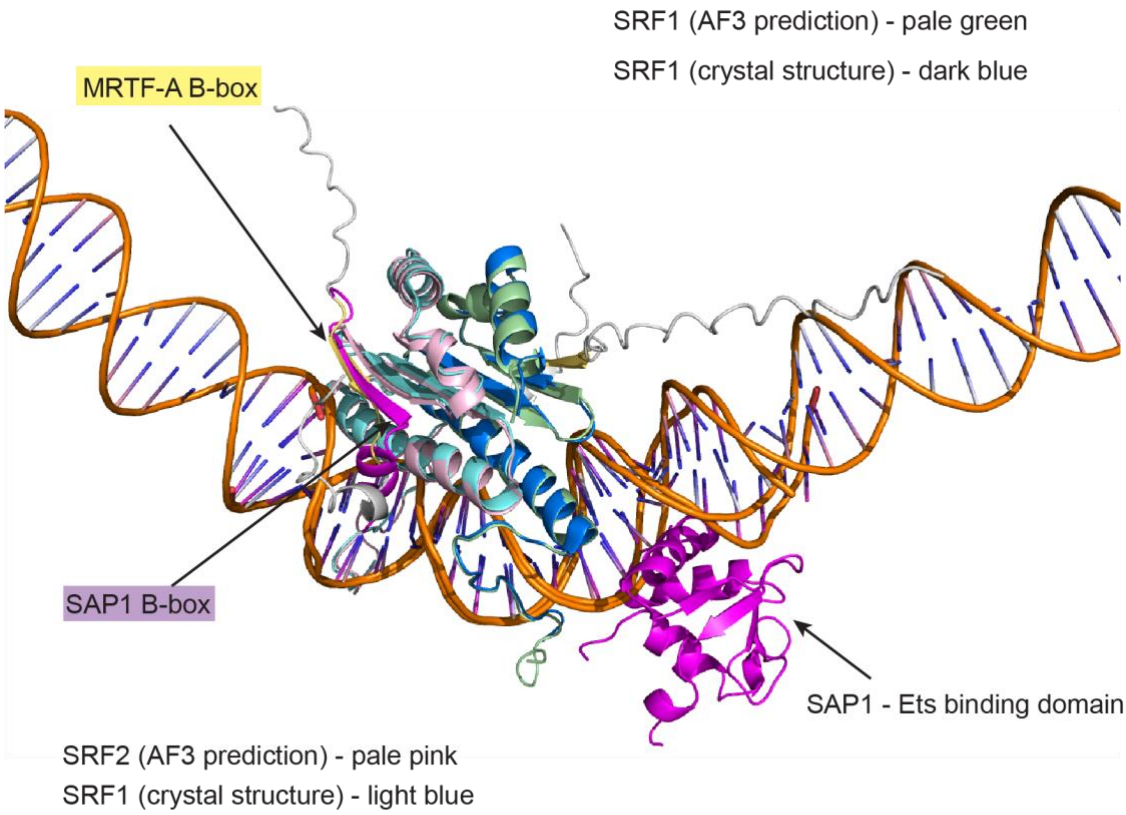

B. B-box position alignment between SAP1 and MRTF

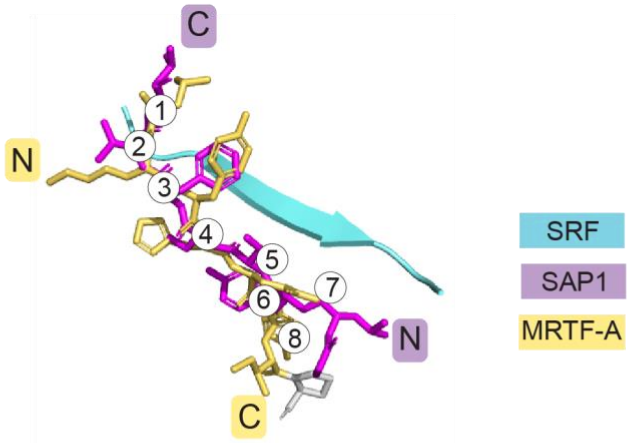

B-box position		1	2	3	4	5	6	7	8	
SAP1 (C<N)	152	L	T	F	S	S	Y	L	G	145
MRTF-A (N>C)	328	L	K	Y	H	Q	Y	I	P	335

Figure 46. Comparison of MRTF and TCF binding to SRF
A. Alignment of the AF3 prediction (SRF-DNA + MRTF B-box) with that of SAP1-SRF-DNA. B-box of both SAP1 and MRTF contacts the same surface on SRF. SAP1 shown in magenta, with the DNA binding domain indicated on the structure (Ets-binding domain). AF3 prediction: SRF1 – pale green SRF2 – pale pink; SAP1-SRF crystal structure: SRF1 – dark blue, SRF2 – light blue. MRTF B-box shown in yellow. **B.** Comparison of the residues in relative positions of the B-box. SAP1 B-box placed in antiparallel manner to SRF, MRTF B-box in parallel.

4.5 Summary

In this chapter I have described the AF2-Multimer prediction of MRTF binding actin and identified a new interaction with Q-box in its sequence. The prediction also identified a small helix in the R3 extension region, which we termed the O helix. The Q-box is placed on top of a hydrophobic actin surface (wall), making multiple contacts. It is also in close proximity to the R3 and O-box, forming a hydrophobic core of interactions between the three. It was also verified that the same interactions occur in the context of five actins binding to the RPEL domain.

R3 motif on its own is the weakest RPEL, as compared to R1 and R2, and the reason for this has been unknown. The main difference can be found between the residues within the RPxxxEL, which in R2 stabilize the Helix α-2 as well as make hydrophobic interactions with actin. Data described in this chapter shows, that in R3 residues in the same position are involved in stabilizing binding of the Q-box and actin.

Based on the structural data, a stable trivalent complex is formed on the first two RPELs and Spacer 1, and only upon stabilization of actin binding on R3, can a pentavalent complex be formed. The proposed model of binding suggested actin loading onto RPELs from the N->C of the sequence (Guettler et al., 2008), with actins binding to R3 and S2 only at high actin concentrations. In the new, revised model, loading of actin begins with R3 and S2 with the facilitating contacts from the Q-box, followed with loading of the trivalent complex on R1-S1-R2. In following chapters of this thesis I will show biochemical data in support of this model.

MRTF-SRF binding is crucial for its target gene activation. It was determined by biochemical studies that the surface of contact on MRTF is the

heptameric peptide within the B-box. Using AF3 I validated the biochemical data, showing that the B-box is placed in a parallel orientation to SRF β-sheet, making contacts with all three subunits of SRF, with high level of confidence. Comparison of the crystal structure of SAP1, a TCF-family member which competes for SRF binding with MRTF, showed they indeed place their basic B-box in the same position relatively to SRF. MRTF contacts SRF in a parallel manner, while TCFs bind with their B-box sequence antiparallel to SRF. This shows that binding of MRTF and TCF to SRF is mutually exclusive and is in agreement with the data showing competition between the two coactivators for MRTF binding.

Next chapters of this thesis will validate the AF2-Multimer prediction using biochemical and mass spectrometry-based analysis.

Chapter 5. Validation of the AlphaFold2 Multimer prediction

AlphaFold-Multimer predicts, that RPEL3 recruits Q helix to bind actin. Q stabilizes the interaction by both, binding to the surface of actin and to the RPEL3 Helix α-2 residues. This has first been predicted in the R3+C protein but has also been confirmed in the context of five actins binding to the RPEL domain.

In this section I will use two biochemical approaches to validate the prediction. First, to investigate conformational changes induced in MRTF by actin binding, I will use Hydrogen-Deuterium exchange (HDX) mass spectrometry. In this assay I will use the intact MRTF with intact RPEL domain and introduce a range of mutations in RPELs and Q to see the difference in how actin-binding induces structural changes in MRTF. Second, to measure the binding affinity and assess which MRTF interactions are required for actin binding, I will use the Bio Layer Interferometry (BLI) assay. Due to technical aspects of this assay and given that R3+C prediction matches that of the pentavalent MRTF-actin binding, I will use the R3+C construct that was used in 3.3, where a range of mutations will be introduced into MRTF based on the AF2-Multimer.Combination of both these methods will allow for identification of exact sequences necessary for actin binding to R3 and validating the AF2-Multimer prediction.

5.1 HDX-MS analysis of MRTF – actin binding interactions

I confirmed that actin binding induces structural changes in MRTF using HDX-MS, a technique, which measures the rate at which amide hydrogens (in the backbone of a protein) exchange with deuterated water.

For disordered proteins, deuterium will exchange rapidly with water, as all the amides are exposed to the solvent (Balasubramaniam and Komives, 2013) For structured proteins or bound regions of protein, deuterium will exchange less rapidly, due to protection of the amides from the solvent. Mass of deuterium is about twice that of a single hydrogen, which allows for detection of

changes in mass where the exchange occurred (Vinciauskaite and Masson, 2023).This allows for identification of protein-protein binding interfaces by quantifying the ratio of deuterium/hydrogen in peptides before and after conformational change induced by partner protein binding. The technique provides single-peptide resolution, not single-residue, since the exchange occurs on peptides with α-1 amide, which is why a good coverage of the sequence is important by obtaining overlapping peptides. The proteins are digested using pepsin which cleaves in the C-terminal site of amino acids Phe, Leu, Tyr and Trp, but the cleavage is variable between experiments, proving difficult to compare between experiments.

MRTF is an intrinsically disordered protein (IDT), unstructured in solution, which is a common feature observed in transcription factors (Brodsky et al., 2020). Actin binding induces structure in RPEL domain of MRTF (Mouilleron et al., 2011), which can be detected using HDX-MS by comparison of the uptake of deuterium between MRTF alone and MRTF bound with actin.

The data can be presented in two ways: as a butterfly plot, which allows for visualization of average relative fractional exchange for all the obtained peptides at different labelling time points. Second, the data can be plotted as a coverage plot, where the relative fractional difference values (in Da) between protein alone and bound can be plotted on top of the peptides covering the protein sequence. Shorter labelling time points allow for obtaining more transient or rapid interactions, as compared to longer times, where deuterium exchange will eventually occur with all the amides. The Mass spectrometry and analysis was done by Sarah Maslen.

5.1.1 Actin-Q contacts detected by HDX-MS

Using HDX-MS, MRTF alone was first tested to assess the exchange rate of the protein in solution. The data is presented as a butterfly plot in Figure 47. MRTF labelling reaction was done at room temperature for 3s, 30s, 300s and 3000s. Even at the earliest time-point tested, all the amides exchange fully with deuterium, indicating that the protein is essentially unstructured in solution.

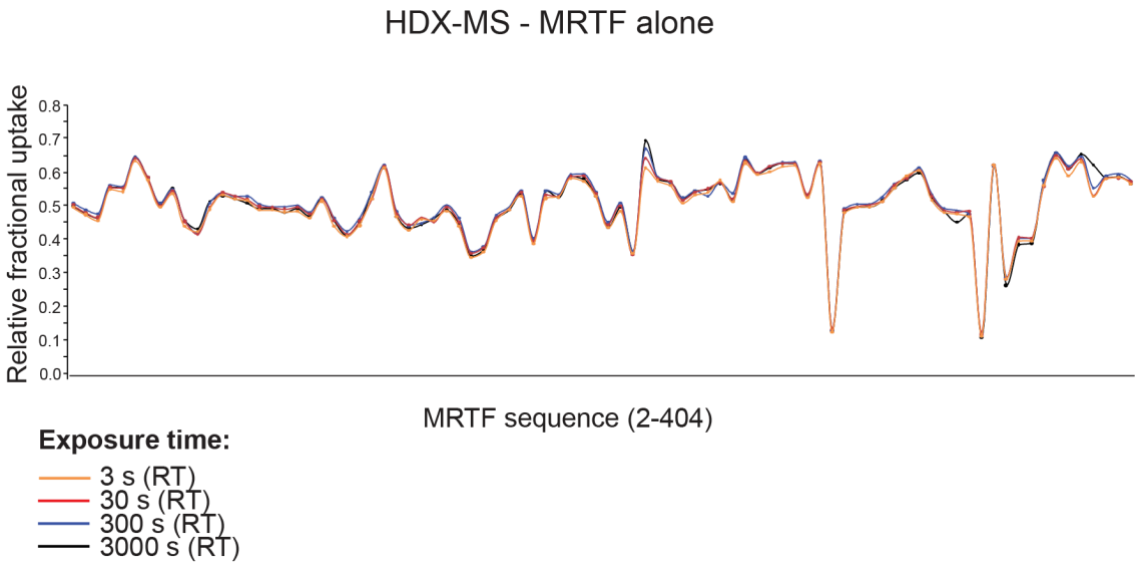

Figure 47. HDX-MS shows MRTF alone is fully deuterated in solution
HDX-MS analysis of MRTF WT alone in solution presented as a butterfly plot - each dot represents a single peptide covering MRTF sequence. Data acquired at four labelling time-points at room temperature (RT): 3s, 30s, 300s, 3000s. Axis: x – MRTF sequence, y – Relative fractional uptake of deuterium. Uptake is dependent on the number of amide hydrogens exchanging within peptide. Peptides are ordered according to the position of their N-terminus. MRTF used at 5µM. Sample run in triplicate.

Actin is known to bind to RPEL1, 2, 3 and the spacer sequences between them (Mouilleron et al., 2011), so the hydrogen-deuterium exchange at these sites should be affected by actin bidning. In pilot experiments, using 3s as the shortest labelling time-point, protection of RPEL1, Spacer 1 and RPEL2 was noted, as well as RPEL3, but no interaction with Spacer 2 was detectable. Indeeed, previous crystallography studies suggest S2 binding is unstable (Mouilleron et al., 2011). To gain more insight into S2-actin interactions, we measured exchange at shorter time points, which allows for detection of weaker or transient interactions. As the exchange rate is temperature dependent, in order to decrease the labelling time, the samples were incubated for 2s at 4°C, which would correspond to approximately 0.2s at room temperature. At this short time point, protection within the S2 could be detected (Figure 48A - peptides overlapping the S2 sequence are annotated on the plot; compare between orange and red lines, representing 2s at 4°C and 3s at RT, respectively), together with all the other well-known actin binding sites on RPEL, which prompted us to using this short timepoint for all experiments.

Difference plot (in Daltons) between MRTF with actin and MRTF alone is shown in Figure 48B.

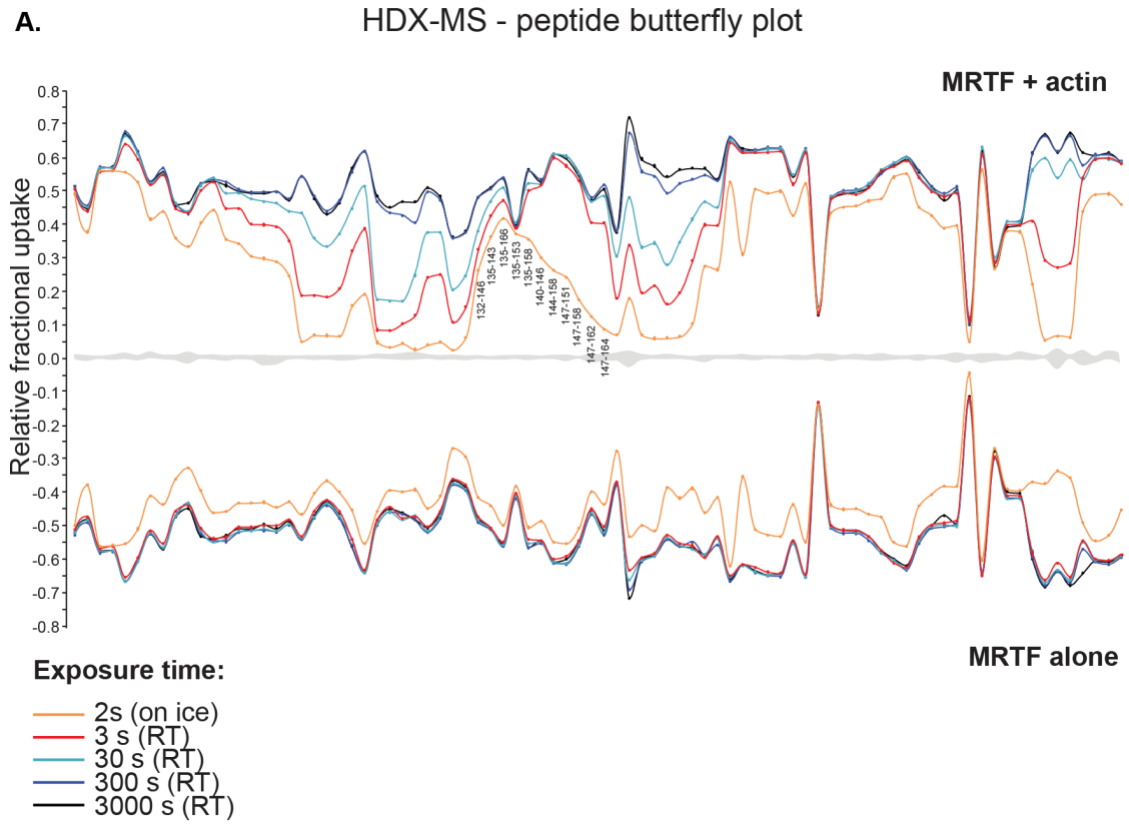

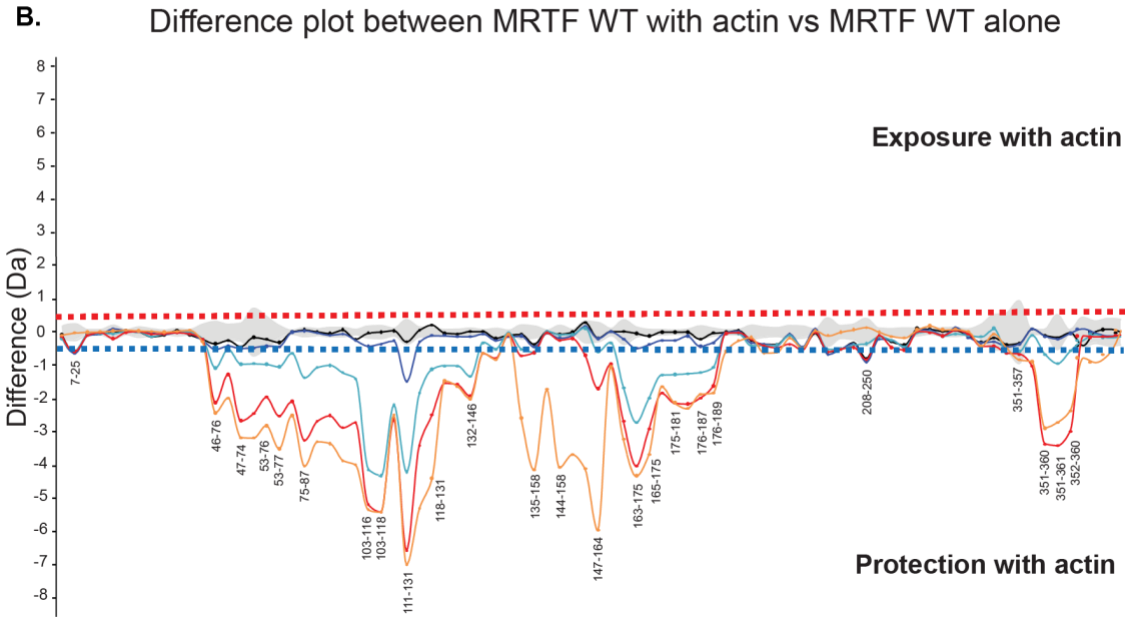

Figure 48. MRTF-actin interactions detected by HDX-MS
A. Butterfly plot of MRTF alone (bottom) and MRTF-actin (top) at 1:1 stochiometric ratio. Labelling time points: 2s at 4°C, 3s RT, 30s RT, 300s RT, 3000s RT. Data for 2s at 4°C was acquired at a different time than the RT samples. Peptides corresponding to Actin-Spacer2 binding annotated on the plot. Axis: x – MRTF sequence, y – Relative fractional uptake of deuterium. Uptake is dependent on the number of amide hydrogens exchanging within peptide. Peptides are ordered according to the position of their N-terminus. MRTF used at 5µM, LatB-skeletal α-actin used at 25µM. Sample run in triplicate. **B.** Difference plot between MRTF-actin and MRTF alone, plotted as difference in mass (Da). Change of mass larger than 0.5Da upon deuterium uptake is considered significant. Positive y-values represent exposure upon binding, negative y-values – protection upon binding.

In order to relate the HDX data to the actin-MRTF interactions shown in our previous crystal structure, the 2s at 4°C labelling time point was plotted in Figure 49. Here the individual peptides, colour coded according to the relative francional uptake difference between MRTF alone and actin bound, are aligned with the MRTF sequence, and actin interactions detected in crystal structure are annotated. There is a high level of protection within the RPEL domain region, with low relative fractional uptake spanning the sequence corresponding to each RPEL motif and the spacers between. This is in accordance with up-to-date knowledge of the MRTF-actin interaction (Guettler et al., 2008; Mouilleron et al., 2011, 2008). Strikingly, the results also revealed additional protection of the Q region, with the highest levels detected within the 351-YAKILQQQQLF-361, in accordance with the AF-Multimer prediction. This data indicates that the *in silico* modelling correctly predicted additional MRTF-actin contacts.

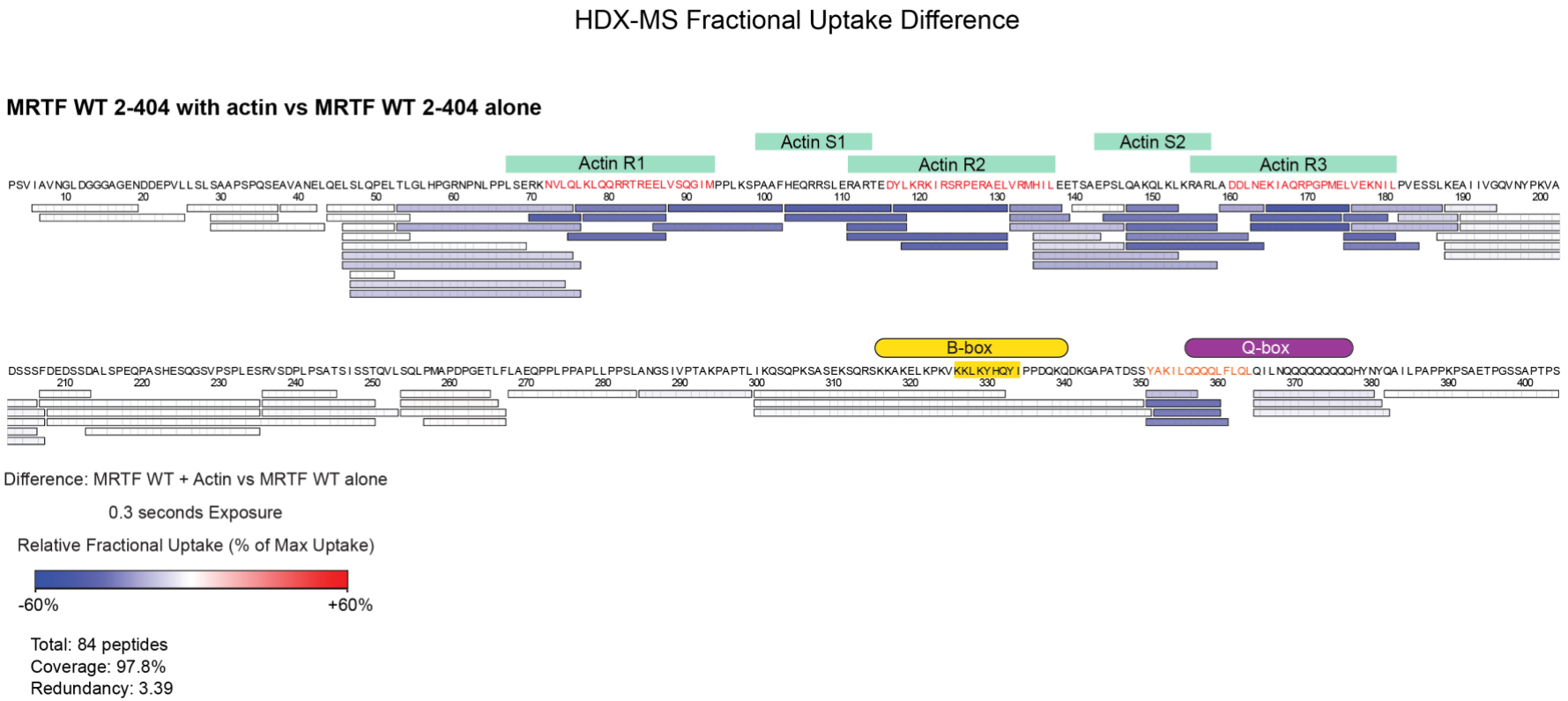

Figure 49. Q-region protection detected in MRTF WT when bound to actin
Fractional uptake difference (%) between MRTF (2-404)/Actin and MRTF alone, plotted for each peptide detected at 2s/4°C labelling time point,aligned over MRTF sequence. Data not normalized to the number of amide hydrogens within peptide and not corrected for back exchange. Total number of peptides detected: 84, coverage of the sequence: 97.8%, redundancy: 3.39. The RPEL motifs are coloured red, known actin binding sites based on structural data (PDB:2YJF) marked in green. The basic region is shaded in yellow, and the classical Q region in grey (Zaromytidou et al., 2006). The conserved Q sequence coloured orange.

Based on the AF2-Multimer prediction, residues downstream of the RPEL domain fold into a small helix, spanning the sequence 185-202 of MRTF, which will be referred to as the O helix. This interaction was not detected in the MRTF WT HDX-MS (Figure 49), however to assess its involvement in actin binding, HDX-MS analysis was performed on an MRTF mutant lacking residues spanning the O helix. As shown in Figure 50, deletion of O-box has no effect on actin binding to RPEL domain and Q-box, which is consistent with the MRTF WT HDX data, as well as the AF2-Multimer prediction, where the O helix interaction is predicted with low confidence.

BLI experiments presented in Section 3.3 showed, that the sequence C-terminal to the RPEL domain, including B and Q increase affinity of actin bidning to RPEL3. The AF2 prediction specified this interaction to occur within the Q region, and this was confirmed by HDX-MS. To check whether the unstructured region between the RPELs and Q is not involved in the binding, a deletion of the disordered loop was introduced to MRTF sequence. MRTF Δloop (Δ207-311) was analysed by HDX-MS and plotted over MRTF sequence as before. Upon loop deletion, a strong protection within the RPEL domain and Q regions can still be detected (Figure 51), suggesting that these regions are not necessary for actin binding and confirming, that Q-box has been correctly identified as involved in actin interactions.

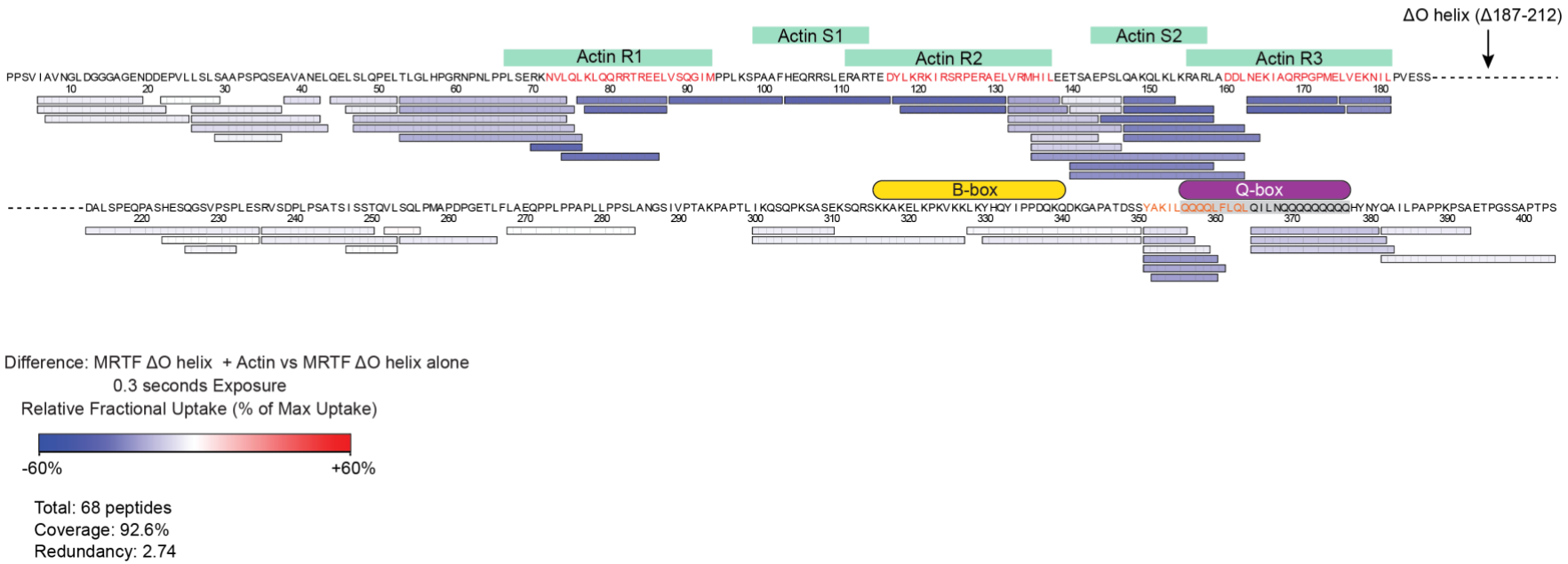

Figure 50. Actin protection on MRTF 2-404 uneffected by O helix deletion

Fractional uptake difference (%) between MRTF ΔO (Δ187-212)/Actin and MRTF ΔO alone, plotted for each peptide detected at 2s/4°C labelling time point, aligned over MRTF sequence. Data not normalized to the number of amide hydrogens within peptide and not corrected for back exchange. Total number of peptides detected: 68, coverage of the sequence: 92.6%, redundancy: 2.74. The RPEL motifs are coloured red, known actin binding sites based on structural data (PDB:2YJF) marked in green. The basic region is shaded in yellow, and the classical Q region in grey (Zaromytidou et al., 2006). The conserved Q sequence coloured orange. Deleted O residues marked as dotted line.

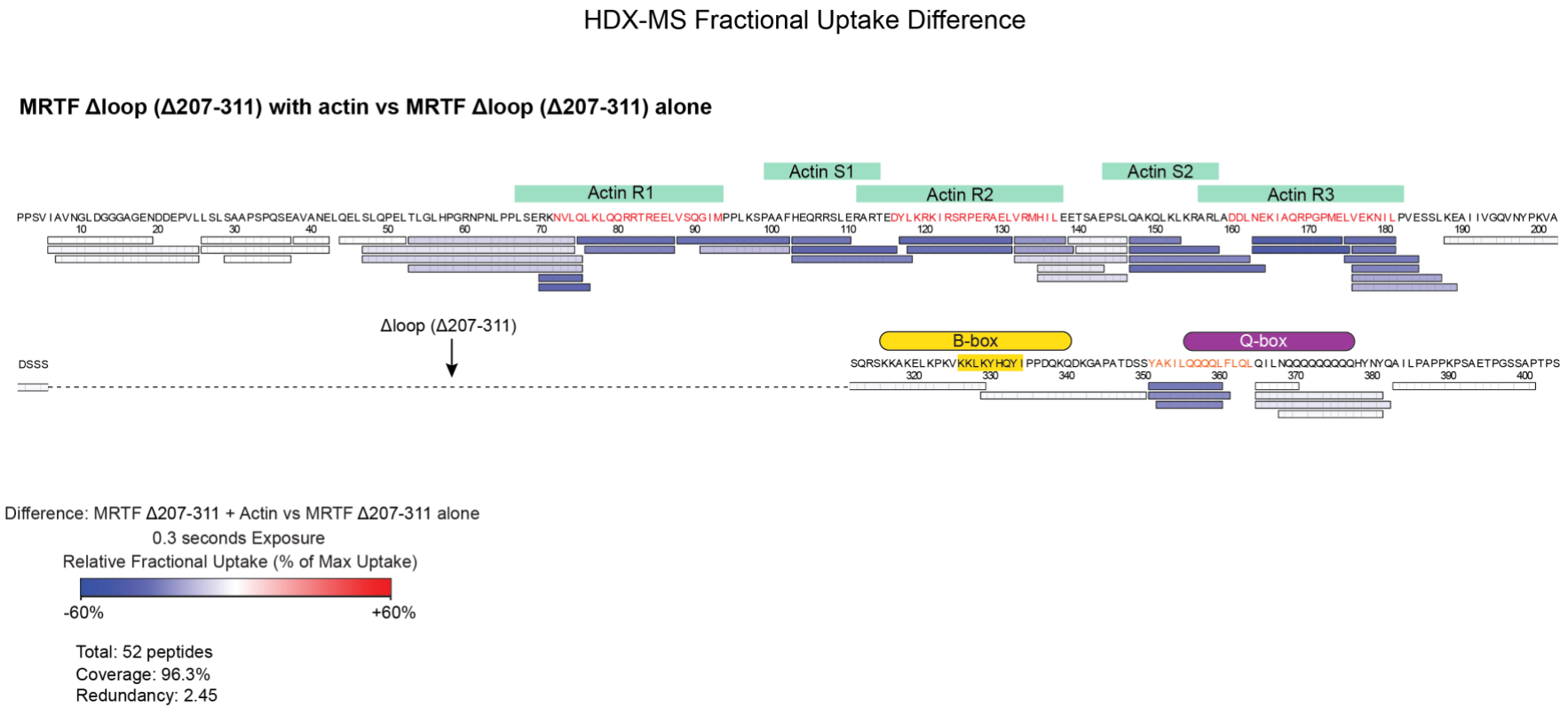

Figure 51. Actin protection on MRTF 2-404 uneffected by loop deletion

Fractional uptake difference (%) between MRTF Δloop (Δ207-311)/Actin and MRTF Δloop alone, plotted for each peptide detected at 2s/4°C labelling time point, aligned over MRTF sequence. Data not normalized to the number of amide hydrogens within peptide and not corrected for back exchange. Total number of peptides detected: 52, coverage of the sequence: 96.3%, redundancy: 2.45. The RPEL motifs are coloured red, known actin binding sites based on structural data (PDB:2YJF) marked in green. The basic region is shaded in yellow, and the classical Q region in grey (Zaromytidou et al., 2006). The conserved Q sequence coloured orange. Deleted loop residues marked as dotted line.

5.1.2 Integrity of RPEL3 is required for interaction with Q

In Chapter 3, I showed that the RPEL3 R169A mutation, which blocks actin interaction with RPEL3 severely impairs the ability of actin to inhibit MRTF-SRF interaction in the DNA pulldown assay. Based on the AF2-Multimer prediction, Q-box stabilizes actin binding to RPEL3. If interaction with the Q region is important for inhibition, R169A mutation might be expected to show altered behaviour in the HDX-MS assay. Accordingly, I tested the behaviour of the MRTF R169A mutant (MRTF-12X). In Figure 52 the top panel represents the MRTF WT binding actin at the same conditions for comparison (top panel). The relative fractional uptake (%) of the difference between MRTF 12X with actin vs MRTF 12X alone has been plotted on top of the peptide sequence (Figure 52 – bottom panel). RPEL1 and RPEL2 actin binding was not disrupted, as seen by dark blue shading of the peptides covering their corresponding sequence. As expected, actin binding to RPEL3 was not detected; moreover, Q region protection was also lost, suggesting that it is dependent on the ability of RPEL3 to bind actin.

This observation is consistent with the AF2-Multimer prediction of a composite interaction between actin and both RPEL3 and Q.

HDX-MS Fractional Uptake Difference

1.MRTF WT with actin vs MRTF WT alone

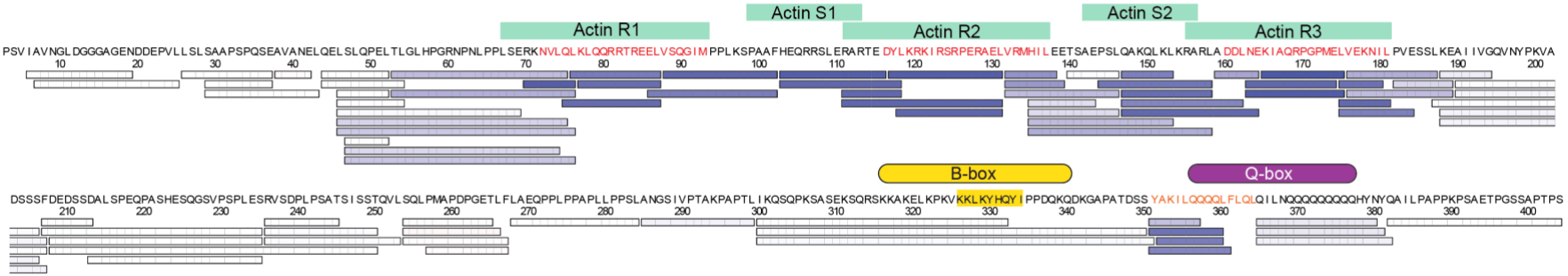

2.MRTF 12X with actin vs MRTF 12X alone

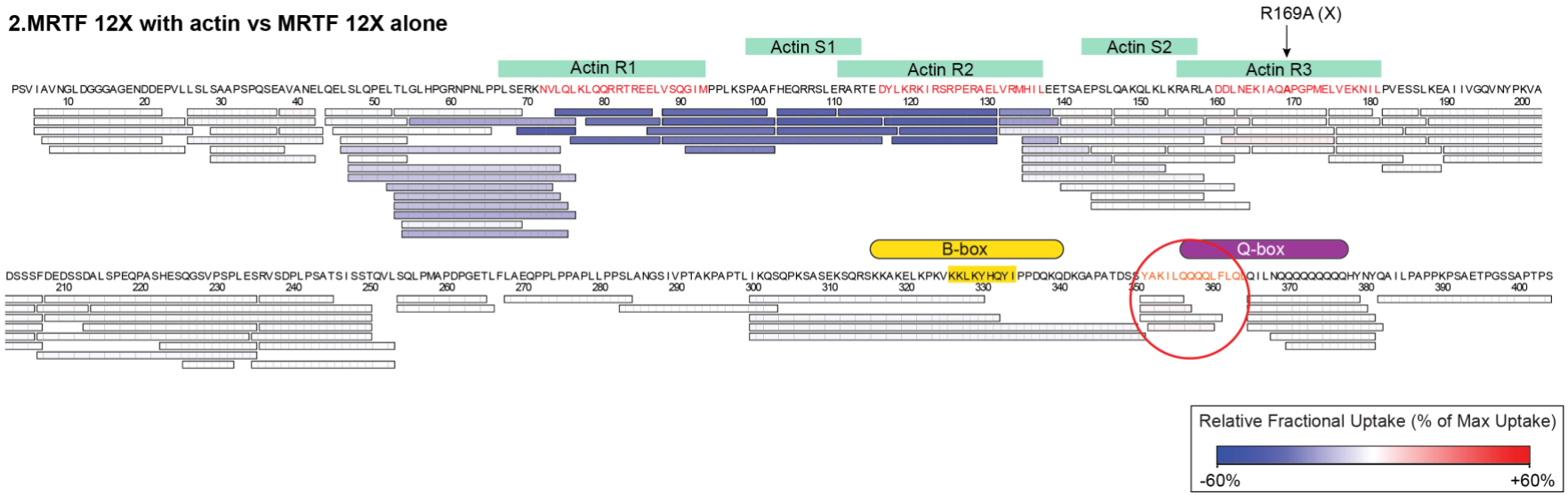

Figure 52. Comparison of HDX-MS data between MRTF WT and 12X with actin Fractional uptake difference (%) between 1. MRTF (2-404)/Actin and MRTF alone; 2. MRTF (2-404) 12X (R169A)/Actin and MRTF 12X alone. Data plotted for each peptide detected at 2s/4°C labelling time point, aligned over MRTF sequence. Data not normalized to the number of amide hydrogens within peptide and not corrected for back exchange. Total number of peptides detected in MRTF WT as described in Figure 3. Total number of peptides detected in MRTF 12X: 119, coverage of the sequence: 98%, redundancy: 4.89. The RPEL motifs are coloured red, known actin binding sites based on structural data (PDB:2YJF) marked in green. The basic region is shaded in yellow, and the classical Q region in grey (Zaromytidou et al., 2006). The conserved Q sequence coloured orange. R169A mutation indicated by an arrow.

5.1.3 Q deletion does not inhibit actin binding to RPELs

To test whether interaction with the Q-box facilitates actin binding to RPEL3, I analysed HDX-MS data on MRTF derivative lacking the Q box (∆356-377), as defined by (Zaromytidou et al., 2006). Relative fractional uptake data was plotted onto peptide sequence of the protein, as before (Figure 53). Actin binding was detected across the entire RPEL domain, although the relative fractional uptake on RPEL3 appeared to be lower than that seen with MRTF WT, consistent with weaker binding and the BLI experiments showing sequences including Q region stabilize actin binding to RPEL3. The deletion of the classical Q removes only half of the docked Q helix, with remaining short peptides spanning the interaction sequences of Q (351-YAKIL-355). Lack of protection in the remaining sequence suggests that the Q binding has been fully disrupted.

Two Q residues were chosen to assess whether single-point mutation can affect recruitment of the Q-box. L362 contacts the hydrophobic surface of actin, according to the AF2 prediction, and a mutation of this residue was expected to result in lack of Q-box recruitment. L364 however contact the predicted O region, and this mutation was thought not to interfere with Q-box binding. HDX-MS data was analysed and plotted, same as before and the results are shown in Figure 54. In both MRTF L362A (Figure 54A) and MRTF L364A (Figure 54B), binding of actin can be detected across the entire RPEL domain. However, only the L362A mutation leads to a loss, or a significant decrease in the protection within the Q, region, indicating to the importance of this interaction for actin binding.

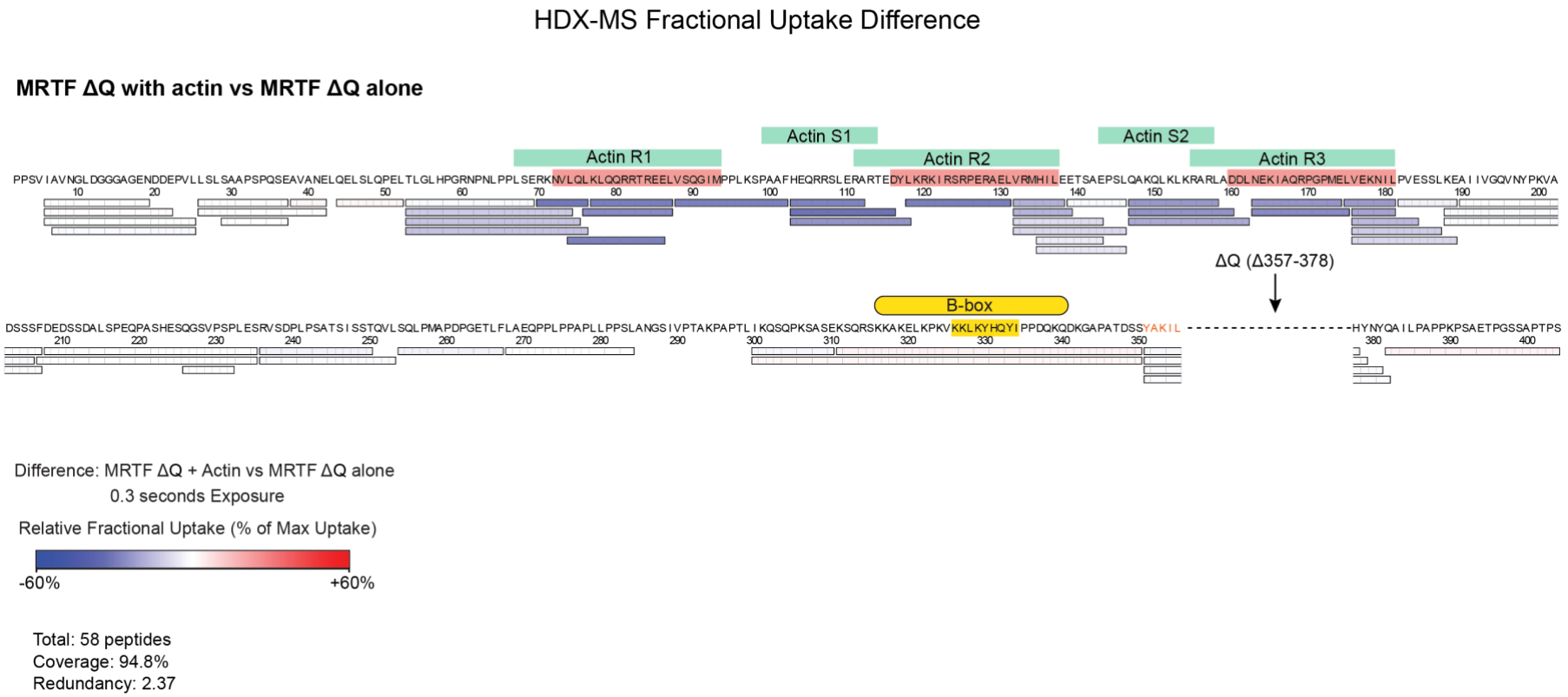

Figure 53. RPEL binding detected in the absence of classical Q sequence

Fractional uptake difference (%) between MRTF ΔQ (Δ357-378)/Actin and MRTF ΔQ alone, plotted for each peptide detected at 2s/4°C labelling time point, aligned over MRTF sequence. Data not normalized to the number of amide hydrogens within peptide and not corrected for back exchange. Total number of peptides detected: 58, coverage of the sequence: 94.8%, redundancy: 2.37. The RPEL motifs are coloured red, known actin binding sites based on structural data (PDB:2YJF) marked in green. The basic region is shaded in yellow, and the classical Q region in grey (Zaromytidou et al., 2006). The conserved Q sequence coloured orange. Residues corresponding to Q deletion are marked as a dotted line.

HDX-MS Fractional Uptake Difference

1.MRTF 2-404 L362A with actin vs MRTF 2-404 L362A alone

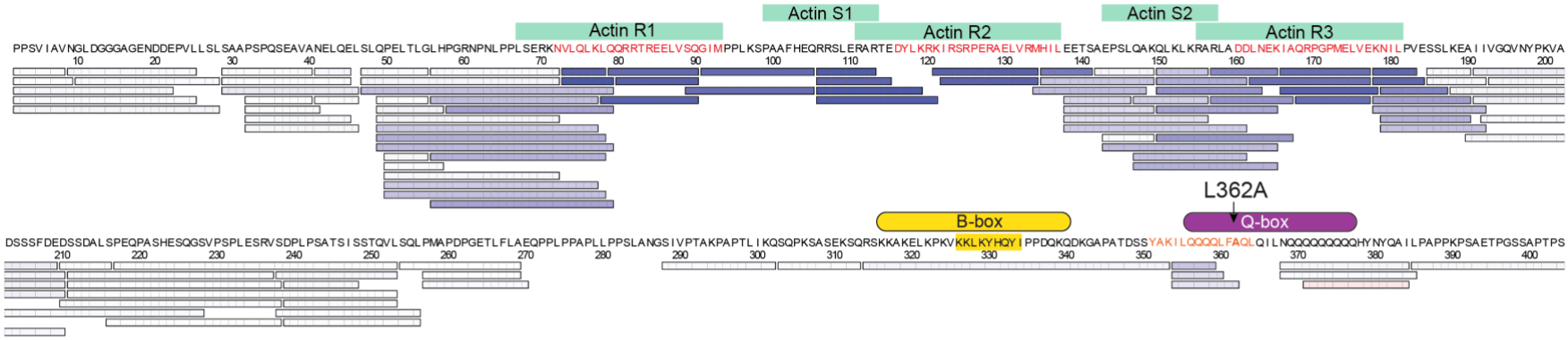

2.MRTF 2-404 L364A with actin vs MRTF 2-404 L364A alone

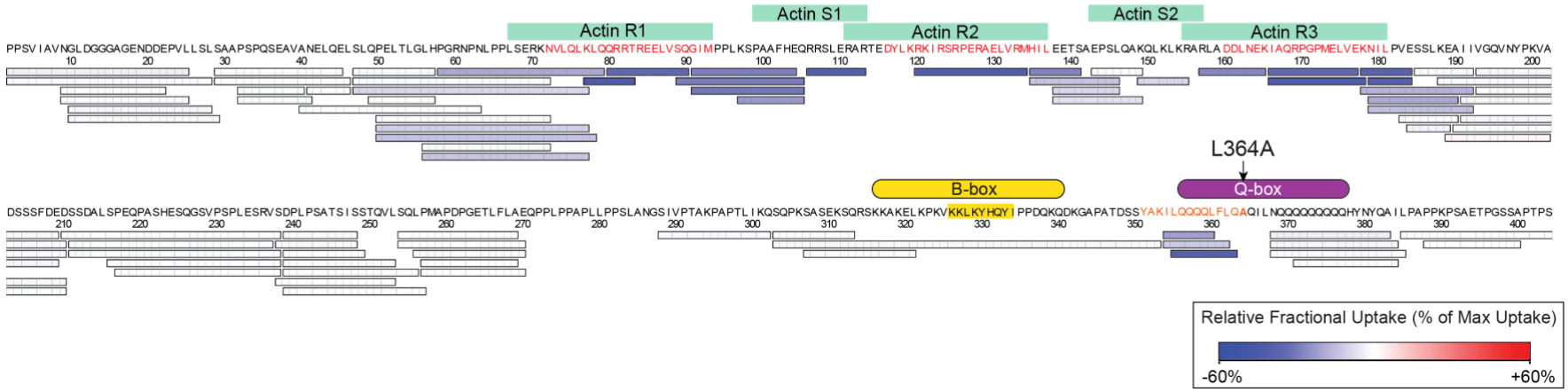

Figure 54. Actin recruitment to RPELs not affected by Q mutations in HDX-MS
Fractional uptake difference (%) between 1. MRTF (2-404) L362A/Actin and MRTF L362A alone; 2. MRTF (2-404) L364A/Actin and MRTF L364A alone, plotted for each peptide detected at 2s/4°C labelling time point, aligned over MRTF sequence. Data not normalized to the number of amide hydrogens within peptide and not corrected for back exchange. MRTF L362A - total number of peptides detected: 112, coverage of the sequence: 94.5%, redundancy: 4.74; MRTF L364A - total number of peptides detected: 84, coverage of the sequence: 93.1%, redundancy: 3.56. The RPEL motifs are coloured red, known actin binding sites based on structural data (PDB:2YJF) marked in green. The basic region is shaded in yellow, and the classical Q region in grey (Zaromytidou et al., 2006). The conserved Q sequence coloured orange. Site of mutation indicated by arrow.

5.1.4 Q binding detected in R3+C

AF prediction was done using the R3+C sequence of MRTF spanning resides 155-404. As this is the construct that will be used for the BLI analysis in the next section to identify specific residues involved in the interaction, MRTF R3+C protein was analysed using HDX-MS. MRTF was mixed with actin at a 1:1 stochiometric ratio (1:1 molar), under the assumption that there is only one actin binding site on the RPEL motif. The data has been plotted for the 2s at 4°C labelling time point on peptides covering the MRTF 155-404 sequence. As shown in Figure 55, protection can be detected both in the RPEL3 and Q regions, confirming the AF2 prediction.

This construct will be used in the further section of this chapter, where the comprehensive analysis of the MRTF-Q-actin interaction will be examined.

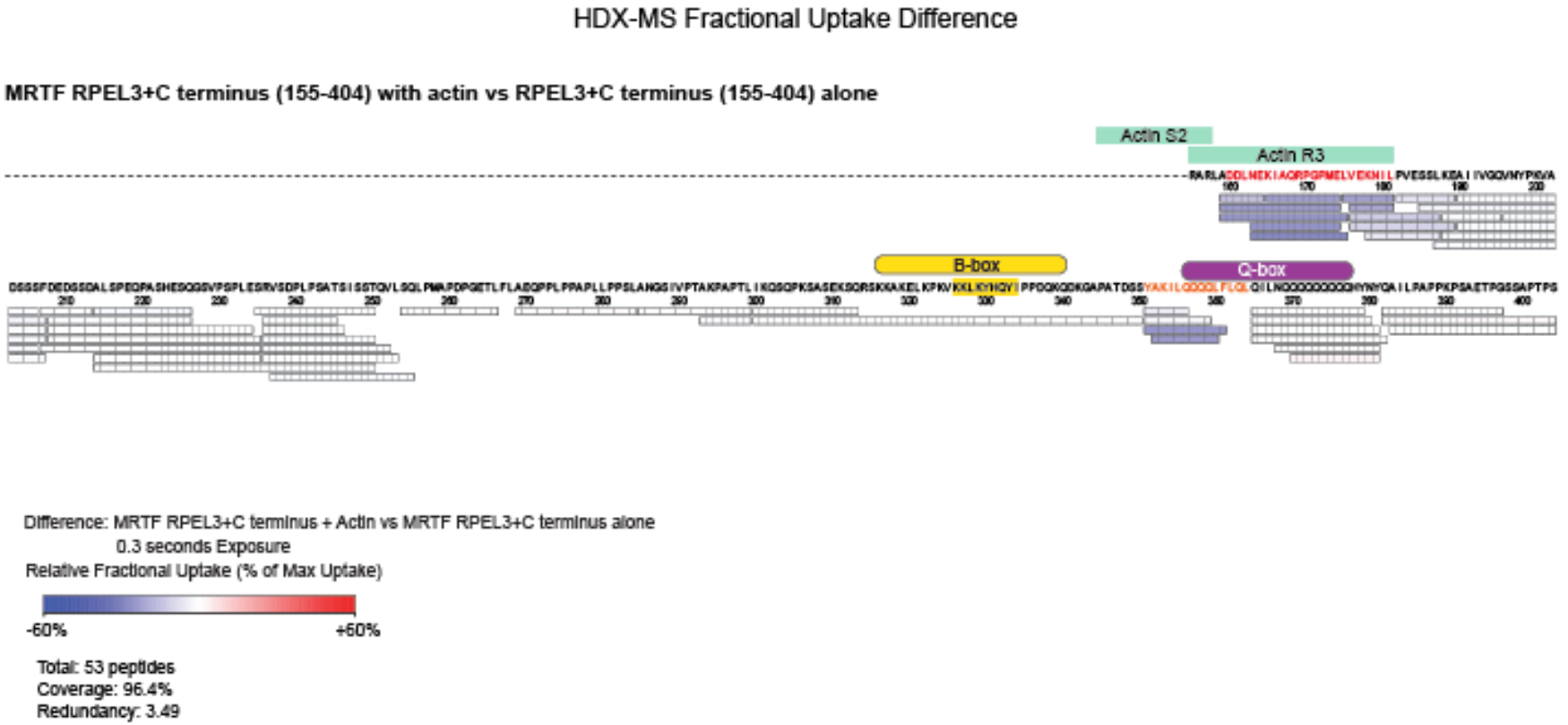

Figure 55. Q binding detected in MRTF 155-404 complexed with actin
Fractional uptake difference (%) between MRTF (155-404)/Actin and MRTF (155-404) alone, plotted for each peptide detected at 2s/4°C labelling time point, aligned over MRTF sequence. Data not normalized to the number of amide hydrogens within peptide and not corrected for back exchange. Total number of peptides detected: 53, coverage of the sequence: 96.4%, redundancy: 3.49. The RPEL motif is coloured red, known actin binding sites based on structural data (PDB:2YJF) marked in green. The basic region is shaded in yellow, and the classical Q region in grey (Zaromytidou et al., 2006). The conserved Q sequence coloured orange.

5.2 Actin-binding affinity studies

The Biolayer Interferometry (BLI) affinity measurement assay was used to determine the binding affinity of MRTF to actin.

In the following experiments, a set of mutations will be introduced to the ligand (MRTF), where the affinity of binding of the analyte (actin) will decrease significantly to that of WT MRTF. For determination of the binding affinity, the Response (thickness of the optical layer in nm) at equilibrium was plotted over concentration of the analyte (see Section 3.3 for a detailed description of the method). In order to estimate a K_d range, the R_{max} of high-affinity actin binder (WT) was used as reference (R_{max}=~1), under the assumption that given a high enough concentration of the analyte, all the mutants would be able to reach R_{max} = WT. Stimulated binding curves were fitted, using a constant R_{max} and a range of K_d values to determine which curve would best fit the data. Through this approach, a range of binding affinities is obtained based on the fit of the curves applied, which allows for comparison of the binding values between mutants and helps to determine the severity of the mutation/deletion on the ability to bind actin.

5.2.1 MRTF interactions with actin specific to the Q region

BLI is a binary assay that allows for measurement of 1:1 binding interaction. MRTF R3+C construct was used, with both AF2-Multimer prediction (Chapter 4) and HDX-MS analysis (section 5.1.4) corroborating the recruitment of Q-box to RPEL3 and actin in this construct, and the BLI analysis shown in Chapter 3 confirming a high affinity for actin binding. Mutations and deletions within the sequence were designed based on AF2-Multimer prediction.

First, I used the AF2-Multimer prediction to design large deletions in MRTF sequence, removing structured or unstructured elements of the R3+C. These include structured O helix, two deletions of the unstructured loop region between O and Q, and classical Q box deletion (Zaromytidou et al., 2006).

The AF prediction suggests the MRTF sequences between RPEL3 and Q are not involved in actin interaction. To test that, I introduced two large

deletions, one including the basic B region, the other leaving it intact (Figure 56 A and B). Neither deletion decreased the actin binding affinity. Next, the residues corresponding to the O helix were deleted, and resulted in a ~2-fold increase in Kd (Figure 56 A and C). These sequences were not implicated by AF2 to be involved in direct actin-interactions. In contrast, deletion of the Q box resulted in a >20-fold increase in K_d value (Figure 56 A and C).

These results show that the enhancement of binding affinity by sequences C terminal to RPEL domain is due to specific interaction with Q, consistent with the AF2 prediction.

A.

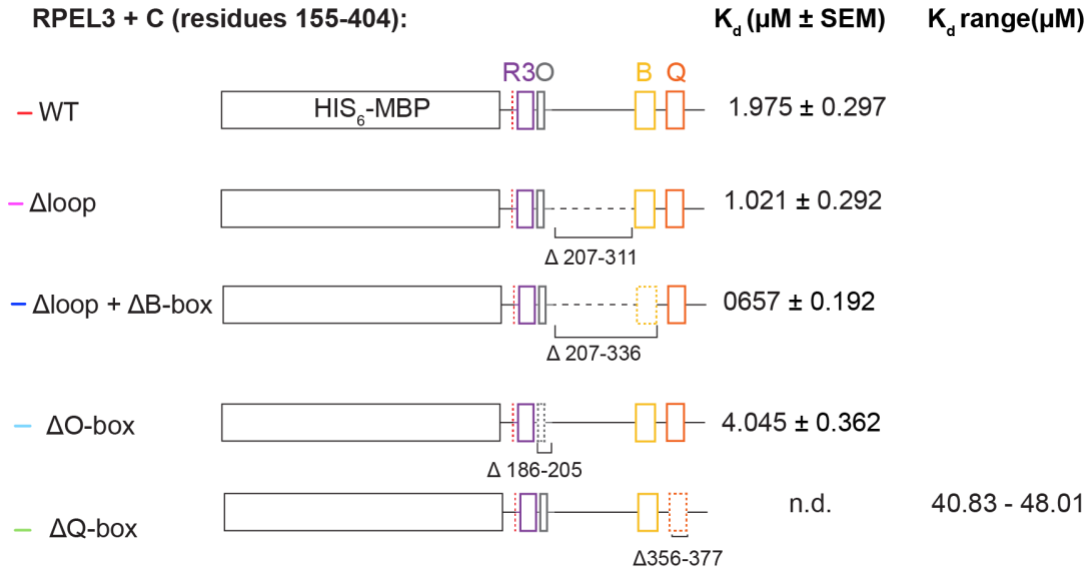

B. **BioLayer Interferometry Assay**

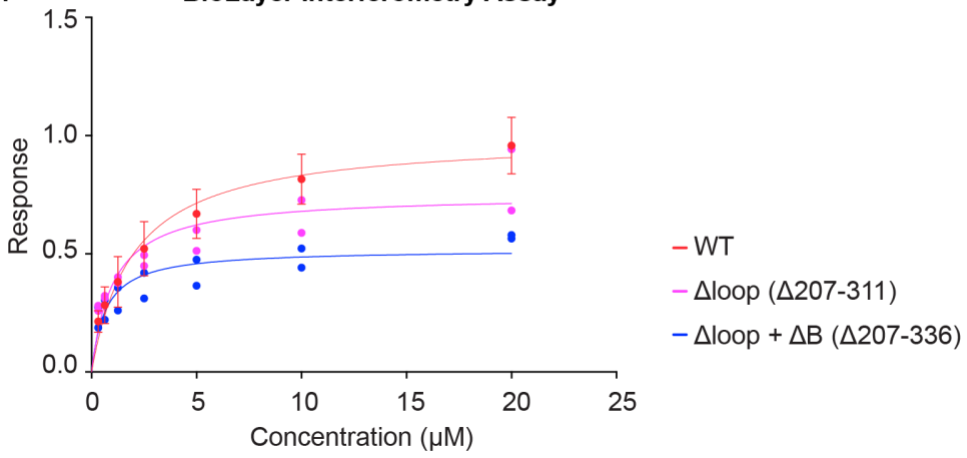

C. **BioLayer Interferometry Assay**

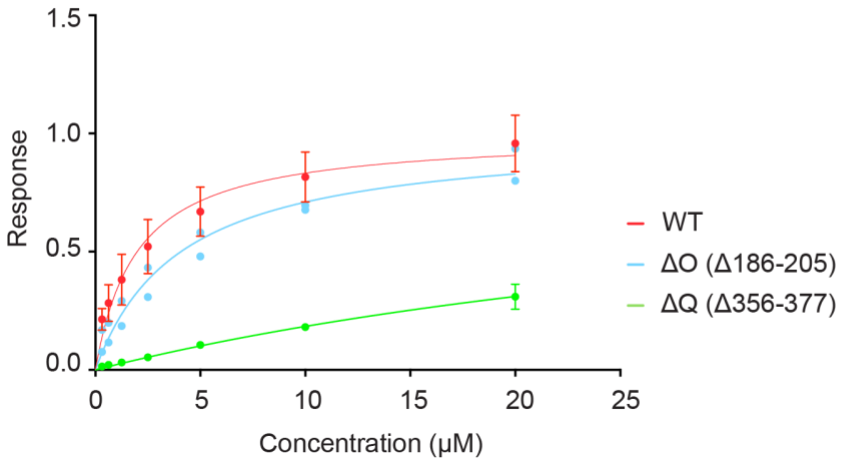

Figure 56. Enhancement of actin binding to RPEL3 specific to Q
BLI assay using HIS_6-MBP R3 + C (155-404) with LatB-rabbit skeletal muscle α-actin (top concentration of actin = 20μM). The values of K_d are based on a non-linear curve fit, with R_{max} constraint =0.9965. K_d values were calculated by steady state, using Response values of each protein over Concentration. For low affinity binders, K_d values shown as range. **A.** Schematic representation of tested proteins. Deletions are indicated on the schematic. **B.** R3+C: WT (n=6), Δloop (207-311) (n=2) and Δloop + ΔB (207-336) (n=2) binding curves. No constraint was put on the Kd calculations, as they bind actin with high affinity. **C.** R3+C WT (n=6), ΔO helix (186-205) (n=2) and ΔQ (356-377) (n=3) binding curves. Technical replicates were performed for each experiment. The error bars indicate SD values for constructs n>3.

Loss of contact alanine substitutions were introduced to the Q region, at positions identified in the AF2-Mutlimer prediction to make contact with either the actin wall (Figure 57A and B) or the RPEL3-O box sequences (Figure 57A and C). Sequence spanning from $Y351^{Q\text{-box}}$ to $I364^{Q\text{-box}}$ has been predicted to make contacts with both actin and RPEL3. Each of the mutations introduced affect actin binding to a varying degree. Residues involved in actin binding – $Y351^{Q\text{-box}}$, $L362^{Q\text{-box}}$ - decrease the affinity of binding >10-fold, with $L355^{Q\text{-box}}$ increasing the K_d >5-fold. $Q358^{Q\text{-box}}$ mutation leads to loss of actin binding affinity, with the K_d values estimated in the high μM range. In contrast, Q residues indicated in RPEL3 and O binding have an overall much milder effect on the binding affinity, increasing the K_d around 5-fold, and L360 increasing the value 2-fold.

A.

RPEL3 + C (residues 155-404):

		K_d (μM):	K_d range (μM):
WT	SYAKILQQQQLFLQLQILNQQQQQQQQQ	1.975 ± 0.172	
Actin contacts:			
Y351A	-A----------	n.d.	25.39 - 30.38
L355A	-----A----------	n.d.	12.12 - 15.28
Q358A	--------A----------	n.d.	141.2 - 190.3
L362A	----------A----------	n.d.	22.35 - 35.85
RPEL3 contacts:			
L360A	----------A----------	3.949 ± 0.223	
I354A	----A----------	n.d.	12.26 - 15.36
O contacts:			
L364A	----------A----------	n.d.	9.890 - 16.63

B.

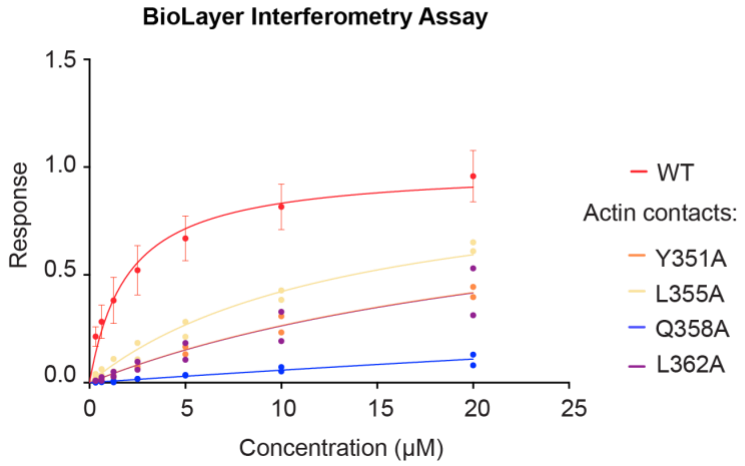

C.

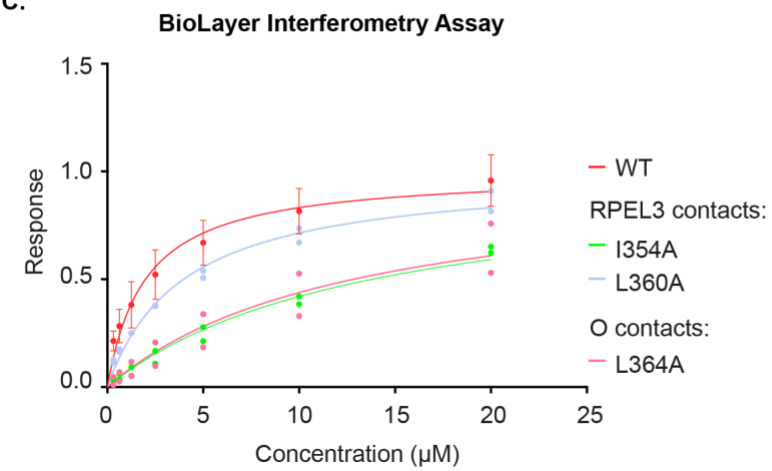

Figure 57. Disrupting Q binding to actin and R3 affects binding affinity
BLI assay using HIS_6-MBP R3 + C (155-404) with LatB-rabbit skeletal muscle α-actin (top concentration of actin = 20μM). The values of K_d are based on a non-linear curve fit, with R_{max} constraint =0.9965. K_d values were calculated by steady state, using Response values of each protein over Concentration. For low affinity binders, K_d values shown as range. **A.** Schematic representation of tested proteins. Mutations are indicated on the schematic. **B.** R3+C: WT (n=6), Y351A (n=2), L355A (n=2), Q358A (n=2) and L362A (n=2) binding curves. **C.** R3+C WT (n=6), I354A (n=2), L360A (n=2) and L364A (n=2) binding curves. Technical replicates were performed for each experiment. The error bars indicate SD values for constructs n>3.

5.2.2 Specific residues within RPEL3 required for Q recruitment

RPEL3 appears to have a specific role in Q-box interactions. As described in Chapter 4, several RPEL3 residues, together with the O region contact the Q-box to stabilize binding. In this section I will address the following: is this RPEL3 specific, or does it also occur on RPEL1 and RPEL2? If it is specific, what is it about RPEL3 that allows for Q recruitment and is that why RPEL3 alone is a weak actin binder? Looking at R1+C and R2+C, as well as substitutions within RPEL3 with individual R1 and R2 residues will help answer these questions.

Loss of contact mutation at the conserved arginine of RPxxxEL (R/A) abolishes the ion pair with actin C terminal carboxylate at $F375^{actin}$ of actin, leading to effective loss of binding (Mouilleron et al., 2008). In the BLI assay, introduction of this change into R3+C resulted in a similar loss of binding (Figure 58A and B), consistent with the effect of this change in HDX-MS (Figure 52). This confirms that the classical interaction with actin is crucial.

In contrast, mutations of residues within the O helix did not significantly affect actin binding affinity (Figure 58A and C). This is consistent with both the AF prediction (Chapter 4), HDX analysis (5.1) and the BLI analysis of O deletion mutant (Figure 50).

A.

RPEL3 + C (residues 155-404):

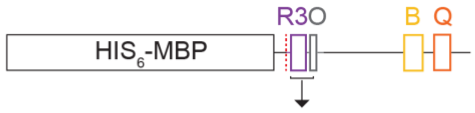

		K_d (μM):	K_d range (μM):
	160 170 180		
WT	RARLA**DDLNEKIAQRPGPMELVEKNIL**PVESS	1.975 ± 0.172	
R169A	----------**A**----------	n.d.	240.3-381.6

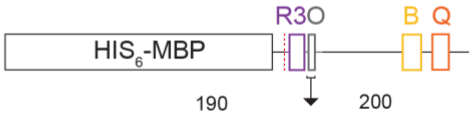

	190 200		
	PVESSLKEAIIVGQVNYPKVAD		
V183A	-**A**----------	4.459 ± 0.392	
L187A	-----**A**----------	2.461 ± 0.235	
I191A	---------**A**----------	4.420 ± 0.248	
V196A	----------**A**-------	4.545 ± 0.748	

B. **BioLayer Interferometry assay**

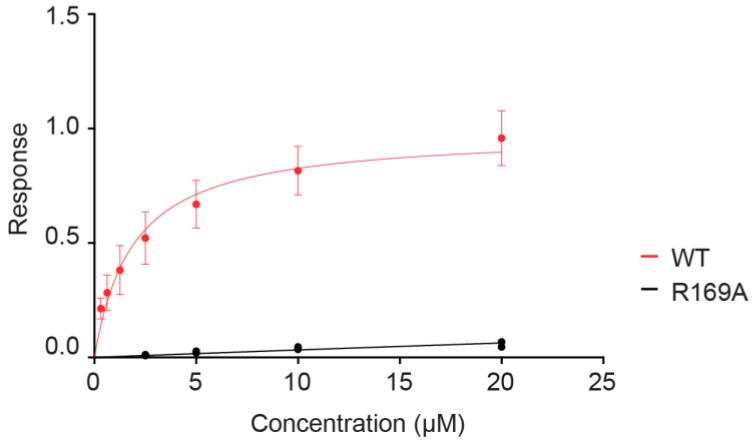

C. **BioLayer Interferometry assay**

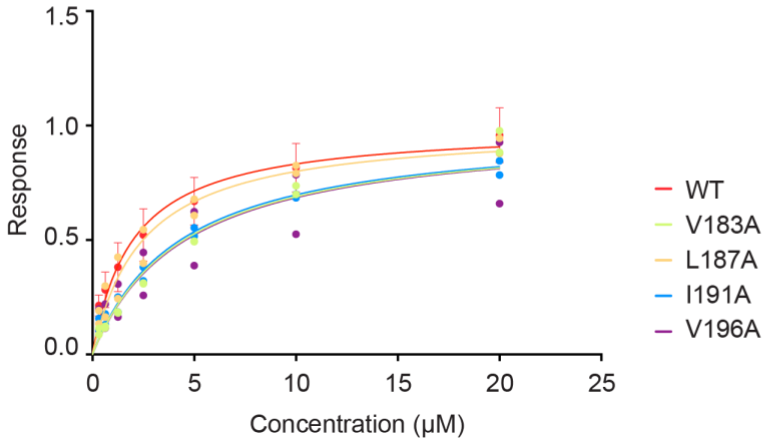

Figure 58. Specific residues in RPEL3 region affect actin binding
BLI assay using HIS_6-MBP R3 + C (155-404) with LatB-rabbit skeletal muscle α-actin (top concentration of actin = 20μM). The values of K_d are based on a non-linear curve fit, with R_{max} constraint =0.9965. K_d values were calculated by steady state, using Response values of each protein over Concentration. For low affinity binders, K_d values shown as range. **A.** Schematic representation of tested proteins. Mutations are indicated on the schematic. **B.** R3+C WT (n=6) and R169A (n=2) binding curves. **C.** R3+C: WT (n=6), V183A (n=2), L187A (n=2), I191A (n=2) and V196A (n=2) binding curves. Technical replicates were performed for each experiment. The error bars indicate SD values for constructs n>3.

Subsequently, to test whether the Q-box interaction is RPEL3 specific, or is it a general RPEL characteristic, RPEL1 and RPEL2 sequences were substituted in place of RPEL3 in the R3+C construct (Figure 59). This led to a significant decrease in actin-binding affinity, with the effect more pronounced for RPEL2 substitution. This confirms RPEL3-Q interaction is unique, even when RPEL1 and RPEL2 sequences were moved in its place.

To understand the differences that lead to different actin binding affinities, a series of single-point mutations was introduced into RPEL3, based on RPEL2 sequence (Figure 60). $G171^{R3}$ and $P172^{R3}$ are in the same position within RPEL3 as $E127^{R2}$ and $R128^{R2}$ in RPEL2. In RPEL2, they play a role in stabilizing binding of actin. Substitution of these residues with G171E or P172R resulted in significant loss of actin binding affinity. In another residue, $M173^{R3}$, loss of contact (M173A) or charge-reversal mutation (M173E) also decreased actin-binding affinity. This shows distinct actin binding mechanisms between the RPELs.

A.

RPEL1 67 LSERK**NVLQLKLQQRRTREELVSQGIM**PPLKS 98

RPEL2 111 RARTE**DYLKRKIRSRPERAELVRMHIL**EETSA 142

RPEL3 155 RARLA**DDLNEKIAQRPGPMELVEKNIL**PVESS 186

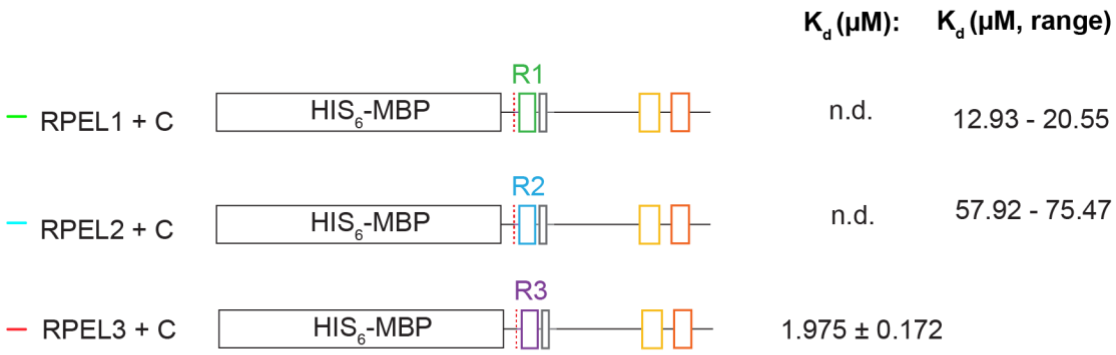

B.

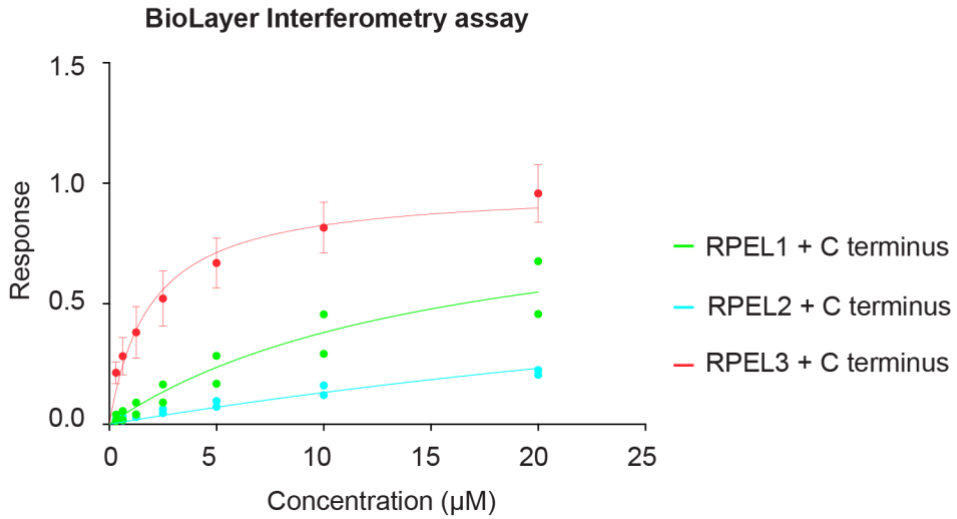

Figure 59. RPEL1 and RPEL2 binding not compatible with Q recruitment
BLI assay using HIS_6-MBP R3 + C (155-404) with LatB-rabbit skeletal muscle α-actin (top concentration of actin = 20μM). The values of K_d are based on a non-linear curve fit, with R_{max} constraint =0.9965. K_d values were calculated by steady state, using Response values of each protein over Concentration. For low affinity binders, K_d values shown as range. **A.** Schematic representation of tested proteins. **B.** R3+C: WT (n=6), R2+C (n=2) and R1+C (n=2) binding curves. Technical replicates were performed for each experiment. The error bars indicate SD values for constructs n>3.

A.

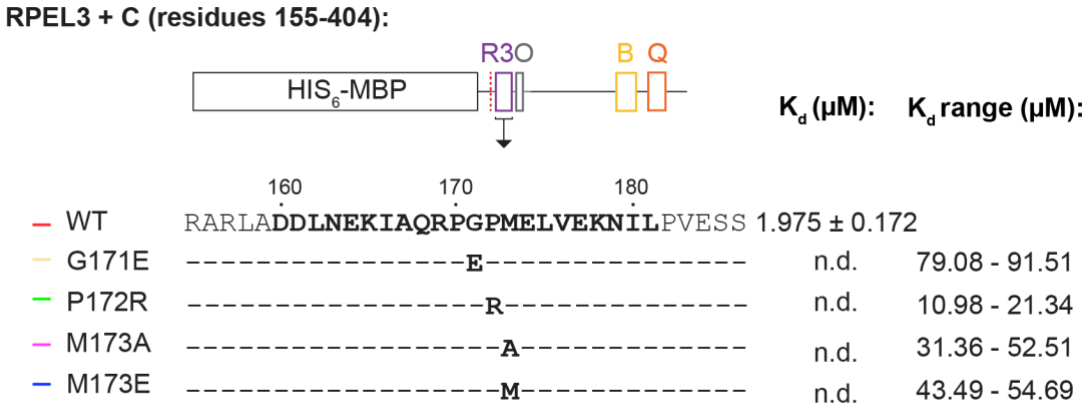

B.

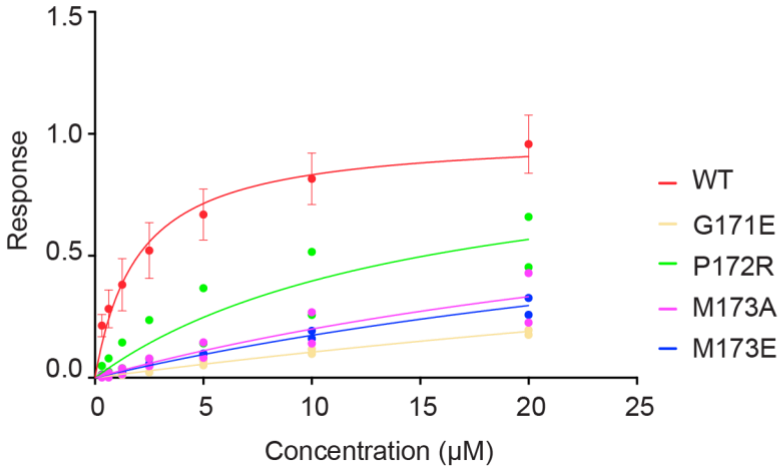

Figure 60. R2-like mutations in R3+C decrease binding affinity
BLI assay using HIS_6-MBP R3 + C (155-404) with LatB-rabbit skeletal muscle α-actin (top concentration of actin = 20μM). The values of K_d are based on a non-linear curve fit, with R_{max} constraint =0.9965. K_d values were calculated by steady state, using Response values of each protein over Concentration. For low affinity binders, K_d values shown as range. **A.** Schematic representation of tested proteins. Mutations indicated on the schematic. **B.** R3+C: WT (n=6), G171E (n=2), P172R (n=2), M173A (n=2) and M173E (n=2) binding curves. Technical replicates were performed for each experiment. The error bars indicate SD values for constructs n>3.

RPEL3 on its own binds actin weakly, as compared to RPEL1 and RPEL2 (Mouilleron et al., 2008). Although the crystal structures of RPEL1 and RPEL2 with actin were resolved, RPEL3-actin crystal structure was not possible to resolve, due to the weak binding affinity. The conservation between the RPEL motifs can be mapped onto the R-Loop and Helix α2 (RPxxxEL). The main residues responsible for the lower affinity of RPEL3 have been determined to

be G171^{R3} and P172^{R3}. G171^{R3} was implicated in introducing flexibility to the R-Loop, while the P172^{R3} is unable to bind the Y169^{actin} in actin, as it's lacking a main chain amide to form a hydrogen bond. As described above, the corresponding residues in RPEL2 are E127^{R2} and R128^{R2}, and play a role in stabilizing actin binding in RPEL2.

Introducing a GP171/172ER mutation into RPEL3 peptide alone led to increase of actin binding affinity of RPEL3 (Mouilleron et al., 2008). This is also the approach that was used to obtain a crystal structure of RPEL domain with five actins (Mouilleron et al., 2011). Same effect could be observed using BLI, where introducing a GP171/172ER mutation into RPEL3 alone increases the affinity for actin binding (Figure 61) compared to RPEL3 WT. By combining this mutation with M173A, to further resemble RPEL2, the binding of RPEL3 was significantly increased.

A.

RPEL3 (residues 155-186):

		K_d (μM):	K_d range (μM):
	160 170 180		
WT	RARLA**DDLNEKIAQRPGPMELVEKNIL**PVESS	n.d.	80.84 - 113.4
GP/ER (171/172)	----------**ER**----------	n.d.	18.61 - 31.13
GPM/ERA (171/172/173)	----------**ERA**----------	10.246 ± 0.287	

B.

BioLayer Interferometry assay

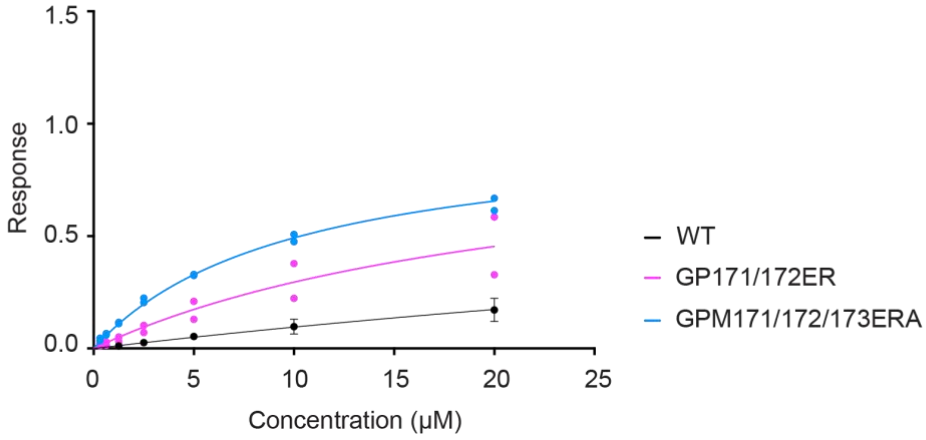

Figure 61. Combined R2-like mutations increase binding affinity of RPEL3 alone
BLI assay using HIS_6-MBP R3 + C (155-187) with LatB-rabbit skeletal muscle α-actin (top concentration of actin = 20µM). The values of K_d are based on a non-linear curve fit, with R_{max} constraint =0.9965. K_d values were calculated by steady state, using Response values of each protein over Concentration. For low affinity binders, K_d values shown as range. **A.** Schematic representation of tested proteins. Mutations indicated on the schematic. **B.** R3: WT (n=3), GP171/172ER (n=2), GPM171/172/173ERA (n=2) binding curves. Technical replicates were performed for each experiment. The error bars indicate SD values for constructs n>3.

As shown in Figure 60, introduction of single-point mutations into R3+C (G171E or P172R) led to a decrease in actin binding affinity, whereas combination of them in RPEL3 alone increased actin binding. $G171^{R3}$ and $P172^{R3}$, based on the AF-Multimer prediction interact with $Q357^{Q\text{-box}}$ of the Q-box. Mutation of these residues could lead to a possible clash with $Q357^{Q\text{-box}}$ within the Q region, especially the P172R substitution. I introduced a double-point mutation GP171/172ER and saw the same residues that make RPEL2 a strong actin-binder, and increase actin binding of RPEL3 alone, are incompatible with the mechanism of Q stabilizing interaction on RPEL3 (Figure 62). Deleting the classical Q region in the GP/ER mutant led to an increase in actin binding affinity. This again confirms that Q-interaction is RPEL3 specific, and that actin binding by RPEL2 and Q is mutually exclusive.

To visualize GP171/172ER R3+C actin binding, I used AF2-Multimer to test whether Q-box recruitment can be observed in the presence of the RPEL2-like residues. As shown in Figure 63A, actin-MRTF interaction is only predicted with low error within RPEL3, whereas the Q is not predicted to be bound by actin (compare with PAE plot in Figure 34). Similarly, the pLDDT plot predicts high confidence interactions within RPEL3, while the previously detected Q binding is abolished (Figure 63B). This confirms the BLI results presented in this section, where RPEL2-like mutations decreased actin binding affinity, suggesting incompatibility with Q-box binding.

The mechanism of actin binding to RPEL3 is different to that of the other RPELs, as it involves additional interaction, which in tandem stabilize actin binding to the RPEL3. Disruption of RPEL3 residues contacting Q-box leads to loss of actin binding.

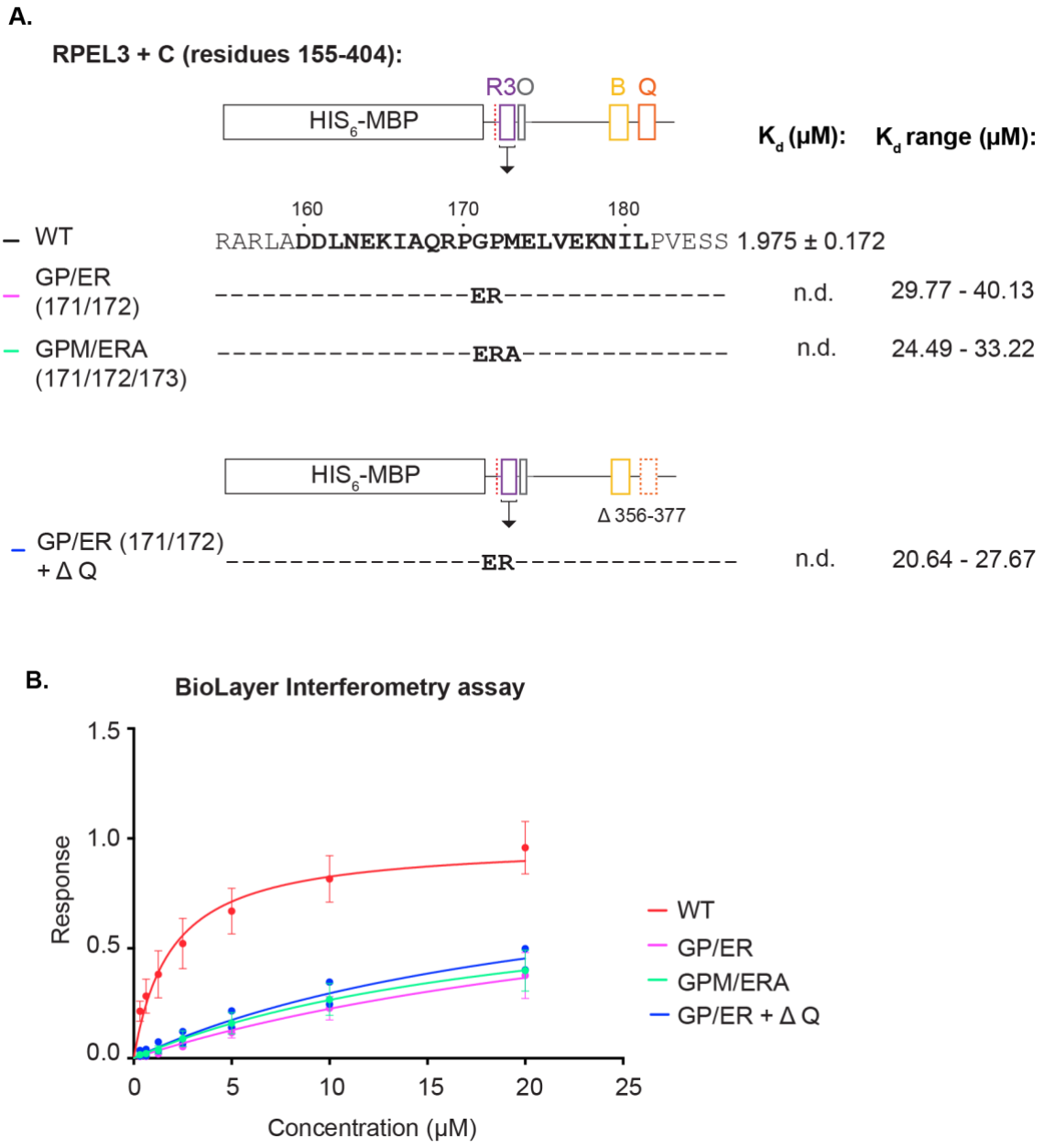

Figure 62. Combined R2-like mutation in R3+C incompatible with Q recruitment
BLI assay using HIS_6-MBP R3 + C (155-404) with LatB-rabbit skeletal muscle α-actin (top concentration of actin = 20μM). The values of K_d are based on a non-linear curve fit, with R_{max} constraint =0.9965. K_d values were calculated by steady state, using Response values of each protein over Concentration. For low affinity binders, K_d values shown as range. **A.** Schematic representation of tested proteins. Mutations and deletions indicated on the schematic. **B.** R3+C: WT (n=6), GP171/172ER (n=3), GPM171/172/173ERA (n=3) and GP171/172ER + ΔQ (356-377) (n=2) binding curves. Technical replicates were performed for each experiment. The error bars indicate SD values for constructs n>3.

A. **PAE of RPEL3+C terminus GP171/172ER with actin (AF-Multimer)**

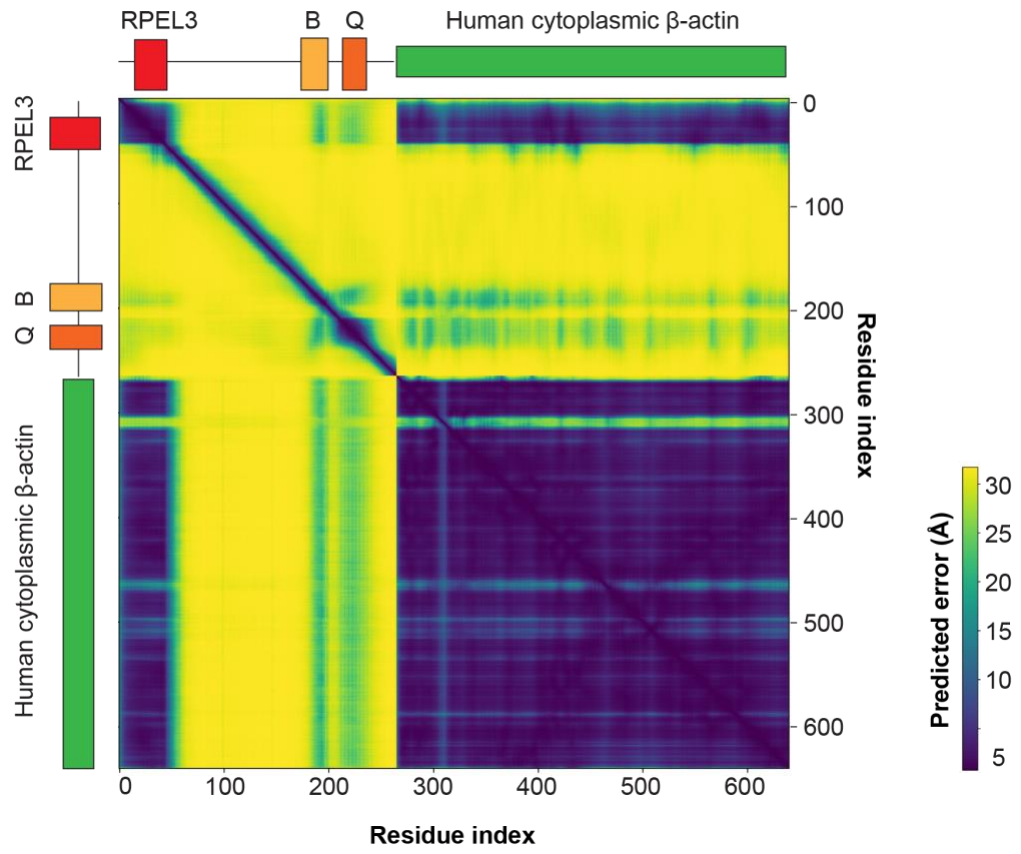

B. **pLDDT of RPEL3+C terminus GP171/172ER with actin (AF-Multimer)**

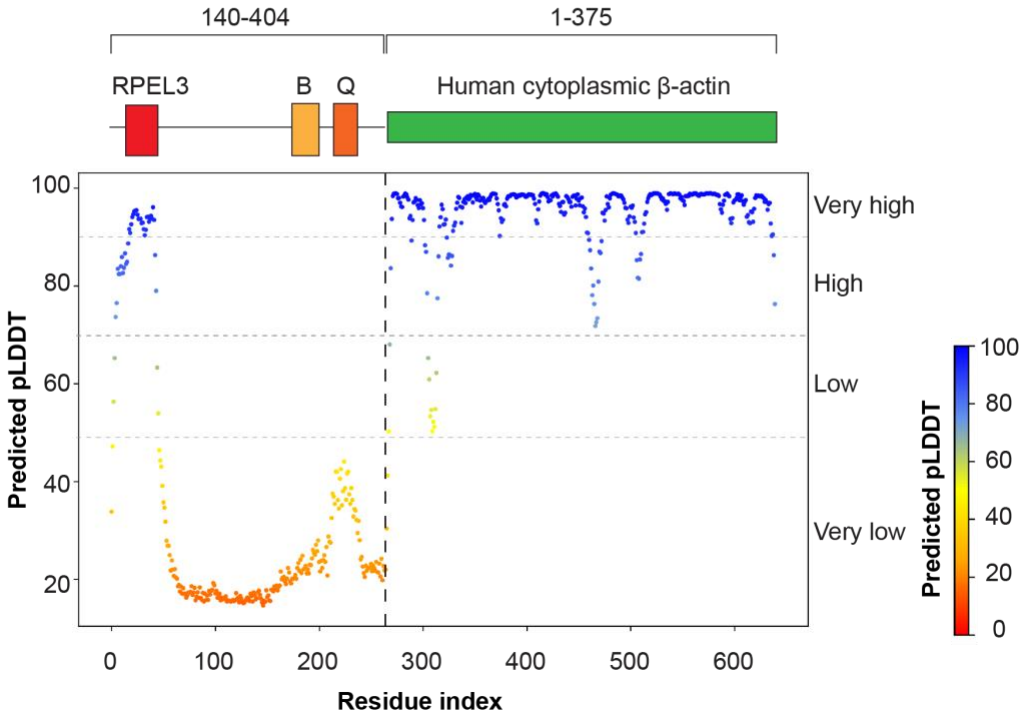

Figure 63. AF-Multimer confidence plot of R3+C GP171/172ER – actin complex
AlphaFold-Multimer prediction using MRTF (140-404) GP171/172ER and human β-cytoplasmic actin (1-375). **A.** Predicted aligned error (PAE) values are coloured on a scale of 1-30, with lower values in dark indicating lower error, and higher values in lighter shade indicating high error of prediction. Sequence schematics have been aligned to the graph to indicate the PEA for specific regions. **B.** pLDDT values are colour-coded on a scale of 1-100, where 90-100=Very high accuracy, 70-90=High accuracy, 50-70=Low accuracy and <50=Very low accuracy.

5.3 Summary

The aim of this chapter was to validate the AF2-Multimer prediction of how Q-box recruitment stabilizes R3-actin binding. Two biochemical assays were used to that effect.

Actin binding to RPEL motifs and spacers between was confirmed in solution using HDX-MS. Actin binding induces structure within the sequence corresponding to the Q region. This interaction was solely dependent on the integrity of RPEL3-actin binding, where loss of actin binding on RPEL3 resulted in loss of Q-box interaction. This showed that the mechanism is RPEL3-dependent. Deletion of structured O helix and the unstructured loop region between O and Q did not result in loss of actin binding to RPEL and Q, consistent with the AF prediction.

Q deletion was designed based on classical Q box (Zaromytidou et al., 2006), leaving several residues predicted in actin binding intact. Due to that, it can be observed that the deletion led to loss of actin binding to the remaining residues of Q, but the RPEL-actin binding could still be detected. It might be that the interaction of actin with the other RPELs stabilizes actin binding to RPEL3 in the absence of Q.

Based on the biochemical data I have shown in section 3.3, absence of the C terminal sequences of MRTF in the context of RPEL3 decreases actin binding. To check the role of Q in the context of 1:1 interaction with MRTF, affinity measurements were used. Deletion of Q, but not of the residues spanning the sequence between R3 and Q led to a significant decrease in actin binding, confirming that the interaction with actin is specific to Q region in MRTF C-terminal sequences.

This mechanism of Q facilitating actin binding is RPEL3 specific, whereby replacing RPEL3 in R3+C with either R1 or R2 resulted in loss of high affinity binding. Substitution of residues within R3 with corresponding ones from R2 led to an increase in binding of RPEL3 alone, but a decrease in the R3+C construct, suggesting that the Q-facilitated actin binding is not compatible with RPEL2. Analysis of the crystal structure and the AF2 prediction indicated that the same positions of residues in RPEL2 and 3 are responsible for different functions: in R2, they stabilize actin binding, whereas in R3 they stabilize Q binding. AF-Multimer prediction of R3 mutants (GP171/172ER) revealed, that Q is not recruited together with actin.

All of the above explains the difference between the binding affinities of the RPELs, where two actin binding mechanisms can be proposed: an RPEL-only actin binding, where no additional interactions are necessary (RPEL1 and RPEL2) and an RPEL-Q actin binding, where for binding to occur, additional Q interactions are crucial (RPEL3).Role of this Q-facilitated actin interaction needs to be further examined in the context of SRF-MRTF-DNA binding.

Chapter 6. Role of multivalent complexes in MRTF regulation

Previous work showed that a stable complex with actin is formed on R1-S1-R2, where upon stabilization of R3-actin binding, five actins could be detected on the RPEL domain (Mouilleron et al., 2011). Biochemical studies of the complex formation suggested cooperativity in actin loading, with a proposed model of actin loading on R1, followed by S1-R2 cooperative binding. Binding to S2-R3 was proposed to occur only at high actin concentrations. In this model the number of actins bound to the RPEL domain determines its cellular localization and activity, with the first trimer formed spontaneously in cells, and loading of the following two actins on Spacer2-RPEL3 being sensitive to the local actin concentration in the cell (Guettler, 2007, PhD Thesis). All the previous work suggested that RPEL3 is weak, due to the fact that all the biochemical and structural data was obtained using sequences lacking the Q region. Based on the data I have shown in the previous chapters, for R3 to bind with high affinity, Q-recruitment is necessary.

To better understand the actin dynamics in the context of new data, actin binding to RPEL domain with the C terminal sequences of MRTF needs to be reanalysed. To that effect, HDX-MS analysis will be used to determine the order of actin loading on MRTF. It provides with a good resolution of individual RPELs and Spacers binding actin, as well as allows for the assay to be done in solution. I will use loss-of-contact mutations in the RPEL domain to assess actin binding to the RPEL domain in solution. This will be followed by actin titration to detect the first actin binding site on MRTF at low concentrations.

6.1 R3-actin binding independent from the R1 and R2

Previous studies show that actin binding to the RPELs is dependent on the integrity of RPEL-actin binding site. The R/A mutation within the RPxxxEL motif led to loss of binding of the individual RPELs. According to the previous model, loss of actin binding on R1 and R2 would result in no actin binding on RPEL3. In gel filtration experiment, where an R/A mutation was introduced on R1

(R81A) and R2 (R125A), no actin binding could be detected in solution to the RPEL domain. This was done using a shorter MRTF construct, without the Q sequence (MRTF 2-261).

To test that in the context of MRTF 2-404 binding, double loss-of-contact mutation was introduced to RPEL1 and RPEL2 (XX3) and the binding with actin at 1:5 molar ratio was analysed by HDX-MS (Figure 64.1). Actin can still be detected on both RPEL3 and Q, with weaker binding on R1 and R2. This is consistent with a model in which actin binding to R3 is independent from the other RPELs and indicates loading from R3. To assess this model further, a mutation was introduced into the MRTF XX3 construct, to stop actin binding to the Spacer2 (LK147/149DD) (Figure 64.2). Actin binding to the RPEL3 and Q-box was intact, while no actin could be detected on RPEL1 and RPEL2. This suggests that actin loading onto MRTF is cooperative and occurs from RPEL 3 to 1, in contrast to the previously proposed model.

HDX-MS Fractional Uptake Difference

1.MRTF 2-404 XX3 with actin vs MRTF 2-404 XX3 alone

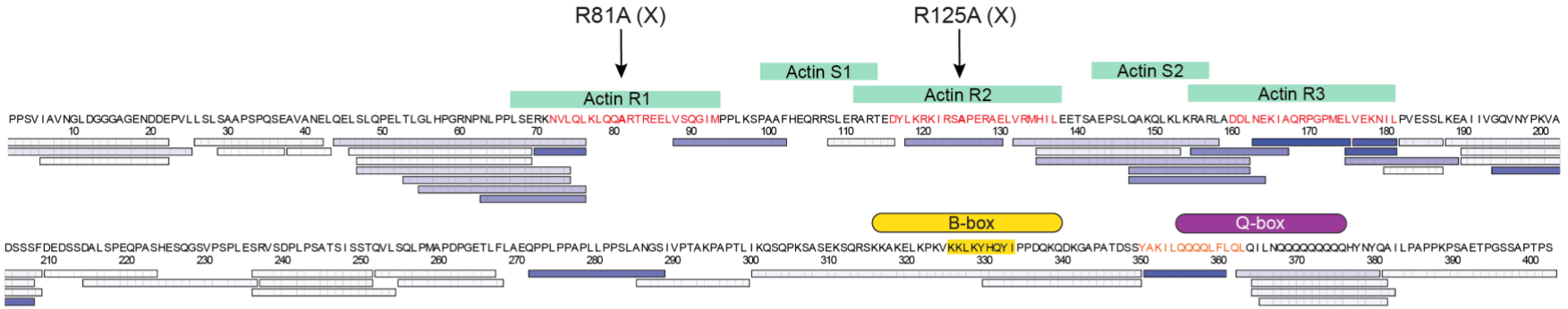

2.MRTF2-404 XX3 LK147/149DD with actin vs MRTF 2-404 XX3 LK147/149DD alone

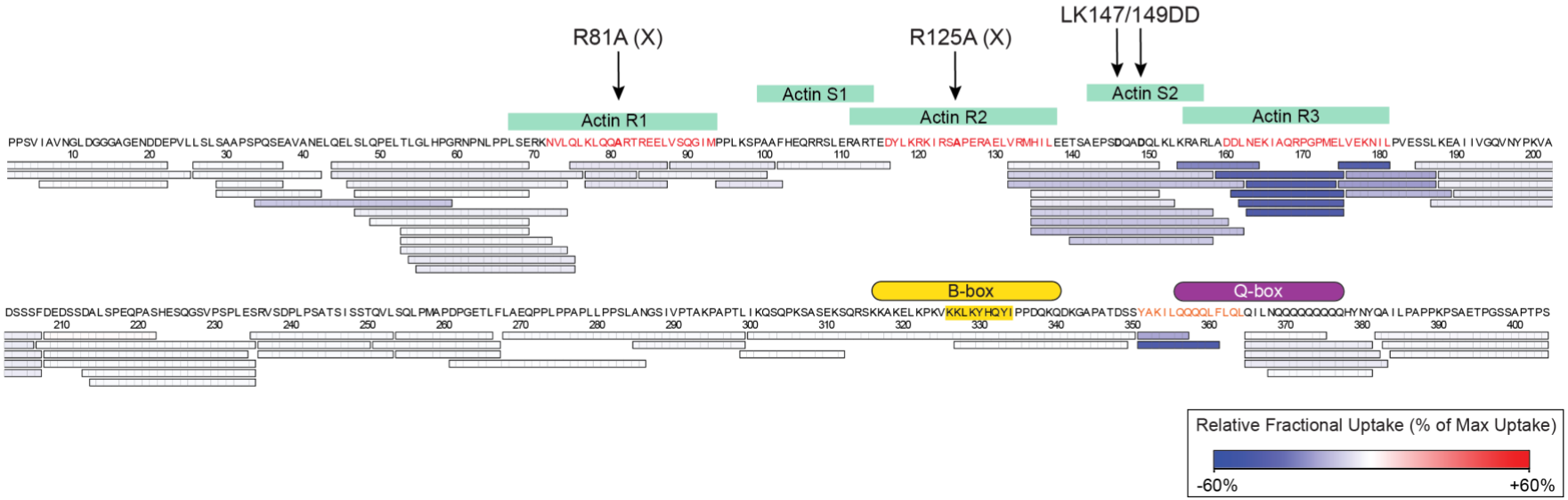

Figure 64. Actin binding on R3-Q independent of R1-S1-R2 actin binding
Fractional uptake difference (%) between 1. MRTF (2-404) XX3 (R81A/R125A)/Actin and MRTF alone; 2. MRTF (2-404) XX3 (R81A/R125A) LK147/149DD/Actin and MRTF alone. Data plotted for each peptide detected at 2s/4°C labelling time point, aligned over MRTF sequence. Data not normalized to the number of amide hydrogens within peptide and not corrected for back exchange. Total number of peptides detected in MRTF XX3: 50, coverage of the sequence: 94.6%, redundancy: 2.30. Total number of peptides detected in MRTF XX3 LK/DD: 78, coverage of the sequence: 95.6%, redundancy: 3.86. The RPEL motifs are coloured red, known actin binding sites based on structural data (PDB:2YJF) marked in green. The basic region is shaded in yellow, and the classical Q region in grey (Zaromytidou et al., 2006). The conserved Q sequence coloured orange. All mutations indicated by an arrow.

6.2 Order of actin loading on MRTF

All the HDX-MS analysis described in Chapter 5 was done at equimolar ratio. In this section, by decreasing the amount of actin in solution, early stages of actin loading on MRTF can be detected and the complex assembly could be followed.

A titration curve of actin onto MRTF WT 2-404 was prepared. As before, HDX data is plotted along MRTF sequence as difference map between MRTF-actin and MRTF alone. At the lowest concentration (MRTF:actin at 1:0.1), a weak actin protection was detected within the RPEL3 and Q regions (Figure 65). No actin binding was detected on the other two RPELs, which suggested that the first RPEL to bind actin is RPEL3 with its associated Q-box sequence. The next titration step (MRTF:actin at 1:0.3) shows the same interaction, with an decreased fractional uptake, suggesting more actin bound to the RPEL3 and Q or stabilization of the interaction at higher concentrations. Next (MRTF:actin at 1:1), the peptides corresponding to RPEL2 and Spacer 1 show protection, indicating actin binding, and only at the highest concentration can actin binding on all five available sites be detected.

The data presented here indicates that in solution the complex formation on MRTF begins from C->N, with actin loading on RPEL3 facilitated by association of the Q-box, followed by binding on RPEL2 and RPEL1.

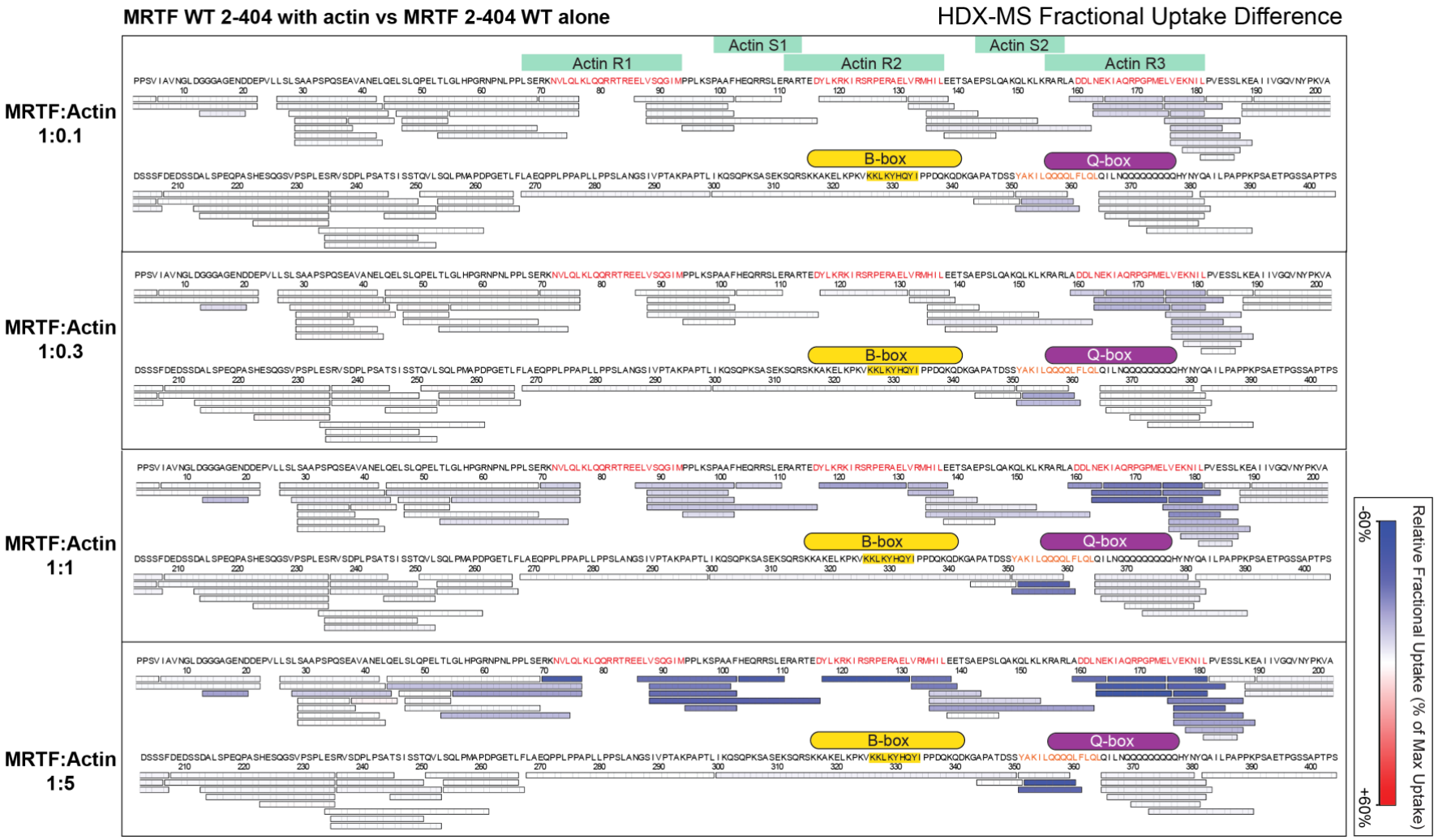
MRTF WT 2-404 with actin vs MRTF 2-404 WT alone
HDX-MS Fractional Uptake Difference
MRTF:Actin 1:0.1
MRTF:Actin 1:0.3
MRTF:Actin 1:1
MRTF:Actin 1:5
Actin S1
Actin S2
Actin R1
Actin R2
Actin R3
B-box
Q-box
Relative Fractional Uptake (% of Max Uptake)
-60%
+60%

Figure 65. The order of MRTF-Actin loading can be detected by HDX-MS
Fractional uptake difference (%) between MRTF (2-404) WT/Actin and MRTF alone at following molar ratio: **1st** actin 0.1:1 MRTF; **2nd** actin 0.3:1 MRTF; **3rd** actin 1:1 MRTF, 4th actin 5:1 MRTF, shown from top to bottom. Data plotted for each peptide detected at 2s/4°C labelling time point, aligned over MRTF sequence. Data not normalized to the number of amide hydrogens within peptide and not corrected for back exchange. Total number of peptides detected: 78, coverage of the sequence: 96.3%, redundancy: 3.09. The RPEL motifs are coloured red, known actin binding sites based on structural data (PDB:2YJF) marked in green. The basic region is shaded in yellow, and the classical Q region in grey (Zaromytidou et al., 2006). The conserved Q sequence coloured orange. All mutations indicated by an arrow.

There is an abundance of structural and biochemical data confirming the formation of a stable, trivalent MRTF-actin complex on R1-S1-R2. Based on the biochemical data shown in Chapter 5, introduction of the GP171/172ER mutation into RPEL3 is incompatible with Q-facilitated actin binding. Weakening this RPEL3-actin interaction by abolishing the additive effect of Q binding could lead to a switch into R1->R3 order of actin loading.

In this experiment, MRTF 2-404 GP171/172ER was subjected to HDX-MS analysis at different actin binding ratios. 1:0.3 ratio was used as the lowest concentration, followed by 1:1, 1:2 and 1:5 MRTF: actin. At the lowest titration point, no difference could be detected between the exchange of MRTF alone vs MRTF with actin (Figure 66 - top). In comparison, at the same concentration, MRTF WT – actin binding could already be detected (Figure 65 , second panel).

This indicates, that by introducing the GP171/172ER mutation, the overall affinity of MRTF for actin has been effectively lowered. At the following point of the titration curve, protection of peptides corresponding to RPEL2 can be detected. Only at the 1:2 MRTF: actin molar ratio, can RPEL1 and RPEL3 binding be detected, with the Relative Fractional Uptake values higher within the RPEL1 and RPEL2 regions. There is no Q-box binding detected throughout the assay. This is consistent with the data suggesting that the R2-like GP171/172ER mutation on RPEL3 prevents the recruitment of Q-box, thus changing the actin binding affinity of the domain as a whole and switching the actin loading order.

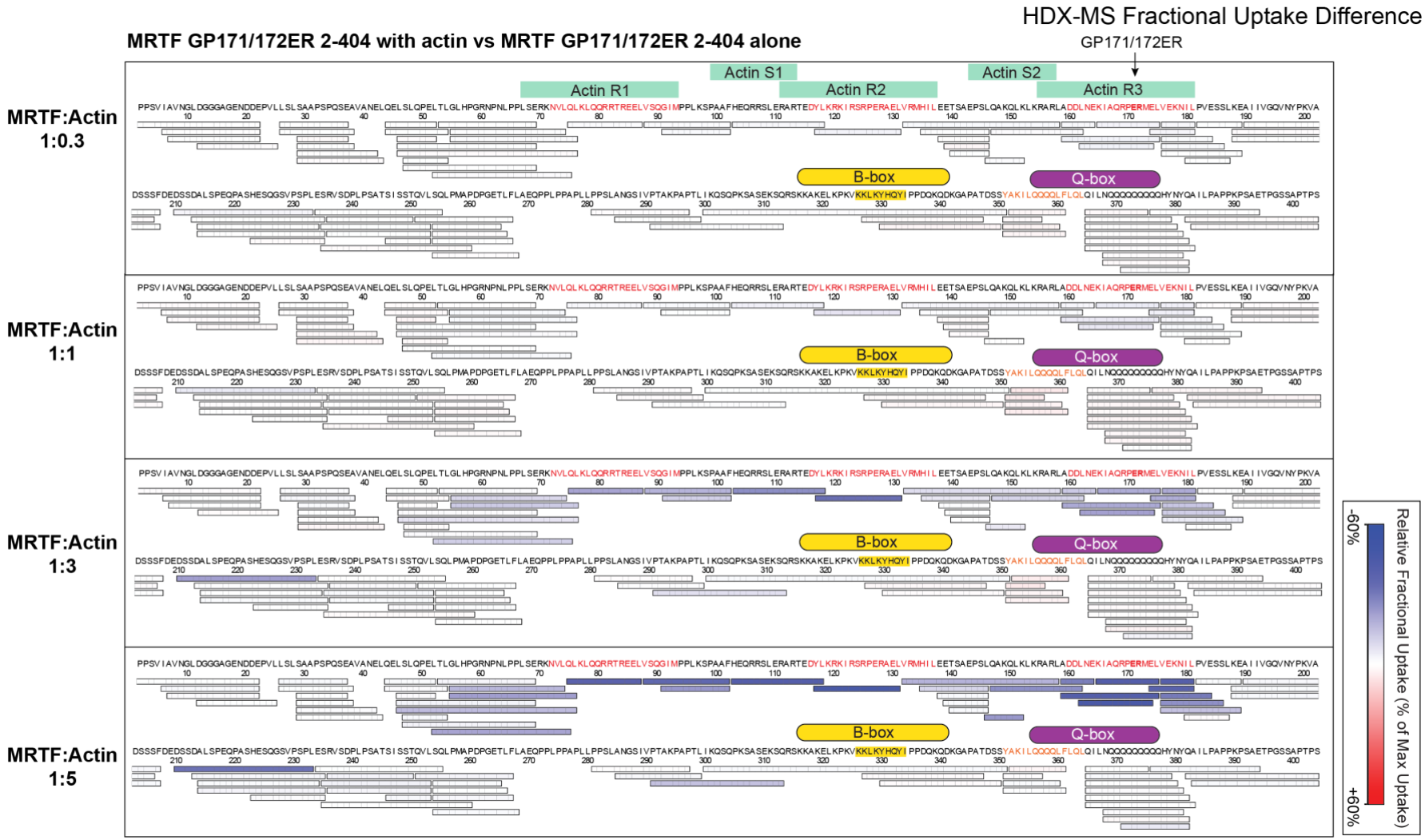
HDX-MS Fractional Uptake Difference
MRTF GP171/172ER 2-404 with actin vs MRTF GP171/172ER 2-404 alone
GP171/172ER
Actin S1
Actin S2
Actin R1
Actin R2
Actin R3
B-box
Q-box
MRTF:Actin 1:0.3
MRTF:Actin 1:1
MRTF:Actin 1:3
MRTF:Actin 1:5
Relative Fractional Uptake (% of Max Uptake)
-60%
+60%

Figure 66. N-terminal actin loading onto MRTF does not involve Q binding
Fractional uptake difference (%) between MRTF GP171/172ER (2-404) /Actin and MRTF alone at following molar ratio: **1st** actin 0.3:1 MRTF; **2nd** actin 1:1 MRTF; **3rd** actin 3:1 MRTF, 4th actin 5:1 MRTF, shown from top to bottom. Data plotted for each peptide detected at 2s/4°C labelling time point, aligned over MRTF sequence. Data not normalized to the number of amide hydrogens within peptide and not corrected for back exchange. Total number of peptides detected: 85, coverage of the sequence: 95.8%, redundancy: 3.43. The RPEL motifs are coloured red, known actin binding sites based on structural data (PDB:2YJF) marked in green. The basic region is shaded in yellow, and the classical Q region in grey (Zaromytidou et al., 2006). The conserved Q sequence coloured orange. All mutations indicated by an arrow.

In the assay, a small peptide with high protection could be detected downstream of the RPEL domain, covering part of the helix sequence that AF2-Multimer predicted in the O region. In a region predicted by AF2-Multimer to be of very low confidence. It could be speculated, that in the absence of Q-box binding, this element becomes more stable, leading to an increase in protection in HDX-MS.

The results presented here show, that actin loading occurs form C->N on RPEL3 with recruitment of the Q-box, but a switch is possible by abolishing the interaction between R3 and Q, and consequently lowering its affinity for actin. GP171/172ER mutation is indeed incompatible with Q-box binding and when actin loading occurs form the N-terminus, the concentration of actin necessary for RPEL domain loading is higher than for the C-terminal loading.

6.3 Summary

In this chapter I summarized the current knowledge regarding actin assembly on MRTF. The N-terminal loading model that has been proposed thus far, is based on the fact that RPEL1-Spacer 1-RPEL2 can form a stable trivalent complex in solution (when using the RPEL domain alone), which was thought to be the order of loading, occurring cooperatively from the amide end. The trivalent complex could be readily formed in cells, and only upon change in the actin concentration would the further two actins load onto Spacer 2-RPEL3, leading to a pentavalent complex formation.

With the findings described thus far in this thesis, it was important to test the assumption that involvement of the C terminal sequences that stabilize

binding on RPEL3 could mean a different order of actin loading, translating into a different model of regulation of MRTF activity.

Here I showed that in the presence of the C terminal Q-box region, we are able to detect actin loading from the carboxyl end, with RPEL3-Q loading occurring first at low actin concentration, followed by stabilization of actin on RPEL2, and concurringly, loading the full actin complex on MRTF. As the first trimer can be formed stably in solution, I tested whether we can change the loading order of actin by introducing a mutation to RPEL3 that is incompatible with Q-binding, changing the affinity of binding on RPEL3 and thus, shifting the loading order. The overall actin binding affinity was lowered, with loading detected only at a higher actin concentration as compared with MRTF WT. The loading occurred from RPEL2-Spacer1-RPEL1, with actin loading onto RPEL3 in the end, and no Q binding could be detected even at high actin concentrations.

Chapter 7. Functional validation of R3-Q interaction with actin

MRTF shuttles constantly between the cytoplasm and the nucleus. Import is regulated by Importin α/β binding to bipartite NLS signal within RPEL domain and an NLS in the basic B-box region. Actin regulates subcellular localization of MRTF by competing with Importin α/β and functionally cooperating with Crm1 (Hirano and Matsuura, 2011; Panayiotou et al., 2016; Pawłowski et al., 2010; Vartiainen et al., 2007), and also controls MRTF in the nucleus by regulating its association with SRF and DNA (Gualdrini, 2016, PhD Thesis; Vartiainen et al., 2007). To test the functional significance of the novel actin-MRTF interactions identified in the previous Chapters, the effect of mutations that disrupt them on MRTF subcellular localization and interaction with SRF was analysed.

7.1 Sub-cellular localization of MRTF

Full-length MRTF (residues 2-1021) sequence was used for expression in mammalian cells, with an N-terminal FLAG-tag for immunofluorescent staining. Mutations and deletions were introduced to the MRTF sequence based on the biochemical analysis presented in previous chapters. Mouse NIH/3T3 fibroblast cells were transiently transfected and stained using anti-FLAG antibody to assess MRTF sub-cellular localization. Cells were serum starved for 24h before the staining. In each set of figures each MRTF mutant was done as separate experiment, with replicates done at different times. The MRTF mutants were then grouped based on the region where the mutation was targeting for the purpose of discussion, and each bar on the graph comes from separate experiment. In resting cells (0.3% FCS for 24h), MRTF WT is predominantly cytoplasmic due to high local concentration of monomeric actin. Serum stimulation, which leads to actin polymerization, effectively lowering the available pool of G-actin in the cell, allows for MRTF accumulation to the nucleus (Figure 67 A and B). Localization of MRTF in the cell is dependent on the integrity of actin-binding sites on the RPEL domain. MRTF XXX, in which a loss-of-contact mutation is introduced to each RPEL motif, is localized to the

cell nucleus in resting cells (Guettler et al., 2008; Miralles et al., 2003) (Figure 67 B and C). Loss-of-contact mutation in single MRTF RPEL motifs has been shown to also affect MRTF sub-cellular localization, although not to the same degree as the MRTF XXX mutant (Guettler et al., 2008). Of the three, the integrity of RPEL3 was most critical, which can also be observed in (Figure 67 B and C).

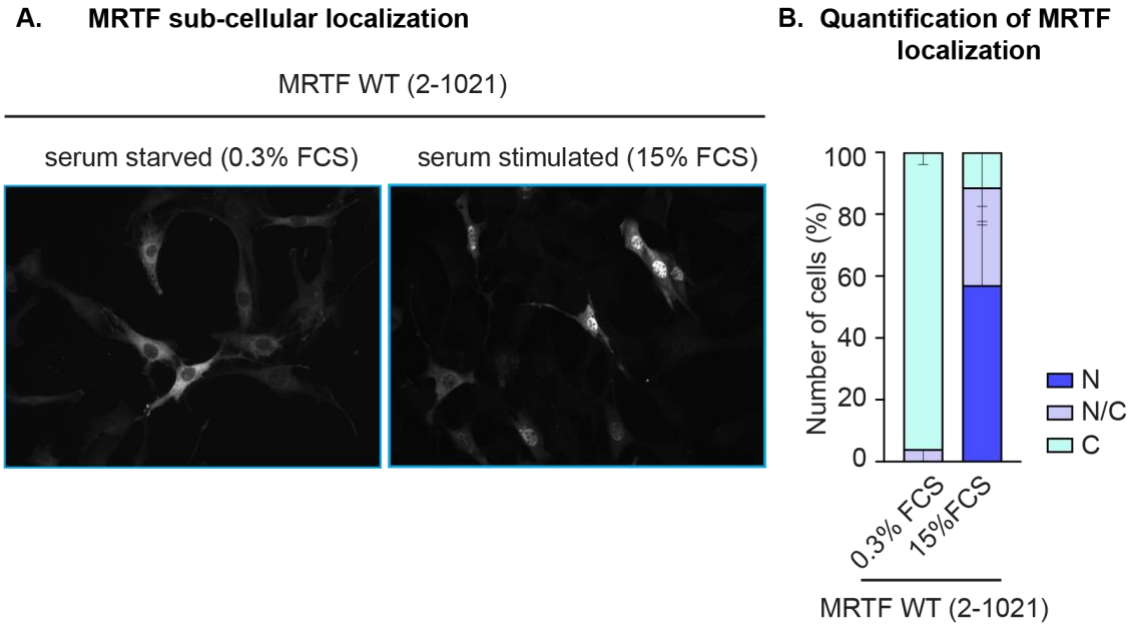

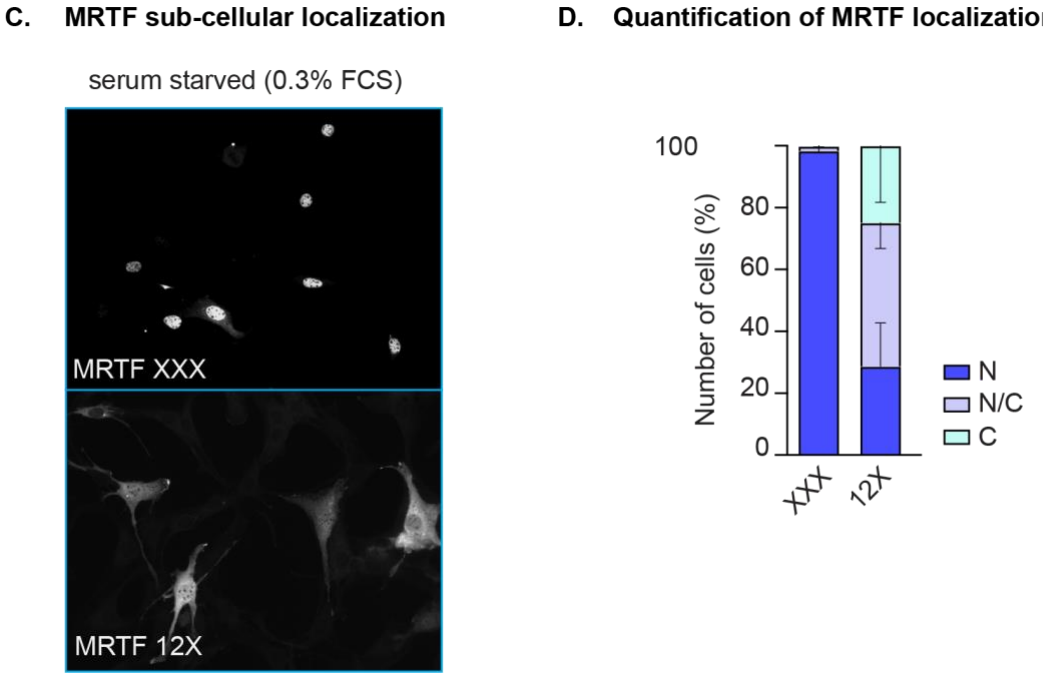

Figure 67. MRTF sub-cellular localization dependent on the integrity RPEL domain
Immunofluorescent staining of FLAG-tag MRTF derivatives. MRTF FL (2-1021) was expressed in NIH3T3 cells. Cells were starved for 24h (0.3%FCS) or starved for 24h and serum stimulated for 30min (15%FCS) and stained using anti-FLAG antibody to assess sub-cellular localization of the indicated MRTF derivatives (MRTF WT, MRTF XXX (R/A mutation on each RPEL), and MRTF 12X (R/A mutation on R3)); n=4, 300 cells counted in each replicate. Cells evaluated by eye as either nuclear, pan cellular or cytoplasmic. **A.** and **C**. a-FLAG staining of MRTF cellular localization. **B**. and **D.** Quantification of the localization presented as % of cells in either cytoplasm, nucleus or throughout the cell. Error bars present SEM of the population. n=number of individual experimental repeats of the derivative.

Mutations within the O-box region were introduced into the sequence. Both deletion of the O-box (Δ186-205) and single point mutations - L187A and I191A did not significantly change MRTF sub-cellular localization (Figure 68). In contrast, R3 mutations – G1712, P172R, M173A and M173E, which significantly reduce actin affinity for RPEL3+C, led to an increase in the number of cells with nuclear MRTF (Figure 68).

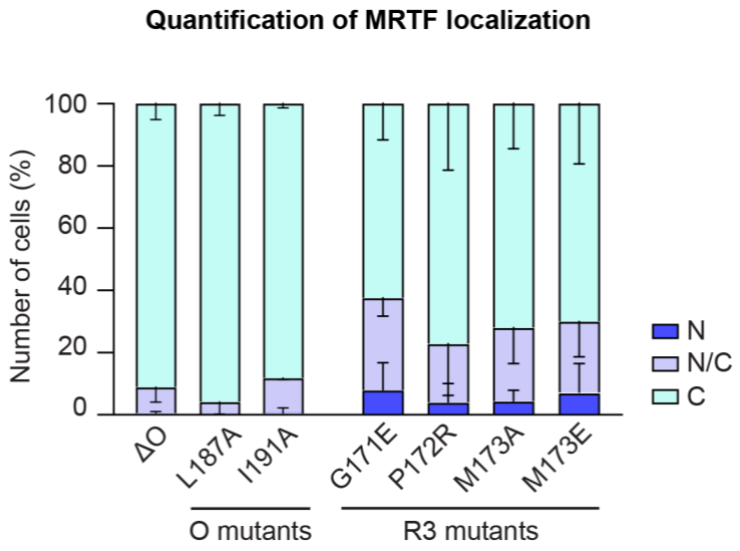

Figure 68. Mutations in the RPEL3 region affect MRTF sub-cellular localization
Immunofluorescent staining of FLAG-tag MRTF derivatives. MRTF FL (2-1021) was expressed in NIH3T3 cells. Cells were starved for 24h (0.3%FCS) and stained using anti-FLAG antibody to assess sub-cellular localization of the indicated MRTF derivatives (MRTF O mutants: ΔO-box (Δ186-205) n=3, L187A n=1, I191A n=1; MRTF R3 mutants: G171E n=3, P172R n=3, M173A n=3, M173E n=3). 300 cells counted in each separate experiment, n=number of individual experimental repeats of the derivative. Cells evaluated by eye as either nuclear, pan cellular or cytoplasmic. Error bars present SEM of the population.

Deletion of the Q-box was previously shown to increase nuclear localization of MRTF, but the cause of that is not clear considering the presence

of an NES signal within the Q-box, as well as Q-box affecting the efficiency of MRTF binding to SRF (Miralles et al., 2003; Muehlich et al., 2008a; Panayiotou et al., 2016; Zaromytidou et al., 2006). Therefore, I assessed the effect of point mutants of the Q-box identified in the AF2-Multimer prediction on MRTF localization (Figure 69). Although Y351, Q358 and L355 are localized outside the predicted Q-box NES, change in MRTF sub-cellular localization can be observed. L362A and L364A mutations can be mapped onto the NES, but do not have as severe of an effect on MRTF as the mutations predicted to disrupt Q-box-actin binding. This helps to uncouple the effect of disrupting the NES and inhibition of R3 – Q-box composite site formation.

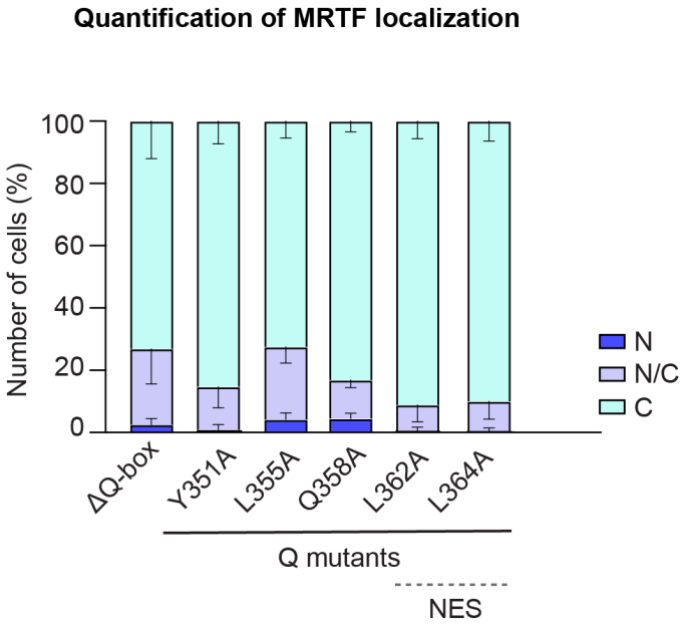

Figure 69. Deletion of Q leads to change in MRTF sub-cellular localization
Immunofluorescent staining of FLAG-tag MRTF derivatives. MRTF FL (2-1021) was expressed in NIH3T3 cells. Cells were starved for 24h (0.3%FCS) and stained using anti-FLAG antibody to assess sub-cellular localization of the indicated MRTF derivatives (MRTF Q-box mutants: ΔQ-box (Δ356-377), Y351A, L355A, Q358A, L362A, L364A). 300 cells counted in each separate experiment, n=3 for all MRTF mutants; n=number of individual experimental repeats of the derivative. Cells evaluated by eye as either nuclear, pan cellular or cytoplasmic. Error bars present SEM of the population.

GP171/172ER mutation was shown to increase the affinity of RPEL3 alone, but decreased the affinity for actin for R3+C. This mutation abolishes recruitment of the Q-box, as seen in the HDX-MS. As a result, GP/ER lowers the effective affinity of the RPEL domain for actin. MRTF GP/ER exhibited

increased nuclear localization, and this was ameliorated by deletion of the Q-box (Figure 70). This result is consistent with a model in which the increased affinity of the RPEL3$^{GP/ER}$ motif can compensate for the loss of the Q-box interaction to maintain cytoplasmic localization.

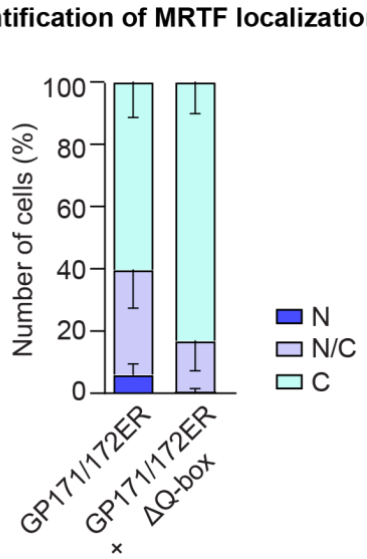

Figure 70. GP171/172ER mutation increases pan-cellular localization of MRTF
Immunofluorescent staining of FLAG-tag MRTF derivatives. MRTF FL (2-1021) was expressed in NIH3T3 cells. Cells were starved for 24h (0.3%FCS) and stained using anti-FLAG antibody to assess sub-cellular localization of the indicated MRTF derivatives (MRTF GP171/172ER and MRTF GP171/172ER + ΔQ-box (Δ356-368)). 300 cells counted in each separate experiment, n=3 for all MRTF mutants; n=number of individual experimental repeats of the derivative. Cells evaluated by eye as either nuclear, pan cellular or cytoplasmic. Error bars present SEM of the population.

7.2 Actin – Q-box interaction is required for inhibition of MRTF-SRF interaction on DNA

As described in Chapter 3, actin binding inhibits recruitment of MRTF to the SRF-DNA complex (Figure 71A). To test whether this reflects recruitment of the Q-box to the actin-bound RPEL domain, I examined the RPEL GP/ER mutant, which blocks actin-mediated Q-box recruitment to RPEL3.

Deletion of the Q-box did not affect recovery of MRTF in the DNA pulldown assay, but reduced the ability of actin to inhibit recovery, and this reflected a reduced overall affinity for actin binding (Figure 71B). Next, I examined RPEL3 GP/ER, which abolishes recruitment of the Q-box to the composite site on R3 with actin but maintains RPEL3 interaction (Figure 71C).

Same effect could be observed, where a higher actin concentration was needed to inhibit MRTF complex formation on SRF and DNA. Both results are consistent with a model, where R3 – Q-box binding is necessary for efficient inhibition of the MRTF-SRF-DNA complex.

A.

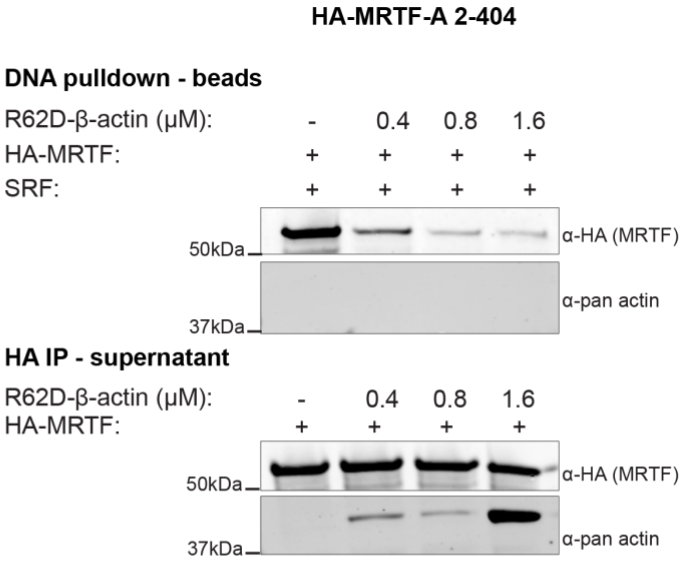
HA-MRTF-A 2-404
DNA pulldown - beads
R62D-β-actin (μM): - 0.4 0.8 1.6
HA-MRTF: + + + +
SRF: + + + +
50kDa
37kDa
α-HA (MRTF)
α-pan actin
HA IP - supernatant
R62D-β-actin (μM): - 0.4 0.8 1.6
HA-MRTF: + + + +
50kDa
37kDa
α-HA (MRTF)
α-pan actin

B.

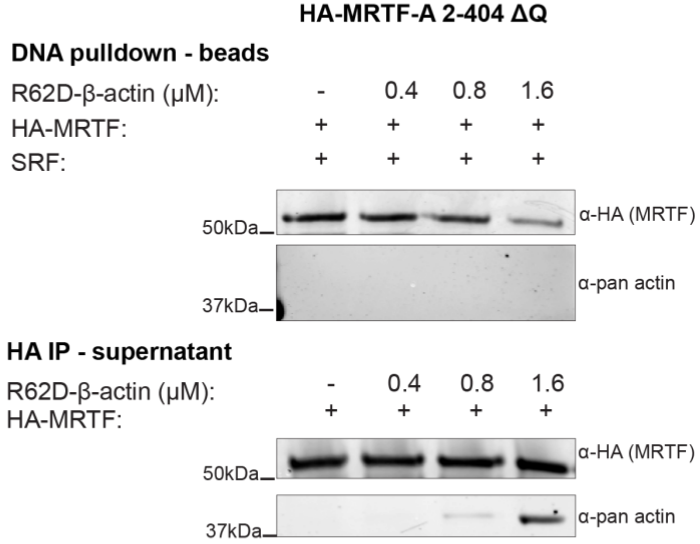
HA-MRTF-A 2-404 ΔQ
DNA pulldown - beads
R62D-β-actin (μM): - 0.4 0.8 1.6
HA-MRTF: + + + +
SRF: + + + +
50kDa
37kDa
α-HA (MRTF)
α-pan actin
HA IP - supernatant
R62D-β-actin (μM): - 0.4 0.8 1.6
HA-MRTF: + + + +
50kDa
37kDa
α-HA (MRTF)
α-pan actin

C.

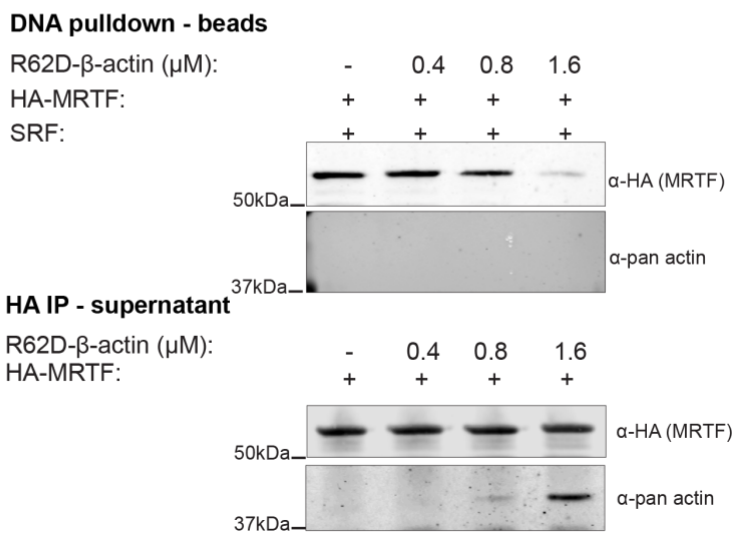
HA-MRTF-A 2-404 GP171/172ER
DNA pulldown - beads
R62D-β-actin (μM): - 0.4 0.8 1.6
HA-MRTF: + + + +
SRF: + + + +
50kDa
37kDa
α-HA (MRTF)
α-pan actin
HA IP - supernatant
R62D-β-actin (μM): - 0.4 0.8 1.6
HA-MRTF: + + + +
50kDa
37kDa
α-HA (MRTF)
α-pan actin

Figure 71. Inhibition of MRTF-SRF binding is dependent on R3 – Q-box interaction DNA pulldown assays included 21pmol DNA, 4pmol SRF.DBD and 10pmol MRTF per reaction, with human cytoplasmic β-actin R62D at 0.4μM, 0.8μM and 1.6μM. Top panels: DNA pulldown, bottom panel: HA IP of the pulldown supernatant. MRTF was detected using anti-HA antibody, actin was detected using anti pan-actin antibody. **A.** HA-MRTF WT (2-404). **B.** HA-MRTF ΔQ (2-404). **C.** HA-MRTF GP171/172ER (2-404).

7.3 Summary

The data presented in this chapter are consistent with a model in which recruitment of actin to RPEL3 *in vivo* is dependent on additional interactions with the Q-box. Mutations in either RPEL3 or the Q-box that reduce actin binding affinity result in increased MRTF nuclear accumulation in resting cells. Q-box recruitment to the RPEL domain is also required for actin to inhibit interactions with SRF on DNA, as its deletion resulted in lowered overall sensitivity for actin with higher actin concentrations needed to disrupt SRF binding. Same could be observed for the GP171/172ER mutation, which disrupts Q-box recruitment to R3-actin composite site. The data presented shows that inhibition of MRTF-SRF interaction requires formation of Q-box – RPEL3 complex. However, the precise mechanism by which this interaction blocks binding of the B-region heptapeptide with the SRF remains unclear.

Chapter 8. Discussion

In this thesis, I have elucidated a new mechanism by which actin controls MRTF activity. MRTF is an SRF coactivator, and its binding is necessary for active transcription of genes regulating the cytoskeletal dynamics (Miralles et al., 2003; Vartiainen et al., 2007). Binding to SRF occurs via a basic element in the sequence - B-box, integrity of which is crucial for the interaction (Zaromytidou et al., 2006). MRTF also acts as a G-actin sensor in the cell, binding actin to its N-terminal RPEL domain (Guettler et al., 2008; Miralles et al., 2003).

Actin regulates MRTFs on two levels: cellular localization (Guettler et al., 2008; Miralles et al., 2003; Panayiotou et al., 2016; Pawłowski et al., 2010) and activity in the nucleus (Gualdrini, 2016, PhD Thesis; Toteva, 2021, PhD Thesis; Vartiainen et al., 2007). MRTF shuttles constantly between the cytoplasm and the nucleus. Binding of G-actin to the RPELs prevents nuclear accumulation of MRTF by competition with Importin α/β for the bipartite NLS localized in the RPEL domain (Pawłowski et al., 2010). Additionally, sequestering of MRTF in the nucleus without disruption of actin binding results in non-productive transcription, with MRTF detected on target promoters, but with no subsequent gene expression (Vartiainen et al., 2007). The mechanism of nuclear actin regulation of MRTF activity is unclear.

In this thesis I used biochemical approaches, structural modelling and biophysical assays to demonstrate that RPEL3-actin also interacts with sequences C-terminal to the RPEL domain, in the region implicated in SRF binding on MRTF.

8.1 The new model of MRTF – actin interaction

It was previously proposed that actin bound to the RPEL domain from N to C (Guettler et al., 2008; Mouilleron et al., 2011) (Figure 72A). In this model a stable trivalent complex is converted to a pentavalent one at high concentrations through binding of actin to the weak RPEL3 motif and the

Spacer 2. This was deemed consistent with the weak affinity of the RPEL3 motif, the stable trivalent complex detected in gel filtration experiments, and the instability of the Spacer2-RPEL3 actins in the crystal structure. It was also in agreement with the strong effect of RPEL3 loss-of-contact mutations *in vivo* (Guettler et al., 2008), and the fact that a MRTF (met) derivative without RPEL1 could still be regulated (Miralles et al., 2003). The model was consistent with observed competition between Importin α/β and actin for RPEL domain binding (Pawłowski et al., 2010), but it does not explain how actin bound to the RPEL domain can inhibit interaction with SRF, nor does it explain how the B1 NLS could be regulated by actin.

The data in this thesis support a revised model for actin regulation shown in Figure 72B. In this model, actin loads cooperatively from C to N, nucleated by a high-affinity RPEL3 – Q-box composite actin-binding site. Actin binding again competes with Importin α/β binding to the RPEL domain, and recruitment of the Q region inhibits interaction of the neighbouring B1 region and possibly its associated importin binding sequence. This model is supported by biochemical data of the effects of actin binding on interaction with SRF and DNA, with direct evidence from HDX-MS studies that show loading of actin from C to N with structural changes in the Q box induced by actin binding.

A.

Old actin binding model

Actin loading N->C

Active states

- no actin bound - or RPEL3 exposed?
- import signals exposed
- competent to bind SRF

Inactive state

- pentavalent actin complex
- import signals occluded
- export competent
- SRF interaction blocked ?

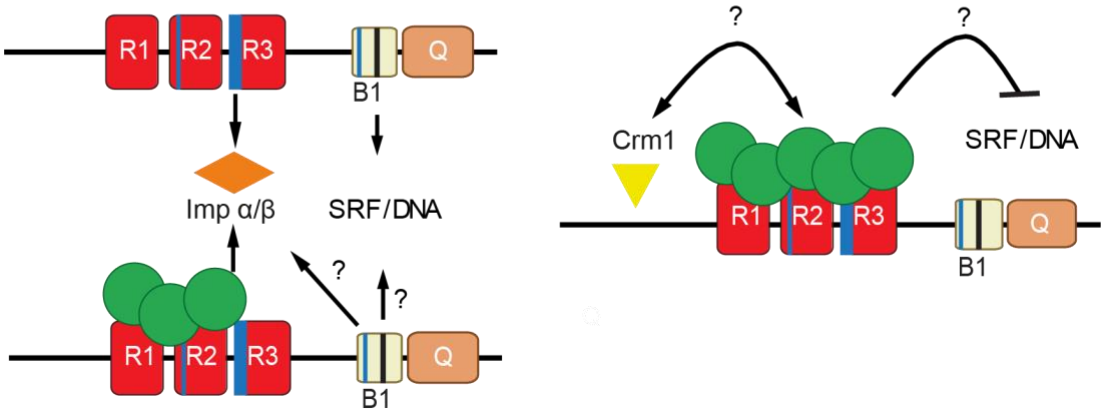

B.

New actin binding model

Actin loading C->N

Active state

- no actin bound
- import signals exposed
- competent to bind SRF

Inactive state

- pentavalent actin complex - RPEL3-actin first to load
- import signals occluded
- export competent
- SRF interaction blocked

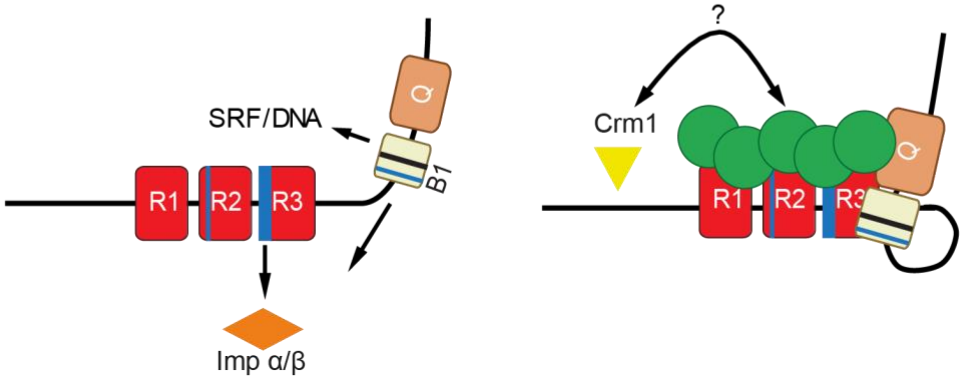

Figure 72. Comparison of the two actin binding models
A. The old model, where actin loading occurred from N->C. **B.** The new model of C->N loading with actin binding to a composite site on R3 – Q-box. Blue boxes indicate the localization of NLS signals on MRTF, with the black box on B1 as the heptapeptide sequence crucial for SRF binding. The arrows show the parts of the presented models that are not fully understood.

8.2 Technical approaches used to validate the model

I used several techniques that allowed for identification of the interactions important for determining the new binding model. Highlighting the advantages and limitations of these methods will allow for better understanding of the data I will discuss in the following sections.

8.2.1 AlphaFold as a useful tool to facilitate biochemical and structural studies

AlphaFold2 is an *in-silico* modelling programme that allows for prediction of interactions between proteins. It takes into account the evolutionary conservation of protein regions between species to generate a probable model of how the protein will be folded. At the beginning of this project, the computing limitations did not allow for visualization of the whole MRTF pentavalent complex, which is the reason why most of the data presented here has been done using the simplified RPEL3 + C MRTF, limiting the interaction to one RPEL-actin binding. This was however sufficient to identify the new interaction with the Q-box and further validate it using biochemical methods. AF2-Multimer is a useful tool to aid biological and structural experiments. It allows for mutagenesis analysis, indicating if the change in the amino acid sequence will result in change in structure or interaction between proteins. This was utilized in this thesis, where disruption of R3 – Q-box binding by introduction a mutation into RPEL3 could be visualized using the programme. AF2-Multimer provides each prediction with two sets of confidence levels, which are highly based on the conservation of the sequences in evolution and the relative position of each residue within that sequence. In this project, a high confidence prediction of the Q-box was validated *in vitro* and confirmed the importance of the interaction for RPEL3-actin binding. Another region predicted by AF2-Multimer was a small

helix downstream of R3, which was termed the “O”-helix. This prediction was of low confidence and was assessed both in solution (HDX) and by BLI affinity measurement not to be important for the interaction. Both examples show that AF2-Multimer confidence can be mirrored in experimental data, showing how it can be useful for aiding structural and biochemical studies.

Development of the newer programme, AlphaFold3 allowed for inclusion of nucleotides, ligands and nucleic acids in the prediction. As MRTF binds to SRF on DNA, and no crystal structure was resolved of the complex, this presented with a valuable tool to visualize the interaction. It was known based on biochemical data, that a heptapeptide in the B-box of MRTF is crucial for the interaction with SRF, and this could be detected with AF3. However, the role of Q-box in the interaction was not clear, but AF3 presented a possible model of how Q-box might stabilize the interaction with SRF. Although the prediction of the Q-box as forming a dimerization interface was of low confidence, it specified which residues might be important for that interaction. This will be useful in choosing a Q-box mutation to test *in vivo* that disrupts actin binding on R3-composite site but does not influence SRF binding.

8.2.2 HDX-MS – an in solution based “footprinting” assay

Hydrogen-Deuterium Exchange Mass Spectrometry is a useful tool for detecting protein-protein interaction in solution with high resolution. It is a particularly good method to use in this project, as MRTF is unstructured in solution, which was shown previously by Circular Dichroism (CD) experiments (Mouilleron et al., 2011). Only upon actin binding it becomes structured, which in CD was seen as an increase in the helical content of the RPEL domain, while with HDX it can map the exact surface which becomes structured upon actin binding. This meant it was possible to detect which binding site of actin is occupied, how that changes when introducing mutations to the protein as well as allows for titration of actin into solution, which was how we observed the loading of MRTF from C->N, with the R3 – Q-box both becoming structured at the lowest concentrations. The limitation of the method is that there is an upper concentration limit that can be used in the assay, which means that for lower-

binding affinity MRTF mutants loading cannot be observed, as the concentration of actin is too low in the assay. Additionally, the resolution of the mapping is dependent on the position of the cleavage site of a given peptide. It also varies between experiments, resulting in difficulty in comparing exact occupied residues between MRTF mutants.

8.2.3 Octet BLI as a good validation tool of structural predictions

Biolayer Interferometry assay is an affinity measurement that was used in this thesis to test multiple MRTF mutations following AF2-Multimer prediction. It allows for 1:1 interaction detection, which is why R3+C MRTF protein was used for all mutagenesis validation. As it was shown to bind with high affinity, it became an effective tool in identifying the residues in the R3 -Q-box composite site that would disrupt the binding. Similar to HDX-MS, the limitation of the assay is the top limit of protein concentration that can be used, with low-affinity binding mutants never reaching R_{max}. This means that an exact K_d cannot be determined, and the range of binding affinities has to be predicted based on curve modelling. Nevertheless, it allows for an efficient validation of binding interactions, and it has been instrumental in carrying out this project.

8.3 How is MRTF binding to SRF regulated?

MRTF binds to SRF in the presence of DNA, with SRF DNA binding domain (DBD) necessary and sufficient for the interaction (Wang et al., 2002; Zaromytidou et al., 2006). The surface on MRTF that was determined to be crucial for SRF binding is localized within the B-box and consists of a heptameric peptide with sequence homology to basic regions of other SRF binding proteins. Although in cells MRTF binds SRF as a dimer, it was shown that monomeric MRTF binding could be detected, although less efficiency than that of a dimer.

I exploited this to develop an MRTF-SRF-DNA interaction assay using recombinant purified components. In this assay, monomeric MRTF binding to SRF DBD on DNA was observed. Inhibition of binding occurred with inclusion of actin in the assay and MRTF-actin binding could be detected in solution. No

actin was detected on the DNA-SRF-MRTF complex, suggesting that actin-MRTF and MRTF-SRF binding is mutually exclusive. Actin inhibition was dependent on the integrity of all binding sites on the RPEL, with no disruption of the MRTF-SRF-DNA complex in the MRTF XXX mutant. Using the MRTF 12X mutant in the assay showed the importance of RPEL3 in DNA binding regulation, as a higher actin concentration was needed to inhibit MRTF-SRF complex formation. This mutation was shown to prevent Q-box recruitment in solution, which shows that formation of the high affinity composite site is crucial for disruption of SRF-MRTF binding. As the B-box is localized in the vicinity of the Q-box, we speculated there might be a competition for binding between actin and SRF.

The importance of the R3 – Q-box led to proposing a model of cooperative binding to RPEL domain from RPEL3 to RPEL1, where mutations disrupting the interaction would lower the overall actin binding affinity of MRTF. If the interaction between actin-MRTF and SRF-MRTF was mutually exclusive, we would never detect actin binding at the same time as SRF. The data I presented in this thesis is consistent with that model, although it does not prove it. For that, a mutation that allows for assembly of the pentavalent actin complex on actin without recruitment of the Q-box would need to be identified, to effectively uncouple the MRTF-actin interaction from the MRTF-SRF binding region. Knowledge of RPEL-actin interactions should allow this, with the GP171/172ER mutation shown to disrupt Q-box binding in solution and by BLI, while increasing the affinity of RPEL3 binding of actin. This could be coupled with a mutation within the Q-box. The residue chosen would have to be important for interaction with R3, with mutations of contacts localized within the evolutionary conserved region of the Q-box (^{351}YAKIL^{355}) shown as having the most severe effect on actin binding to RPEL3. This region was also outside of the predicted interaction surface between two Q-box helices in SRF-DNA complex, as well as outside the previously mapped region of interactions facilitating SRF binding (Zaromytidou et al., 2006). With this, both SRF and actin binding to MRTF will remain intact and should allow for proving whether binding of both is mutually exclusive.

8.3.1 Implication of the proposed model for Myocardin regulation

There is high degree of homology of the RPEL3 motif between MRTF and Myocardin, but not with RPEL1 and RPEL2, suggesting to an evolutionary conservation of the RPEL3 sequence. Additionally, the conserved part of the Q-box region, that was also identified to be crucial for actin interaction is homologous in Myocardin. However, there is no indication that Myocardin is regulated by actin. Myocardin binds to SRF as a monomer, and the integrity of both B-box and Q-box sequences is crucial for regulation. In MRTF the Q-box is not necessary and seems to fill a more facilitating role in SRF binding. This difference could be due to MRTF binding as a dimer, and Myocardin as a monomer, where Q-box might play a more important part in stabilizing the complex.

Myocardin is constitutively active in cells and its activity is not regulated by actin (Wang et al., 2001). This was tested in fibroblast cells, where Myocardin would localize to the nucleus in resting conditions, but a hybrid between Myocardin and MRTF, where the R1 and R2 sequences on Myocardin were replaced with those of MRTF, could effectively reinstate regulation by actin (Guettler et al., 2008). As Myocardin possesses the regulatory R3+C sites, it could be considered that in cells with higher actin concentrations than those present in fibroblasts (for example in muscle cells), the activity of Myocardin could be regulated in the same way as MRTF.

8.4 Why is there a difference in actin binding between RPELs?

The three RPELs have different affinities for actin binding on their own, with R3-actin binding of the lowest affinity (Mouilleron et al., 2008). The differences between the RPELs were determined to be the amino-acid composition of the motifs, with residues G171 and P172 of R3 not making the same contacts with actin, as R1 and R2 in their respective positions (Mouilleron et al., 2011). Identification of the Q-box as an interacting surface that facilitates actin binding to the RPEL3 provided the answer to why there is a difference between the RPELs in sequence. The same residues that are missing in R3 as

compared to R1 and R2 have been identified as crucial for binding to the Q-box in the AlphFold2-Multimer prediction and have been verified by BLI. The conserved region of the Q-box is predicted in interaction with both actin and R3. Importantly, $I354^{Q\text{-}box}$ binds RPEL3 residues $G171^{R3}$ and $P172^{R3}$, with $Q357^{Q\text{-}box}$ also contacting $P172^{R3}$ through hydrophobic interactions. $G171^{R3}$ and $P172^{R3}$ are the residues that were thought to be responsible for lowering the affinity for actin biding when compared to R1 and R2. This reveals that these amino acid differences are actually crucial for this new regulatory mechanism.

Detection of the Q-box in solution was dependent on the integrity of RPEL3. In the absence of R3-actin binding, Q-box was not recruited to any other RPEL-actin site on MRTF. This could be due to a possible steric clash between the residues of RPEL1 and RPEL2 in the positions that in RPEL3 facilitate binding, and the Q-box. This was a useful finding, as it allowed for identification of mutations that can be used to uncouple the RPEL3 and Q-box interaction, while maintaining high affinity of binding of a “strong” RPEL motif.

In the C->N loading model, actin binding to the composite site on R3 – Q-box would lead to cooperative loading of actins onto R2 and R1. The low affinity of R3 alone prevents actin loading when bound to SRF, but an increase in actin concentration would lead to R3-Q-box recruitment, with the R2 and R1 having the ability to efficiently load the rest of actins due to their autonomously high affinity.

8.5 What constitutes an RPEL motif?

RPEL motif containing proteins compose a unique family of G-actin binding proteins. RPEL motif of each of the families occupies the same binding surface on actin, making contacts along the hydrophobic cleft and ledge between the SD1/3 of actin (Diring et al., 2019a; Mouilleron et al., 2012, 2008). Nevertheless, comparing the mechanism of binding with actin between the different RPELs allows for classification of the RPEL-actin binding into three different models.

The RPEL motifs of MRTF - R1 and R2 – bind to actin with high affinity, without any additional interaction necessary. The crystal structure of both motifs

binding actin was resolved, and their interactions with actin constitute a classical RPEL motif (Figure 73A). A second model of RPEL-actin binding can be observed in another family – ArhGAPs. ArhGAP12 has only one RPEL motif, which binds actin with high affinity. However, an additional interaction with the GAP domain localized C-terminal to the RPEL can be detected in the crystal structure, which binds to another hydrophobic surface of actin on SD1 – the hydrophobic niche (Figure 73B). Although this binding is not necessary for actin interaction, association of the GAP domain to actin increases the affinity 70-fold. This additive mechanism of C-terminal sequences was one of the reasons behind considering an additional role of sequences other than the RPEL in actin binding, that were subsequently presented in this thesis. The RPEL3 motif – actin binding of MRTF is the third, new identified model. Here, the RPEL domain C-terminal sequences also increase the binding affinity for actin, but the binding of Q-box is localized to a different surface of actin than that of ArhGAP12 GAP domain, and it is necessary for the RPEL3 to bind actin (Figure 73C). The different mechanisms described suggest to the complex role that actin-binding plays in regulation of the protein's activity. The presence of two different models within MRTF emphasizes the intricate regulatory mechanism that is involved in its regulation.

A. MRTF-A RPEL2 motif - actin (PDB:2V52)

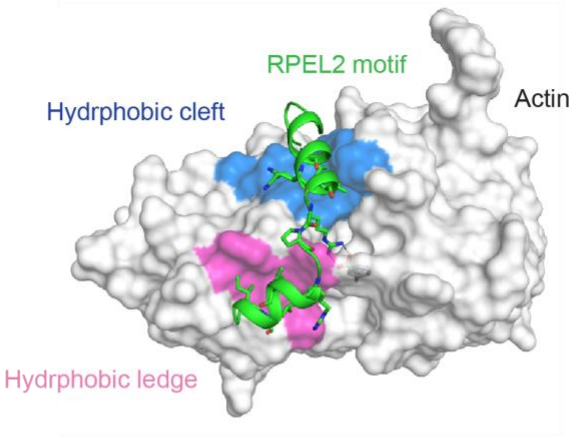

B. ArhGAP12 - actin (PDB:6GVC)

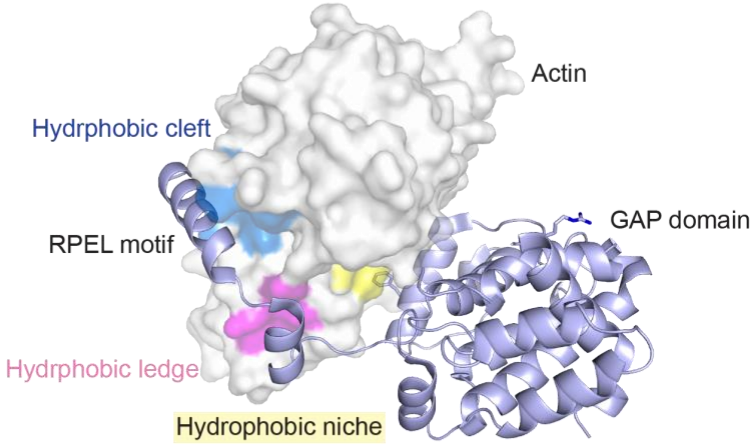

C. MRTF-A RPEL3 motif + Q-box - AF2-Multimer

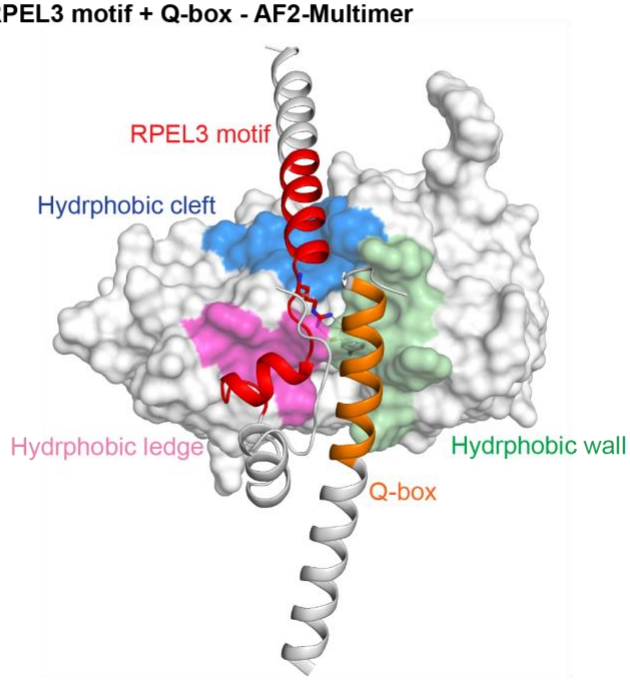

Figure 73. Different types of RPEL motif-actin binding
A. Crystal structure of RPEL2 motif (MRTF) with rabbit skeletal α-actin (PDB:2V52). **B.** RPEL motif and GAP domain of ArhGAP12 with rabbit skeletal α-actin (PDB: 6GVC). **C.** AlphaFold2-Multimer prediction of RPEL3 (MRTF) and Q-box with human cytoplasmic β-actin.

8.6 Multiple roles of the Q-box

In literature, the role of Q-box was never specifically identified. Q-box was originally described as a glutamine-rich region of Myocardin (Wang et al., 2001). However, subsequent analysis of the sequence conservation in evolution extended the region to include residues five base pairs upstream of the initial classified region. ^{351}YAKILQQQQLFLQLQ^{367} has the highest level of homology between vertebrates and invertebrates, pointing to the role of these sequences in evolution (Zaromytidou et al., 2006).

Q-box regulates the nuclear export of MRTF, with an NES signal localized within the sequence mapped to the region ^{360}LFLQLQILNQQQQ^{372}. Mutation or deletion of that sequence led to higher pan cellular distribution of MRTF in resting cells (Panayiotou et al., 2016; Zaromytidou et al., 2006). Nuclear export of MRTF is dependent on its phosphorylation state, which correlates to the ability to bind actin. It has been proposed, that for MRTF nuclear export, it needs to be bound to actin, and specifically, the Q-box NES was implicated in this process. It was thought that actin binding to the MRTF domain results in a conformational change in the protein structure resulting in exposure of the region for export (Muehlich et al., 2008b; Panayiotou et al., 2016). With the model of R3 – Q-box binding, this could be the conformational change that is necessary for MRTF export. This role in MRTF regulation of the Q-box NES will be taken under consideration when designing a mutation to introduce for functional validation.

Another aspect of the Q-box – actin binding is the formation of a high affinity complex, which when disturbed by deletion of the Q box leads to lowering the overall affinity for actin binding. This has several implications for nuclear import for MRTF. There are two NLS signals within the RPEL domain, localized within R2 and S2-R3 sequences, which form a composite binding site for Importin α/β (Pawłowski et al., 2010). Another NLS signal is localized in the

B1 region. Previous studies show that B1 NLS works inefficiently in the context of the full-length protein (Vartiainen et al., 2007). The new model of actin binding could provide an explanation, as it predicts that importin binding on B1 might be outcompeted by actin binding to the Q-box – RPEL3. Binding of actin to the composite site would lead to recruitment of Q, possibly occluding both B2/B3 NLS on the RPEL domain and B1 of MRTF from Importin. Considering this, disruption of the interaction between R3 and the Q-box would result in a higher nuclear localization of MRTF in resting cells, as the B1 would be exposed and possibly B2 at low actin concentrations. In preliminary experiments I have shown that actin competes with Importin α/β for binding to MRTF (2-404), which includes both B2 and B1. In future work I will extend these experiments to confirm that Importin is binding to both B1 and B2 in MRTF (2-404) and that these sites are functionally independent. The role of the Q-box in regulating both the import and export of MRTF highlights the complexity of the new identified model of actin-binding. Both these aspects will need to be carefully considered when choosing a mutation that disrupts R3 – Q-box binding, while does not affect MRTF regulation.

Q-box has also been implicated in SRF binding of MRTF. Mapping of the residues affecting the efficiency of SRF binding in MRTF showed I354, L355, L362, L364 and L366 of the evolutionary conserved ^{351}YAKILQQQQLFLQLQ^{367} to be important (Zaromytidou et al., 2006). AF3 modelling of SRF-MRTF on DNA does not provide additional information that would confirm the role these residues might play in SRF binding. It does, however with low confidence, predict the two Q-box helices as forming an antiparallel coiled-coil-like structure on top of the SRF dimer. Coiled-coils are a ubiquitous dimerization and stabilization mechanism (Mason and Arndt, 2004), and might explain why the Q-box facilitates interaction with SRF. Only two residues could be identified (with low confidence) that might be involved in Q-Q interaction, F361 and N368. There were no additional contacts detected between the Q-box and SRF, which would exclude the possibility of direct competition between SRF and actin for binding to the Q-box. Interestingly, inclusion of actin in the MRTF-SRF-DNA prediction resulted in actin binding to the RPEL3 with recruitment of the Q-box

to form a composite site. This led to displacement of the Q-helices from the dimerization coiled-coil like unit and this change of the Q-box significantly reduced the predicted confidence of the B-box placement Figure 74. Although AlphaFold2-Mulitmer predicts all the proteins can be successfully docked simultaneously, the reduced confidence of the B-box prediction may be indicative of steric hindrance introduced by Q-box displacement. This would be in agreement with the C->N loading model, where at low concentrations of actin, binding to R3 and the Q-box would be sufficient to dissociate the MRTF-SRF complex, acting an efficient regulatory mechanism of MRTF activation.

AF3 prediction: DNA - SRF - MRTF

pLDDT change in the B-box prediction with inclusion of actin

A. Prediction without Actin (pLDDT on B-box)

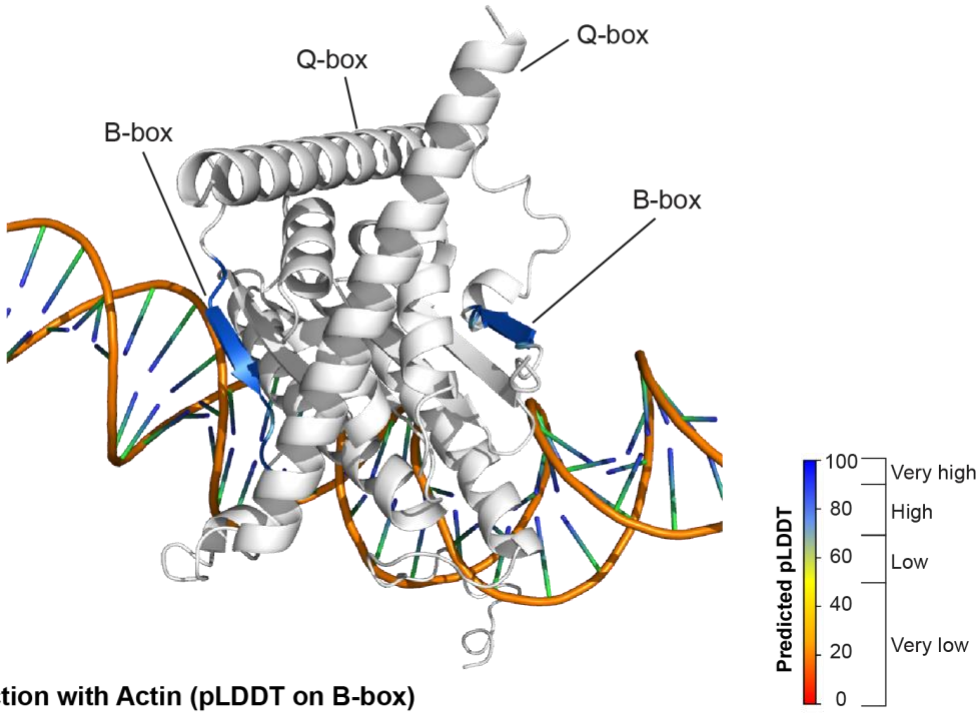

B. Prediction with Actin (pLDDT on B-box)

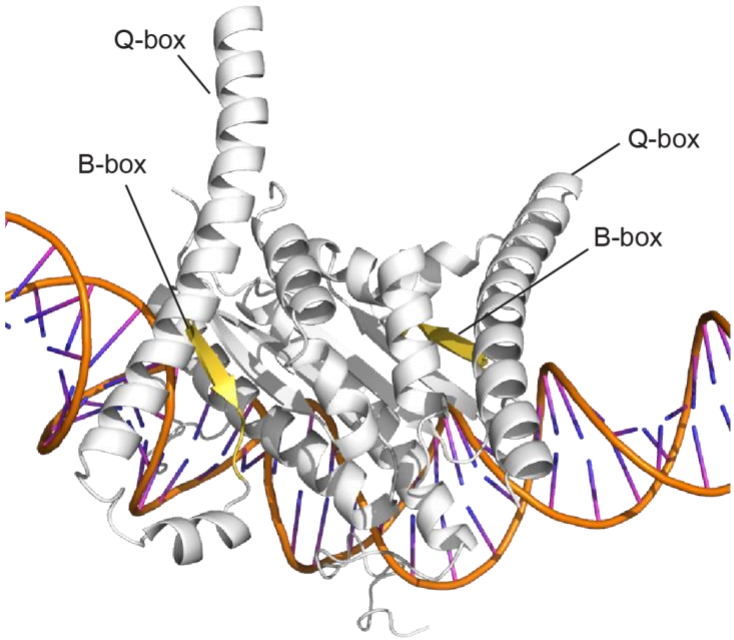

*Only MRTF B-box and Q-box sequence shown, actin omitted for clarity

Figure 74. AF3 prediction of B-box confidence with and without actin in the DNA-SRF-MRTF prediction.
AF3 prediction of: DNA (c-fos promoter, 70bp), 2xSRF.DBD, 2xMRTF 2-404 and human cytoplasmic β-actin (only in B). The figure shows only parts of the prediction relevant for the discussion for clarity: MRTF B-box and Q-box, whole prediction of SRF on DNA. No actin and RPEL domain is shown in the prediction. The pLDDT values were plotted on the structure of the B-box (pLDDT values are colour-coded on a scale of 1-100, where 90-100=Very high accuracy, 70-90=High accuracy, 50-70=Low accuracy and <50=Very low accuracy). All other protein sequences shown in white. A. Prediction without actin. B-box prediction of very high confidence (shown in blue). B. Prediction with actin. B-box prediction of low confidence (shown in yellow).

Most importantly, Q-box involvement in all the processes described in this section is due to its ability to bind actin. Q-box was predicted by AlphaFold2-Multimer to fold into a nine-turn helix, placed on the hydrophobic surface of actin which we termed the “wall”. It’s positioned in a way that allows for contacts with both actin and RPEL3. $Y351^{Q\text{-}box}$ makes hydrophobic contacts with $Q354^{actin}$, $M355^{actin}$ and $K373^{actin}$ of actin, $I354^{Q\text{-}box}$ contacts the side chain of $F375^{actin}$ through hydrophobic interactions, and $L355^{Q\text{-}box}$ makes contact with $R372^{actin}$. The interaction with R3 is exerted through $I354^{Q\text{-}box}$, $Q357^{Q\text{-}box}$, $L361^{Q\text{-}box}$ and $F361^{Q\text{-}box}$. This means that the whole region conserved in evolution is involved in interaction with both RPEL3 and actin. Binding of the Q-box with actin and RPEL3 was tested in BLI and confirmed these interactions to be crucial for a high composite-site formation. This is in agreement with the new model, where the R3 – Q-box binds actin with the highest affinity. This is also confirmed by change in loading order of actins when Q-box recruitment is inhibited by the GP/ER mutation. Although GP/ER increases the affinity of RPEL3 alone, it’s of much lower affinity than that of R3 – Q-box or of R1-actin binding, and results in primary loading from N->C, again showing the validity of the new proposed model.

8.7 Considerations for in vivo validation of actin-regulated SRF interactions

To confirm that the actin – Q-box interaction is responsible for control of MRTF – SRF interaction *in vivo*, I aim to test the effect of mutations that block Q-box recruitment to RPEL3 on actin-mediated inhibition of SRF recruitment.

This will be assayed using Chromatin Immunoprecipitation assay under conditions of low or high G-actin.

All the aspects discussed in the previous section will need to be taken under consideration when designing an MRTF mutation for *in vivo* validation of the biochemical and structural data. The goal would be to uncouple RPEL-actin binding from the Q-box interacting region. The following criteria will be used when designing the mutation:

1. Disruption of R3 – Q-box binding, while maintaining the higher affinity for actin binding on RPEL3
2. Preserving the integrity of the regulatory elements in MRTF – both the NLS and NES signals, to uncouple the effect on DNA binding from that of disruption of MRTF sub-cellular localization

Based on the biochemical data presented here, the GP171/172ER mutation is a good candidate that meets both criteria. It disrupts Q-box recruitment to the composite site, switching to an N->C loading model, while maintaining the ability of RPEL3 to bind actin, although with lower overall affinity than that of the composite site binding. Two types of additional mutation may also be tested:

1. Additional RPEL3 mutation to further increase its affinity as an autonomously actin binding motif – M173A. The GPM171/172/173ERA mutant was shown to bind actin with higher affinity than GP/ER.
2. Mutations of the Q-box that block its interaction with actin. For this purpose, the residues in the ^{351}YAKIL^{355} sequence are the best candidate, as these do not affect other potential Q-box functions.

I will use CRIPSR-Cas9 to introduce the RPEL3 mutation into cells, while testing of the double mutation in both RPEL3/Q-box will be done using a doxycycline-inducible re-expression system in MRTF A/B KO cells.

Assuming the chosen mutation will successfully uncouple actin binding to the RPEL domain form Q-box interactions, there should be a noticeable difference in the effect that actin has on the MRTF-SRF-DNA complex formation in cells. To induce MRTF-DNA binding I will use serum stimulation, followed by treatment of cells with LatB, which will increase the concentration of monomeric actin available for MRTF binding. In WT MRTF, it was shown that this leads to rapid dissociation of MRTF from DNA (Gualdrini, 2016, PhD Thesis; Toteva, 2021, PhD Thesis). However, in the R3 – Q-box mutant, this should not be readily observed, as the B-box interaction with SRF should remain unaffected by actin binding on the RPEL domain. Disruption of binding might occur either at higher actin concentrations or over longer periods of time. It might also be possible to detect both actin and SRF bound to MRTF. The presence of actin on the target DNA will be tested, although it is unclear whether that will occur, as there is no actin detected in the *in vitro* DNA pulldown. However, this will add another layer of confirmation to the model, where actin and SRF binding to MRTF is mutually exclusive.

8.8 Future directions

The work presented in this thesis has allowed development of a new model for the mechanism regulating MRTF in the cell. Due to time constraints, functional validation of the model *in vivo* could not be done within the course of this PhD. This section therefore presents the experimental agenda of immediate experiments to be completed to publish this work. There are also experiments that would present a good project to work on in the future.

8.8.1 Immediate plans

8.8.1.1 Generating of the mutant MRTF cells using CRISPR-Cas9

NIH/3T3 mouse cell line was chosen for the *in vivo* validation. As there are two MRTFs in the cells, MRTF-A and MRTF-B which share a high degree of homology, there is a question as to their redundancy in the role they play in cells (Mokalled et al., 2015; Singh et al., 2023; Velasquez et al., 2013). MRTF-A

and MRTF-B also poses the ability to heterodimerize (Selvaraj and Prywes, 2003). Considering that, introducing the mutation into both sequences would assure that the observed phenotype is not influenced by the presence of WT MRTF in the cell. However, a simpler approach will be to delete MRTF-B in the cells, followed by introducing the mutation into MRTF-A. I will also assess the feasibility of testing re-expression of MRTF-A mutants in MRTF A/B KO cells.

I will describe the CRIPSR-Cas9 Knock-In approach for the GPM/ERA mutation on RPEL3 but following identification of any additional mutation that needs to be introduced, the same steps will be followed.

In the first step, I will use the CRISPR-Cas9 system, where a single-stranded oligonucleotide matching the MRTF-A target region with the substitution of the GPM171/172/173ERA residues will be delivered to the cells. This will be done in parallel with transfection of a SpCas9 plasmid (*S. pyogenes* Cas9), along with a gRNA designed to cut within RPEL3 (Exon 7). This will allow for HDR repair of the region using the ssOligonucleotide as a template, introducing the mutation into the cells. An additional screening tool that allows for determining which cells were transfected is a red fluorescent marker (mCherry) encoded in the backbone, which will be expressed together with Cas9. This permits single cell sorting of the cells based on the presence of mCherry, followed by genotyping using intronic primers, sequencing to detect the presence of the mutation (Figure 75), and Western Blotting to check whether the protein is intact. Secondary screening will be done to guarantee an intact mRNA product, using exonic primers located in the exons surrounding the targeted site. This is to make sure, that both alleles have the same final product. Genomic screening will be done all clones. Chosen clones with the mutation will be tested on cDNA to test that Exon7 is present on both alleles, as Exons 6-8 are in frame and will generate aberrant protein. All the abovementioned steps have already been optimized.

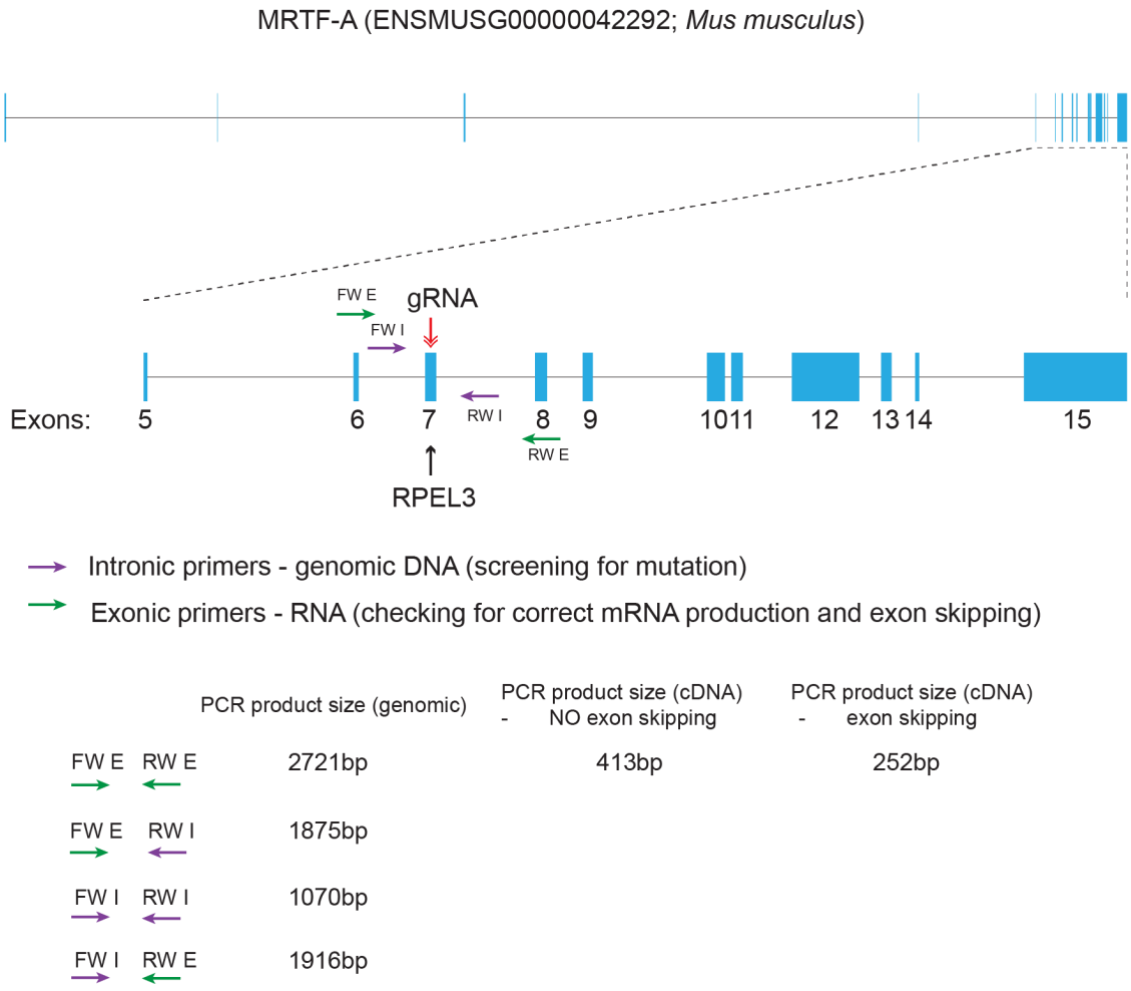

Figure 75. Strategy for introducing GPM/ERA mutation into MRTF-A
MRTF-A sequence with exons and introns indicated on the schematic (introns – black, exons – blue). gRNA targeted to the sequence of RPEL3 on Exon 7 will be inserted into a spCas9 plasmid, and will be introduced into cells using transfection, together with a donor ssOligonucleotide sequence carrying the mutation for HDR. The cells will be screened using intronic primers (purple) around the targeted exon to check for correct mutation insertion, as well as using exonic primers (green) localized in Exon 6 and Exon 8, to test for correct mRNA product on both alleles.

The second step after obtaining a clone with mutation within RPEL3, will be a Knock-Out of MRTF-B in the cells. Initial experiments used the sgRNA targeting a region in MRTF-B Exon 5, which was shown to cut the DNA with high efficiency. This region, however, has a high degree of homology with MRTF-A, and although the guide has five mismatches between MRTF-A and B sequences, a high percentage of cells tested were targeted on both genes. A new sgRNA will be designed to target a region of the protein with a lower level of homology, to obtain a product with MRTF-B KO and an intact MRTF-A. The

cells will be screened following the steps used for MRTF-A Knock-In. The cells will be then assayed to test the effect of disrupting R3 – Q-box interaction on DNA binding *in vivo*, as described in Section 8.7.

8.8.2 Long-term plans

8.8.2.1 Resolving the crystal structure of the MRTF-actin complex and MRTF-SRF-DNA binding

The pentavalent structure of MRTF with actin was resolved using the RPEL3 GP/ER mutation (Mouilleron et al., 2011). Having mapped the sequence of MRTF-A and identifying the regions involved in interaction with both SRF and actin should allow for generating better approaches for resolving the crystal structure of the complexes. As X-ray crystallography does not permit detection of unstructured regions, modifying the protein sequence of MRTF to contain the relevant elements should allow for resolving the crystal structure of both MRTF-Actin with Q-box and MRTF-SRF-DNA. Primary experiments were done to determine whether deletion of the unstructured region between the RPEL domain and the Q-box will affect actin binding in BLI and showed no negative effect on actin-binding affinity.

Reference List

Abramson J, Adler J, Dunger J, Evans R, Green T, Pritzel A, Ronneberger O, Willmore L, Ballard AJ, Bambrick J, Bodenstein SW, Evans DA, Hung C-C, O'Neill M, Reiman D, Tunyasuvunakool K, Wu Z, Žemgulytė A, Arvaniti E, Beattie C, Bertolli O, Bridgland A, Cherepanov A, Congreve M, Cowen-Rivers AI, Cowie A, Figurnov M, Fuchs FB, Gladman H, Jain R, Khan YA, Low CMR, Perlin K, Potapenko A, Savy P, Singh S, Stecula A, Thillaisundaram A, Tong C, Yakneen S, Zhong ED, Zielinski M, Žídek A, Bapst V, Kohli P, Jaderberg M, Hassabis D, Jumper JM. 2024. Accurate structure prediction of biomolecular interactions with AlphaFold 3. *Nature* **630**:493–500. doi:10.1038/s41586-024-07487-w

Alberts AS. 2001. Identification of a Carboxyl-terminal Diaphanous-related Formin Homology Protein Autoregulatory Domain*. *J Biol Chem* **276**:2824–2830. doi:10.1074/jbc.m006205200

Alekhina O, Burstein E, Billadeau DD. 2017. Cellular functions of WASP family proteins at a glance. *J Cell Sci* **130**:2235–2241. doi:10.1242/jcs.199570

AlphaFold open source code. https://github.com/deepmind/alphafold">https://github.com/deepmind/alphafold. n.d. https://github.com/deepmind/alphafold

Ampe C, Markey F, Lindberg U, Vandekerckhove J. 1988. The primary structure of human platelet profilin: Reinvestigation of the calf spleen profilin sequence. *FEBS Lett* **228**:17–21. doi:10.1016/0014-5793(88)80575-1

Aravind L, Koonin EV. 2000. SAP – a putative DNA-binding motif involved in chromosomal organization. *Trends Biochem Sci* **25**:112–114. doi:10.1016/s0968-0004(99)01537-6

Armelin HA, Armelin MCS, Kelly K, Stewart T, Leder P, Cochran BH, Stiles CD. 1984. Functional role for c-myc in mitogenic response to platelet-derived growth factor. *Nature* **310**:655–660. doi:10.1038/310655a0

Arsenian S, Weinhold B, Oelgeschläger M, Rüther U, Nordheim A. 1998. Serum response factor is essential for mesoderm formation during mouse embryogenesis. *EMBO J* **17**:6289–6299. doi:10.1093/emboj/17.21.6289

Ayadi A, Zheng H, Sobieszczuk P, Buchwalter G, Moerman P, Alitalo K, Wasylyk B. 2001. Net-targeted mutant mice develop a vascular phenotype and up-regulate egr-1. *EMBO J* **20**:5139–5152. doi:10.1093/emboj/20.18.5139

Balasubramaniam D, Komives EA. 2013. Hydrogen-exchange mass spectrometry for the study of intrinsic disorder in proteins. *Biochim Biophys Acta (BBA) - Proteins Proteom* **1834**:1202–1209. doi:10.1016/j.bbapap.2012.10.009

Balzer CJ, Wagner AR, Helgeson LA, Nolen BJ. 2019. Single-Turnover Activation of Arp2/3 Complex by Dip1 May Balance Nucleation of Linear versus Branched Actin Filaments. *Curr Biol* **29**:3331-3338.e7. doi:10.1016/j.cub.2019.08.023

Balzer CJ, Wagner AR, Helgeson LA, Nolen BJ. 2018. Dip1 Co-opts Features of Branching Nucleation to Create Linear Actin Filaments that Activate WASP-Bound Arp2/3 Complex. *Curr Biol* **28**:3886-3891.e4. doi:10.1016/j.cub.2018.10.045

Bernander R, Lind AE, Ettema TJG. 2011. An archaeal origin for the actin cytoskeleton: Implications for eukaryogenesis. *Commun Integr Biol* **4**:664–667. doi:10.4161/cib.16974

Blanchoin L, Pollard TD. 1999. Mechanism of Interaction of Acanthamoeba Actophorin (ADF/Cofilin) with Actin Filaments*. *J Biol Chem* **274**:15538–15546. doi:10.1074/jbc.274.22.15538

Bos JL, Rehmann H, Wittinghofer A. 2007. GEFs and GAPs: Critical Elements in the Control of Small G Proteins. *Cell* **129**:865–877. doi:10.1016/j.cell.2007.05.018

Brodsky S, Jana T, Mittelman K, Chapal M, Kumar DK, Carmi M, Barkai N. 2020. Intrinsically Disordered Regions Direct Transcription Factor In Vivo Binding Specificity. *Mol Cell* **79**:459-471.e4. doi:10.1016/j.molcel.2020.05.032

Burtnick LD, Koepf EK, Grimes J, Jones EY, Stuart DI, McLaughlin PJ, Robinson RC. 1997. The Crystal Structure of Plasma Gelsolin: Implications for Actin Severing, Capping, and Nucleation. *Cell* **90**:661–670. doi:10.1016/s0092-8674(00)80527-9

Cairns JT, Habgood A, Edwards-Pritchard RC, Joseph C, John AE, Wilkinson C, Stewart ID, Leslie J, Blaxall BC, Susztak K, Alberti S, Nordheim A, Oakley F, Jenkins G, Tatler AL. 2020. Loss of ELK1 has differential effects on age-dependent organ fibrosis. *Int J Biochem Cell Biol* **120**:105668. doi:10.1016/j.biocel.2019.105668

Campellone KG, Welch MD. 2010. A nucleator arms race: cellular control of actin assembly. *Nat Rev Mol Cell Biol* **11**:237–251. doi:10.1038/nrm2867

Cao L, Ghasemi F, Way M, Jégou A, Romet-Lemonne G. 2023. Regulation of branched versus linear Arp2/3-generated actin filaments. *EMBO J* **42**:e113008. doi:10.15252/embj.2022113008

Carlier M-F, Ducruix A, Pantaloni D. 1999. Signalling to actin: the Cdc42-N-WASP-Arp2/3 connection. *Chem Biol* **6**:R235–R240. doi:10.1016/s1074-5521(99)80107-0

Cen B, Selvaraj A, Burgess RC, Hitzler JK, Ma Z, Morris SW, Prywes R. 2003. Megakaryoblastic Leukemia 1, a Potent Transcriptional Coactivator for Serum Response Factor (SRF), Is Required for Serum Induction of SRF Target Genes. *Mol Cell Biol* **23**:6597–6608. doi:10.1128/mcb.23.18.6597-6608.2003

Ceron RH, Carman PJ, Rebowski G, Boczkowska M, Heuckeroth RO, Dominguez R. 2022. A solution to the long-standing problem of actin expression and purification. *P Natl Acad Sci Usa* **119**:e2209150119. doi:10.1073/pnas.2209150119

Cochran BH, Lillquist JS, Stiles CD. 1981. Post-transcriptional control of protein synthesis in Balb/C-3T3 cells by platelet-derived growth factor and platelet-poor plasma. *J Cell Physiol* **109**:429–438. doi:10.1002/jcp.1041090308

Cochran BH, Zullo J, Verma IM, Stiles CD. 1984. Expression of the c-fos Gene and of an fos-Related Gene Is Stimulated by Platelet-Derived Growth Factor. *Science* **226**:1080–1082. doi:10.1126/science.6093261

Cooper JA. 1987. Effects of cytochalasin and phalloidin on actin. *J Cell Biol* **105**:1473–1478. doi:10.1083/jcb.105.4.1473

Costello P, Nicolas R, Willoughby J, Wasylyk B, Nordheim A, Treisman R. 2010. Ternary Complex Factors SAP-1 and Elk-1, but Not Net, Are Functionally Equivalent in Thymocyte Development. *J Immunol* **185**:1082–1092. doi:10.4049/jimmunol.1000472

Costello P, Sargent M, Maurice D, Esnault C, Foster K, Anjos-Afonso F, Treisman R. 2015. MRTF-SRF signaling is required for seeding of HSC/Ps in bone marrow during development. *Blood* **125**:1244–1255. doi:10.1182/blood-2014-08-595603

Costello PS, Nicolas RH, Watanabe Y, Rosewell I, Treisman R. 2004. Ternary complex factor SAP-1 is required for Erk-mediated thymocyte positive selection. *Nat Immunol* **5**:289–298. doi:10.1038/ni1038

Curran T, Peters G, Beveren CV, Teich NM, Verma IM. 1982. FBJ murine osteosarcoma virus: identification and molecular cloning of biologically active proviral DNA. *J Virol* **44**:674–682. doi:10.1128/jvi.44.2.674-682.1982

Dalton S, Treisman R. 1992. Characterization of SAP-1, a protein recruited by serum response factor to the c-fos serum response element. *Cell* **68**:597–612. doi:10.1016/0092-8674(92)90194-h

Dandamudi A, Akbar H, Cancelas J, Zheng Y. 2023. Rho GTPase Signaling in Platelet Regulation and Implication for Antiplatelet Therapies. *Int J Mol Sci* **24**:2519. doi:10.3390/ijms24032519

Diring J, Mouilleron S, McDonald NQ, Treisman R. 2019a. RPEL-family rhoGAPs link Rac/Cdc42 GTP loading to G-actin availability. *Nat Cell Biol* **21**:845–855. doi:10.1038/s41556-019-0337-y

Dominguez R. 2004. Actin-binding proteins – a unifying hypothesis. *Trends Biochem Sci* **29**:572–578. doi:10.1016/j.tibs.2004.09.004

Dominguez R, Holmes KC. 2011. Actin Structure and Function. *Annu Rev Biophys* **40**:169–186. doi:10.1146/annurev-biophys-042910-155359

Dopie J, Skarp K-P, Rajakylä EK, Tanhuanpää K, Vartiainen MK. 2012. Active maintenance of nuclear actin by importin 9 supports transcription. *Proc National Acad Sci* **109**:E544–E552. doi:10.1073/pnas.1118880109

Du KL, Chen M, Li J, Lepore JJ, Mericko P, Parmacek MS. 2004. Megakaryoblastic Leukemia Factor-1 Transduces Cytoskeletal Signals and Induces Smooth Muscle Cell Differentiation from Undifferentiated Embryonic Stem Cells*. *J Biol Chem* **279**:17578–17586. doi:10.1074/jbc.m400961200

Dubois E, Bercy J, Descamps F, Messenguy F. 1987. Characterization of two new genes essential for vegetative growth in Saccharomyces cerevisiae: nucleotide sequence determination and chromosome mapping. *Gene* **55**:265–275. doi:10.1016/0378-1119(87)90286-1

Edwards M, Zwolak A, Schafer DA, Sept D, Dominguez R, Cooper JA. 2014. Capping protein regulators fine-tune actin assembly dynamics. *Nat Rev Mol Cell Biol* **15**:677–689. doi:10.1038/nrm3869

Epstein FH, Lee WM, Galbraith RM. 1992. The Extracellular Actin-Scavenger System and Actin Toxicity. *N Engl J Med* **326**:1335–1341. doi:10.1056/nejm199205143262006

Esnault C, Stewart A, Gualdrini F, East P, Horswell S, Matthews N, Treisman R. 2014. Rho-actin signaling to the MRTF coactivators dominates the immediate transcriptional response to serum in fibroblasts. *Gene Dev* **28**:943–958. doi:10.1101/gad.239327.114

Evans R, O'Neill M, Pritzel A, Antropova N, Senior A, Green T, Žídek A, Bates R, Blackwell S, Yim J, Ronneberger O, Bodenstein S, Zielinski M, Bridgland A, Potapenko A, Cowie A, Tunyasuvunakool K, Jain R, Clancy E, Kohli P, Jumper J, Hassabis D. 2022. Protein complex prediction with AlphaFold-Multimer. *Biorxiv* 2021.10.04.463034. doi:10.1101/2021.10.04.463034

Fedoryshchak RO, Přechová M, Butler AM, Lee R, O'Reilly N, Flynn HR, Snijders AP, Eder N, Ultanir S, Mouilleron S, Treisman R. 2020. Molecular basis for substrate specificity of the Phactr1/PP1 phosphatase holoenzyme. *eLife* **9**:e61509. doi:10.7554/elife.61509

Feuer G, Molnar F. 1948. Studies on the composition and polymerization of actin. *Hung acta Physiol* **1**:150–63.

Finkel MP, Biskis BO, Jinkins PB. 1966. Virus Induction of Osteosarcomas in Mice. *Science* **151**:698–701. doi:10.1126/science.151.3711.698

Fukata Y, Kaibuchi K, Amano M, Kaibuchi K. 2001. Rho–Rho-kinase pathway in smooth muscle contraction and cytoskeletal reorganization of non-muscle cells. *Trends Pharmacol Sci* **22**:32–39. doi:10.1016/s0165-6147(00)01596-0

Garrels JI, Gibson W. 1976. Identification and characterization of multiple forms of actin. *Cell* **9**:793–805. doi:10.1016/0092-8674(76)90142-2

Gille H, Sharrocks AD, Shaw PE. 1992. Phosphorylation of transcription factor p62TCF by MAP kinase stimulates ternary complex formation at c-fos promoter. *Nature* **358**:414–417. doi:10.1038/358414a0

Gille H, Strahl T, Shaw PE. 1995. Activation of ternary complex factor Elk-1 by stress-activated protein kinases. *Curr Biol* **5**:1191–1200. doi:10.1016/s0960-9822(95)00235-1

Gilman MZ, Wilson RN, Weinberg RA. 1986. Multiple Protein-Binding Sites in the 5′-Flanking Region Regulate c-fos Expression. *Mol Cell Biol* **6**:4305–4316. doi:10.1128/mcb.6.12.4305-4316.1986

Gineitis D, Treisman R. 2001. Differential Usage of Signal Transduction Pathways Defines Two Types of Serum Response Factor Target Gene*. *J Biol Chem* **276**:24531–24539. doi:10.1074/jbc.m102678200

Giovane A, Pintzas A, Maira SM, Sobieszczuk P, Wasylyk B. 1994. Net, a new ets transcription factor that is activated by Ras. *Genes Dev* **8**:1502–1513. doi:10.1101/gad.8.13.1502

Görlich D, Kostka S, Kraft R, Dingwall C, Laskey RA, Hartmann E, Prehn S. 1995. Two different subunits of importin cooperate to recognize nuclear localization signals and bind them to the nuclear envelope. *Curr Biol* **5**:383–392. doi:10.1016/s0960-9822(95)00079-0

Graham R, Gilman M. 1991. Distinct Protein Targets for Signals Acting at the c-fos Serum Response Element. *Science* **251**:189–192. doi:10.1126/science.1898992

Greenberg ME, Ziff EB. 1984. Stimulation of 3T3 cells induces transcription of the c-fos proto-oncogene. *Nature* **311**:433–438. doi:10.1038/311433a0

Gualdrini F. 2016. PhD Thesis.

Gualdrini F, Esnault C, Horswell S, Stewart A, Matthews N, Treisman R. 2016. SRF Co-factors Control the Balance between Cell Proliferation and Contractility. *Mol Cell* **64**:1048–1061. doi:10.1016/j.molcel.2016.10.016

Guettler S. 2007. PhD Thesis.

Guettler S, Vartiainen MK, Miralles F, Larijani B, Treisman R. 2008. RPEL Motifs Link the Serum Response Factor Cofactor MAL but Not Myocardin to Rho Signaling via Actin Binding. *Mol Cell Biol* **28**:732–742. doi:10.1128/mcb.01623-07

Gunning P, Ponte P, Okayama H, Engel J, Blau H, Kedes L. 1983. Isolation and Characterization of Full-Length cDNA Clones for Human α-, β-, and γ-Actin mRNAs: Skeletal but Not Cytoplasmic Actins Have an Amino-Terminal Cysteine that Is Subsequently Removed. *Mol Cell Biol* **3**:787–795. doi:10.1128/mcb.3.5.787-795.1983

Gunning PW, Ghoshdastider U, Whitaker S, Popp D, Robinson RC. 2015. The evolution of compositionally and functionally distinct actin filaments. *J Cell Sci* **128**:2009–2019. doi:10.1242/jcs.165563

Gupton SL, Gertler FB. 2007. Filopodia: The Fingers That Do the Walking. *Sci's STKE* **2007**:re5. doi:10.1126/stke.4002007re5

Gurbuz I, Ferralli J, Roloff T, Chiquet-Ehrismann R, Asparuhova MB. 2014. SAP domain-dependent Mkl1 signaling stimulates proliferation and cell migration by induction of a distinct gene set indicative of poor prognosis in breast cancer patients. *Mol Cancer* **13**:22–22. doi:10.1186/1476-4598-13-22

Hakoshima T. 2017. eLS. doi:10.1002/9780470015902.a0005049.pub2

Hall A. 1994. Small GTP-Binding Proteins and the Regulation of the Actin Cytoskeleton. *Annu Rev Cell Dev Biol* **10**:31–54. doi:10.1146/annurev.cellbio.10.1.31

Hayashi K, Morita T. 2013. Differences in the Nuclear Export Mechanism between Myocardin and Myocardin-related Transcription Factor A*. *J Biol Chem* **288**:5743–5755. doi:10.1074/jbc.m112.408120

Heasman SJ, Ridley AJ. 2008. Mammalian Rho GTPases: new insights into their functions from in vivo studies. *Nat Rev Mol Cell Biol* **9**:690–701. doi:10.1038/nrm2476

Helgeson LA, Prendergast JG, Wagner AR, Rodnick-Smith M, Nolen BJ. 2014. Interactions with Actin Monomers, Actin Filaments, and Arp2/3 Complex Define the Roles of WASP Family Proteins and Cortactin in Coordinately Regulating Branched Actin Networks*. *J Biol Chem* **289**:28856–28869. doi:10.1074/jbc.m114.587527

Herrera RE, Shaw PE, Nordheim A. 1989. Occupation of the c-fos serum response element in vivo by a multi-protein complex is unaltered by growth factor induction. *Nature* **340**:68–70. doi:10.1038/340068a0

Herschman HR. 1991. Primary Response Genes Induced by Growth Factors and Tumor Promoters. *Annu Rev Biochem* **60**:281–319. doi:10.1146/annurev.bi.60.070191.001433

Hertzog M, Heijenoort C van, Didry D, Gaudier M, Coutant J, Gigant B, Didelot G, Préat T, Knossow M, Guittet E, Carlier M-F. 2003. The beta-thymosin/WH2 domain; structural basis for the switch from inhibition to promotion of actin assembly. *Cell* **117**:611–23. doi:10.1016/s0092-8674(04)00403-9

Hill CS, Treisman R. 1995. Differential activation of c-fos promoter elements by serum, lysophosphatidic acid, G proteins and polypeptide growth factors. *Embo J* **14**:5037–5047. doi:10.1002/j.1460-2075.1995.tb00186.x

Hill CS, Wynne J, Treisman R. 1995. The Rho family GTPases RhoA, Racl , and CDC42Hsregulate transcriptional activation by SRF. *Cell* **81**:1159–1170. doi:10.1016/s0092-8674(05)80020-0

Hill CS, Wynne J, Treisman R. 1994. Serum-regulated transcription by serum response factor (SRF): a novel role for the DNA binding domain. *EMBO J* **13**:5421–32. doi:10.1002/j.1460-2075.1994.tb06877.x

Hipskind RA, Roa VN, Muller CGF, Raddy ESP, Nordheim A. 1991. Ets-related protein Elk-1 is homologous to the c-fos regulatory factor p62TCF. *Nature* **354**:531–534. doi:10.1038/354531a0

Hirano H, Matsuura Y. 2011. Sensing actin dynamics: Structural basis for G-actin-sensitive nuclear import of MAL. *Biochem Bioph Res Co* **414**:373–378. doi:10.1016/j.bbrc.2011.09.079

Holmes KC, Popp D, Gebhard W, Kabsch W. 1990. Atomic model of the actin filament. *Nature* **347**:44–49. doi:10.1038/347044a0

Huehn AR, Bibeau JP, Schramm AC, Cao W, Cruz EMDL, Sindelar CV. 2020. Structures of cofilin-induced structural changes reveal local and asymmetric perturbations of actin filaments. *Proc Natl Acad Sci* **117**:1478–1484. doi:10.1073/pnas.1915987117

Iwasa M, Maeda K, Narita A, Maéda Y, Oda T. 2008. Dual Roles of Gln137 of Actin Revealed by Recombinant Human Cardiac Muscle α-Actin Mutants*. *J Biol Chem* **283**:21045–21053. doi:10.1074/jbc.m800570200

Jaffe AB, Hall A. 2005. RHO GTPASES: Biochemistry and Biology. *Cell Dev Biol* **21**:247–269. doi:10.1146/annurev.cellbio.21.020604.150721

Janknecht R, Zinck R, Ernst WH, Nordheim A. 1994. Functional dissection of the transcription factor Elk-1. *Oncogene* **9**:1273–8.

Jumper J, Evans R, Pritzel A, Green T, Figurnov M, Ronneberger O, Tunyasuvunakool K, Bates R, Žídek A, Potapenko A, Bridgland A, Meyer C, Kohl SAA, Ballard AJ, Cowie A, Romera-Paredes B, Nikolov S, Jain R, Adler J, Back T, Petersen S, Reiman D, Clancy E, Zielinski M, Steinegger M, Pacholska M, Berghammer T, Bodenstein S, Silver D, Vinyals O, Senior AW, Kavukcuoglu K, Kohli P, Hassabis

D. 2021. Highly accurate protein structure prediction with AlphaFold. *Nature* **596**:583–589. doi:10.1038/s41586-021-03819-2

Kabsch W, Mannherz HG, Suck D, Pai EF, Holmes KC. 1990. Atomic structure of the actin: DNase I complex. *Nature* **347**:37–44. doi:10.1038/347037a0

Kang H, Bradley MJ, Elam WA, De La Cruz EM. 2013. Regulation of Actin by Ion-Linked Equilibria. *Biophys J* **105**:2621–2628. doi:10.1016/j.bpj.2013.10.032

Kelly K, Cochran BH, Stiles CD, Leder P. 1983. Cell-specific regulation of the c-myc gene by lymphocyte mitogens and platelet-derived growth factor. *Cell* **35**:603–610. doi:10.1016/0092-8674(83)90092-2

Kim AS, Kakalis LT, Abdul-Manan N, Liu GA, Rosen MK. 2000. Autoinhibition and activation mechanisms of the Wiskott–Aldrich syndrome protein. *Nature* **404**:151–158. doi:10.1038/35004513

Konno K. 1987. Functional, chymotryptically split actin and its interaction with myosin subfragment 1. *Biochemistry* **26**:3582–3589. doi:10.1021/bi00386a050

Kudryashov DS, Grintsevich EE, Rubenstein PA, Reisler E. 2010. A Nucleotide State-sensing Region on Actin*. *J Biol Chem* **285**:25591–25601. doi:10.1074/jbc.m110.123869

Li J, Zhu X, Chen M, Cheng L, Zhou D, Lu MM, Du K, Epstein JA, Parmacek MS. 2005. Myocardin-related transcription factor B is required in cardiac neural crest for smooth muscle differentiation and cardiovascular development. *Proc Natl Acad Sci* **102**:8916–8921. doi:10.1073/pnas.0503741102

Li S, Chang S, Qi X, Richardson JA, Olson EN. 2006. Requirement of a myocardin-related transcription factor for development of mammary myoepithelial cells. *Mol Cell Biol* **26**:5797–808. doi:10.1128/mcb.00211-06

Littlefield R, Almenar-Queralt A, Fowler VM. 2001. Actin dynamics at pointed ends regulates thin filament length in striated muscle. *Nat Cell Biol* **3**:544–551. doi:10.1038/35078517

Liu T, Cao L, Mladenov M, Jegou A, Way M, Moores CA. 2024. Cortactin stabilizes actin branches by bridging activated Arp2/3 to its nucleated actin filament. *Nat Struct Mol Biol* **31**:801–809. doi:10.1038/s41594-023-01205-2

Luan Q, Liu S, Helgeson LA, Nolen BJ. 2018. Structure of the nucleation-promoting factor SPIN90 bound to the actin filament nucleator Arp2/3 complex. *EMBO J* **37**. doi:10.15252/embj.2018100005

Ma L, Rohatgi R, Kirschner MW. 1998. The Arp2/3 complex mediates actin polymerization induced by the small GTP-binding protein Cdc42. *Proc Natl Acad Sci* **95**:15362–15367. doi:10.1073/pnas.95.26.15362

Ma Z, Morris SW, Valentine V, L M, Herbrick J-A, Cui X, Bouman D, Li Y, Mehta PK, Nizetic D, Kaneko Y, Chan GCF, Chan LC, Squire J, Scherer SW, Hitzler JK. 2001a. Fusion of two novel genes, RBM15 and MKL1, in the t(1;22)(p13;q13) of acute megakaryoblastic leukemia. *Nat Genet* **28**:220–221. doi:10.1038/90054

Ma Z, Morris SW, Valentine V, L M, Herbrick J-A, Cui X, Bouman D, Li Y, Mehta PK, Nizetic D, Kaneko Y, Chan GCF, Chan LC, Squire J, Scherer SW, Hitzler JK. 2001b. Fusion of two novel genes, RBM15 and MKL1, in the t(1;22)(p13;q13) of acute megakaryoblastic leukemia. *Nat Genet* **28**:220–221. doi:10.1038/90054

Machesky LM, Atkinson SJ, Ampe C, Vandekerckhove J, Pollard TD. 1994. Purification of a cortical complex containing two unconventional actins from Acanthamoeba by affinity chromatography on profilin-agarose. *J cell Biol* **127**:107–115. doi:10.1083/jcb.127.1.107

Marais R, Wynne J, Treisman R. 1993. The SRF accessory protein Elk-1 contains a growth factor-regulated transcriptional activation domain. *Cell* **73**:381–393. doi:10.1016/0092-8674(93)90237-k

Mason JM, Arndt KM. 2004. Coiled Coil Domains: Stability, Specificity, and Biological Implications. *ChemInform* **35**:no-no. doi:10.1002/chin.200415270

McCullough BR, Grintsevich EE, Chen CK, Kang H, Hutchison AL, Henn A, Cao W, Suarez C, Martiel J-L, Blanchoin L, Reisler E, De La Cruz EM. 2011. Cofilin-Linked Changes in Actin Filament Flexibility Promote Severing. *Biophys J* **101**:151–159. doi:10.1016/j.bpj.2011.05.049

McGough A, Pope B, Chiu W, Weeds A. 1997. Cofilin Changes the Twist of F-Actin: Implications for Actin Filament Dynamics and Cellular Function. *J Cell Biol* **138**:771–781. doi:10.1083/jcb.138.4.771

Mercher T, Coniat MB-L, Monni R, Mauchauffé M, Khac FN, Gressin L, Mugneret F, Leblanc T, Dastugue N, Berger R, Bernard OA. 2001. Involvement of a human gene related to the Drosophila spen gene in the recurrent t(1;22) translocation of acute megakaryocytic leukemia. *Proc Natl Acad Sci* **98**:5776–5779. doi:10.1073/pnas.101001498

Messenguy F, Dubois E. 2003. Role of MADS box proteins and their cofactors in combinatorial control of gene expression and cell development. *Gene* **316**:1–21. doi:10.1016/s0378-1119(03)00747-9

Miralles F, Posern G, Zaromytidou A-I, Treisman R. 2003. Actin Dynamics Control SRF Activity by Regulation of Its Coactivator MAL. *Cell* **113**:329–342. doi:10.1016/s0092-8674(03)00278-2

Mockrin SC, Korn ED. 1980. Acanthamoeba profilin interacts with G-actin to increase the rate of exchange of actin-bound adenosine 5'-triphosphate. *Biochemistry* **19**:5359–5362. doi:10.1021/bi00564a033

Mokalled MH, Carroll KJ, Cenik BK, Chen B, Liu N, Olson EN, Bassel-Duby R. 2015. Myocardin-related transcription factors are required for cardiac development and function. *Dev Biol* **406**:109–116. doi:10.1016/j.ydbio.2015.09.006

Mokalled MH, Johnson A, Kim Y, Oh J, Olson EN. 2010. Myocardin-related transcription factors regulate the Cdk5/Pctaire1 kinase cascade to control neurite outgrowth, neuronal migration and brain development. *Development* **137**:2365–2374. doi:10.1242/dev.047605

Moll J, Sansig G, Fattori E, Putten H van der. 1991. The murine rac1 gene: cDNA cloning, tissue distribution and regulated expression of rac1 mRNA by disassembly of actin microfilaments. *Oncogene* **6**:863–6.

Morton WM, Ayscough KR, McLaughlin PJ. 2000. Latrunculin alters the actin-monomer subunit interface to prevent polymerization. *Nat Cell Biol* **2**:376–378. doi:10.1038/35014075

Mosaddeghzadeh N, Ahmadian MR. 2021. The RHO Family GTPases: Mechanisms of Regulation and Signaling. *Cells* **10**:1831. doi:10.3390/cells10071831

Mouilleron S, Guettler S, Langer CA, Treisman R, McDonald NQ. 2008. Molecular basis for G-actin binding to RPEL motifs from the serum response factor coactivator MAL. *Embo J* **27**:3198–3208. doi:10.1038/emboj.2008.235

Mouilleron S, Langer CA, Guettler S, McDonald NQ, Treisman R. 2011. Structure of a Pentavalent G-Actin•MRTF-A Complex Reveals How G-Actin Controls Nucleocytoplasmic Shuttling of a Transcriptional Coactivator. *Sci Signal* **4**:ra40. doi:10.1126/scisignal.2001750

Mouilleron S, Wiezlak M, O'Reilly N, Treisman R, McDonald NQ. 2012. Structures of the Phactr1 RPEL Domain and RPEL Motif Complexes with G-Actin Reveal the Molecular Basis for Actin Binding Cooperativity. *Structure* **20**:1960–1970. doi:10.1016/j.str.2012.08.031

Muehlich S, Wang R, Lee S-M, Lewis TC, Dai C, Prywes R. 2008a. Serum-Induced Phosphorylation of the Serum Response Factor Coactivator MKL1 by the Extracellular Signal-Regulated Kinase 1/2 Pathway Inhibits Its Nuclear Localization. *Mol Cell Biol* **28**:6302–6313. doi:10.1128/mcb.00427-08

Mullins RD, Heuser JA, Pollard TD. 1998. The interaction of Arp2/3 complex with actin: Nucleation, high affinity pointed end capping, and formation of branching networks of filaments. *Proc Natl Acad Sci* **95**:6181–6186. doi:10.1073/pnas.95.11.6181

Murai K, Treisman R. 2002. Interaction of Serum Response Factor (SRF) with the Elk-1 B Box Inhibits RhoA-Actin Signaling to SRF and Potentiates Transcriptional Activation by Elk-1. *Mol Cell Biol* **22**:7083–7092. doi:10.1128/mcb.22.20.7083-7092.2002

Nag S, Larsson M, Robinson RC, Burtnick LD. 2013. Gelsolin: The tail of a molecular gymnast. *Cytoskeleton* **70**:360–384. doi:10.1002/cm.21117

Narumiya S, Tanji M, Ishizaki T. 2009. Rho signaling, ROCK and mDia1, in transformation, metastasis and invasion. *Cancer Metastasis Rev* **28**:65–76. doi:10.1007/s10555-008-9170-7

Noguchi TQP, Kanzaki N, Ueno H, Hirose K, Uyeda TQP. 2007. A Novel System for Expressing Toxic Actin Mutants in Dictyostelium and Purification and Characterization of a Dominant Lethal Yeast Actin Mutant*. *J Biol Chem* **282**:27721–27727. doi:10.1074/jbc.m703165200

Norman C, Runswick M, Pollock R, Treisman R. 1988. Isolation and properties of cDNA clones encoding SRF, a transcription factor that binds to the c-fos serum response element. *Cell* **55**:989–1003. doi:10.1016/0092-8674(88)90244-9

Oda T, Iwasa M, Aihara T, Maéda Y, Narita A. 2009. The nature of the globular- to fibrous-actin transition. *Nature* **457**:441–445. doi:10.1038/nature07685

Oh J, Richardson JA, Olson EN. 2005a. Requirement of myocardin-related transcription factor-B for remodeling of branchial arch arteries and smooth muscle differentiation. *Proc National Acad Sci* **102**:15122–15127. doi:10.1073/pnas.0507346102

Olson EN, Nordheim A. 2010. Linking actin dynamics and gene transcription to drive cellular motile functions. *Nat Rev Mol Cell Bio* **11**:353–365. doi:10.1038/nrm2890

Onuh JO, Qiu H. 2021. Serum response factor-cofactor interactions and their implications in disease. *Febs J* **288**:3120–3134. doi:10.1111/febs.15544

Oosterheert W, Klink BU, Belyy A, Pospich S, Raunser S. 2022. Structural basis of actin filament assembly and aging. *Nature* **611**:374–379. doi:10.1038/s41586-022-05241-8

Otterbein LR, Cosio C, Graceffa P, Dominguez R. 2002. Crystal structures of the vitamin D-binding protein and its complex with actin: Structural basis of the actin-scavenger system. *Proc Natl Acad Sci* **99**:8003–8008. doi:10.1073/pnas.122126299

Paavilainen VO, Oksanen E, Goldman A, Lappalainen P. 2008. Structure of the actin-depolymerizing factor homology domain in complex with actin. *J Cell Biol* **182**:51–59. doi:10.1083/jcb.200803100

Panayiotou R, Miralles F, Pawlowski R, Diring J, Flynn HR, Skehel M, Treisman R. 2016. Phosphorylation acts positively and negatively to regulate MRTF-A subcellular localisation and activity. *Elife* **5**:e15460. doi:10.7554/elife.15460

Pantaloni D, Carlier M-F. 1993. How profilin promotes actin filament assembly in the presence of thymosin β4. *Cell* **75**:1007–1014. doi:10.1016/0092-8674(93)90544-z

Passmore S, Elble R, Tye BK. 1989. A protein involved in minichromosome maintenance in yeast binds a transcriptional enhancer conserved in eukaryotes. *Genes Dev* **3**:921–935. doi:10.1101/gad.3.7.921

Paunola E, Mattila PK, Lappalainen P. 2002. WH2 domain: a small, versatile adapter for actin monomers. *FEBS Lett* **513**:92–97. doi:10.1016/s0014-5793(01)03242-2

Pawłowski R, Rajakylä EK, Vartiainen MK, Treisman R. 2010. An actin-regulated importin α/β-dependent extended bipartite NLS directs nuclear import of MRTF-A. *Embo J* **29**:3448–3458. doi:10.1038/emboj.2010.216

Pellegrini L, Tan S, Richmond TJ. 1995. Structure of serum response factor core bound to DNA. *Nature* **376**:490–498. doi:10.1038/376490a0

Pollard TD. 2016. Actin and Actin-Binding Proteins. *Cold Spring Harb Perspect Biol* **8**:a018226. doi:10.1101/cshperspect.a018226

Pollard TD. 2007. Regulation of Actin Filament Assembly by Arp2/3 Complex and Formins. *Annu Rev Biophys Biomol Struct* **36**:451–477. doi:10.1146/annurev.biophys.35.040405.101936

Pollard TD, Borisy GG. 2003. Cellular Motility Driven by Assembly and Disassembly of Actin Filaments. *Cell* **112**:453–465. doi:10.1016/s0092-8674(03)00120-x

Pollard TD, Cooper JA. 2009. Actin, a Central Player in Cell Shape and Movement. *Science* **326**:1208–1212. doi:10.1126/science.1175862

Posern G, Sotiropoulos A, Treisman R. 2002. Mutant Actins Demonstrate a Role for Unpolymerized Actin in Control of Transcription by Serum Response Factor. *Mol Biol Cell* **13**:4167–4178. doi:10.1091/mbc.02-05-0068

Posern G, Treisman R. 2006. Actin' together: serum response factor, its cofactors and the link to signal transduction. *Trends Cell Biol* **16**:588–596. doi:10.1016/j.tcb.2006.09.008

Price MA, Rogers AE, Treisman R. 1995. Comparative analysis of the ternary complex factors Elk-1, SAP-1a and SAP-2 (ERP/NET). *EMBO J* **14**:2589–601. doi:10.1002/j.1460-2075.1995.tb07257.x

Pring M, Evangelista M, Boone C, Yang C, Zigmond SH. 2003. Mechanism of Formin-Induced Nucleation of Actin Filaments. *Biochemistry* **42**:486–496. doi:10.1021/bi026520j

Prywes R, Roeder RG. 1987. Purification of the c-fos Enhancer-Binding Protein. *Mol Cell Biol* **7**:3482–3489. doi:10.1128/mcb.7.10.3482-3489.1987

Rao JN, Madasu Y, Dominguez R. 2014. Mechanism of actin filament pointed-end capping by tropomodulin. *Science* **345**:463–467. doi:10.1126/science.1256159

Remedios CGD, Chhabra D, Kekic M, Dedova IV, Tsubakihara M, Berry DA, Nosworthy NJ. 2003. Actin Binding Proteins: Regulation of Cytoskeletal Microfilaments. *Physiol Rev* **83**:433–473. doi:10.1152/physrev.00026.2002

Rexach M, Blobel G. 1995. Protein import into nuclei: association and dissociation reactions involving transport substrate, transport factors, and nucleoporins. *Cell* **83**:683–692. doi:10.1016/0092-8674(95)90181-7

Richmond TJ, Hassler M. 2001. The B-box dominates SAP-1±SRF interactions in thestructure of the ternary complex.

Robinson RC, Turbedsky K, Kaiser DA, Marchand J-B, Higgs HN, Choe S, Pollard TD. 2001. Crystal Structure of Arp2/3 Complex. *Science* **294**:1679–1684. doi:10.1126/science.1066333

Rubenstein PA, Martin DJ. 1983. NH2-terminal processing of actin in mouse L-cells in vivo. *J Biol Chem* **258**:3961–3966. doi:10.1016/s0021-9258(18)32761-3

Sasazuki T, Sawada T, Sakon S, Kitamura T, Kishi T, Okazaki T, Katano M, Tanaka M, Watanabe M, Yagita H, Okumura K, Nakano H. 2002. Identification of a Novel Transcriptional Activator, BSAC, by a Functional Cloning to Inhibit Tumor Necrosis Factor-induced Cell Death*. *J Biol Chem* **277**:28853–28860. doi:10.1074/jbc.m203190200

Schröter H, Shaw PE, Nordheim A. 1987. Purification of intercalator-released p67, a polypeptide that interacts specifically with the c-fos serum response element. *Nucleic Acids Res* **15**:10145–10158. doi:10.1093/nar/15.24.10145

Sells MA, Pfaff A, Chernoff J. 2000. Temporal and Spatial Distribution of Activated Pak1 in Fibroblasts. *J Cell Biol* **151**:1449–1458. doi:10.1083/jcb.151.7.1449

Selvaraj A, Prywes R. 2003. Megakaryoblastic Leukemia-1/2, a Transcriptional Co-activator of Serum Response Factor, Is Required for Skeletal Myogenic Differentiation*. *J Biol Chem* **278**:41977–41987. doi:10.1074/jbc.m305679200

Shaw PE, Schröter H, Nordheim A. 1989. The ability of a ternary complex to form over the serum response element correlates with serum inducibility of the human c-fos promoter. *Cell* **56**:563–572. doi:10.1016/0092-8674(89)90579-5

Silva JC, Denny R, Dorschel CA, Gorenstein M, Kass IJ, Li G-Z, McKenna T, Nold MJ, Richardson K, Young P, Geromanos S. 2005. Quantitative Proteomic Analysis by Accurate Mass Retention Time Pairs. *Anal Chem* **77**:2187–2200. doi:10.1021/ac048455k

Singh AK, Rai A, Weber A, Gericke M, Janssen K-P, Moser M, Posern G. 2023. MRTF-A gain-of-function in mice impairs homeostatic renewal of the intestinal epithelium. *Cell Death Dis* **14**:639. doi:10.1038/s41419-023-06158-4

Skarnes WC, Auerbach BA, Joyner AL. 1992. A gene trap approach in mouse embryonic stem cells: the lacZ reported is activated by splicing, reflects endogenous gene expression, and is mutagenic in mice. *Genes Dev* **6**:903–918. doi:10.1101/gad.6.6.903

Smith JC, Stiles CD. 1981. Cytoplasmic transfer of the mitogenic response to platelet-derived growth factor. *Proc Natl Acad Sci* **78**:4363–4367. doi:10.1073/pnas.78.7.4363

Solomon LR, Rubenstein PA. 1985. Correct NH2-terminal processing of cardiac muscle alpha-isoactin (class II) in a nonmuscle mouse cell. *J Biol Chem* **260**:7659–7664. doi:10.1016/s0021-9258(17)39659-x

Sommer H, Beltrán JP, Huijser P, Pape H, Lönnig WE, Saedler H, Schwarz-Sommer Z. 1990. Deficiens, a homeotic gene involved in the control of flower morphogenesis in Antirrhinum majus: the protein shows homology to transcription factors. *EMBO J* **9**:605–613. doi:10.1002/j.1460-2075.1990.tb08152.x

Sotiropoulos A, Gineitis D, Copeland J, Treisman R. 1999. Signal-Regulated Activation of Serum Response Factor Is Mediated by Changes in Actin Dynamics. *Cell* **98**:159–169. doi:10.1016/s0092-8674(00)81011-9

Spector I, Shochet NR, Kashman Y, Groweiss A. 1983. Latrunculins: Novel Marine Toxins That Disrupt Microfilament Organization in Cultured Cells. *Science* **219**:493–495. doi:10.1126/science.6681676

Spudich JA, Watt S. 1971. The Regulation of Rabbit Skeletal Muscle Contraction I. Biochemical studies of the interaction of the tropomyosin-troponin complex with actin and the proteolytic fragments of myosin. *J Biol Chem* **246**:4866–4871. doi:10.1016/s0021-9258(18)62016-2

Stüven T, Hartmann E, Görlich D. 2003. Exportin 6: a novel nuclear export receptor that is specific for profilin·actin complexes. *Embo J* **22**:5928–5940. doi:10.1093/emboj/cdg565

Sun Y, Boyd K, Xu W, Ma J, Jackson CW, Fu A, Shillingford JM, Robinson GW, Hennighausen L, Hitzler JK, Ma Z, Morris SW. 2006. Acute Myeloid Leukemia-Associated Mkl1 (Mrtf-a) Is a Key Regulator of Mammary Gland Function. *Mol Cell Biol* **26**:5809–5826. doi:10.1128/mcb.00024-06

Tan S, Richmond TJ. 1998. Crystal structure of the yeast MATα2/MCM1/DNA ternary complex. *Nature* **391**:660–666. doi:10.1038/35563

Tanaka K, Takeda S, Mitsuoka K, Oda T, Kimura-Sakiyama C, Maéda Y, Narita A. 2018. Structural basis for cofilin binding and actin filament disassembly. *Nat Commun* **9**:1860. doi:10.1038/s41467-018-04290-w

Tang Y, Yu J, Field J. 1999. Signals from the Ras, Rac, and Rho GTPases Converge on the Pak Protein Kinase in Rat-1 Fibroblasts. *Mol Cell Biol* **19**:1881–1891. doi:10.1128/mcb.19.3.1881

Tomchick DR, Otomo T, Otomo C, Panchal SC, Machius M, Rosen MK. 2005. Structural basis of actin filament nucleation and processive capping by a formin homology 2 domain. *Acta Crystallogr Sect A: Found Crystallogr* **61**:c75–c75. doi:10.1107/s0108767305096844

Toteva T. 2021. PhD Thesis

Treisman R. 1995. Journey to the surface of the cell: Fos regulation and the SRE. *EMBO J* **14**:4905–4913. doi:10.1002/j.1460-2075.1995.tb00173.x

Treisman R. 1994. Ternary complex factors: growth factor regulated transcriptional activators. *Curr Opin Genet Dev* **4**:96–101. doi:10.1016/0959-437x(94)90097-3

Treisman R. 1987. Identification and purification of a polypeptide that binds to the c-fos serum response element. *EMBO J* **6**:2711–2717. doi:10.1002/j.1460-2075.1987.tb02564.x

Treisman R. 1986. Identification of a protein-binding site that mediates transcriptional response of the c-fos gene to serum factors. *Cell* **46**:567–574. doi:10.1016/0092-8674(86)90882-2

Treisman R. 1985. Transient accumulation of c-fos RNA following serum stimulation requires a conserved 5′ element and c-fos 3′ sequences. *Cell* **42**:889–902. doi:10.1016/0092-8674(85)90285-5

Treisman R, Marais R, Wynne J. 1992. Spatial flexibility in ternary complexes between SRF and its accessory proteins. *EMBO J* **11**:4631–40. doi:10.1002/j.1460-2075.1992.tb05565.x

Uruno T, Liu J, Li Y, Smith N, Zhan X. 2003. Sequential Interaction of Actin-related Proteins 2 and 3 (Arp2/3) Complex with Neural Wiscott-Aldrich Syndrome Protein (N-WASP) and Cortactin during Branched Actin Filament Network Formation*. *J Biol Chem* **278**:26086–26093. doi:10.1074/jbc.m301997200

Vandekerckhove J, Weber K. 1978. At least six different actins are expressed in a higher mammal: An analysis based on the amino acid sequence of the amino-terminal tryptic peptide. *J Mol Biol* **126**:783–802. doi:10.1016/0022-2836(78)90020-7

Vartiainen MK, Guettler S, Larijani B, Treisman R. 2007. Nuclear Actin Regulates Dynamic Subcellular Localization and Activity of the SRF Cofactor MAL. *Science* **316**:1749–1752. doi:10.1126/science.1141084

Velasquez LS, Sutherland LB, Liu Z, Grinnell F, Kamm KE, Schneider JW, Olson EN, Small EM. 2013. Activation of MRTF-A–dependent gene expression with a small molecule promotes myofibroblast differentiation and wound healing. *Proc Natl Acad Sci* **110**:16850–16855. doi:10.1073/pnas.1316764110

Vinciauskaite V, Masson GR. 2023. Fundamentals of HDX-MS. *Essays Biochem* **67**:301–314. doi:10.1042/ebc20220111

Wagner AR, Luan Q, Liu S-L, Nolen BJ. 2013. Dip1 Defines a Class of Arp2/3 Complex Activators that Function without Preformed Actin Filaments. *Curr Biol* **23**:1990–1998. doi:10.1016/j.cub.2013.08.029

Wagner BJ, Hayes TE, Hoban CJ, Cochran BH. 1990. The SIF binding element confers sis/PDGF inducibility onto the c-fos promoter. *EMBO J* **9**:4477–4484. doi:10.1002/j.1460-2075.1990.tb07898.x

Wang D-Z, Chang PS, Wang Z, Sutherland L, Richardson JA, Small E, Krieg PA, Olson EN. 2001. Activation of Cardiac Gene Expression by Myocardin, a Transcriptional Cofactor for Serum Response Factor. *Cell* **105**:851–862. doi:10.1016/s0092-8674(01)00404-4

Wang D-Z, Li S, Hockemeyer D, Sutherland L, Wang Z, Schratt G, Richardson JA, Nordheim A, Olson EN. 2002. Potentiation of serum response factor activity by a family of myocardin-related transcription factors. *Proc National Acad Sci* **99**:14855–14860. doi:10.1073/pnas.222561499

Wang D-Z, Olson EN. 2004. Control of smooth muscle development by the myocardin family of transcriptional coactivators. *Curr Opin Genet Dev* **14**:558–566. doi:10.1016/j.gde.2004.08.003

Wang Z, Wang D-Z, Hockemeyer D, McAnally J, Nordheim A, Olson EN. 2004. Myocardin and ternary complex factors compete for SRF to control smooth muscle gene expression. *Nature* **428**:185–189. doi:10.1038/nature02382

Wang Z, Wang D-Z, Pipes GCT, Olson EN. 2003. Myocardin is a master regulator of smooth muscle gene expression. *Proc National Acad Sci* **100**:7129–7134. doi:10.1073/pnas.1232341100

Wasylyk B, HAHN SL, GIOVANE A. 1993. The Ets family of transcription factors. *Eur J Biochem* **211**:7–18. doi:10.1111/j.1432-1033.1993.tb19864.x

Wheeler AP, Ridley AJ. 2004. Why three Rho proteins? RhoA, RhoB, RhoC, and cell motility. *Exp Cell Res* **301**:43–49. doi:10.1016/j.yexcr.2004.08.012

Wittmann T, Waterman-Storer CM. 2001. Cell motility: can Rho GTPases and microtubules point the way? *J Cell Sci* **114**:3795–3803. doi:10.1242/jcs.114.21.3795

Yanofsky MF, Ma H, Bowman JL, Drews GN, Feldmann KA, Meyerowitz EM. 1990. The protein encoded by the Arabidopsis homeotic gene agamous resembles transcription factors. *Nature* **346**:35–39. doi:10.1038/346035a0

Zaromytidou A-I, Miralles F, Treisman R. 2006. MAL and Ternary Complex Factor Use Different Mechanisms To Contact a Common Surface on the Serum Response Factor DNA-Binding Domain. *Mol Cell Biol* **26**:4134–4148. doi:10.1128/mcb.01902-05